Application of Blue Light for Phototherapy of Dental Tissues

by:

Sherif Abdelsalam Mohamad

A thesis submitted to the University of Birmingham for the degree of Doctor of Philosophy

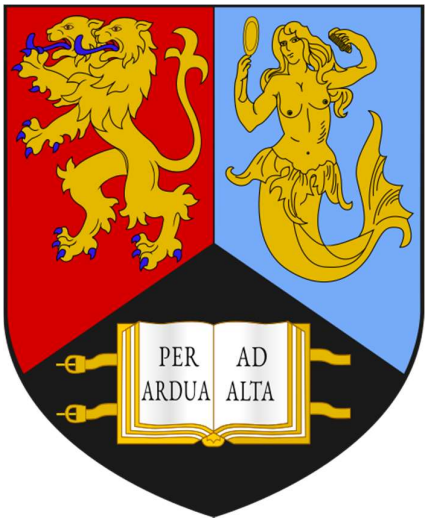

School of Dentistry

University of Birmingham

September 2021

Abstract

The direct application of blue light provides a non-invasive modality for both disinfecting dentine (photodisinfection) as well as enhancing the mineralisation processes of dental pulp cells (photobiomodulation) using a single wavelength. Dentine acquires the highest absorption for blue wavelengths of light. This permits the delivery of relatively higher doses of light limiting the cariogenic bacterial infections (*Streptococcus mutans*) within dentine, while allowing lower doses to reach the pulp cells stimulating odontoblastic differentiation. However, previous studies in the literature have not reported the orientation of dentine discs used as bacterial substrate surfaces. Notably, there has been variations among the experimental set-ups and irradiation parameters for both bacteria and mesenchymal stem cells, the stem cell type existing within the dental pulp. This study aimed to i) characterize the pattern of transmission of 405 nm light through coronal molar dentine at different tooth locations, and ii) determine the irradiation parameters that are antibacterial for *Streptococcus mutans* and iii) stimulatory for dental pulp cells.

To determine the effect of dentinal tubule orientation on light transmission, the amount of light (470 - 4054 mW/cm^2) transmitted through occlusal, oblique and buccal dentine (1, 2, 3 mm) was investigated by recording the irradiance of the traversed light. Scanning electron micrographs of 2 mm outer (dentine-enamel junction) and inner (pulp) dentine sections were analysed to detect the influence of tubular density on light transmission. Regarding photodisinfection studies, cariogenic bacteria were irradiated at a range of doses (110 – 1254 J/cm^2) in agar lawns, planktonic cultures and

mature biofilms. For photobiomodulation investigations, human dental pulp cells were irradiated using doses of 2, 4, 5 and 6 J/cm^2. Data indicated that dentine thickness as well as dentinal tubule orientation and density significantly affected 405 nm light transmission. Occlusal and oblique dentine allowed higher transmission compared with buccal dentine. Blue light irradiation inhibited initial biofilm formation as demonstrated by zones of inhibition. The 405 nm wavelength also killed bacteria in planktonic cultures and mature biofilms. At lower doses, blue light enhanced the mineralisation processes of human dental pulp cells. These data suggest that phototherapy approaches utilising a 405 nm wavelength have therapeutic potential to both limit cariogenic bacterial infections within dentine and stimulate the mineralisation potential of pulp cells. However, limiting bacterial infections can be restricted by the bacterial species irradiated, its oxidative state and anti-oxidative potential. The protocols established in the current investigation can be further explored in ex-vivo models, clinical trials, along with the development of a therapeutic light source.

This thesis is dedicated to my parents.

Primarily, in the memory of my beloved late dad

Medhat Abdelsalam Mohamad,

as well as to my mum,

Soha Negm El-Din

Acknowledgments

I would like to express my gratitude and appreciation to all of my supervisors for their help throughout my PhD. Special acknowledgments to my main supervisors Professors Paul Cooper and Mike Milward who have been endlessly supportive from day one. Professor Cooper supported my second year tuition fees, and even though he moved to New Zealand one year after I started my PhD, he was always there to help and guide. Professor Milward supported my second and third year's bench fees and always helped me reach my targets on site. Both mentored and guided me throughout my writings, analysis and critical thinking. I could feel my skills develop and progress along the way due to their efforts. There is not enough words to express how grateful I am for both of them.

This work would not have been possible without the help of the technical staff in the School of Dentistry. I am very thankful to Michelle Holder, Gay Smith, Helen Wright, Changxiang Wang, Jonathan James, Jianguo Liu and Lisa Shriane for their lab assistance.

Warmest thanks to all my fellow PhD students and postdocs. Ajoy, Ben, Farah, Hannah, Jasper, Jewlew, Maria, Mark, Menisha, Mincy, Nessma, Nina, Olga, Rebecca, Samir, Satnam, Satvir, Soher and Sophie: it has been a great pleasure and an enjoyable company.

Finally, I would like to thank my friends and family whom I will always be indebted. Without their infinite encouragement and support, I would not have gotten this far.

Contents

List of Tables

List of Figures

List of Abbreviations

ADMSCs:	Adipose derived Mesenchymal stem cells
AhpC:	Alkyl hydroperoxide reductase C
ALA:	Aminolevulinic acid
ALP:	Alkaline phosphatase
ATP:	Adenosine tri-phosphate
BCHC:	Birmingham community healthcare
BHI:	Brain heart infusion
BMMSCs:	Bone marrow Mesenchymal stem cells
BMP2:	Bone morphogenic protein-2
BSA:	Bovine serum albumin
cAMP:	Cyclic adenosine monophosphate
cDNA:	Complementary DNA
CFU:	Colony forming unit
CO_2:	Carbon dioxide
COL1:	Collagen-1
COX:	Cytochrome C oxidase
CRY:	Cryptochrome gene
DEJ:	Dentine-enamel junction
DMP1:	Dentine matrix protein-1
DPCs:	Dental pulp cells
Dpr:	Dipeptide repeat protein
DSPP:	Dentine sialophosphoprotein
E. coli:	*Escherichia* coli
E. faecalis:	*Enterococcus faecalis*
EDTA:	Ethylene-diamine-tetraacetic acid

EPR:	Electron paramagnetic resonance
FAD:	Flavin adenine dinucleotide
FBS:	Fetal bovine serum
F. nucleatum:	*Fusobacterium nucleatum*
GAPDH:	Glyceraldehyde 3-phosphate dehydrogenase
GPX:	Glutathione peroxidase
H_2O_2:	Hydrogen peroxide
HeNe:	Helium Neon
H. pylori:	*Helicobacter pylori*
HRP:	Horseradish peroxidase
IT/DP:	Increased time/Decreased power
IP/DT:	Increased power/Decreased time
IR:	Infra-red
L. acidophilus:	*Lactobacillus acidophilus*
L. lactis:	*Lactococcus lactis*
LED:	Light emitting diode
MB:	Methylene blue
MEM:	Minimum essential medium
MMP:	Matrix metalloproteinase
MSCs:	Mesenchymal stem cells
NAD(P)H:	Nicotinamide adenine dinucleotide (phosphate)
NIR:	Near Infra-red
NO:	Nitric oxide
Nox:	NADH oxidase
NRF2:	Nuclear factor erythroid 2-related factor 2
OCN:	Osteocalcin
OD:	Optical density
OPN:	Osteopontin

P. aeruginosa:	*Pseudomonas aeruginosa*
PBM:	Photobiomodulation
PBS:	Phosphate buffered saline
PCR:	Polymerase chain reaction
PDT:	Photodynamic therapy
PER:	Period gene
P. gingivalis:	*Porphyromonas gingivalis*
pNPP:	Para-nitrophenylphosphate
R:	Red
ROS:	Reactive oxygen species
RUNX2:	Runt-related transcription factor-2
S. agalactiae:	*Streptococcus agalactiae*
S. aureus:	*Staphylococcus aureus*
SD:	Standard deviation
SEM:	Scanning electron microscope
S. epidermidis:	S*taphylococcus epidermidis*
S. mutans:	*Streptococcus mutans*
S. sanguinis:	*Streptococcus sanguinis*
S. sobrinus:	*Streptococcus sobrinus*
SOD:	Superoxide dismutase
TB:	Toluidine blue
TCA:	Tricarboxylic acid
TGF-β 1:	Transforming growth factor-βeta 1
TMB:	Tetramethylbenzidine
UV:	Ultraviolet
ZOI:	Zone of inhibition

Chapter 1: Introduction and Aims

1.1 General introduction

Dental caries is a common oral health disorder which affects wide sectors of various communities worldwide. Even though there are regular advancements in treatment, it remains a remarkable healthcare and economic burden, costing more than 4% of the health expenditure globally. Disease progression can cause significant pain and can ultimately lead to tooth loss **[1]**,**[2]**. The major etiological factor is dental plaque breaking down carbohydrates and secreting acids. The main causative bacterial specie is *Streptococcus mutans* (*S.mutans*) **[3]**. After demineralising the outer layer of enamel, the lesion becomes cavitated and ultimately extends into the underlying dentine, with increased bacterial proliferation yielding increased acid production **[4]**. In advanced carious lesions, persistent infection and deepening of the lesion could eventually lead to pulp tissue necrosis and a peri-apical pathology **[5]** [see **Figure 1**]. Importantly, the tooth vitality is crucial for combating the bacterial invasion in dentine. Vital teeth were found to be significantly more resistant to bacterial progression into the dentinal tubules **[6]**. Notably, dentinal fluid is inside the tubules as well as the odontoblastic processes can maintain an outward constant pressure and fluid flow **[7-10]**. Indeed, the dentinal fluid contains a range of immunoglobulins (IgG, IgA, IgM) enhancing the tooth's defence mechanisms **[11-13]**. Additionally, only healthy odontoblasts allocated at the periphery of a vital pulp are able to promote the decalcified dentine remineralisation and repair **[14]**.

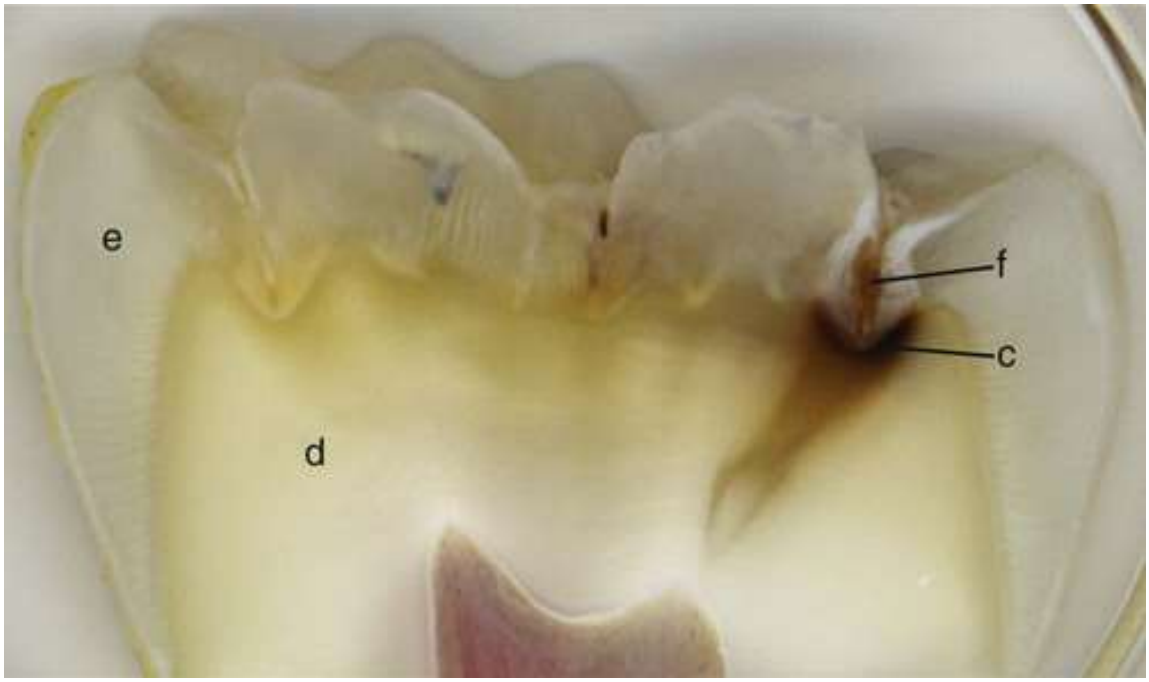

Figure 1: Longitudinal section in a tooth with a carious lesion. Fissure (f) at junction of lobes allows accumulation of nutrients and bacteria predisposing the tooth to dental caries (c). Enamel (e). Dentine (d). Source: Boushell LW, Sturdevant JR. Clinical Significance of Dental Anatomy, Histology, Physiology, and Occlusion. In: Heyman HO, Swift Jr. EJ, Ritter AV. Sturdevant's art and science of operative dentistry. Elesvier 2013.

Effective caries disease management should therefore aim to eliminate or at least control cariogenic bacterial colonisation and subsequent acid production. Other key aspects include facilitating the re-mineralization and restoration of lost tooth structure **[15]**. Routine management of carious lesions involves excavation of carious tissue and restoration placement. However, residual infection in sound tissue within the prepared cavities leads to recurrent caries. Not to mention, restorations have a finite lifespan and require periodic replacement resulting in additional tooth tissue loss over time. Deeper lesions might require pulp tissue extirpation if infection reaches the pulp; nonetheless, a conservative approach can be utilised if no signs of irreversible

inflammation or necrosis is encountered. A key aspect for conservative disease management is the induction of the regenerative odontoblastic processes. Consequently, the tertiary or repair dentine deposited acts as a barrier against carious disease progression and can retain pulp vitality. Current vital pulp therapy protocols involve removal of infected tissue, followed by application of materials that aid the initiation of the reparative responses of the pulp (*i.e.* calcium hydroxide and mineral trioxide aggregate). However, there are challenges regarding the delivery and dosage control when using materials **[16-19]**. One of the main problems is that carious lesions are difficult to detect before the cavitation is observed and subsequently operative dentistry is required **[20]**. One strategy to prevent carious tooth tissue loss is local delivery of chemical antibacterial compounds (i.e. mouth rinses) to inhibit the biofilm colonisation and growth. However, some compounds such as chlorhexidine have been reported to give a less than ideal outcome due to poor penetration in the established plaque biofilm as well as other complications such as staining. Fluoride containing mouth rinses are not effective against high caries challenges **[21-23]**. Other chemical disinfectants such as triclosan have been utilised but these are shown to have transient oral retention and a short activity half-life, and therefore are limited in their use **[24]**.

Utilisation of light for bacterial disinfection has focused conventionally on the use of photodynamic therapy (PDT). This method of inhibiting and killing bacteria utilises a light- excited sensitizer that produces free radicals inhibiting or killing the bacteria **[25]**. However, results indicated that disinfection of ex-vivo carious dentine models was less effective than when applied in a planktonic suspension **[26]**. Additionally,

photosensitizers exhibit diffusion difficulties in carious lesions, making it more resistant to the treatment **[27]**. Another recent approach has been the use of the direct antimicrobial effect of light without the application of a photosensitizer. This approach has the advantage of direct light delivery to bacteria in order to excite endogenous chromophores/photo-absorbers for each bacterial species, resulting in bacterial killing **[28]**. The mechanism involved does not rely on photo-thermal eradication as reported using infra-red (IR) diode and carbon dioxide (CO_2) lasers, which would be hazardous to host tissues **[29],[30]**. The mechanism by which direct light irradiation causes antimicrobial action is reported to be via porphyrin activation which have been proposed as the main endogenous photosensitizers within bacteria. They have an absorption peak within the violet/blue spectral range **[31]**. Porphyrins are macromolecules essential for bacterial synthesis of heme **[32],[33]**. They include a range of intermediate compounds starting with aminolevulinic acid (ALA) precursor **[34]**, and exhibit fluorescent properties with light absorbance between the wavelengths of 390 and 425 nm. Porphyrins absorb light photons, leading to the production of inhibitory levels of reactive oxygen species (ROS) including hydroxyl radicals, superoxide anions and singlet oxygen **[31],[35-43]**. Normal low levels of ROS which are secreted for signalling and haemostasis result in bacterial proliferation; however, higher levels of ROS can be produced when irradiation is performed in the 400-500 nm / blue light spectral range **[44]**. Recent research studies have shown that blue light can exert a bactericidal or bacteriostatic effects on cariogenic bacteria. This characteristic offers the potential to use light irradiation to inhibit biofilm cariogenic activity, which can be achieved either directly by inhibiting the cariogenic bacteria

residing in the biofilm or indirectly by interfering with the bacterial cell metabolism preventing bacterial colonisation and biofilm maturation **[45-47]**.

Research using the cariogenic bacteria *S. mutans* showed variability among the bacterial substrate surfaces and irradiation conditions reported. PDT studies showed variability in the irradiation parameters used **[48-50]**. Needless to say, the orientation of the sectioned dentine - which typically affects light transmission - was not reported **[48],[50-52]**. In direct light studies, there were notable inconsistencies in characterising the light sources used as well as reporting the delivered dose **[45],[53]**. Additionally, dentine is a complex tissue. It is an optically anisotropic tissue, meaning that its optical properties are dependent upon the light propagation direction. This takes place due to the dentine's non-homogenous structure comprising dentinal tubules. Light propagation also differs according to age, tooth type, dentine thickness, dentinal tubules density and orientation. The microstructural pathway of the tubules affect dentine's refractive index. Different tooth types show different scattering and absorption properties. Needless to mention, biological variations within the same tooth type comprising transparent or sclerotic dentine **[51],[52]**,**[54-59]**.

Photobiomodulation (PBM) or Low level light therapy (LLLT) effects were first reported by Endre Mester in 1967 following the discovery of ruby lasers. His work initially investigated the possibility that laser light induced cancer; however, he discovered that the irradiation was not carcinogenic but actually promoted hair growth in mice. PBM utilises light at relatively low power settings, which is absorbed by endogenous chromophores within various mammalian cells including but not limited to fibroblasts, keratinocytes, neural and endothelial cells. Photo-absorbers are mainly redox proteins

such as cytochrome C oxidase (COX), nicotinamide adenine dinucleotide phosphate (NADPH) oxidase and NADPH dehydrogenase. After light absorption, a photochemical response is induced that has been reported to significantly increase proliferation rates, growth factors (basic fibroblast growth factor, vascular endothelial growth factor and transforming growth factor-βeta (TGF-β 1)) as well as wound healing inflammatory mediators (interleukins 1 and 8) **[60],[61]**. Several investigations have reported that red (R) (620-660 nm) and near infra-red (NIR) (800-980 nm) light can enhance the proliferation in mesenchymal stem cells (MSCs) **[62],[63]**; this cell type can be found within the dental pulp and is termed dental pulp stem cells (DPCs). Other studies have also reported osteo- and odonto-blastic differentiation effects following irradiation by R/NIR light **[64],[65-73].** Blue lasers or Light Emitting Diodes (LED) (400-500 nm) – at lower irradiation parameters than those applied to inhibit bacteria – have recently been shown to enhance the mineralization processes in MSCs **[74-78]**. The most widely accepted theory for the R/NIR PBM effects are in response to light absorption by COX, which subsequently leads to stimulation of the respiratory chain and associated adenosine tri-phosphate (ATP) production **[79].** The mode of action of blue light is reportedly primarily mediated via a relatively small increase in ROS levels after the light has been absorbed by flavin-bound enzymes (NADPH oxidase and NDPH dehydrogenase) **[80],[81].** Notably**,** MSCs redox state has major influence on proliferation and mineralisation **[82],[83].**

Light dose/radiant exposure/energy density (J/cm^2) depends on both the irradiance/power density (mW/cm^2) and irradiation time (seconds). The irradiance varies with the light source's output power, spot size and distance to target tissue.

Irradiance is also affected by the pulse frequency and duty cycle in case of using a pulsed light source. PBM effects show a biphasic dose-response relationship and biostimulation for each specific tissue occurs only via a window of doses. A low light dose has no effect, a slightly higher dose causes biostimulation, while a much higher dose leads to inhibitory effects. Accordingly, the Arndt-Schulz law is frequently quoted as an appropriate model to describe these biphasic responses. This law states that small doses of any substance leads to stimulatory effects and moderate or high doses result in inhibition. The Arndt-Schultz law is displayed over a curve where low doses have bi-stimulatory effects, while higher doses - higher irradiance or longer exposure times - cause inhibition [see **Figure 2**]. PBM effects also defies reciprocity, meaning that if the light dose is kept constant while changing other settings (irradiance and irradiation time), outcomes will not be the same. Other irradiation parameters can also affect the outcomes such as the mode of operation, i.e. continuous wave or pulsed, and the wavelength applied **[84-88]**. Notably, the energy of photons depends on the wavelength, e.g. blue light photons emit more energy than red light photons. So it is important to optimise the irradiation parameters to ensure the desired therapeutic effects and avoid undesirable side effects such as cellular injury subsequent to oxidative stress **[61]**.

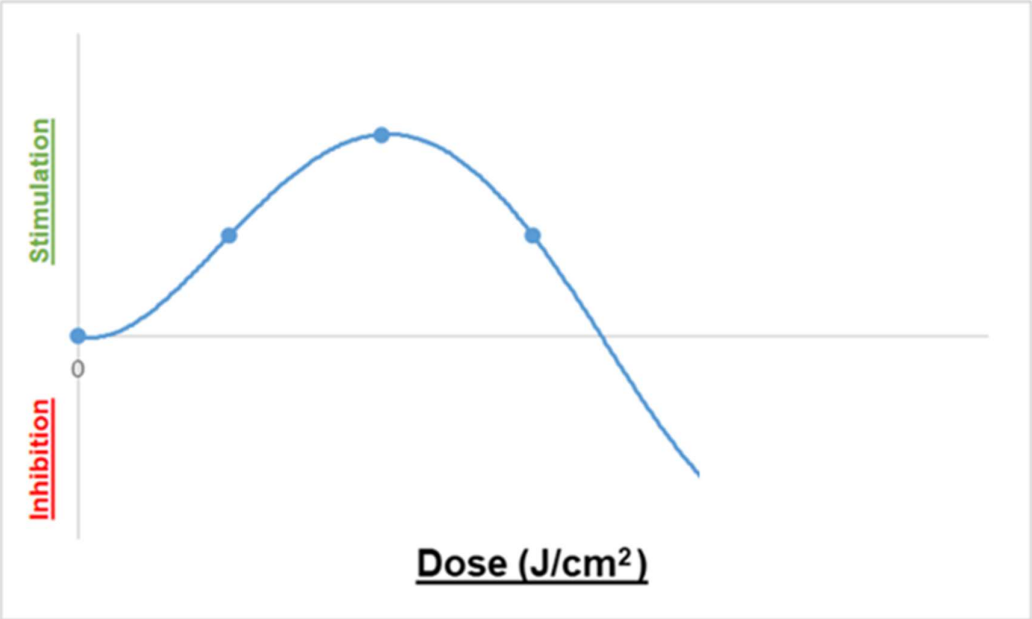

Figure 2: An illustration of the Arndt Schultz curve. Lower light dose exerts no effect, higher dose causes stimulatory effects, while much higher doses (higher irradiance or irradiation time) can lead to inhibitiory effects.

To summarise, PDT approaches may have drawbacks, it reportedly works better in planktonic suspensions rather than in ex-vivo carious dentine models mostly due to the limited diffusibility of the photosensitizer in a complex medium such as dentine **[26],[27]**. Pathogenic bacteria residing within the dentinal tubules are not embedded in a broth medium which might facilitate the absorption of a photosensitizer into the bacterial cells. To overcome the diffusion obstacles, direct application of light has been proposed to directly control the bacterial infection on the tooth surface as well as within dentinal tubules. When light interacts with a tissue, photons are either absorbed or scattered. Eventually, the scattered photons will be absorbed by bacteria residing in the tubules **[61]**. Light propagation in dentine depends mainly on the pathway of the dentinal tubules, meaning light has a tendency to propagate through the tubules with a lower refractive index compared with peritubular dentine lining the tubules **[52]**.

PBM also offers the potential to stimulate stem cell differentiation in the dentine-pulp complex and consequently promote reparative dentine deposition which is beneficial in caries management. Moreover, blue light exhibits the highest absorption coefficient in dentine **[89-91]**, enabling a potential way to deliver lethal doses to pathogenic bacteria located within the dentinal tubules, while allowing only a residual lower light energy to pass through to the dental pulp to bio-modulate the cells and reduce inflammation. However, in order to optimise the delivery of blue light for both purposes, the optical characteristics of dentine, irradiation parameters that are inhibitory for *S. mutans* and stimulatory for DPCs must be investigated. The differences in absorption / transmission patterns at a variety of anatomical tooth locations will influence how light could be delivered to optimise the desired therapeutic outcomes. These outcomes could help prevent carious lesion progression, pulpal inflammation / necrosis and potential tooth loss.

1.2 Dental caries, dentine-pulp complex biology and hard tissue repair

Carious lesions are initiated primarily by *S. mutans*, a Gram positive, facultative anaerobic bacteria which grows optimally in a microaerophilic atmosphere; however, it can also survive in aerobic conditions. Notably**,** *sobrinus*, *rattus*, *mutans*, *ferus* and *cricetus* are collectively known as *Mutans Streptococci*. It grows rapidly at a temperature of 37^{o}C, ferments a range of sugars, i.e. lactose, sorbitol, mannitol, insulin, raffinose, mannose, salicin and trehalose, producing lactic acid. It is more acidogenic than other streptococci and can synthesize water-soluble/insoluble extracellular polysaccharides (e.g. glucan – fructan) from sucrose, which enhance bacterial colonization and growth on the tooth surface. *S. mutans* can be isolated from incipient and cavitated carious lesions **[92],[93]** and it is regarded as the most cariogenic of all streptococcal bacteria **[15]**. Other bacterial species contribute later in the caries process as the lesion progresses such as *Enterococcus*, *Actinomyces*, *Lactobacillus* and *Eubacterium spp*. Their presence depend on each specie's aciduricity and the local pH **[3],[4],[94]**. The biofilm causing caries comprises of bacteria and extra-cellular polysaccharides in a complex matrix that develops with time and is influenced by environmental factors such as salivary flow and frequency of sugar intake. Carious lesions primarily begin by demineralising the outer highly mineralized layer of enamel as a result of key cariogenic bacteria resident in the biofilm generating lactic, acetic and propionic acid from dietary components **[94-97]**. The bacterial by-

products (pathogen-associated molecular patterns) eventually reach the dental pulp via the dentinal tubules, inducing inflammatory responses **[98]**.

The dental pulp consists of a range of cell types that include odontoblasts, fibroblasts secreting collagen fibres types I and III, a microcirculatory system, a neuronal system and DPCs which are self-renewing mesenchymal cells with multi-lineage differentiation capacity **[99-103]**. Odontoblasts, the cells that form dentine, originate from the ectomesenchymal progenitor cells. After developmental dentinogenesis is complete, odontoblasts remain aligned at the periphery of the dental pulp in order to continuously deposit secondary dentine throughout the tooth's life; also, their activity can be up-regulated in response to tissue injury or disease **[104]**. Notably, tertiary dentine, which is repair dentine deposited after a tooth has erupted, could either be: a) reactionary, produced by surviving post-mitotic odontoblasts or b) reparative, produced by a new generation of odontoblast-like cells after the death of the original post-mitotic cells [see **Figure 3**]. When a reparative action is required, the undifferentiated mesenchymal cells, situated within the pulpal tissue, are signalled to differentiate into odontoblast-like cells resulting in reparative dentine production. This occurs only when there are sufficient oxygen levels and minimal levels of inflammation. Histologically, it can be difficult to distinguish between both types of repair dentine; however, reparative dentine can be more dysplastic and exhibit similarities with bone and is subsequently termed osteodentine. Conversely, reactionary dentine has a tubular structure and maintains a non-uniform junction with odontoblasts. Extracellular matrices of dentine contain significant amounts of TGF-β 1 which has a well-characterised influence upon odontoblastic differentiation and

secretory activity. Acids demineralizing dentine, produced by cariogenic bacteria, could lead to the release of TGF-β1 from the dentine extracellular matrix which then mediates the odontoblastic cell response to mild or arrested dental caries. Notably, the deposition of either reactionary or reparative dentine can be due to internal or external stimuli **[105-109]**.

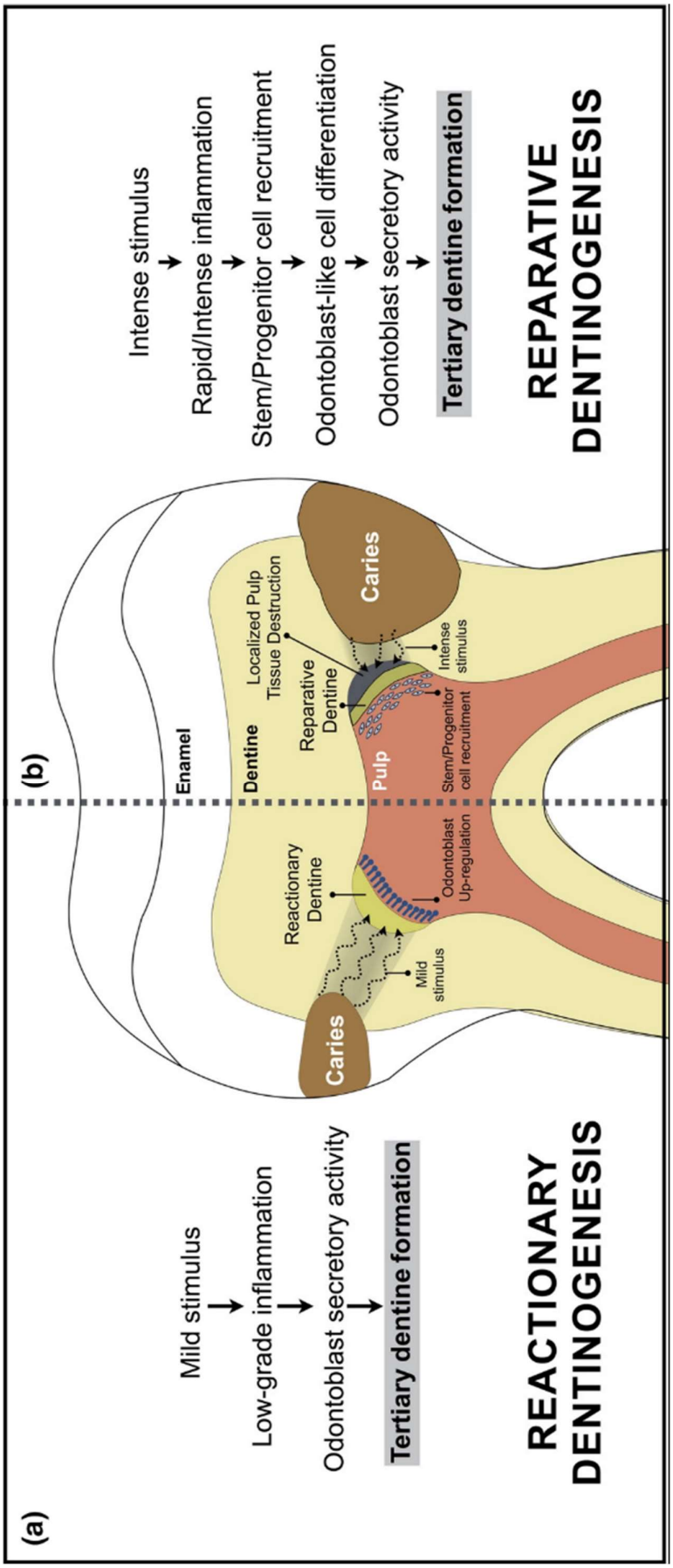

Figure 3: The processes and steps involved in reactionary and reparative dentine formation. Source: da Rosa WLO, Piva E, da Silva AF. Disclosing the physiology of pulp tissue for vital pulp therapy. International Endodontic Journal 2018; 51(8):829-846. https://doi.org/10.1111/iej.12906

Dentine permeability has been proposed to be a key factor which dictates the pulpal response to a carious challenge. Compared to demineralised tissue, tertiary dentine provide a more intact hard tissue base to protect the pulp against carious lesions. Consequently, in response to more severe injuries, the tissue secreted by newly differentiated odontoblasts exhibits discontinuity in tubular structure in attempts to maintain the pulp tissue vitality. It has been also reported that the reparative process begins with a primitive osteodentine or fibrodentine matrix - secreted by cells other than odontoblast-like cells - in order to pave the way to the more tissue specific response by odontoblast-like cells. Nonetheless, these reports suggests that the secretion of atubular tissue is an essential precursor to depositing the more complex tissue. Reparative and reactionary dentine deposition overlap specially in cases of pulp exposure. It is also worth reporting that fibroblasts have been proposed to be able to differentiate into odontoblast-like cells, with fibrocytes participating in the healing process. Therefore, successful outcomes of vital pulp therapy depend on both controlling the infection as well as stimulating a dentinogenesis response. Initiation of an endogenous reparative response is indeed better than invasive protocols. Furthermore, maintaining a healthy pulpal blood circulation is important for eliminating toxins produced by carious infections enabling odontoblastic differentiation at the dentine-pulp interface. Obviously, infection elimination results in improved tissue repair outcomes. It has been proven clinically that reducing the bacterial challenge, through partial and full pulpotomies, is essential towards achieving a better prognosis **[16-18]**.

1.3 Dentine microstructure and optical properties

Dentine is composed mainly of mineralized hydroxyapatite (70% in weight), organic matrix - mainly collagen (20%) - and water (10%). The dentinal tubules have a diameter which ranges from 2-3 µm near the pulp to 0.5-1 µm at the dentine-enamel junction (DEJ) **[110],[111]**. The outer layer of dentine demonstrate relatively thin and abundant tubules with terminal branches at the DEJ. The central layer exhibits two separate tubular morphologies: type 1 with no nodular structures and more branches and type 2 having more circular nodules that surround the tubules. Type 1 dentine is more prevalent in young individuals (10-12 years old) while type 2 dentine is more prevalent in older individuals (32-58 years). The nodular structures, linked by thin branches, is proposed as a connection between intertubular and peritubular dentine. Also, the nodules were suggested to be dentinal tubules in the first place, containing cytoplasmic processes derived from the odontoblasts **[112]** [see **Figure 4**].

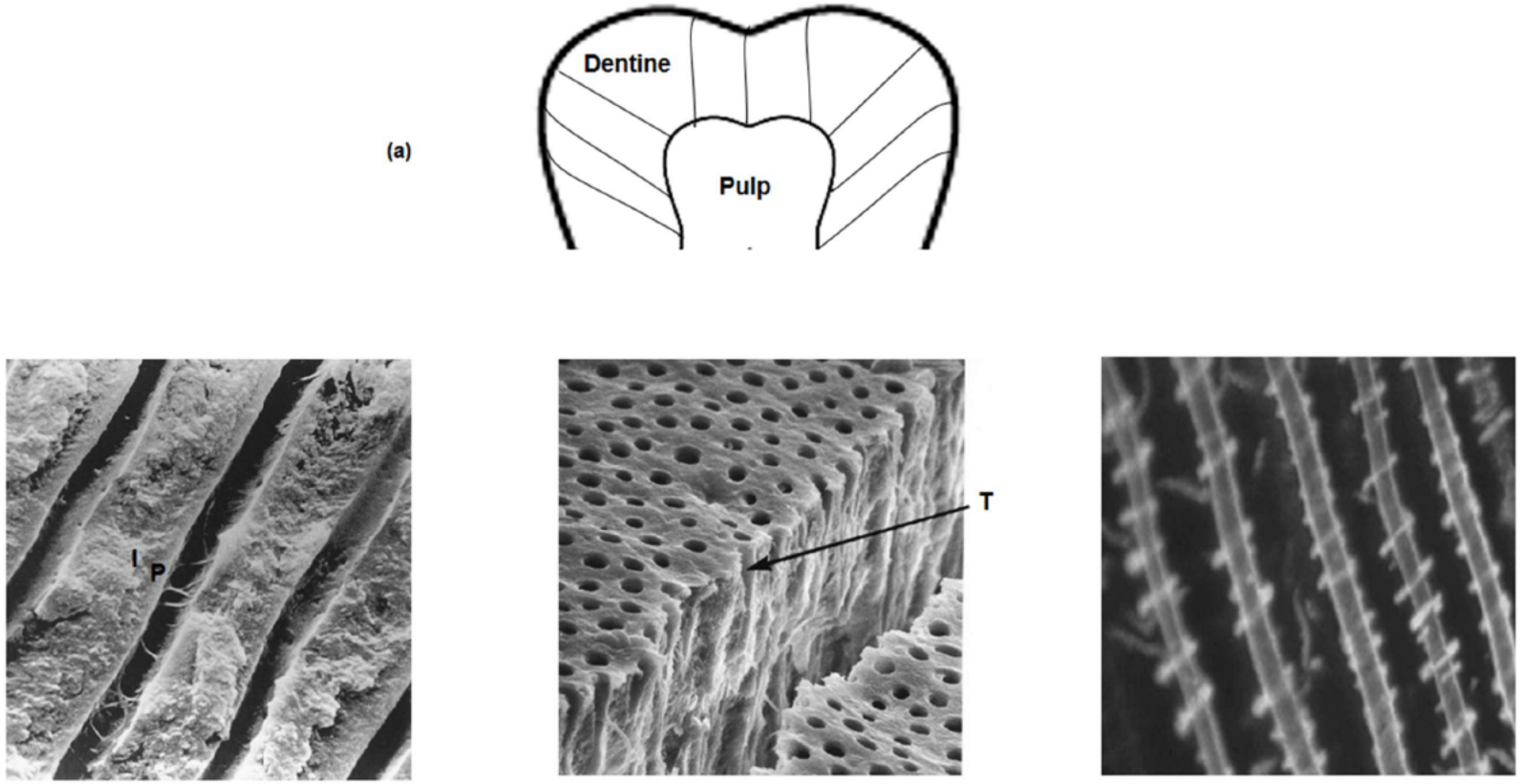

Figure 4: **(a)** Schematic diagram showing the change in tubular orientation at different tooth sections. **(b)** Dentinal tubules in cross-section showing both Peri-tubular (P) and inter-tubular dentine (I). **(c)** Scanning electron microscope image of a ground dentinal surface where an artificial crack shows the dentinal tubule (T) structure. Source (b) & (c): Brännström M: Dentin and pulp in restorative dentistry. Wolfe Medical London 1982. **(d)** Fluorescent micrographs showing dentinal tubules having numerous nodules. Source: Kagayama M, Sasano, Y, Sato H, Kamakura S, Motegi K, Mizoguchi I. Confocal microscopy of dentinal tubules in human tooth stained with alizarin red. Anatomy and Embryology 1999; (3):233-8. http://doi.org/10.1007/s004290050224.

Kienle *et al.* excluded the concept that the dentinal tubules might be transmitting light in a similar way to fibre-optics where light propagates down a fibre by multiple total internal reflections, at an incident angle greater than the critical angle. This hypothesis was proposed as peritubular dentine has a higher refractive index compared with the hollow tubules, intertubular dentine and collagen fibres. However, this did not explain light propagation when incident light is at an angle less than the critical angle. They affirmed that the fibre-optic theory was not valid, as the dentinal tubules and peritubular dentine appeared darker compared to the surrounding tissue when investigating the transmitted light. Not to mention, the sigmoid pathway of the tubules. Anisotropy of dentine was explained to be due to the tubules divergence towards the pulp, acting like a wave-guide system. This theory was confirmed by their findings where light intensity in occlusal-pulpal direction was higher than through pulpal-occlusal direction. Applying Maxwell's equation for infinite long cylinders, with a small angle between the incident light beam and the dentinal tubules, light would be scattered in a cone with a small apex angle. The following scattering takes place by the nearby tubules and so on, demonstrating that light photons propagates along the tubules direction by multiple scatterings **[113]**. Zijp *et al.* evaluated several theoretical models for light scattering in dentine. The calculated values from a Fraunhofer diffraction model showed minimal impact on light propagation. Nonetheless, cylinder scattering values were comparable to the ones measured which supported the hypothesis that dentinal tubules are mainly the light scatterers. Scattering measured in a plane parallel to the tubules was less than scattering measured in a plane perpendicular to the tubules, and values throughout the parallel plane were also not

equal to absolute zero. The reason for this was attributed to the tubules not being perfectly straight circular cylinders **[114]**. A scattering effect takes place due to the difference in physical properties of the tissue along its different axes. The scattering is relatively high throughout the Ultraviolet (UV) - NIR spectrum, and occurs mostly along the dentinal tubule direction, perpendicular to the tooth surface. The refractive index of dentine depends mainly on the direction of light propagation due to both the hydroxyapatite crystals and the uniform orientation of the tubules. Accordingly, it has been reported that dentine has a double refraction/birefringence **[51],[52],[54-58]**.

Notably, dentine's light absorption and its subsequent re-emitted luminescence showed a maximum value at 400 nm **[115],[116]**. Three additional wavelengths showed absorption peaks; 350 – 360 nm, 405 – 410 nm and 440 – 450 nm. Emission occurred at 525 nm through demineralized dentine, and this is attributed to the collagen crosslinking within the hydroxyapatite **[117-119]**. A study was undertaken by Dogandzhiyska *et al.* who calculated the absorption and transmission of a range of wavelengths of light (350-1000 nm) through a 1 mm dentine specimen. Light absorption was found to be dependent on wavelength within the spectral range of 350-600 nm; however, higher transmission was evident at wavelengths above 600 nm. The highest penetration/lowest absorption was found in the NIR range 750-1000 nm, and the least penetration/highest absorption occurred in the UV – blue spectrum of 315-400 nm **[89]**. Similarly, when 0.2, 0.5 and 1 mm dentine specimens were irradiated using three different wavelengths of LED light at 450, 630 and 850 nm, light attenuation was the highest when using the 450 nm blue light and declined at the higher wavelengths of 630 nm and 850 nm. These data indicated that transmittance

increased as wavelength increased **[90]**. Using a more complex approach, Palin *et al.* utilised 1, 2 and 3 mm dentine specimens sectioned through the pulp either perpendicular to the crown, the buccal surface or obliquely. They determined that there were no differences between irradiance of transmitted LED light at 400-900 nm and laser light at 660-810 nm. The highest absorption coefficient for dentine was found to be at a wavelength of 400 nm. **[90]**. Shorter wavelengths of light exhibited more refraction and would therefore need a relatively high critical angle to exit an optically dense medium such as dentine **[120]**.

The light absorption and its resultant forward scattering taking place in the dentinal tissue is not reportedly a function of mineral content **[57]**, and is due to the organic components (i.e. collagen and amino acids) present in the intertubular dentine **[58].** The mineral scattering coefficient is regarded as being too low and is not sufficient to cause Rayleigh scattering and therefore does not contribute towards light propagation **[114]**. Berg *et al.* also confirmed these findings, as they could not identify any trends correlating wavelength and mineral content. In their studies, they analysed sclerotic apical dentine (Cemento-Enamel Junction) and irradiated it with a 1300 nm light source **[121]**. Absorption was found to be independent of wavelength at irradiations below 400 nm; however, at 400 nm there was a rise in absorption coefficient likely due to the presence of collagen. The amino acids found within the collagen crosslinks results in dentine fluorescing three times more than enamel. This was evident by 4 fluorescence bands identified at 350, 400, 450 and 520 nm with their respective excitation bands being at 300, 325, 380 and 410 nm. Chromophores for the first two excitation/emission are tryptophan and hydroxypyridinium, and the latter two were

not identified, although it was hypothesized to be due to organic components. Notably, scattering slowly decreased with increase in wavelength, which suggests it occurred due to dentinal tubules **[57],[122]**. Nikonenko *et al.* reported that blue light scattering occurs more than red light. Scattering is due to tubules being 1000 times greater in size compared with the mineralised tissue crystals **[55]**. However, scattering patterns might fluctuate according to location as nearer the DEJ, scattering is reportedly less likely due to the decreased and smaller diameter tubules compared with scattering in deeper tissue where there are increased and wider diameter tubules **[57]**. Notably, scattering is a result of the intertubular dentine whose axes are aligned with the axes of the dentinal tubules leading to a radial-optical anisotropy model. This means that there are various refractive indices along as well as transverse to the tubules, and therefore dentine can be called a uniaxial crystal only if the mineral crystals are uniformly distributed inside the tubules. Dentinal tubules have a biaxial gradient though since it is composed of several uniaxial crystals with multiple optical axes **[123]**. Any isotropic component can be added to this anisotropic model **[58]**. Consequently, this anisotropy can vary with dentine thickness. Fried *et al.* assessed the scattering properties of two types of dentine approximately 300 µm in thickness. They studied three wavelengths 543 nm, 632 nm and 1053 nm. Specimens of more than 300 µm thickness showed no anisotropy due to the continuous change of tubular orientation with depth, while specimens less than 300 µm in thickness exhibited increased anisotropy as light diffracts in a plane perpendicular to the dentinal tubules. Within the dentine sections of 30 - 200 µm, relatively strong scattering and weak absorption effects were mostly observed in the visible-NIR light spectrum. Notably,

both scattering and absorption coefficients did not vary considerably with the wavelengths studied **[51]**.

Light propagates along dentinal tubules which contain peritubular dentine with a high refractive index, and the odontoblasts which exhibit a refractive index similar to that of water. Subsequently, the tubules could act predominantly as a uni-axial crystal whose optical axis is parallel to the tubules themselves. The central part of dentinal tissue can yield optical magnification/reduction due to the more symmetrical distribution of the tubules **[123]**, while the periphery of the coronal dentine has an exceptional polarization potential **[54],[124]**. Accordingly, it can be stated that light scattering and eventual propagation can either be a symmetric process due to the effect of hydroxyapatite and collagen or asymmetric caused by the dentinal tubules themselves **[51]**. Additionally, the orientation of the tubules affects the amount of light transmitted. Lower refractive index values resulted among the cross cut samples compared with discs dissected both longitudinally and obliquely. Hariri *et al.* determined the refractive indices and optical tomography signals of 300 - 400 µm dentine discs dissected cross-sectionally, longitudinally or obliquely. A range of outcomes were observed and lower refractive index values resulted among the cross cut samples compared with the other two sectioning approaches. This was attributed to the anisotropic structure of dentine and its tubular orientation, eventually leading to different indices which affected the light propagation **[52]**. A study examining the influence of dentine's microstructure and anisotropy utilised two groups of dentine exposed to either 543 nm or 633 nm wavelength light generated by a Helium Neon (HeNe) laser. In order to analyse the diversity in the dentine structure, two sample

groups were sectioned, one at a 20 µm thickness with dentinal tubules either parallel or perpendicular to the surface. The second group were of 200 µm thickness and had tubules at a 30 degree angle to the surface. The scattering coefficient was calculated to be zero and the transmitted intensity peaks for each wavelength of laser used were determined to be due to the diffraction effects of the tubules **[58]**. It is also important to take into account that the optical characteristics of dentine can change with tooth type. Incisors, canines and molars show similar spectral behaviour although significant differences in the magnitude of the patterns were observed. Canines demonstrated the highest scattering and light reflectivity, while molars exhibited the highest light transmittance and absorption. The degree of absorption was similar between all three types of teeth **[59]**.

1.4 Dental tissue photodisinfection

1.4.1 Photodynamic therapy:

1.4.1.1 Mechanism

PDT is a method of inhibiting and killing bacteria that utilises a light activated sensitizer that produces free radicals, which subsequently reacts with the bacterial cell components causing cell damage and death. A similar outcome could also be achieved if the stimulated sensitizer transfers energy to molecular oxygen, yielding singlet oxygen states which are more powerful oxidants for cellular constituents **[25]** [see **Figure 5**]. There are many studies examining the effect of light on cariogenic bacteria and involving the use of photo-activated stains/dyes **[26],[27],[48 – 50],[125 – 128]**. The process termed PDT can involve the use of toluidine blue (TB), methylene blue (MB), disulfonate phthalocyanine and curcumin. Currently, it is however not possible to identify any studies within the literature which examine the effect of these sensitizers on host cells, so there is a possibility that the photosensitizer may have a detrimental impact on local host cells.

1.4.1.2 Cariogenic bacteria photodynamic therapy in-vitro studies

Zanin *et al.* assessed the effect of a 660 nm diode laser on *S. mutans and S. sobrinus* using TB photosensitizer. After delivering a light dose of 28.8 J/cm^2, total bacterial killing was only observed when the light and the TB where both used. Neither the laser nor the dye alone affected the viability of the bacteria **[125]**. Additionally, similar outcomes were obtained for the same bacteria grown on enamel slabs and irradiated

using a 638.8 nm LED (85.7 J/cm^2) and utilising TB **[126]**. Melo *et al.* obtained similar results using TB sensitized *S. mutans* and *Lactobacillus spp.* photo-activated by a 630 nm laser (94 J/cm^2). Notably, these bacterial species were directly harvested from human carious dentine lesions **[127]**. Furthermore, a combined therapy applying both MB and 660 nm diode laser (320 J/cm^2) twice a day resulted in a marked *S. mutans* reduction. This effect was comparable with conventional chlorhexidine usage **[128]**. Williams *et al.* irradiated *S. mutans* treated with TB under two conditions, either in a collagen matrix or using *ex vivo* carious dentine to replicate oral cavity conditions. They used a 633 nm laser and the disinfection process in carious dentine was shown to be less effective than when assessed in a planktonic suspension due to restricted diffusibility. Interestingly there was more deviation in $\log_{10}$ (CFU/ml) reductions obtained when using carious dentine, which is attributed to the variability in dentine's microstructure **[26]**. In a similar study, bacteria were treated with one of two conditions, TB + 633 nm HeNe laser or aluminium disulfonate phthalocyanine + 660 nm laser, each applied in either a collagen matrix or on artificially demineralized dentine slices. While the longer they exposed the bacteria to light the greater the killing effect, no relationship was detected between the extent of tissue demineralisation and the treatment's ability to eradicate the bacteria **[50]**. *S. mutans* and *L. acidophilus* biofilms, as well as carious dentine colonized specimens were exposed to curcumin, LED 450 nm (5.7 J/cm^2) or curcumin + LED. Only PDT curcumin + LED reduced the viability of the biofilms. However, due to curcumin drug diffusion difficulties, carious lesions were more resistant to the treatment **[27]**.

With regards to the variability in reporting the irradiation parameters, in their PDT study, Ricatto *et al.* initially infected 2 mm dentine fragments from bovine incisors with planktonic suspensions. They reported the irradiation protocol was executed relying on Lima *et al.'*s protocol. The mentioned parameters in Lima *et al.'s* study were only the output power of a 638 nm LED - 40 mW, spot size of 9.5 mm, as well as irradiation distance of 2 mm from human dentine slabs. Still, Ricatto *et al.* stated that the irradiation was done at 2 cm delivering the same dose - 94 J/cm^2 **[48],[49]**. On the other hand, Burns *et al.* experimented a PDT set-up with a 150 µm human dentine slabs interposed between the light source and *S. mutans* planktonic cultures. They reported that the irradiance at the surface of the culture was measured in the presence and absence of the dentine slab **[50]**.

1.4.2 Direct light irradiation

1.4.2.1 Mechanism

Porphyrins are macromolecules essential for the bacterial synthesis of heme **[32],[33]**. They exhibit fluorescence spectra at ~600 nm with wavelengths of light absorbance between 390 and 425 nm **[35]**. Notably, bacterial cells containing porphyrins are sensitive to blue and red visible light **[42],[43]**. Indeed, Hamblin *et al.* indicated that blue light at 405 nm sensitizes the photoactive porphyrins in *H. pylori* cells, which leads to antibacterial killing **[31]**.

Porphyrins are metal-free intermediate compounds that share common basic structures which include four pyrrole rings linked together by a methine bridge at their

alpha carbon bonds. Due to their common structure, they exhibit blue light absorbance. After porphyrins absorb light photons, an electron is elevated from ground state to an excited state. The excited electron then returns to the ground state through two different mechanisms. One mechanism is through releasing one photon to induce a fluorescence effect, whilst the other mechanism involves the electron moving to a less excited state (triplet state). Once the electron has reached the triplet state, it can either return to the ground state discharging one photon to generate phosphorescence or in the presence of oxygen, the photosensitizer will transfer energy to an oxygen molecule. If energy transfer to oxygen occurred, then two potential reactions can occur, a type I or type II reaction. In the type I reaction, ROS such as hydroxyl and superoxide anion radicals are produced, which are not specifically reactive with biologic tissues; however, they can react with themselves forming more reactive species such as hydrogen peroxide (H_2O_2). In type II reactions, the energy released from the photosensitizer is up-taken by a triplet oxygen, transforming it into a much more excited singlet oxygen which is highly reactive and understood to have the major effect in the photodisinfection process **[35-41]** [see **Figure 5**]**.** Notably, ROS generated at high levels affects the cell wall, cell membrane, mitochondria, nucleus, DNA, as well as ATP levels. Moreover, lipids are oxidised and proteins are crosslinked. Early investigations using exogenous porphyrins as novel photosensitizers suggested that porphyrins bind to either the bacterial cell wall, inner membrane or translocates to the cytoplasm **[129]**. To confirm the role of both porphyrins and ROS in the process, Lipovsky *et al.* recorded higher levels of ROS production when bacteria were illuminated with blue light (400-500 nm) compared with red light (500-600 nm).

Notably, the phototoxic effect of light reportedly relies on porphyrin content as well as the antioxidative potential of the cell **[130].** The phototoxic effect was consequently diminished when the bacteria were irradiated in the presence of ROS scavengers including superoxide dismutase (SOD), catalase, ascorbic acid and dimethylthiourea **[131]**.

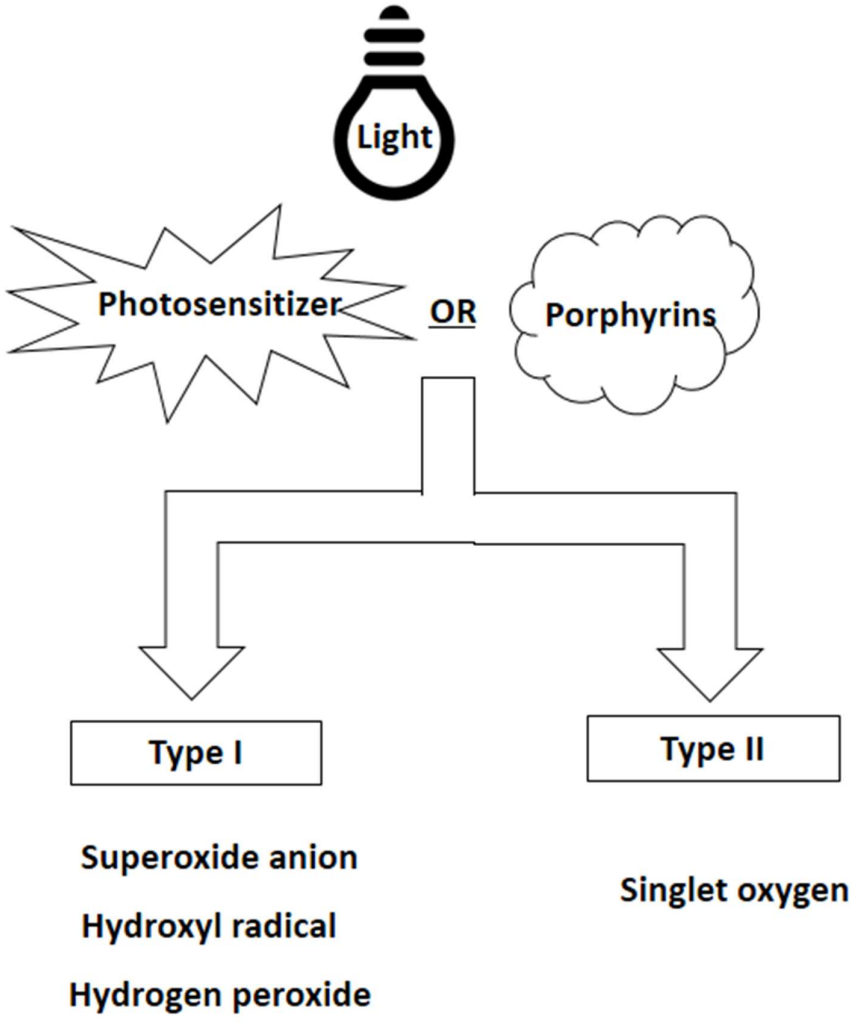

Figure 5: Schematic showing the process of ROS production after light absorption by either an exogenous photosensitizer or endogenous porphyrins in bacterial cells. The Type I reaction leads to the production of fewer reactive superoxide anions, hydroxyl radicals and hydrogen peroxide. The Type II reaction leads to the production of singlet oxygen which is highly reactive and understood to have the major effect in the photodisinfection process.

1.4.2.2 Application of direct light for photodisinfection: in-vitro studies

1.4.2.2.1 Red light

Ahmed *et al.* used a 670 nm dioder laser (30 mW power) to irradiate *S. mutans* harvested from carious lesions at different exposure times of 5, 10, 15, 20 and 25 seconds. The bacterial biofilms were grown in broth then transferred to healthy rabbit teeth to estimate the bacteria's cariogenic potential. Only 15, 20 and 25 seconds exposure times maintained a caries-free environment, while bacteria treated at 5 and 10 seconds showed latent caries **[132]**. Utilising a 630 nm LED, and to better imitate oral cavity conditions, Lee *et al.* studied *S. mutans* irradiated in three different human dentine thicknesses of 500, 1000 and 2000 µm. They investigated a range of power settings; 0.5, 1, 3, 5, 7 and 9 W. LED application at 7 W power along with distilled water cooling led to a 97.7% killing as assessed by colony forming unit assay through the 500 µm dentine thickness. Results were not significantly different from the 5 W exposure group which resulted in 90.8% killing **[133].**

1.4.2.2.2 Blue light

De Sousa *et al.* cultured *S. mutans* biofilms on saliva-coated hydroxyapatite discs. Twice daily 420 nm blue light exposure (72 J/cm^2) for 5 days was applied which led to a significant decrease in the presence of extracellular polysaccharides and this was a greater effect than bacteria treated with either sodium chloride or chlorhexidine alone **[45]**. Equally, a 5 minutes irradiation from a 405 nm quantitative light-induced fluorescence caries detection system (xenon arc lamp with a blue light filter) indicated

a capacity to lower metabolic activity of *S. mutans* with / without the presence of sucrose **[47]**. Using the same wavelength, Al Mamoori *et al.* utilized a diode pumped solid state laser to examine its effect on *S. mutans*. They studied the exposure at different times from 2.5 - 40 minutes (5.3 – 84.9 J/cm^2). Results indicated that 22 minutes was sufficient to kill bacteria at 405 nm, also, increasing exposure times lead to energy densities able to significantly damage the bacterial cell and diminish its survival rate **[134]**.

As highlighted in PDT studies, there were issues in reporting irradiation parameters in direct light investigations. In De Sousa *et al.*'s study, the irradiance of the device was reported as 95.5 mW/cm^2 as well as an energy density of 72 J/cm^2. Although they mentioned the output irradiance, they did not state whether characterisation of the light source was done at the irradiation distance outlined - 1 cm **[45].** Gomez *et al.* investigated the effect of a 405 nm light on *S. mutans* grown on top of 2 mm human dentin specimens. Nonetheless, the only parameters reported were light irradiance of the device on a tooth surface (as reported by the manufacturer) – 13 mW/cm^2 as well as the irradiation distance – 2 cm at the underside of the well which contained the infected dentine sample **[53]**. Other studies did not report any parameters except the power output and irradiation time **[47]**.

1.4.2.3 Aminolevulinic acid, heme and flavins in *S. mutans*

Even though the most accepted theory for the mechanism underpinning the direct antimicrobial action of blue light is via its absorption by porphyrins present in bacteria, blue light has also shown antimicrobial effects towards species where no heme-proteins or cytochromes (heme-containing redox proteins) have been identified such as *S. mutans*. Notably this bacterial species relies mainly on flavin adenine dinucleotide (FAD)-enzymes for oxygen metabolism. Endogenous porphyrins have been found in a range of anaerobic as well as facultative anaerobic bacterial species **[135-139].** Interestingly, other bacterial species including *S. mutans*, which do not synthesise or require heme for growth, **[140]** also have shown susceptibility towards blue light **[45-47],[134].**

The iron-bound heme synthetic cascade begins with ALA as a precursor molecule **[34]**. Notably, ALA stimulates oxidative phosphorylation by enhancing COX and inhibiting glycolysis in eukaryotic cells **[141],[142].** The supplementation of bacteria capable of synthesizing heme with ALA enhances their porphyrin production and examples include *E. coli*, *P. aeruginosa* and *S. aureus*. Increased levels of porphyrins have subsequently been shown to increase the bacteria's susceptibility to light exposure in both the blue (407–420 nm) and the red (635 nm) light spectrum **[142-146].** Interestingly, ALA supplementation has also been shown capable of enhancing the inhibitory effect of both blue (440 nm) and red light (635 nm) in *S. mutans* **[147],[148]** even though this bacteria is incapable of synthesizing heme**.** Similarly, *E. faecalis* - another lactic acid-producing bacteria - did not show any porphyrin synthesis following ALA treatment **[143]**; yet, also exhibited photo-inhibitory effects following ALA

supplementation and red light (633 nm) irradiation **[149]**. It has been shown that higher levels of ALA can induce oxidative damage without light irradiation **[144],[146].** ALA caused and increase in *E. coli* cytochrome levels, elevating its redox state **[150].** Unexpectedly, ALA at high concentrations can also inhibit *S. mutans* unaccompanied by light exposure **[147],[148].**

SOD, peroxidase and catalase are enzymes which bacteria use to manage excessive intracellular oxidative stress levels **[140].** SOD converts superoxide anions to H_2O_2 and molecular oxygen, while catalase is the enzyme responsible for degrading H_2O_2 to water and oxygen **[151]**. *S. mutans* has an iron/manganese-bound SOD; however, it lacks heme-bound catalase and cannot synthesise cytochromes for full aerobic respiration and energy metabolism **[152-154].** Even *though S. mutans* does not perform oxidative phosphorylation **[155]**, it utilises an incomplete tricarboxylic acid (TCA) cycle **[156],[157]** and depends mainly on glycolysis for ATP generation **[158].** Conversely, it has been also reported that *S. mutans* can undertake oxygen metabolism**.** Flavins which are essential for growth and energy metabolism have been reported to mediate several redox functions in the process **[159].** *S. mutans* adapts to oxidative environments using FAD- bound enzymes such as NADH oxidases (Nox-1 and Nox-2) as well as alkyl hydroperoxide reductase C (AhpC) **[154],[160].** Nox-1 and Nox-2 enable lactate dehydrogenase to oxidize NADPH by reducing molecular oxygen. However, Nox-1 generates H_2O_2, while Nox-2 generates water and plays a greater role in the regeneration of NAD for the steady operation of glycolysis. H_2O_2 generated by both SOD and Nox-1 is eliminated by AhpC **[158]**; therefore, Nox-1 can operate as a NADH peroxidase only combined with AhpC **[160].** Notably, the Nox system operates

at the converging point of several pathways involved in oxidative stress responses and energy metabolism. It controls and is itself affected by these pathways to maintain *S. mutans* survival **[161]**. For example, Nox-2 deficient *S. mutans* cannot undertake the lactate dehydrogenase pathway due to their inability to oxidise the NADH generated **[154].** *S. mutans* also has an ability to resist oxidative stress by means of a dipeptide repeat protein (Dpr); albeit, not through a direct interaction with ROS. Dpr sequestrates iron, which prevents further hydroxyl radical formation through the Fenton reaction. Dpr deficient bacteria restored their survival rates only by supplementing the cultures with deferoxamine or catalase **[140],[162]**.

Due to their unique potential adapting to various environmental changes, it is proposed that generally all lactic acid-producing bacteria ancestors had the cytochrome gene - cyd; however, multiple gene loss has occurred over time. Currently there are species that show preference towards aerobic metabolism under appropriate conditions. Exogenous heme is shown to promote cytochrome formation in *L. lactis*, as well as catalase and cytochrome activity in *E. faecalis*. The cytochrome bd gene - cydABCD - within *L. lactis* improves cellular survival and oxidative stress resistance by inducing a proton motive force. Conversely however, the cytochrome bd genes have not been identified in other lactic acid-producing bacteria including *S. mutans* and *S. sanguinis* **[151],[163],[164].** Notably, exogenous heme was consumed only to synthesise cytochromes and not to alter the mode of respiration **[165].**

Confirming the enigmatic nature of heme acquisition and synthesis in prokaryotes, it was also suggested that that all Gram-positive bacteria use non-canonical pathways for protoheme synthesis. Gram-positive bacteria rely on alternate routes through the last

three enzymatic steps, compared with Gram-negative bacteria and eukaryotic cells **[166],[167].** Genes involved in heme bio-synthesis have been also identified in species not requiring heme for growth. *E. faecalis* contains the gene HemH (ferrochelatase) whose only function is to insert ferrous iron into either protoporphyrin IX or coproporphyrin III **[151].** Interestingly, heme and heme-protein/cytochrome synthesis are totally separate, meaning that neither heme abundance nor deficiency affects heme-protein levels. **[168].** Furthermore, stimulating intrinsic cytochromes formation through supplementing cultures with exogeneous ALA is significantly more effective than exogenous heme supplementation **[169].** Notably, it has been recently reported that *S. mutans* contains an extracellular electron transport system, which likely contains both flavins and cytochromes for full operation – flavo-cytochromes or flavo-porphyrins **[170-172].** Overall, it is possible that *S. mutans* might possesses the potential of utilising ALA to generate heme-proteins and cytochromes; however, the underlying pathways are not elucidated yet. Nonetheless, the presence of FAD-enzymes means that this species can endure oxidative conditions.

1.5 Photobiomodulation

1.5.1 Mechanism

1.5.1.1 Photobiomodulation signal transduction in the red / near infra-red spectrum

After absorbing photons, an electronically excited molecule exerts biologic effects by modulating intracellular metabolic pathways. Depending on the delivered dose, light absorption causes enhancement in ATP and cyclic adenosine monophosphate (cAMP) levels during biostimulation or destruction of cytochromes in the case of inhibitory effects. In either process these changes have been proposed to take place inside the mitochondria of eukaryotic cells **[173].** The primary photoreceptor or chromophore reportedly absorbing photons of light is COX. COX is a terminal enzyme in the respiratory chain, playing a major regulatory role in the process of oxidative phosphorylation. It is constituted of two heme, two copper, one magnesium and one zinc site. COX functions to transfer electrons from cytochrome C to molecular oxygen, which leads to the oxidation of ferrocytochrome C and the reduction of a di-oxygen molecule, inducing proton pumps from the mitochondria to the cytosol. Eventually, energy produced from this redox process leads to the production of ATP **[174],[175]**.

Karu *et al.* established the first direct link between light exposure in the UV-NIR spectrum (300-900 nm) and stimulation of both DNA and RNA synthesis in HeLa cells. DNA synthesis stimulation peaks were recorded at wavelengths of 400, 630, 680 and 760 nm, while those of RNA synthesis were detected at 400, 615, 680, 780 and 820

nm. Stimulation peaks were always lower in the UV-blue region of the spectrum for DNA synthesis. These data confirmed that light was not absorbed directly by the nucleic acid but that light regulated nucleic acid synthesis indirectly **[176].** To elucidate the photoabsorber, a narrower spectrum (580-860 nm) light source was utilized. Four peaks for DNA and RNA synthesis were identified, two within the red spectrum (613-623 nm and 667-683 nm) and two in the IR spectrum (750-772 nm and 812-846 nm). Results supported the hypothesis that COX was the main endogenous chromophore, as the 613 - 623 nm absorbance wavelength was within the same absorbance maxima for reduced COX, while the 667- 683 nm wavelength also conformed to one of the COX intermediates - compound A (fluoromethyl-2,2-difluoro-1-trifluoromethyl vinyl ether). Moreover, peaks recorded at 750 -772 nm correlated with oxidized COX **[79].** Results showed that nitric oxide (NO) - a COX inhibitor - eliminated the bio-stimulatory effects of R-NIR light and this process was accompanied by significant changes in COX absorption **[177]**. NO is known to compete with oxygen for the binding at the COX copper (CuB) nuclear center. However, light reportedly dissociates the binding of NO from COX, which can then enhance cellular respiration / oxygenation through reversing the hypoxic conditions in stressed cells. In turn, this increases electron transfer and ATP production, subsequently inducing transcription factors which can enhance cellular migratory, proliferative and differentiation responses **[177-179]**. Wong-Riley *et al.* investigated the effects of five different irradiation wavelengths (670, 728, 730, 830 and 880 nm) after pre-treating neuronal cells with potassium cyanide, an irreversible inhibitor of COX that bind to the same CuB nuclear site. Delivered light demonstrated an ability to restore COX and ATP levels. The most efficient stimulatory

wavelengths (630 and 830 nm) correlated with the absorbance spectrum of oxidised COX. Nonetheless, the fact that the neurotoxin could have been bound to other proteins such as catalase, NO synthase, cytochrome b and cytochrome C did not rule them out as prospective chromophores **[180].** An LED (670 nm) exposure fully restored COX levels after administrating tetrodotoxin, a neurotoxin that decreases ATP demand and supresses COX activity **[181].**

It has also been proposed that ROS resulting from redox changes in the electron transport chain might - in part - be initiating the cellular modulatory response **[182]** [see **Figure 6**]. PBM takes place due to the increase in ATP levels accompanied by a simultaneous production of relatively low amounts of ROS **[175].** Interestingly, the COX theory has been challenged recently and the interfacial water layers bound to the mitochondria have been advocated to be the main NIR light absorbers. Changes in cytosol volume promotes accelerated proliferation, while reduction in water viscosity causes ATP up-regulation **[183].**

1.5.1.2 Blue light signal transduction

Early reports have indicated that porphyrins absorb blue light, triggering the release of singlet oxygen and increasing intracellular calcium levels, processes which enhance mitosis. Nevertheless, at higher irradiation doses, inhibitory effects could occur due to the extensive reactivity of the singlet oxygen **[179], [184].** Moreover, flavin-bound NADPH dehydrogenase **[174]** and NAPDH oxidase have been proposed as blue light chromophores. Hydroxyl radicals have been shown to be induced in sperm cells after

receiving irradiation from a broadband visible light source (400-800 nm). Hydroxyl radicals were produced only in the 400-500 nm spectral range. The free radical electron paramagnetic resonance (EPR) signal was strongest in the cytosolic fraction; flavin in similar intracellular concentrations produced a matching signal when irradiated. Moreover, reduced cytochrome C fluorescence was also reported in the absorption spectrum of the cytosolic fraction which was attributed to its weak bond to the mitochondrial membrane. However, cytochrome C did not generate free radicals in either forms, oxidised or reduced **[80]**. Nonetheless, enhanced mitochondrial fluorescence after irradiation suggested that light also increased the levels of ROS inside mitochondria. The addition of an extracellular scavenger (SOD) led to a reduction in the hydroxyl radical EPR signal, which supported the hypothesis that ROS is also produced at the cell membrane level due to the sensitization of NADPH oxidase. Notably, the levels of hydroxyl radicals were directly proportional to both the cell density and irradiation dose **[185].**

Intracellular ROS generated were mainly superoxide anions, H_2O_2 and hydroxyl radicals **[186],[187]**; however, these molecules were not necessarily produced in the same manner or sequence. Similar to prokaryotic cells, ROS formation can occur due to a type I or type II reaction. In type I, the excited sensitizer transfers electrons to oxygen generating a superoxide anion and H_2O_2, which is then transformed to hydroxyl radicals through the Haber Weiss / Fenton reactions. The Haber Weiss reaction is catalysed by iron ions and involves two main sequential reactions. The first reaction takes place through the interaction of ferric iron with superoxide anion generating ferrous iron and oxygen. The second reaction is the Fenton reaction which involves the

interaction of ferrous iron and H_2O_2 to produce ferric iron and hydroxyl radicals. Type II reaction involves the production of singlet oxygen after the energy released from the photosensitizer is absorbed by a triplet oxygen. Nevertheless, singlet oxygen can also be produced through a type I reaction through the direct interaction between H_2O_2 and superoxide anion. It has been hypothesised that a type I reaction conforms to the ascending part of the Arndt Schultz curve, when light irradiation up to a certain dose generates non-cytotoxic levels of ROS stimulating cellular processes [see **Figure 2**]. Longer irradiation times or increased light dosage correlates with the descending part of the curve, when activation of the cellular scavenging system takes place negatively affecting the redox balance of the cell. This takes place when H_2O_2 reacts with two hydrogen ions and two electrons to produce two molecules of water. A concomitant elevation in intracellular calcium levels accompanied the excessive elevation in ROS levels. Thus, it was proposed that a transient increase in calcium, caused by H_2O_2, might be associated with the bio-stimulatory effects. Notably, sharp increases in calcium levels causes inhibitory effects, in line with the reduction of H_2O_2 to water **[81]** [see **Figure 6**].

Two FAD containing cryptochromes (CRY1 and CRY2), circadian rhythm proteins, have been also proposed as prospective blue light absorbers in humans **[188]**. CRY1 share common structure with photolyase, although it does not exhibit photolyase activity. Circadian rhythms control a range of periodic biochemical mechanisms which are necessary for regulating cell and tissue haemostatic functions **[189],[190]** [see **Figure 6**]. CRY1 and CRY2 acts as a negative feedback regulator of the circadian clock. Positive regulators include period genes (PER) as well as brain and muscle aryl hydrocarbon

receptor nuclear translocator-like protein-1 **[191]**. Lack of CRY1 and CRY2 has been shown to increased bone formation in *in vivo* models **[192]** [see **Figure 6**].

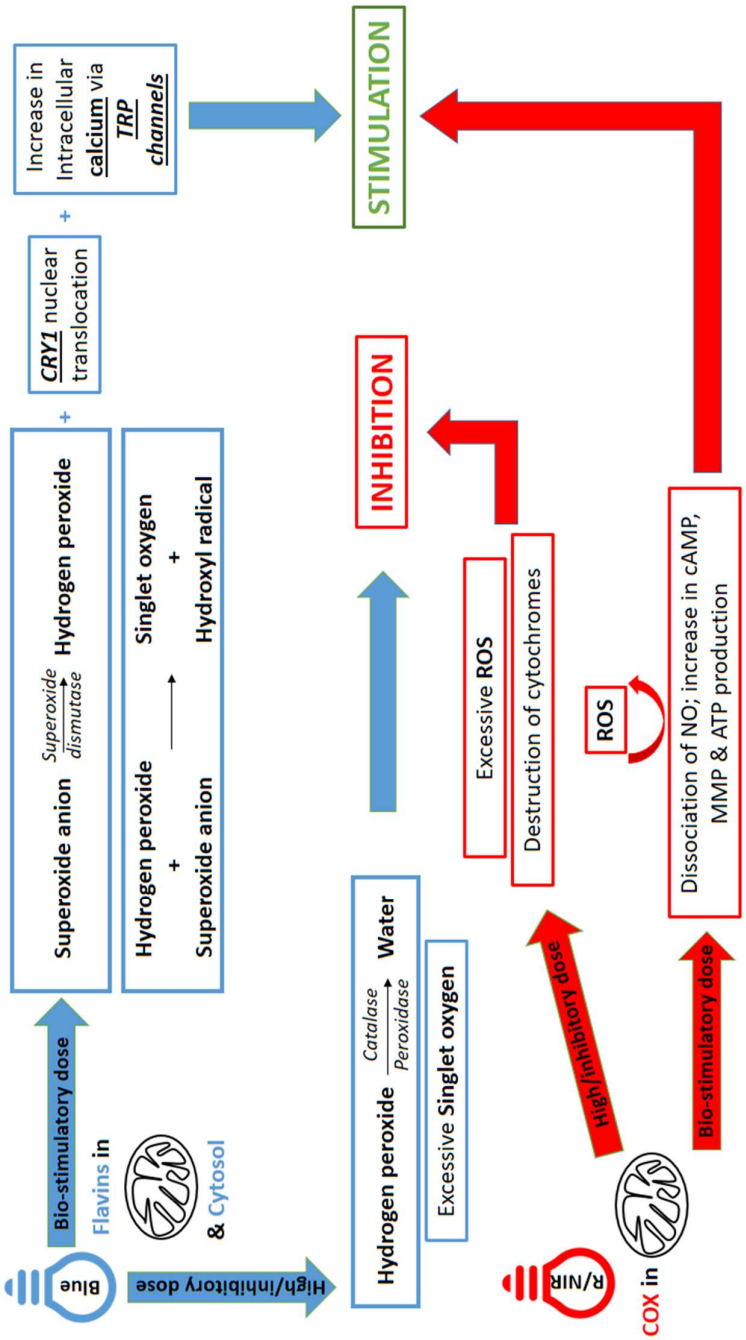

Figure 6. Schematic diagram showing potential blue and red / near infra-red (R/NIR) light bio-modulatory mechanisms. At the stimulatory dose, blue light (absorbed by flavins in both mitochondria and cytosol) induces the production of stimulatory levels of hydrogen peroxide, causing an elevation in intracellular calcium levels through transient receptor potential (TRP) channels. These effects are accompanied by decreased crytochrome-1 (CRY1) activity. R/NIR light dissociates nitric oxide (NO) bound to cytochrome c oxidase (COX) inside the mitochondria, enhancing cyclic adenosine monophosphate (cAMP), mitochondrial membrane potential (MMP), and adenosine tri-phosphate (ATP) production. At higher doses, blue light can cause inhibition due to the up-regulation of the scavenging system (catalase/peroxidase). Inhibitory effects of a higher dose of R/NIR light can occur due to the destruction of cytochromes. Nevertheless, both spectral ranges can cause inhibition due to the excessive production of ROS. Source: Mohamad SA, Milward MR, Hadis MA, Kuehne SA, Cooper PR. Photobiomodulation of mineralisation in mesenchymal stem cells. Photochem Photobiol Sci 2021; 20:699-714. https://doi.org/10.1007/s43630-021-00047-5

1.5.2 Reactive oxygen species regulate mesenchymal stem cell haemostasis and mineralisation processes

Due to the pivotal role of ROS in blue light PBM as well as determining MSCs fate, it is necessary to understand how ROS regulates cellular functions and pathways. ROS are generated within mitochondria during electron transport via a variety of enzymes including NO synthase, lipoxygenase, mono amide oxidase, heme oxygenase, cytochrome P450, cyclooxygenase, NADPH oxidase and myeloperoxidase **[193-195].** Other locations besides mitochondria for ROS generation are endoplasmic reticulum (NAPDH oxidase) **[196],[197]**, plasma membrane (NADPH oxidase / lipooxygenase), the cytosol (NO synthase / lipooxygenase), **[198-200]** and peroxisomes **[201].** ROS can be also produced by membrane bound NADPH oxidase which yields superoxide anions **[202]**. During oxidative phosphorylation and proton pumping, 0.1-0.2% of consumed oxygen is transformed to ROS **[203]**. Superoxide anion is the first ROS produced by mitochondria which is converted to a more stable H_2O_2 by SOD. Subsequently, H_2O_2 can be eliminated by catalases / peroxidases and converted to water and oxygen by glutathione peroxidase (GPX), or it can act as a signalling molecule **[204-206].** ROS can modulate cellular activity by interacting directly with key receptors such as p21ras, a proto-onco gene that exhibits guanosine triphosphate-binding properties. Indirectly, ROS can interact with redox-triggered proteins, a process mediated through protein kinases and phosphatases **[207],[208].**

The balance between self-renewal and regeneration in MSCs is partially controlled by ROS. Redox mechanisms are proposed to be involved in the communication between the mitochondria and nucleus. Mitochondria are however the major source of ROS,

with H_2O_2 acting as the main ROS involved in intracellular signalling. GPX, glutathione reductase, SOD and catalases are enzymes which control ROS levels in MSCs haemostatic states. However, if ROS reach certain threshold levels when cellular protective mechanisms are unable to regulate their action, cellular injury can occur due to oxidation of proteins, lipids and nucleotides. Notably, cells can lower their ROS levels by diverting metabolic pathways away from oxidative phosphorylation. Consequently, ROS act as transitional molecules regulating cell fate and their levels are controlled by multiple and complex mitochondrial mechanisms **[209]**.

MSCs preferentially utilise glycolysis rather than oxidative phosphorylation in their undifferentiated state **[210]**. Non-differentiated MSCs contain relatively low levels of ROS and express high levels of antioxidant enzymes; however, the opposite state exists for MSCs following differentiation **[211],[212]**. During osteogenic differentiation, MSCs switch to aerobic oxidative phosphorylation. Indeed, oligomycin - which facilitates glycolysis through inhibiting ATPase - has been shown to inhibit osteogenesis **[82]**. A limited up-regulation in ROS levels is also essential for initiating MSCs proliferation **[213]**. Intracellular ROS levels play a key role in maintaining the pluripotency of MSCs **[214]** as well as during differentiation. ROS are generated during differentiation from NADPH oxidase, complex I (NADH coenzyme Q oxidoreductase) and complex III (ubiquinol cytochrome C oxidoreductase) **[215].** However, excessive levels of ROS generally inhibit both proliferation and osteogenic differentiation **[216]**.

In support of ROS ability to promote the mineralisation processes several studies have reported on the effects of exogenous sources of ROS (H_2O_2 and NO) on the cellular differentiation capacity. At relatively low concentrations (0.1-0.2 mM), H_2O_2 marginally

increased cell proliferation. However, these same exposure conditions significantly increased the odontoblastic/osteoblatic differentiation marker expression including osteopontin (OPN) and osteocalcin (OCN) in DPCs **[217]**, as well as runt-related transcription factor-2 (RUNX2) and bone morphogenic protein-2 (BMP2) in adipose derived MSCs (ADMSCs) **[218]**. Conversely, at similar exposure concentrations, alkaline phosphatase (ALP) levels decreased in human bone marrow MSCs (BMMSCs). At higher concentrations (up to 0.5 mM), H_2O_2 severely affected proliferation and cell viability **[82]**. Another source of ROS, NO (0.01 mM) improved the expression of mineralisation markers at early (ALP, collagen-1 (COL1), RUNX2, dentine matrix protein-1 (DMP1)) as well as late stages (dentine sialophosphoprotein (DSPP), bone gamma-carboxyglutamic acid-containing protein) of differentiation in DPCs. A significant increase in mineral deposition was also detected; nonetheless, all these effects were reversed by 2-(4-Carboxyphenyl)-4,4,5,5-tetramethylimidazoline-1-oxyl-3-oxide potassium salt (Carboxy-PTIO) - a NO scavenger **[219]**.

Nuclear factor erythroid 2-related factor 2 (NRF2) is a key transcription factor that responds to oxidative stress and promotes antioxidant mechanisms necessary for cell survival. Up-regulation of the NRF2 pathway was observed when H_2O_2 was administrated at concentrations as low as 0.1 mM, along with concomitant up-regulation of the osteogenic markers – ALP and RUNX2. Confirming how a fine-tune in ROS levels can have the total opposite outcomes, NRF2 was also up-regulated when cells were treated with a higher concentration of H_2O_2 (0.4 mM). However, this accompanied by the down-regulation of these same osteogenic markers **[218],[220]**.

NREF2 knockout increased bone formation, suggesting a negative interplay between NRF2 and cellular autophagy is regulating the differentiation process **[218]**.

1.5.3 Photobiomodulation of mesenchymal stem cells in-vitro

1.5.3.1 Red Light

Red light (620-660 nm) significantly increased the proliferation of BMMSCs **[65-67]** and periodontal ligament cells **[67]** when irradiated at doses of 1, 2 and 4 J/cm^2. Notably, doses as low as 2 and 4 J/cm^2 were capable of promoting osteogenic differentiation. This was evident by a notable up-regulation in levels of ALP, OCN, bone gamma-carboxyglutamate protein **[65-68]**, RUNX2 **[66-68]**, BMP2 **[67],[68]**, COL1 **[66]** and insulin-like growth factor-1 **[67]**. Importantly, data also demonstrated significant increases in mineral deposits **[66-68]**. In one particular study, Yang *et al.* irradiated umbilical cord derived MSCs using a 620 nm LED at a dose of 2 J/cm^2 using a pulsed mode (frequency of 50 Hz). Significantly higher proliferation rates were observed compared with the non-irradiated control. Additionally, the irradiated cells exhibited higher levels of ALP, OPN and calcified nodule formation **[69]**.

These positive bio-stimulatory effects occurred when cells were irradiated either once daily **[67],[68]** or every other day **[65],[66]**. Interestingly, a higher irradiance for any assigned dose resulted in enhanced outcomes compared with a lower irradiance. Moreover, multiple exposures initiated greater outcomes in contrast with one single exposure **[65].** It is notable that PBM effects were inhibited by culture supplementation with SQ22536, an adenylyl cyclase inhibitor, supporting the role of cAMP and respiratory chain signalling in the photo-transduction process **[68].**

1.5.3.2 Near infra-red irradiation

NIR diode irradiation (810-850 nm) stimulated the proliferation **[70]** and osteo-/odonto-blastic potential of BMMSCs **[70],[221]**, ADMSCs **[71]**, DPCs **[64]** and stem cells from human exfoliated deciduous teeth **[222]** at doses ranging from 0.5 to 4 J/cm2. Irradiated cell cultures exhibited higher levels of mineralisation markers such as ALP **[64], [222],[70],[71]** COL-I, DMP1 and DSPP **[222].** Even at a doses as high as 64 J/cm^2, a diode laser (808 nm) significantly increased mineral deposition in BMMSCs via the up-regulation of ALP, RUNX2, TGF-β1 and Osterix **[221**].

Both, an *Erbium*-doped Yttrium Aluminium Garnet *laser* (Er:YAG) (2,940 nm) and a diode laser (820 nm) stimulated cellular proliferation and mineralisation in DPCs. There were also differences in differentiation rates and gene expression levels of matrix metalloproteinase-2 (MMP-2), MMP-20 and DSPP between irradiated and non-irradiated cultures **[72]**. Exposure of BMMSC cultures to a Neodymium-doped Yttrium Aluminium Garnet (ND:YAG) laser (1064 nm) also enhanced proliferation as well as calcified nodule deposition. The authors concluded these cellular events were mediated by increased expression of ALP, RUNX2 and OCN **[73]**.

1.5.3.3 Blue light

Since blue light PBM has only been recently investigated, there are significant diversity in the irradiation parameters applied and the outcomes. A 470 nm blue LED inhibited the proliferation of BMMSCs at a range of doses from 1 to 72 J/cm^2, and also inhibited the mineralisation processes at 12 J/cm^2. Notably, cells were irradiated daily **[223]**. Similarly, when gingival MSCs were irradiated with 420–480 nm LED (1, 2, 4 or 6 J/cm^2) every other day, results indicated a significant reduction in proliferation. However, elevation in both ALP levels and calcified nodule formation was observed. The same light source (1, 2, 3 and 4 J/cm^2) enhanced the mineralisation of stem cells from apical papilla through the up-regulation of DMP1, OCN and DSPP **[77]**,**[78]**. At day 28, an increase in calcified nodules formation was noted in a dose-dependent manner, suggesting that lower doses stimulated early differentiation, while higher doses stimulatory effects are observed at a latent stage **[77]**. Only five exposures to a 420 nm LED (3 J/cm^2) also increased the expression of the mineralisation markers OCN and RUNX2 in ADMSCs at day 21 **[76]**.

Interestingly, a single exposure to a continuous wave laser (405 nm) at much higher doses of 9, 18, 27, 36 and 54 J/cm^2, enhanced BMMSCs mineralisation in a dose-dependent manner. These effects were mediated through an increase in OCN and ALP proteins. The nuclear trans-location of CRY1 and PER2 was confirmed by immuno-staining. CRY1 down-regulation occurred in a dose-dependent relationship at doses above 18 J/cm^2 proposing that blue light could reset the circadian clock in MSCs. Notably, however, CRY1 expression was not affected by either 664 or 808 nm light irradiation **[74],[75].** The bio-stimulatory effects of blue light were reversed by

transient receptor potential channel antagonists, SKF96365 and capsazepine. This results suggests that blue light PBM is mediated by slight increase in ROS levels, accompanied by an increase in calcium levels which was transduced by light-gated ion channels **[76],[80],[81]**.

Interestingly, there has been variations among the irradiation parameters reported. Different studies reported fixed irradiance settings even though irradiation was carried out in different culture dishes. Different plate usage also results in different irradiance at target, different cell density and different light-cellular interaction due to the discrepancies between the size of the light source and surface area irradiated. All blue light studies applied a fixed distance to target; however, in Wang *et al.*'s study **[76]** they reported adjusting the irradiation distance with various plate arrangements to maintain the same spot size and irradiance. Other dissimilarities in experimental set-ups were also reported in efforts to maintain homogeneity of delivered light and decrease light bleed. In one study, plates were wrapped in aluminium foil except for an aperture to let light through **[76]**. While the aluminium foil can cause multiple light reflections and affect the final dose of light reaching the cells, others preferred using black-walled well plates **[74],[75]**. Another important observation is the fact that temperature measurements are never taken into consideration. *In-vivo* heat dissipation depends on the cell/tissue thermal relaxation time in addition to the irradiation time, irradiance, pulse duration and pulse frequency of the light source **[224]**. It is also worth mentioning that non-irradiated controls throughout all experimental designs were kept outside the incubator for the same amount of time it took their counterparts to be irradiated. This means that depending on the room

temperature, the irradiated cultures could encounter a rise in temperature below their heat tolerance, which is not the case in a clinical setting. Although PBM is mostly accepted as a non-thermal response **[84]**; however, hyperthermia - on its own - can lead to an increase in mitochondrial ROS production **[225]**.

1.6 Aims and objectives

Based on the background information presented above, it is reasonable to hypothesize that both photodisinfection and PBM can be achieved using the same light source/wavelength. As dentine is the main tissue through which light will reach cariogenic bacteria and/or DPCs, the differences in absorption / transmission patterns at a variety of anatomical tooth locations will influence how light could be delivered clinically to optimise both antimicrobial and PBM activities.

Therefore, this study aims at exploring the use of a single wavelength of blue light for photodisinfection and PBM. However, for clinical applications, the optimisation of conditions for administrating blue light requires elucidation of the interaction of light individually with dentine, *S. mutans* and DPCs. Accordingly, this study aims specifically to:

1) Characterize the transmission of blue light through dentine at key anatomical sites to allow a better understanding of the dentinal tubules' optical characteristics.

2) Determine blue light irradiation parameters that are required to directly inhibit *S. mutans*. Furthermore, asses how different redox states affect the susceptibility of bacteria to blue light.

3) Determine blue light irradiation parameters that are bio-stimulatory for the mineralisation potential of DPCs.

Chapter 2: Materials and Methods

2.1 405 nm blue light transmission through dentine

2.1.1 Dentine specimens

Seventy-five non-carious maxillary and mandibular human molars were used in this study (Ethical approval Birmingham community healthcare (BCHC) Ref.: BCHCDent398.ToothBank / Research ethics committee Ref.: 14/EM/1128 / Integrated research application system Ref.: 161303). Teeth were stored at -80°C prior to processing and use.

2.1.2 Dentine preparation for light transmission studies

Forty-five teeth were randomly selected and fixed in acrylic blocks using impression compound sticks (Kerr®, USA) to facilitate the sectioning process. A water-cooled low speed saw (Isomet™, Buehler®, USA) was used for sectioning. A primary cut was made to remove the surface enamel. Subsequently, dentine discs (n=45) were sliced and distributed into three main groups, 1) cross sectional occlusal, 2) cross sectional oblique and 3) longitudinal buccal sections [see **Figure 7**]. Each group contained three sub-groups with different thicknesses, 1 mm, 2 mm and 3 mm (n=5 each). Specimens were sectioned 0.5 mm thicker than needed to allow for smoothing of the surface by using a fine grade carborundum stone (Carborundum®, France), after which discs were washed under running tap water for 10 seconds and stored in distilled water (E-pod®,

Millitrack®, Germany) at room temperature until light transmission measurements were performed. Compressed air was used to surface dry specimens before testing. A spectrometer, USB4000-VIS-NIR (Ocean Optics, USA), connected with 200 µm optical fibre/detector and a glass cosine corrector (5 mm) were calibrated using a deuterium/halogen light source DH2000 (Ocean Optics, USA). A 405 nm light source (Aura light engine®, lumencor®, USA) with a wide range of power outputs was used. 405 nm light transmission for each sample was recorded with the dentine disc aligned vertically between the light source (7 mm) above and the detector below [see **Figure 7**]. Specimens were oriented with the pulpal side downward. Increasing levels of irradiation were applied to determine optimal parameters that would allow dentine penetration and antimicrobial decontamination in a clinically appropriate time-frame. An irradiance reading (mW/cm^2) was obtained at 10 graduated power outputs (10 - 100 %) of the light source (470, 968, 1473, 1923, 2360, 2774, 3152, 3503, 3768 and 4054 mW/cm^2). Each reading was recorded three times and an average was calculated. The percentage of light transmitted was calculated with reference to initial light source characterization measuring its absolute irradiance at distances 1, 2, 3 mm between the light source and the sensor through atmospheric air. This percentage was calculated based on an average of 10 measurements at power settings 10-100% for each sample, after which, a mean from 5 measurements (per group) was calculated.

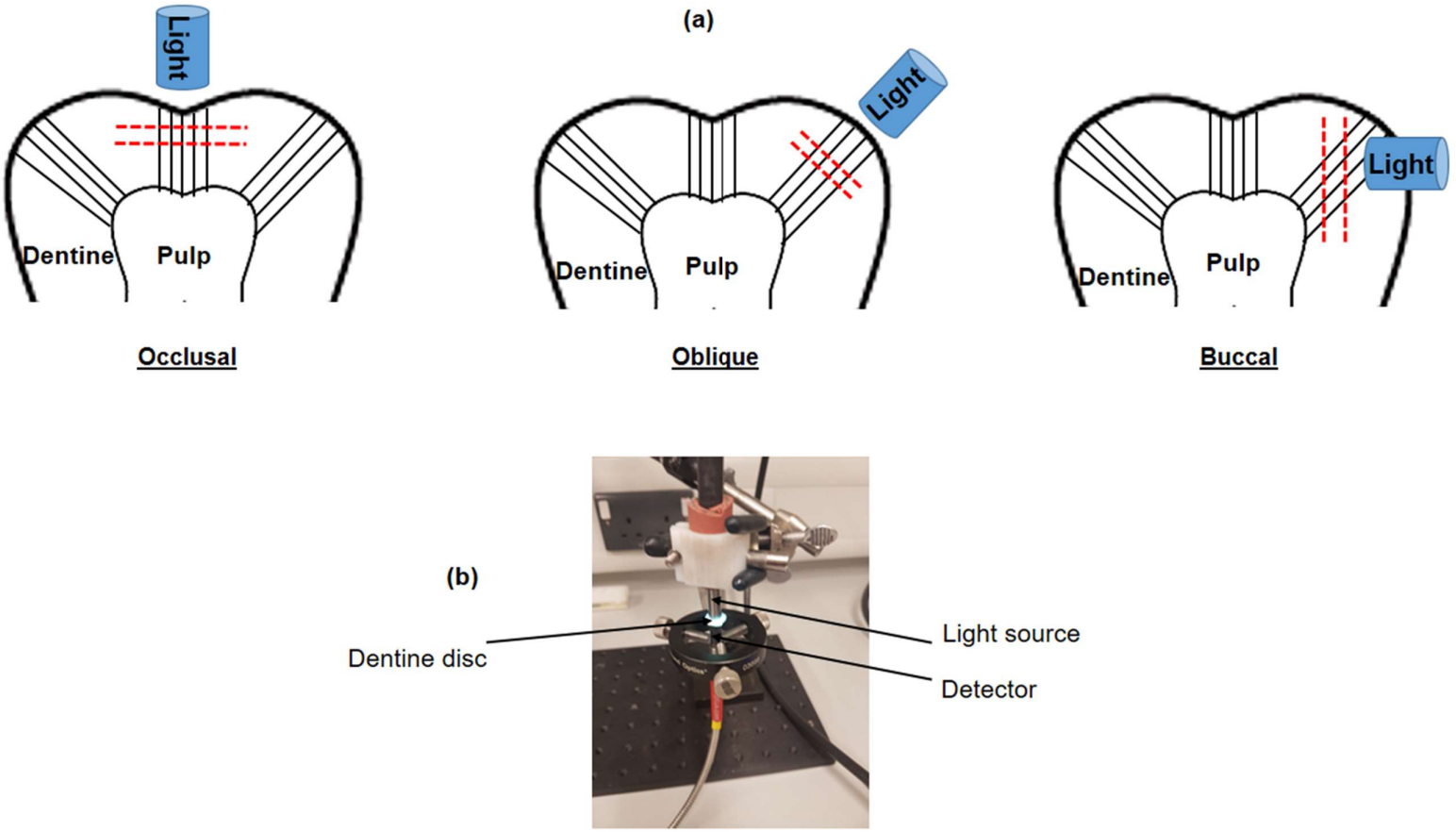

Figure 7: (a) Schematic diagram showing the direction of incident 405 nm light irradiation in relation to the orientation of dentinal tubules in occlusal, oblique, and buccal dentine sections. Black lines represent dentinal tubules, while red lines represent how each dentine disc was sectioned. **(b)** Image of the experimental set-up showing a dentine disc sandwiched between the light source (AURA light engine®, lumencor®, USA) above and the detector below. The dentine specimen was oriented with its occlusal side upward and pulpal side downward.

2.1.3 Characterisation of dentinal tubule density

Thirty non-carious molar teeth were randomly selected, and dentine discs (n=30) were sectioned and assigned to six groups (2 mm thick) (n=5 per group). To assess the dentinal tubule density at different depths, three groups (occlusal, oblique and buccal) were obtained with two sub-groups within each group, namely outer and inner. Outer sections were located adjacent to the DEJ, while inner sections were located adjacent to the pulp chamber.

All sectioning procedures were performed using the protocol described above [see **section 2.1.2**]. To ensure complete smear layer removal in preparation for imaging, dentine discs were rinsed under running tap water, and treated in an ultrasonic bath (In-Ceram Vitasonic, VITA, Germany) for 10 minutes in a mixture of 5% sodium hypochlorite (Acros Organics, Fisher Scientific, UK) and 17% ethylene-diamine-tetraacetic acid (EDTA) (CanalPro EDTA 17%, COLTENE) **[226]**. This was followed by another 10 minute treatment in an ultrasonic bath containing distilled water. Specimens were dried in a 37°C oven (Hybaid Shake 'n' Stack, ThermoFisher Scientific, USA) for at least 72 hours before imaging.

After drying, specimens were gold sputter coated (Emitech K550X, Quorum Technologies, UK) under argon for 3 minutes at 20 mA at a distance of 45 mm to obtain a gold coating thickness of 21 nm. Specimens were subsequently loaded into a scanning electron microscope (SEM) (EVO MA10, Carl Zeiss, Germany) and micrographs were captured at 2000x magnification under high vacuum and electron high tension (EHT) voltage of 20 kV.

The dentinal tubules were quantified manually using the multipoint counter tool of ImageJ software (National Institutes of Health, USA). Subsequently, the number of tubules per unit area (mm^2) were calculated using the following formula: *'n X 10^6 / Z'*, where *'n'* is the actual tubules count per image and *'Z'* is the area of the image in μm^2 **[227]**. Area of the image was calculated using the square area selection tool, after setting the scale bar using the straight line tool.

2.2 Light irradiation characterisation for culture exposures

2.2.1 Light source calibration

2.2.1.1 Irradiation of bacterial lawns grown on agar

Initially, light characterisation was performed under two conditions, (a) with the light source in contact with the top surface of the culture plate lid and (b) in contact with the underside of the plate. Closed plate irradiation was preferred in order to maintain complete seal and isolation of the bacteria to avoid contamination. A Spectrometer, USB4000-VIS-NIR (Ocean Optics, USA), connected with 200 µm optical fibre/detector and a glass cosine corrector were calibrated using a deuterium/halogen light source DH2000 (Ocean Optics, USA).To determine the irradiance for top surface irradiation, a window was drilled in the underside of the plate, and the detector was levelled with the surface of the agar and orientated towards the lid of the agar plate [see **Figure 8(a)**]. For underside irradiation, the detector was in contact with the agar surface orientated towards the underside of the agar dish [see **Figure 8(b)**]**.** Using the 405 nm wavelength (Aura light engine®, lumencor®, USA), the irradiance readings (mW/cm^2) were obtained at 10 gradual power outputs. Each reading was recorded three times and an average was obtained. Data were then used to generate a standard / calibration curve, this curve was used to estimate irradiation dose under each condition '*Dose (J/cm^2) = Irradiance (W/cm^2) X Time (seconds)'.*

Irradiation from beneath the plates was preferred to minimize the Rayleigh scattering of blue light in air **[228]** and maximize its penetration within bacterial layers **[229]**.

Bottom irradiation was also preferred as there was less light irradiance recorded on the agar surface and therefore potentially less temperature elevation.

After conducting preliminary experiments using the light source in contact with the underside of the plate, and to better mimic the application of light in a clinical setting, irradiation was performed at a distance of 5 mm from the bottom surface of the culture plate. This set-up better represents the use of light in a cavity where direct application to the base or axial wall of the cavity would not be possible. The 405 nm light was characterised at this distance [see **Figure 8(c)**].

2.2.1.2 Irradiation of bacterial planktonic cultures, biofilms and dental pulp cells

A calibration curve, similar to the one described for agar plates [see **section 2.2.1.1**], was also generated with the light source in contact with the flat transparent well bottom of a black 96 well plate (4titude®, UK). The sensor was in contact with the base of the well (6 mm) [see **Figure 8(d)**]. As the diameter of the light source (7 mm) and the well were comparable, this experimental set-up ensured consistent saturation of the light beam within each black-walled well in the culture plate. No light leakage between wells was detected.

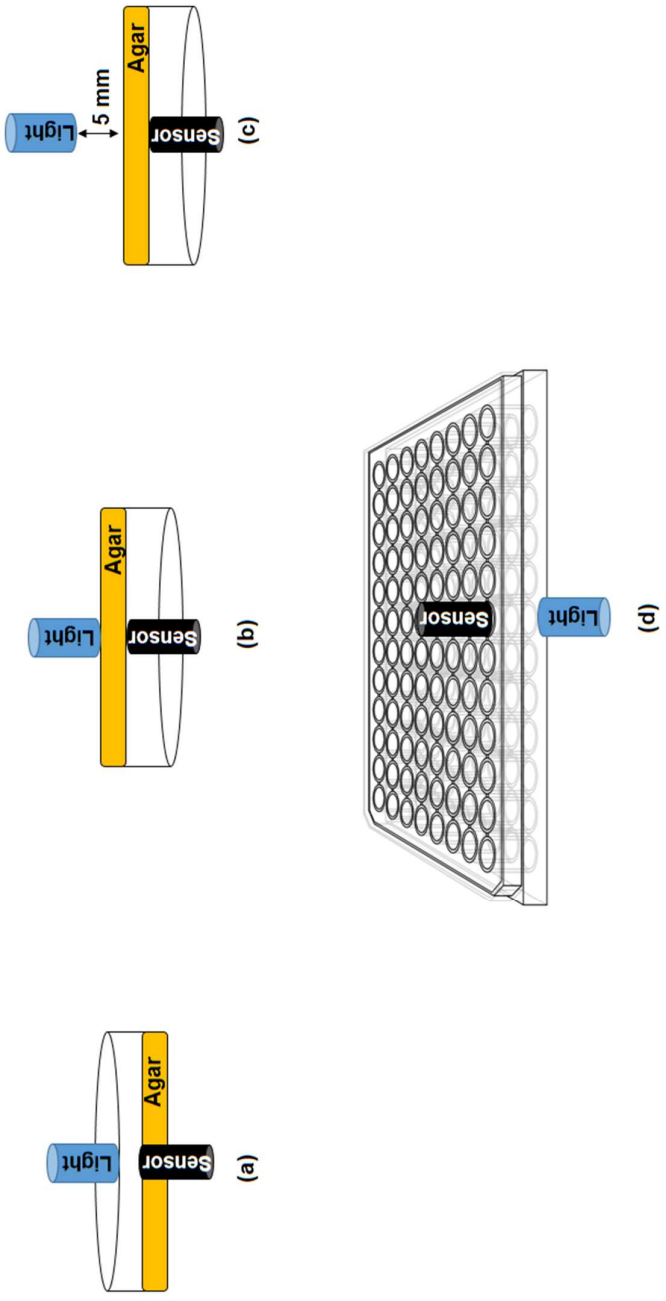

Figure 8: Schematic diagrams showing 405 nm light delivery and characterization for the different experimental set-ups. **(a)** Light irradiation from above the agar plate with the lid on, a window was drilled in the bottom of the plate, and the sensor was levelled with the surface of the agar. **(b)** Light irradiation from beneath the plate, and the sensor was placed in contact with the upper surface of the agar. **(c)** Light irradiation from below at a 5 mm distance. **(d)** Irradiation from the underside of the well in a 96-well plate, the sensor was located inside the well and was in contact with its base.

2.2.2 Light absorption and temperature change measurements in bacterial and cell culture media

2.2.2.1 Media absorption

Bacterial Agar cultures:

Measurements determined that the average distance between the bottom of the Petri dish and the surface of the agar was 6.5 mm – for 20 ml of poured agar after setting [see **section 2.3.1.1**]. Six separate plates were measured at 4 different point across each plate using a calliper. The USB 4000 spectrometer along with the 200 µm detector were fixed at 6.5 mm, while the 405 nm light delivery was characterized at a 5 mm irradiation distance. The absolute irradiance obtained was then used as references. The light characterisation data obtained previously - with the plate containing agar [see **section 2.2.1.1**] - were deducted from the references to calculate the amount of light absorbed by the agar. The percentage of light absorbed was based on an average of 6 measurements

Bacterial Broth and cell culture minimum essential medium: Applying the formula 'Absorbance (Optical Density) = - $\log_{10}$ Transmittance' **[230]**. Absorbance (405 nm) was read for 200 µl fresh brain heart infusion (BHI) broth (Sigma-Aldrich®, USA) [see **section 2.3.3.1**] and minimum essential medium (MEM) (Gibco, ThermoFisher Scientific, USA) [see **section 2.4.2**] in a black-walled 96 well plate using the microplate reader ELx800™ Microplate Reader (BioTek™, USA). Consequently, the transmission

percentage was calculated. The absorbance readings were repeated three times and in triplicate.

2.2.2.2 Temperature measurements

Agar cultures: To determine temperature changes of media following irradiation a K-type thermocouple attached to a TC-08 data logger (Pico Technology, UK) was used for temperature measurements. The edge of the thermocouple was attached to the top surface of the agar in the petri dish. All doses studied were at a 5 mm irradiation distance and maximum temperatures were recorded [see **section 2.3.2**].

Broth and minimum essential medium cultures: a window was drilled in the lid of a 96 well plate to permit the thermocouple to be included while irradiation of the 200 µl BHI broth/MEM from beneath was performed. For bacterial broth, the maximum temperatures reached for irradiated samples were recorded [see **section 2.3.3.1**]. As for cell culture MEM, the plates were taken out of the incubator and immediately started measuring temperature change (decrease) for control and irradiated samples [see **section 2.4.2**]. All doses were run as was performed for the irradiation studies and measurements were carried out at room temperature. Measurements were carried out three times.

2.3 Effects of blue light on bacterial growth and viability

2.3.1 Bacterial cultures and media preparation

2.3.1.1 Media preparation

BHI Agar was prepared by adding 26 g of BHI agar powder (Sigma-Aldrich®, USA) to 500 ml distilled water (E-POD®, Millitrack®, Germany), which was sterilised by autoclaving for 27 minutes at 121°C (Labo MLS-3781L, Sanyo, Japan). Twenty-ml agar was then was decanted into each petri dish using a serological pipette. For the broth media, it was prepared by dissolving 18.5 g of BHI broth (Sigma-Aldrich®, USA) in 500 ml of distilled water, which was subsequently autoclaved as described above. Media was stored at room temperature for a maximum duration of 1 month prior to use.

2.3.1.2 Bacterial cultivation

S. mutans (ATCC 3209) and *E. faecalis* (ATCC 29212) frozen cryobeads (-80°C) were retrieved from archive stocks and streaked onto BHI agar and incubated (37 °C) aerobically (5% CO_2) (Heracell™ 150i, ThermoFisher Scientific, USA) for 24 hours. Colony morphology of both species was subsequently verified. *S. mutans* showed relatively small, droplet-like, heaped, rough colonies. *E. faecalis* demonstrated relatively large, creamy white, well defined and smooth colonies. Subsequently, a single representative colony was inoculated into 10 ml of BHI broth using a sterile plastic inoculation loop, and incubated aerobically overnight (24 hours) in a shaking incubator (NB-205, N-Biotek, Korea) at 100 rpm. The resulting bacterial suspension was gram stained to confirm bacterial morphology and lack of contamination.

2.3.2 Bacterial lawns

Preliminary experiments were undertaken administrating six irradiation doses (84, 147, 200, 358, 443 and 590 J/cm^2) to *S. mutans* lawns- with the 405 nm light source (Aura light engine®, lumencor®, USA) in contact with the bottom surface of the petri dish. A non-irradiated plate (with *S. mutans* lawn) served as the negative control. Each separate seeded agar plate received a single light irradiation dose. The irradiation parameters used are shown in **Table 1**.

To mimic the application of using blue light clinically, a series of studies – using *S. mutans* and *E. faecalis* - with two modifications were undertaken. Initially, irradiation was performed at a distance of 5 mm from the underside surface of the culture plate. Secondly, each dose was delivered using two different protocols, either with i) increased time/decreased power (IT/DP) or ii) increased power/decreased time (IP/DT) [see **Table 2**]. This second modification was adapted to represent the clinical application and ensure minimal impact of any potential *in vivo* temperature rise. Experimental culture plates were exposed at six increasing doses including 110, 154, 273, 366, 456 and 573 J/cm^2.

Overnight bacterial broth cultures were diluted 10 % using fresh BHI in a 1 ml cuvette to record their optical density (OD) using a 7315 spectrophotometer (Jenway, UK) at wavelength of 600 nm. Afterwards, the overnight culture was diluted in fresh BHI broth to an OD of (0.1) ($\simeq 10^8$ Colony forming unit (CFU)/ml) using the following formula: '*C1 X V1=C2 X V2'*, where *C1* is the desired OD (0.1), *C2* is the obtained OD from the overnight culture, *V1* is the volume of the final diluted sample and *V2* is the transfer volume from the overnight culture. Using a sterile cotton swab (Sterilin™,

Thermofisher Scientific, USA) dipped once in the diluted culture, *S. mutans* and *E. faecalis* were separately lawned on BHI agar. Plates were then tightly sealed using Parafilm M™ (Bemis™, USA) to prevent contamination. After receiving the assigned light irradiation dose, plates were incubated at 37 °C for 24 hours.

On the following day, standardized images were obtained (SX620 HS, Canon, Japan) for each plate. Images were captured at a fixed distance between the camera and the base of the agar plate ($\simeq$ 41.5 cm) in a dark room with only bench light illumination. Zones of inhibition (ZOI) diameters were measured using ImageJ software (National Institutes of Health, USA), where the diameter of the plate was calibrated at 87 mm and measurements were taken using the straight line tool in the software. Each ZOI was measured three times at different orientations (horizontal, vertical and diagonal), and an average ZOI diameter was obtained. Experiments with the light source in contact with the underside of the agar plate were repeated three times, while experiments at 5 mm irradiation distance were repeated four times.

405 nm light irradiation settings applied on bacterial lawns

Irradiance (mW/cm^2)	Irradiation time	Dose (J/cm^2)
93	15 min	84
163	15 min	147
222	40 min	200
199	30 min	358
246	30 min	443
246	40 min	590

Table 1: Irradiation settings applied when irradiating at 405 nm *S. mutans* culture lawns. The light source was in contact with the bottom surface of the agar plate.

Irradiance (mW/cm^2)	Irradiation time	Dose (J/cm^2)
122	15 min	110
251	7 min + 13 sec	110
172	15 min	154
251	10 min + 12 sec	154
152	30 min	273
251	18 min + 6 sec	273
122	50 min	366
191	31 min + 54 sec	366
152	50 min	456
191	39 min + 42 sec	456
191	50 min	573
251	38 min	573

Table 2: Irradiation setting applied when irradiating (405 nm) *S. mutans* and *E. faecalis* lawns. Light source at 5 mm distance from the bottom of the agar plate.

2.3.3 Irradiation of planktonic cultures

2.3.3.1 Determining the effect of light irradiation on *S. mutans* planktonic growth

For initial bacterial growth determination, planktonic turbidity investigations were performed. *S. mutans* was grown, sub-cultured and diluted using the same methodology previously described [see s**ection 2.3.2**]. Subsequently, 200 µl of the diluted culture was allocated to wells of a black- walled 96 well plate (4titude®, UK). Two wells were used as controls and received no light irradiation. Culture wells received a range of light doses including 249, 340, 608, 831, 1014 and 1254 J/cm^2 [see **Table** 3]. Experimental design ensured that each plate was removed from the incubator and was at room temperature for less than 1 hour.

Following irradiation, plates were returned to the incubator at 37 °C for 24 hours. On the following day, the OD of all wells were read (600 nm) using an ELx800™ Microplate Reader (BioTek™, USA). The survival rate was calculated based on the equation: *'Treated well OD / Control well OD X 100'*. This experiment was repeated three times.

405 nm light irradiation settings applied on bacterial planktonic cultures

Irradiance (mW/cm^2)	Irradiation time	Dose (J/cm^2)
277	15 min	249
539	7 min + 40 sec	249
378	15 min	340
539	10 min + 30 Sec	340
338	30 min	608
539	18 min + 48 sec	608
281	50 min	831
418	33 min + 7 sec	831
338	50 min	1014
418	40 min + 25 sec	1014
418	50 min	1254
539	38 min + 46 sec	1254

Table 3: Irradiation settings applied when exposing planktonic cultures to 405 nm light. The light source was used in contact with the bottom surface of the wells of a 96 well plate.

Two light doses were selected for subsequent assays, as representative of one high and a low dose. The doses investigated were 340 J/cm^2 (378 mW/cm^2 for 15 minutes) and 831 J/cm^2 (418 mW/cm^2 for 33 minutes). Additionally, experiments was repeated three times (biological replicates), each in a duplicate (two plates per experiment – technical replicates).

2.3.3.2 Viability / Colony Forming Unit assay

Overnight cultures of *S. mutans* and *E. faecalis* were grown, sub-cultured and diluted as described previously [see **section 2.3.2**]. Afterwards, 200 µl of the diluted culture was assigned to three wells per plate (black- walled 96 well plate), one well for each dose and a non-irradiated control well. Plates were then incubated for 24 hours.
At 24 hours, the contents of each well was mixed 3 times using a sterile pipette to ensure an even distribution of bacteria, before 20 µl was mixed with 180 µl sterile phosphate buffered saline (PBS) (Sigma-Aldrich®, USA) (10^{-1}) to produce a serial dilution (up to 10^{-10}) in a sterile 96 well plate using the Miles and Misra method **[231]**. Two BHI agar plates were divided into three partitions, and labelled based on dilutions used for the CFU assay, each plate contained three dilutions (10^{-5} – 10^{-10}). In each partition, three 20 µl volumes of the specific dilution were inoculated and plated. The agar plates were then incubated for 24 hours, after which the colonies were counted. The number of colonies per millilitre (CFU/ml) was calculated using the formula: '*Average number of colonies for a dilution x 50 x dilution factor*'. Subsequently, the '$\log_{10}$' of each (CFU/ml) was calculated.

2.3.4 Mature biofilms live / dead assay

For biofilm growth, BHI broth was supplemented with 1% sucrose (Sigma-Aldrich®, USA). 5 g sucrose were dissolved in 5 ml distilled water, which was filter sterilised using a sterile 0.22 µm filter (Millex-GP, Merck, Germany) and a 5 ml sterile plastic syringe (Terumo, Belgium) into 500 ml autoclaved BHI broth.

Overnight cultures of *S. mutans* and *E. faecalis* were vortexed, then centrifuged (IEC Centra CL2, Thermofisher Scientific, USA) at 5,000 RPM for 5 minutes. Afterwards, the supernatant media was removed and replaced with 10 ml of fresh PBS, vortexed and then centrifuged (5,000 RPM for 5 minutes) again. The final step was repeated, before replacing the supernatant with 10 ml of fresh PBS. Subsequently, the OD was recorded in a 1 ml cuvette and adjusted to 0.5 McFarland standard (Pro-Lab Diagnostics, UK) (equivalent to 1.5 X 10^8 CFU / ml) using PBS.

Forty-µl of the diluted culture was pipetted in each well, supplemented with 160 µl of BHI broth (with 1% sucrose). Culture plates were incubated for 4 days with shaking at 80 rpm with media changed daily. Two control wells were included in this experiment including one positive and another negative.

On the fourth day, media was removed from each well and replaced with PBS in preparation for light irradiation. Directly after delivering the treatment, the live/dead staining protocol (Filmtracer™ LIVE/DEAD™ Biofilm Viability Kit, ThermoFisher Scientific, USA) was carried out. To prepare a working solution, 3 µl of SYTO® 9 stain and 3 µL of propidium iodide were added to 1 ml sterile PBS in a bijou container covered in foil. After light treatment, PBS was removed and 200 µl of the working solution was added to each well, the plate was then incubated in the dark - covered in

foil - at room temperature for 30 minutes. Subsequently, the stains were washed with PBS and each biofilm was gently disrupted by gentle aspiration, prior to pipetting 100 µl of the mixture into a µ-Dish 35 mm high Glass Bottom (ibidi ®, Germany) in preparation for viewing using confocal microscopy (LSM 700, Carl Zeiss, Germany). The excitation/emission maxima used for SYTO® 9 stain was 480/500 nm, while that of propidium iodide was 490/635. Objective was set at 20X. The negative control wells were treated with 70% ethyl alcohol for 20 minutes.

Image analysis for quantification of the dead bacterial cell percentages was determined using ImageJ software. Initially, channels were split into green and red, then each channel was converted to 8 bit. To estimate the number of dead cells, the 'Find Maxima' function was applied along with adopting the 'Point Selection' output. The 'Noise Tolerance' was adjusted so that all background staining is excluded, and only cellular foci are counted. Finally, the percentages of dead cells were calculated according to the following formulas: '*Percentage of Dead Cells = (Dead Cells/Total Cell Number) X 100*'

2.3.5 Effects of hemin supplementation on bacterial viability in response to blue light

For preparation of a stock solution of hemin, 0.45 g of hemin (Sigma-Aldrich®, USA) was dissolved in 18 ml of 1.4 M ammonium hydroxide (Fisher Scientific, UK) to give a concentration of 25 mg/ml. Stock solution was stored at 4°C until further use. Next, 120 µl of the stock solution was added to 300 ml of BHI broth to achieve a final concentration of 0.01 g/L. The broth was autoclaved.

Frozen stocks of *S. mutans* and *E. faecalis* were grown aerobically at 37°C on blood agar plates (Sigma-Aldrich®, USA) for 24 hours. A single representative colony was transferred to the BHI broth supplemented with 0.01 g/L hemin and incubated overnight.

Overnight cultures were vortexed then centrifuged at 5,000 RPM for 5 minutes. Subsequently, the supernatant was removed and replaced with 10 ml of fresh PBS, vortexed and centrifuged again. The final step was repeated, before replacing the supernatant with 10 ml of fresh BHI broth without hemin. The resulting bacterial suspension was diluted to an OD of 0.1 ($\simeq 10^8$ CFU/ml).

Two-hundred-µl of the diluted culture was pipetted into three wells per plate (black-walled 96 well plate), two wells received irradiation and a control well received no light irradiation. Plates were then incubated for 24 hours, before a CFU assay (Miles and Misra method) **[231]** was performed and colony counts were undertaken after 24 hours incubation.

2.3.6 Effects of application of 5-Aminolevulinic acid on bacterial susceptibility to blue light irradiation and flavin adenine dinucleotide levels

Five-hundred mg of 5-ALA hydrochloride (Sigma-Aldrich®, USA) was dissolved in 10 ml sterile PBS to achieve an initial concentration of 50 mg/ml. This stock solution was further diluted to a concentration of 2 mg/ml (≃ 12 mM) and stored at -20°C until further use.

Overnight cultures of *S. mutans* and *E. faecalis* were diluted according to the protocol previously described [see **section 2.3.4**]. One hundred µl of the diluted cultures (1.5 X 10^8 CFU/ml) along with an additional 100 µl of the prepared ALA (2 mg/ml) were added to three wells per plate (black- walled 96 well plate **[131]** (two doses and a control receiving no light). The final ALA concentration was 1 mg/ml (≃ 6 mM). The plates were incubated aerobically at 37°C in the dark (foil wrapped). For each plate in this set of experiments, another plate was prepared where there was only a 100 µl of the diluted culture in three wells, two receiving light and one non-irradiated control. Following irradiation a CFU assay (Miles and Misra method) **[231]** was executed for all samples with colony counts performed after 24 hours.

To quantify FAD levels, overnight cultures of *S. mutans* and *E. faecalis* were diluted according to the protocol previously described [see **section 2.3.4**]. 100 µl of the diluted cultures (1.5 X 10^8 CFU/ml) were transferred to Eppendorf tubes. Samples either received no or 100 µl of ALA (6 mM) before aerobic incubation (37°C) in the dark for 1 hour.

To quantify FAD content, FAD Assay and Deproteinizing Preparation Kits (Abcam®, UK) were used according to manufacturer's instructions. All FAD Assay kit reagents were stored at -20°C, while the Deporoteinizing kit materials were stored at room temperature. All reagents and samples were kept on ice during use.

The FAD standard (1 nmol) was reconstituted in 100 µl of dimethyl sulfoxide to reach an initial concentration of 10 µM, then 10 µl of the reconstituted standard was further diluted in 490 µl assay buffer to reach a final concentration of 0.2 pM/µl. The FAD standard was further diluted using the assay buffer in a fresh 96-well plate to concentrations of 0.4, 0.8, 1.2, 1.6 and 2 pM of FAD per well.

Samples were vortexed, centrifuged (IEC Centra CL2, Thermofisher Scientific, USA) at 5,000 RPM for 5 minutes, the resulting pellet was washed with PBS, and then re-suspended in 400 µl assay buffer and homogenized. Samples were centrifuged at 10,000 RPM for 5 minutes at 4°C (accuSpin™ Micro 17 Microcentrifuge, ThermoFisher Scientific, USA) and the supernatant was transferred to fresh tubes.

Subsequently, samples were deproteinized by mixing 150 µl of the cell lysate with 15 µl of trichloroacetic acid, kept on ice for 15 minutes and then centrifuged at 12,000 RPM for 5 minutes at 4°C. Finally, 10 µl of potassium hydroxide (30 weight %) was added to neutralize the samples and samples were vented on ice for 5 minutes.

FAD concentrations (pM) were calculated using an OxiRed colorimetric assay undertaken in fresh 96-well plates. A master mix for the reaction mix was prepared containing 46 µl assay buffer, 2 µl OxiRed Probe and 2 µl Enzyme mix per sample/standard. 50 µl of the reaction mix was pipetted into each assigned well before adding 50 µl of the samples and the FAD standards.

Absorbance was read at 570 nm using the Spark® micro-plate reader (Tecan©, Switzerland) every 5 minutes and the maximum linear readings were recorded for each sample/standard.

2.4 Blue light irradiation of human dental pulp cells

2.4.1 Cell culture

Human DPCs (BCHC Ref.: BCHCDent334.1533.TB) - were retrieved from archive stocks (-80°C). Cells were previously harvested from caries-free wisdom teeth according to a previously published protocol **[232]**.

Cells were maintained and expanded in MEM with no phneol (Gibco, ThermoFisher Scientific, USA) supplemented with 10% fetal bovine serum (FBS), 1% penicillin-streptomycin and 1% L-Glutamine (Sigma-Aldrich®, USA). 7 ml sterile penicillin-streptomycin and L-Glutamine were added to 500 ml of MEM, afterwards, 45 ml of that MEM were mixed with 5 ml FBS in 50 ml falcon tubes for further use. Media was stored at 4°C.

For preparation of mineralisation-inducing media, the MEM containing 10% FBS was supplemented with 0.2 mM ascorbic acid, 10 mM beta-glycerophosphate and 100 nM dexamethasone (Sigma-Aldrich®, USA) **[76]**. 0.108 g beta-glycerophosphate and 0.0029 g ascorbic acid were weighed in bijou containers, dissolved in sterile MEM (10% FBS), then filtered into 50 ml falcon tubes (MEM (10% FBS)) using an 0.22 µm filter (Millex-GP, Merck, Germany) and a 5 ml syringe (Terumo, Belgium). For dexamethasone, 0.098 g was dissolved in 50 ml 100% ethanol, filter-sterilised into fresh tubes after which 1 µL was added into 50 ml falcon tubes containing MEM (10% FBS).

Cryovials containing DPCs were thawed using a heating block (Dri-Block® Db.2A, Techne®, UK) at 37°C, before adding the contents to 3 ml fresh media. Cells were centrifuged at 1,000 RPM for 3 minutes (Hettich® Universal 320 R, Hettich zentrifugen, Germany), after which the supernatant was discarded and the pellet was re-suspended

in 2 ml fresh media. Cells were then added to either a T25 (containing 4 ml media) or a T75 (10 ml media) flask (Nunc™, ThermoFisher Scientific, USA) and incubated at 37°C in 5% CO_2 (Heracell™ 150i, ThermoFisher Scientific, USA). Cultures were visually inspected daily using light miscroscopy (Primo Vert, Carl Zeiss, Germany) and media was changed twice per week until cultures were 70-100% confluent [see **Figure 9**].

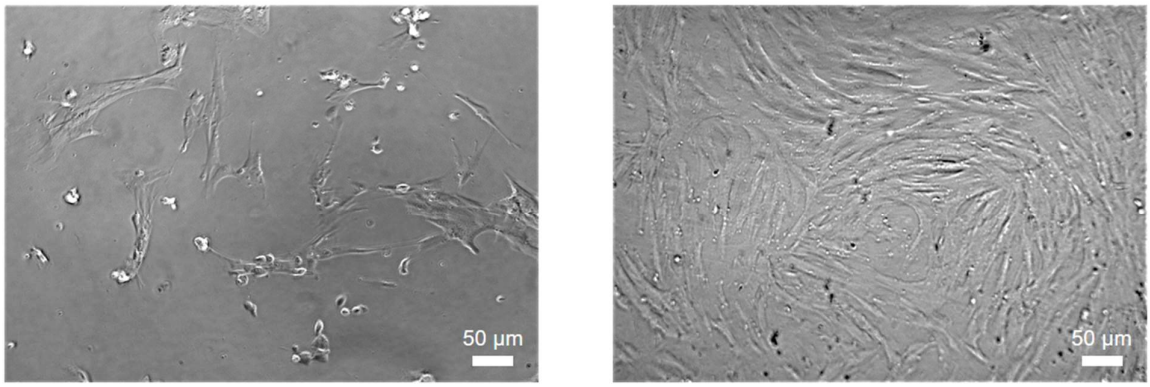

Figure 9: Phase contrast microscopy (Primo Vert, Carl Zeiss, Germany) images of human DPCs captures **(a)** 24 hours culture after cell thawing and **(b)** at confluence. Cells were grown in 5% CO_2 at 37°C. Images were obtained at an objective of 10X.

2.4.2 Cell seeding for biological assays

Confluent cell monolayers were washed with sterile PBS (no calcium or magnesium) (Gibco, ThermoFisher Scientific, USA) then 0.05% trypsin (Sigma-Aldrich®, USA) was added and flasks were incubated at 37°C for a further 1-2 minutes to allow cells to detach. Freshly heated media was then added to de-activate the trypsin. If operating with cells in a T25 flask, volumes used were 3 ml PBS, 1 ml trypsin and 3 ml media. As for T75 flask, volumes used were 5 ml PBS, 3 ml trypsin and 5 ml media.

Cells were pipetted into a 15 ml falcon tube and centrifuged at 1,000 RPM for 3 minutes, after which the supernatant was discarded and the cell pellet re-suspended in 2 ml fresh non-mineralising media. Afterwards, 10 µL of the cell suspension was mixed with 40 µL of 0.4% trypan blue solution (Sigma-Aldrich®, USA) in an Eppendorf tube for cell counting. 10 µL of the mix was loaded into a hemacytometer (Bright-Line™, Reichert Technologies®, USA) - beneath a glass coverslip. Cells on the four corner squares of the hemacytometer were counted, and the average number of cells per ml was calculated based on the formula '*Average number of cells X 5 X 10,000*'.

Cells were seeded at a density of 10,000 cells/ml using the formula: '*C1 X V1=C2 X V2*', where *C1* is the desired number of cells/ml/well multiplied by the number of wells, *C2* is the obtained number of cells/ml in each flask, *V1* is the volume of the final diluted sample in fresh media and *V2* is the transfer volume from the cell suspension. After preparing a master mix, 200 µL was pipetted into each well in a black-walled 96 well plate, and cells were incubated at 37°C in 5% CO_2 for 48 hours to allow initial cell attachment to the cultureware. After 48 hours, media (200 µL) was changed with mineralisation-inducing media and blue light irradiation was delivered. For all assays,

light was administrated at an irradiance of 57.7 mw/cm^2 for 35, 69, 90 or 104 seconds, respectively, delivering light doses of 2, 4, 5 and 6 J/cm^2. However, for the polymerase chain reaction (PCR) assay, only 2 and 4 J/cm^2 exposures were investigated. Control wells received no light exposure.

For the viability (Alamar blue), proliferation (BrdU), ALP and DMP1 assays (described below), cells either received one (day 1) or two irradiations (days 1 and 3). Viability and proliferation were investigated 24 hours post initial irradiation (day 2 for cells receiving one exposure) as well as 72 hours post initial irradiation (day 4 for cells receiving two exposures). ALP and DMP1 levels were investigated at day 3 (one exposure) and day 5 (two exposures).

For the PCR and mineralised nodules assays, cells were exposed to 405 nm blue light on alternate days for 5 days (*i.e.* 3 irradiations at days 1, 3 and 5). OCN expression was investigated on day 7, while the mineralized nodules formation was determined at 7, 14 and 21 days. The effect of extended light irradiation (every other day beyond the initial 3 irradiations) on mineralized nodules formation was also investigated for the full duration of the 14 (6 irradiations) and 21 days (9 irradiations) time points. Media was changed twice a week.

All experiments were carried out in mineralisation-inducing media as described in **section 2.4.1**. All experiments were carried out using cells at passages between 4 and 8. Experiments were repeated three times (biological replicates) in duplicate (technical replicates) except for the PCR assay. For PCR analyses, experiments were repeated three times in triplicate, the RNA was collected from 3 samples (per group in each repeat) and pooled to produce a single sample.

2.4.3 Biological assays

2.4.3.1 Alamar blue assay

The effect of blue light on DPCs growth was detected using the Alamar blue assay. A stock solution of Invitrogen™ Resazurin (ThermoFisher Scientific, USA) was prepared by dissolving 0.015 g in 15 ml PBS, which was subsequently filter sterilised and stored at 4°C in the dark until further use. To prepare 10 % Alamar blue solution, 1 ml was mixed with 9 ml MEM (10% FBS).

Media was gently aspirated from each well, 200 µL of the 10 % Alamar blue solution was pipetted in, and plates were incubated at 37°C in 5% CO_2 (Heracell™ 150i, ThermoFisher Scientific, USA) for 4 hours wrapped in foil. Absorbance of the samples was measured using the ELx800™ microplate Reader (BioTek™, USA) at both wavelengths 570 and 600 nm. Cell growth was calculated as a percentage difference in Alamar blue dye reduction between irradiated and control cells applying the formula '*Percentage reduction of Alamar blue= [(O2 X A1) – (O1 X A2)] / [(O2 X P1) – (O1 X P2)] X 100*' where:

O1 is the molar extinction coefficient (E) of oxidized Alamar blue at 570 nm (80586).

O2 is the E of oxidized Alamar blue at 600 nm (117216).

A1 is the absorbance of irradiated samples at 570 nm.

A2 is the absorbance of irradiated samples at 600 nm.

P1 is the absorbance of the control wells at 570 nm.

P2 is the absorbance of the control wells at 600 nm.

2.4.3.2 Proliferation (BrdU) assay

The BrdU Cell Proliferation ELISA Kit (Abcam®, UK) was used according to the manufacturer's instructions. The wash buffer was diluted 50-fold by adding 40 ml to 1,960 ml of distilled water (E-POD®, Millitrack®, Germany), while the BrdU reagent was diluted 500-fold by mixing 6 µL of the reagent with 3 ml of fresh culture media. For the peroxidase anti-mouse IgG conjugate, it was diluted 2,000-fold by adding 6 µL to 12 ml of the conjugate diluent. All materials were stored at -20°C until further use.

40 µL of the media containing the BrdU reagent was added immediately following light irradiation either on day 1 or day 3, and the plates were incubated for 24 hours at 37°C. The media was then discarded, replaced with 200 µL of fixing solution and the cells were incubated for 30 minutes at room temperature. After discarding the fixing solution, each well was washed three times using 300 µL wash buffer and the plates were blotted dry on paper towels. Subsequently, 100 µL of the anti-BrdU monoclonal detector antibody was added to each well and incubated for 1 hour at room temperature. Plates were washed three times, blotted dry, and 100 µL of the peroxidase anti-mouse IgG conjugate was added to the cells and incubated for 30 minutes at room temperature. Afterwards, the plates were washed/dried as described previously, they then received a final wash using distilled water. Afterwards, 100 µL of tetramethylbenzidine (TMB) peroxidase substrate was pipetted into each well and incubated for 30 minutes at room temperature in the dark – wrapped in aluminium foil. Finally, 100 µL of stop solution was added and the OD was read using the microplate reader (ELx800™ Microplate Reader, BioTek™, USA) at 450 nm.

2.4.3.3 Alkaline phosphatase assay

The ALP assay Kit (Abcam®, UK) was used according to the manufacturer's instructions. The protocol uses p-nitrophenylphosphate (pNPP) as an ALP substrate. The ALP enzyme was reconstituted using 1 ml assay buffer; and for plotting the standard curve, the pNPP (5 mM) was diluted to concentrations of 4, 8, 12, 16 and 20 nM. The assay buffer and stop solution were stored at -20°C, while the pNPP and ALP enzyme were stored at 4°C.

Cells were washed once with PBS, then 80 µL of assay buffer was added to each well. For homogenization, cells were scraped from the bottom of the wells using a sterile needle (BD Microlance™ Stainless Steel Needles, Fisher Scientific, UK) – 0.9 mm in diameter and 20 G gauge. The samples were transferred to Eppendorf tubes and centrifuged (accuSpin™ Micro 17 Microcentrifuge, ThermoFisher Scientific, USA) at 13,000 RPM for 15 minutes at 4°C, then samples were placed on ice for 5 minutes before transferring to a fresh 96-well plate and 50 µL of pNPP (5mM) was added to each sample. 10 µL of the ALP enzyme was added to each diluted pNPP standard well and the plate was incubated for one hour in the dark – wrapped in foil at room temperature.

The reaction was stopped by adding 20 µL of the stop solution (3 N sodium hydroxide) and the OD of the samples was measured at an absorbance of 405 nm. ALP activity was calculated according to the formula: *'ALP activity = B/ ΔT'*, where 'B' is the amount of pNPP in µM and '*ΔT'* is the reaction time in minutes. Afterwards, values were relativized to the control (non-irradiated) wells in each plate.

2.4.3.4 Dentine matrix protein-1 assay

Human DMP-1 DuoSet ELISA and DuoSet ELISA Ancillary Reagent Kit 2 (R & D systems©, USA) were used. High-binding flat bottom 96-well plates and plate sealers were provided. The wash buffer concentrate was diluted to 4%, while the reagent diluent (bovine serum albumin (BSA)) was diluted to 1% using distilled water. The capture antibody (720 µg) was reconstituted with 1 ml PBS. The detection antibody (180 µg) and the DMP1 standard were reconstituted with 1 and 0.5 ml BSA, respectively. Substrate Streptavidin horseradish peroxidase (HRP) was diluted 200-fold in 1% BSA. All reagents were aliquoted and stored at -80°C, except the Streptavidin HRP and the colour reagents (H_2O_2 and TMB) which were stored at 4°C until further use. Before each assay, reagents were diluted to their working concentrations using 1% BSA. 25 µl of each of the capture and the detection antibodies was mixed with 4.5 ml of 1% BSA to achieve a final concentrations of 1 and 4 µg/ml, respectively. The substrate solution was prepared by adding 1:1 volumes (2.5 ml) from each colour reagent. For the standard curve, 150 µl of the reconstituted standard (10,000 pg/ml) was the start point of seven point 2-fold serial dilutions in fresh Eppendorf tubes – to achieve up to 156 pg/ml.

All assay incubations were carried out with sealed plates at room temperature. 24 hours before the intended detection time, 96-well plates were coated with 100 µL of the capture antibody and incubated. Each well was then washed three times and blotted dry as described previously [see **section 2.4.3.2**], and the wells were blocked by adding 100 µL 1% BSA and incubated for 1 hour. Subsequently, the 1% BSA was discarded, wells washed and 100 µL of samples supernatants /standards were

incubated for 2 hours. After washing the plates, 100 µL of the detection antibody was added, incubated for a further 2 hours, re-washed and 100 µL of Streptavidin HRP added prior to incubation for 20 minutes in the dark.

Following a final wash, 100 µL of substrate solution was added to each well and incubated for 20 minutes in the dark and finally 50 µL of the stop solution (2 N sulphuric acid) was added. OD (450 nm) of the samples was measured using a microplate reader (ELx800™ Microplate Reader, BioTek™, USA). DMP1 levels (pg/ml) were retrieved from the calibration curve then values were relativized to the control (non-irradiated) wells in each plate.

2.4.3.5 Mineralised nodule formation / Alizarin red assay

Cultures were washed twice with PBS, fixed with 10% neutral buffered formalin (Sigma-Aldrich®, USA), re-washed and incubated with 200 µl alizarin red stain solution (Sigma-Aldrich®, USA) with gentle agitation (DENLEY orbital mixer) for 30 minutes at room temperature . Afterwards, cells were washed 3-6 times until all excess stain was removed. Images were captured at an objective of 10X using an inverted phase contrast light microscope (Eclipse TE300, Nikon, Japan) along with a digital camera (D5100, Nikon, Japan).

To extract the stain for quantitative data, 200 µl 10% acetic acid (Sigma-Aldrich®, USA) were added to each well and the plates were incubated at room temperature with gentle agitation. Using a 20 G gauge sterile needle (BD Microlance™ Stainless Steel Needles, Fisher Scientific, UK), cells were removed by scraping from the bottom of the wells then the cells along with the acetic acid were transferred to Eppendorf tubes.

Cells were heated in a water bath (85°C) using a hot plate (Isotemp™, Fisher Scientific, UK) for 10 minutes, transferred to ice for 5 minutes and centrifuged at 14,000 RPM for 15 minutes (Jouan, UK). Subsequently, the supernatants were transferred to fresh Eppendorf tubes and the pH was neutralized by adding 75 µl 10% ammonium hydroxide (Sigma-Aldrich®, USA). All samples were transferred to a fresh 96 well plate and the OD was read at 405 nm (ELx800™ Microplate Reader-BioTek™, USA). A calibration curve using a range of concentrations of alizarin red (0.47-30 µM) - in a dilution buffer- was generated to quantify the amounts of the stain present within each sample (µM).

2.4.3.6 Semi-quantitative polymerase chain reaction analysis of Osteocalcin mRNA expression

Cell lysis and RNA extraction was performed using the RNeasy® Mini kit (Qiagen, Germany). To prepare 70% ethanol, 35 ml of molecular biology grade ethanol (Fisher Scientific, UK) were added to 15 ml of molecular biology grade water (Invitrogen™ UltraPure™ DNase/RNase-Free Distilled Water, Fisher Scientific, UK) in sterile falcon tubes. To prepare the working solution of the RPE buffer, 44 ml of 70% ethanol were added to the stock solution provided. The entire protocol was carried out on ice. All kits and reagents were stored at -20°C, except for the RNA extraction kit which was stored at room temperature.

Cells were washed twice with sterile PBS then 350 µl of the lysis buffer was added to each well. Cells were scraped from the bottom of the wells using a 20 G sterile needle and then transferred to sterile spin columns – in collection tubes. Subsequently, 350 µl

of 70% ethanol was added to each sample, centrifuged for 30 seconds at 10,000 RPM (Centrifuge 5425 D, Eppendorf, UK) and the flow-through was discarded from the collection tubes. 350 µl of RW1 buffer was then added to the samples, centrifuged (30 seconds, 10,000 RPM) and the flow-through discarded.

For DNA digestion, the On-Column DNase I Digestion Set (Sigma-Aldrich®, USA) was used. A master mix was prepared in sterile Eppendorf tubes, which included 70 µl digest buffer and 10 µl DNase deoxyribonuclease I per sample. 80 µl of the master mix was added to each sample and left to incubate on ice for 15 minutes, after which 350 µl RW1 buffer was added and the spin columns were centrifuged (30 seconds, 10,000 RPM) and the flow-through discarded.

500 µl of the RPE buffer was added to each sample, centrifuged (30 seconds, 10,000 RPM) and the flow-through discarded. This process was repeated; however, samples were centrifuged for 2 minutes at 10,000 RPM. Spin columns were placed in fresh collection tubes and centrifuged for 1 minute at 13,200 RPM. Columns were placed in sterile Eppendorf tubes, and 30 µl of DNase/RNase-free water was added to each sample before centrifuging for 1 minute at 10,000 RPM. Finally, the eluted RNA from each group (represented by triplicate samples) was collected in a sterile Eppendorf tube.

For detection of RNA purity, a Genova Plus Life Science spectrophotometer (Jenway, UK) was used. 2 µl of DNase/RNase-free water were added to the detector to blank the spectrometer, before adding 2 µl of the extracted RNA and the 260/280 absorbance ratio was recorded. Samples which only recorded a ratio of 1.8-2 were included. Samples were stored at -80°C until further use.

To prepare complementary DNA (cDNA), the bioline tetro cDNA synthesis Kit (meridian BIoscience ™, USA) was used. A master mix was prepared containing the following concentrations per sample: 1 µl Oligo deoxythymine, 1 µl deoxyribose nucleotide triphosphate mix, 4 µl reverse transcriptase buffer, 1 µl RNase inhibitor and 1 µl reverse transcriptase. In sterile 0.2 ml PCR tubes, 8 µl from the master mix was mixed with 19 µl of the extracted RNA and 1 µl of DNase/RNase-free water. Afterwards, the reaction was initiated by incubating the samples at 45°C for 60 minutes (Applied Biosystems' GeneAmp™ PCR System 2700, Biocompare, USA), and the reaction was terminated by further incubation at 85°C for 5 minutes. 40 µl of DNase/RNase-free water were added and samples were stored at -20°C until further use.

For preparation of the primer master mix, volumes used per sample were 60 µl of DNase/RNase-free water, 10 µl of the forward primer and 10 µl of the reverse primer. As for the PCR master mix, the Redtaq® ReadyMix™ PCR Reaction Mix (Sigma-Aldrich®, USA) was used, containing 12.5 µl REDTaq, 9.5 µl DNase/RNase-free water and 2 µl of the primers master mix. The forward primer sequence for OCN was 'GGCAGCGAGGTAGTGAAGAG', while the reverse was 'CTGGAGAGGAGCAGAACTGG'. Glyceraldehyde 3-phosphate dehydrogenase (GAPDH) was used as a housekeeping gene; forward primer sequence was 'CTCCTGTTCGACAGTCAG' while reverse's sequence was 'GCCCAATACGACCAAATC'. Primers were purchased from (Sigma-Aldrich®, USA). Subsequently, 1.5 µl of cDNA was added to 24 µl of the PCR master mix in fresh sterile 0.2 ml PCR tubes and thermocycled for 27 cycles. 6 µl was removed from each sample and stored on ice, before thermocycling the remainder for a further 3-6 cycles. For the first 27 cycles, DNA denaturation was performed at 94°C for 5

minutes followed by 20 seconds extension, while annealing was undertaken at 60.5°C for 20 seconds then 68°C for another 20 seconds. A final extension was carried out at 72°C for 10 minutes. Further thermocycling of the samples was undertaken using the same settings, except for the first and last steps - denaturation (94°C) and extension (72°C) - which were done for only 1 minute.

To prepare a 1.5% agarose gel, 0.9 g of agarose powder (meridian Bioscience™, USA) was added to 60 ml 1X Tris-acetate-EDTA buffer (ThermoFisher Scientific, USA), and microwaved for 2 minutes. After cooling down under tap water for 10 seconds, 5 µl of SYBR® Safe DNA gel stain (Sigma-Aldrich®, USA) was added to the mix and poured onto a casting tray with a comb inserted to create loading wells. Samples were loaded into the gel which was then placed in an electrophoresis tank (Fisherbrand™ Midi Plus Horizontal Gel System, Fisher Scientific, UK), and underwent electrophoresis (120 V / 40 mA) for 30 minutes using a VWR® power source (Avantor®, USA). The gel was viewed using UV light (G-box HR, Syngene, UK), and images were taken by GeneSnap software (Syngene, UK). Quantification of the bands fluorescence intensity was analysed using GeneTools software (Syngene, UK). Expression values were normalized to GAPDH, then values were relativized to the non-irradiated controls.

2.5 Statistical analysis

Light transmission through dentine and tubule quantification data were analysed using one-way ANOVA for comparisons of more than two groups. *Tukey*'s post hoc test was applied for pairwise comparisons. For antimicrobial and PBM data, the *Kruskal-Wallis* test was used to determine significant differences between groups. The *Bonferroni test* was applied for pairwise comparisons. The significance value was set at $p \leq 0.05$. Data were analyzed using SPSS 17 (IBM®, USA).

Chapter 3: Results

Blue light has been reported to have the highest absorption and lowest penetration through dentine **[89-91]**. The 405 nm wavelength has previously been shown to have antibacterial activity against *S. mutans* **[45-47],[134]** as well as an ability to enhance the mineralisation processes of MSCs **[74-78]**. Based on this information, the current investigations were performed.

To estimate the blue light irradiance delivered to either the cariogenic bacteria residing within the dentinal tubules or the DPCs during different clinical applications, 405 nm wavelength transmission through dentine was characterised. Analyses were performed using dentine sectioned occlusally, obliquely and buccally at three different thicknesses; 1, 2 and 3 mm. The percentage of light transmitted was calculated with reference to an initial characterisation of the light source in atmospheric air. The 405 nm light source was characterised prior to each irradiation experimental set-up for both bacterial and cell cultures to determine the light irradiance and doses delivered. Subsequently, the effects of blue light were investigated on cariogenic bacterial growth and viability. The susceptibility of bacteria to light after supplementation with hemin and ALA, as well as the effect of ALA on the bacteria's FAD levels were also studied. Finally, the effects at relatively lower doses of 405 nm blue light on human DPCs proliferation and odontoblastic differentiation were investigated.

Results showed that both dentinal tubule orientation and density have a significant effect on 405 nm blue light transmission. Additionally, 405 nm blue light inhibits the growth of *S. mutans* and *E. facalis* lawn biofilms, as well as exerts a killing effect on

bacteria grown in planktonic cultures and in 4 day mature biofilms. The susceptibility of bacteria to blue light was affected by its redox state through supplementation with hemin and ALA indicating the photochemical – oxidative stress mediated – mechanism of inhibition. Moreover, at relatively low doses, 405 nm blue light inhibited the proliferation but potentially enhanced the mineralisation potential of human DPCs.

3.1 Characterisation of the light source

3.1.1 Characterisation of blue light in atmospheric air

To determine the percentage of light transmitted through dentine sections with different thicknesses, characterisation of the light source was carried out initially by measuring the absolute irradiance at 1, 2 and 3 mm distance between the light source from above and the spectrophotometer sensor below [see **Section 2.1.2**]. The light source was operated at 20 regular interval power outputs of between 5 - 100 % [see **Figure 10**]. Irradiance slightly decreased as the distance between the light source and the detector increased; however, there was no significant differences in irradiance at any power output used.

(a)

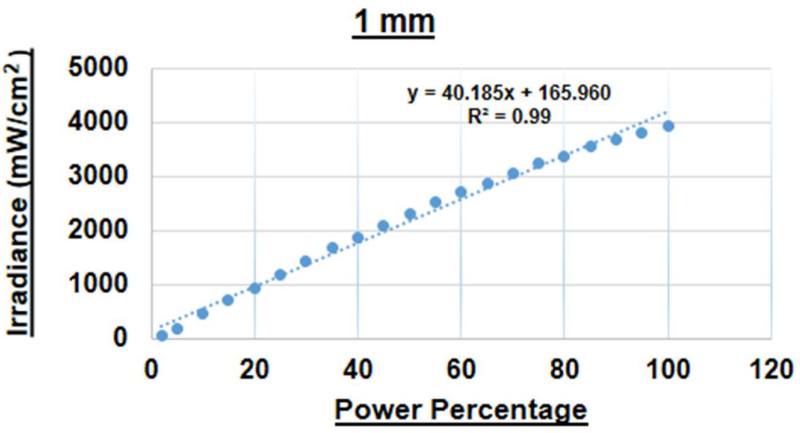

(b)

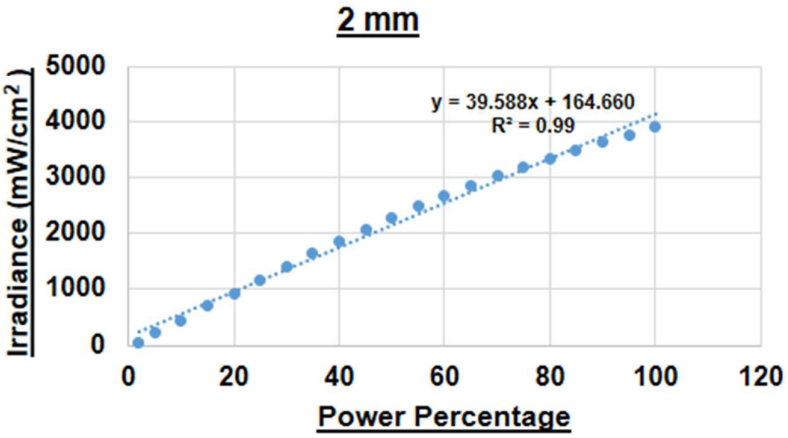

(c)

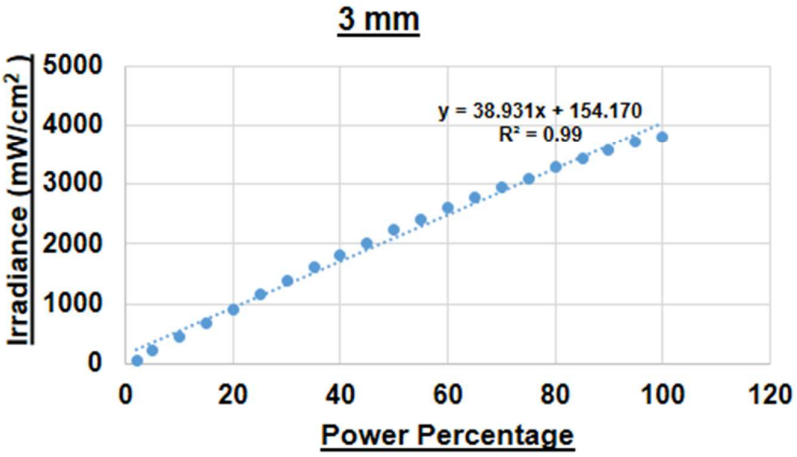

Figure 10: Scatter graphs showing mean irradiance (n=3) recorded relative the operating power percentages of the light source at 1 **(a)**, 2 **(b)** and 3 **(c)** mm distance between the light source and the sensor in atmospheric air. A linear regression curve fit was applied. The fitting formula is used to estimate the operating power percentage of the light source based on the desired incident irradiance.

3.1.2 Characterisation of light irradiation for use in bacterial and human cell cultures

To enable selection of the irradiance assigned for each specific dose when irradiating bacterial and cell cultures, the light source was characterised for each irradiation set-up. Bacterial lawns were grown on BHI agar, while planktonic cultures, biofilms and DPCs experiments were performed in 96-well plates [see **Section 2.2.1** & **Figure 8**]. The light source was operated at 6 increasing power outputs of between 10 - 60 % [see **Figure 11**]. Comapred with direct contact, there was a slight decrease in irradiance as the light source was positioned at 5 mm from the underside of the agar plate. However, these values markedly increased when positioning the light source in direct contact with the 96-well plate base. To select the light source's operating power output, the desired irradiance was calculated from each calibration curved obtained. Subsequently, the light dose was calculated based on the formula *'Dose (J/cm^2) = Irradiance (mW/cm^2) X Time (seconds).'*

(a)

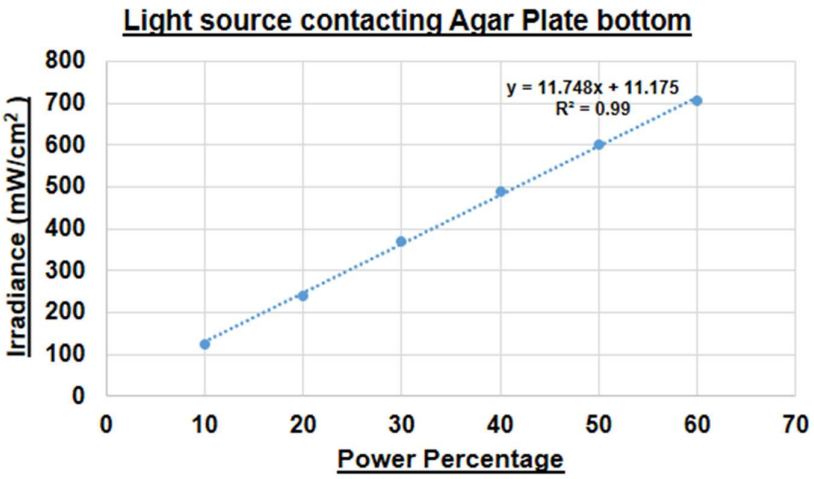

(b)

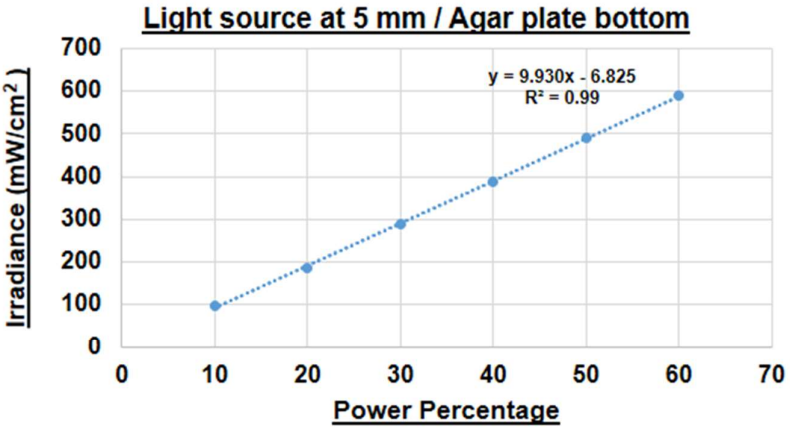

(c)

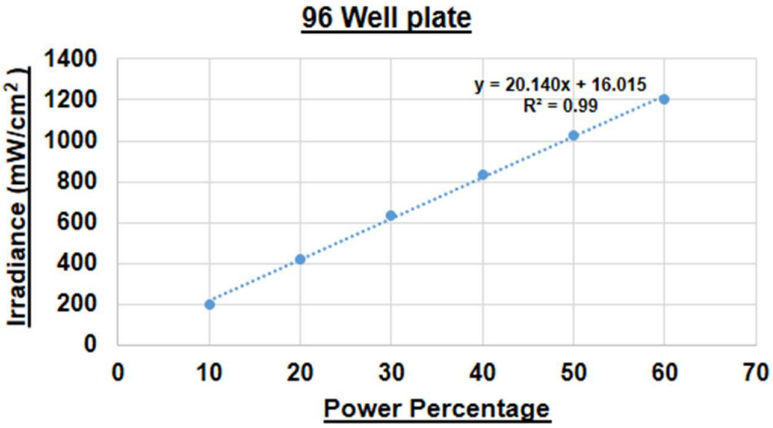

Figure 11: Scatter graphs showing mean irradiance recorded relative to the operating power percentages of the light source when the light source was in contact with the agar plate base **(a)** or at 5 mm from agar plate base **(b)**, as well as contacting the base of a well in a 96 well plate **(c)** (n=3). A linear curve fit was applied.

3.1.3 Media absorption and temperature measurements

3.1.3.1 Media absorption

For the bacterial cultures, the amount of blue light transmitted to the upper surface of the BHI agar was 67.9 % ± 2 when irradiating the plate at a 5 mm distance. These data indicated that the percentage of blue light absorbed / scattered before reaching the agar surface was 32.1 %. The percentage of light transmitted through the BHI broth was calculated to be 29.4 % ± 0.2. Therefore, the amount of light absorbed in the broth was 70.6 %. The percentage of light transmitted through the MEM cell culture media was 74 % ± 1.5, indicating the percentage of blue light absorbed in the MEM was 26 %.

3.1.3.2 Temperature measurements

Temperature elevation in the bacterial cultures was consistently directly related to the power/ irradiance setting administrated regardless of either the duration of exposure or the eventual dose. Once the irradiation commenced, temperatures increased until a stationery plateau phase was reached. The room temperature was between 19-22°C. The highest temperature reached at the BHI agar surface was 31.18°C, and 37.99°C for the BHI broth [see **Figure 12**]. Both temperatures are within the normal range of growth for both *S. mutans* and *E. faecalis* **[233],[234]**.

The irradiance parameter used for DPCs studies was considerably lower than those used to irradiate the bacterial cultures. The irradiation times were also relatively shorter. Accordingly, there was no elevation in the MEM temperature. The temperature of the MEM cell culture media began decreasing once the 96-well plates were removed from the incubator, the average temperature decrease over 104

seconds (maximum irradiation time) was 7.22°C. There was no significant difference in the temperature decrease between the non-irradiated control and the irradiated samples [see **Figure 13**].

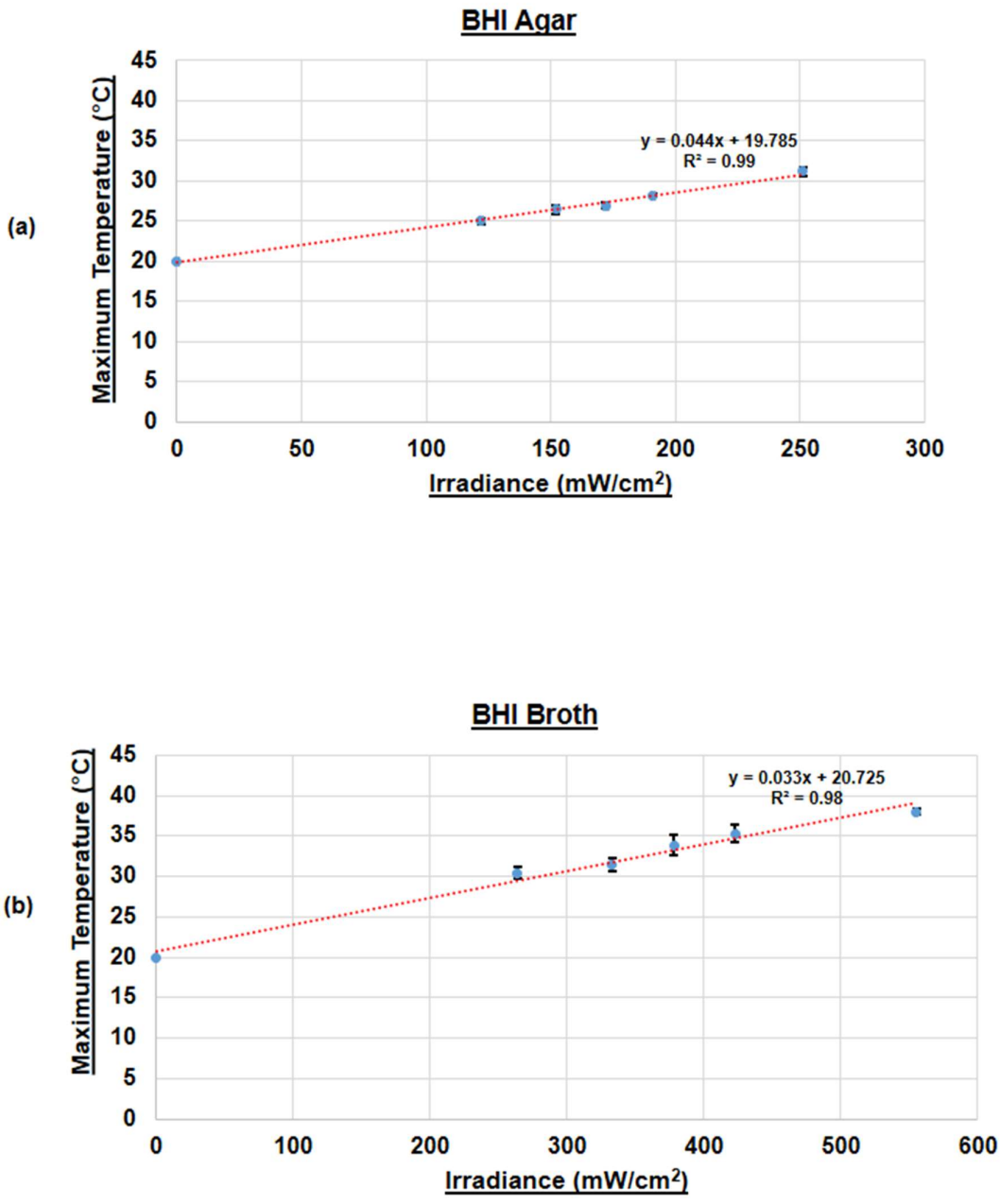

Figure 12: Scatter graphs showing average temperatures reached (n=3) corresponding to each irradiance applied throughout the photodisinfection studies. Irradiance settings used on agar **(a)** were 122,152,172,191 and 254 mW/cm^2. Irradiance settings for broth cultures **(b)** were 277, 338, 378, 418 and 539 mW/cm^2. A linear curve fit was applied.

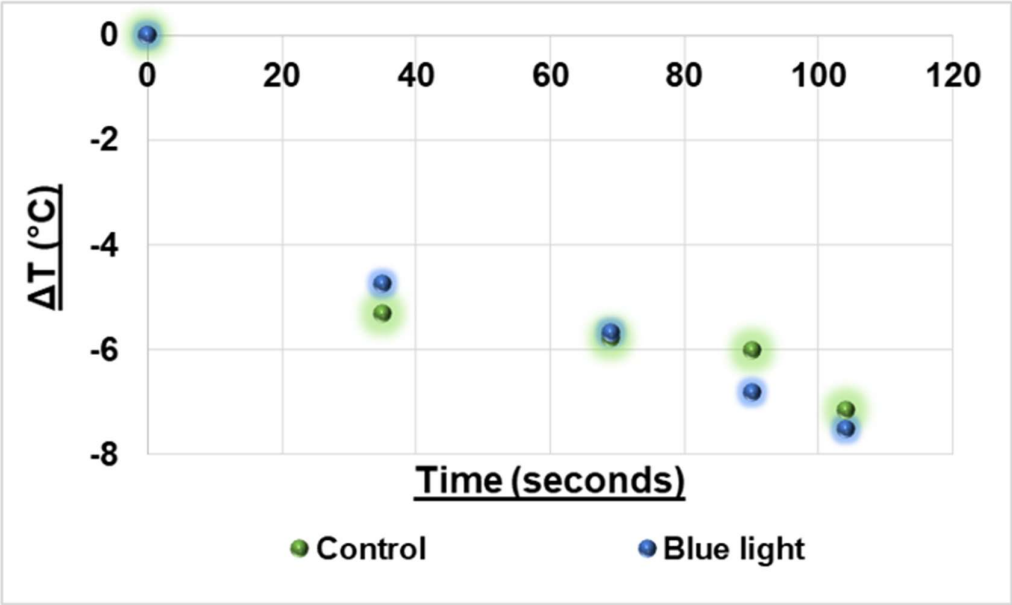

Figure 13: Mean temperature change (ΔT) (n=3) measured in both the irradiated (57.7 mW/cm^2) and non-irradiated controls at different time points; 35, 69, 90 and 104 seconds.

3.2 Effect of dentinal tubule orientation and density on 405 nm blue light transmission

3.2.1 Dentine orientation and thickness

To determine the percentage of light transmitted through different dentine specimens, the absolute irradiance was measured in each dentine specimen aligned vertically between the light source and the sensor (pulpal side downwards) [refer to **Section 2.1.2** and **Figure 7**]. The light source was operated at 10 gradual power outputs of between 10-100% and was initially characterised in atmospheric air [see **Figure 14**]. Results indicated that light transmission decreased as dentine thickness increased at all orientations. The percentage of light transmitted through 1 mm dentine in all sections (occlusal, oblique, buccal) was significant compared with both the 2 and 3 mm dentine specimens ($P<0.001$). The amount of light transmitted through either occlusal or oblique sections was consistently greater than the amount of light transmitted through buccal sections at all three thicknesses studied [see **Figure 15**].

No significant differences were found between occlusal and oblique dentine in terms of light transmission in the thicknesses tested. In the 1 and 3 mm dentine sections, light transmission in occlusal sections was significantly greater than in buccal dentine sections ($P=0.033$ and $P=0.040$, respectively). In 2 mm dentine sections, although light transmitted in the occlusal and oblique sections was higher than in buccal sections, there was no significant difference between all three groups analyzed. It is notable that the percentage of light transmitted through each specimen was not significantly different regardless of the light source's power output.

(a)

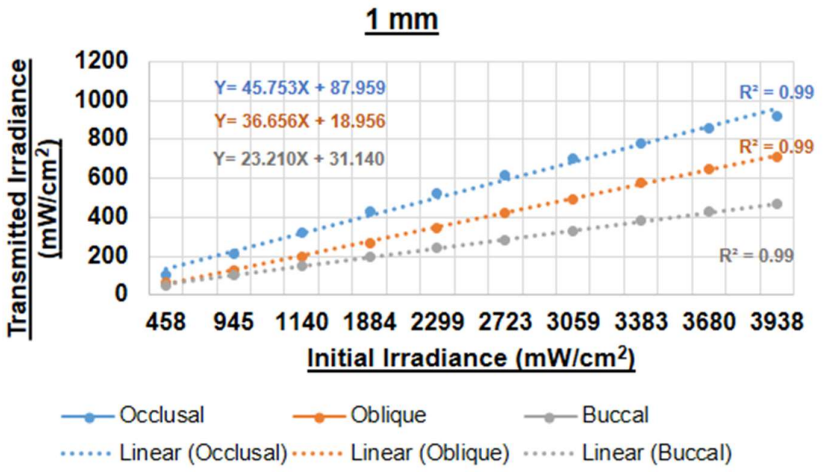

(b)

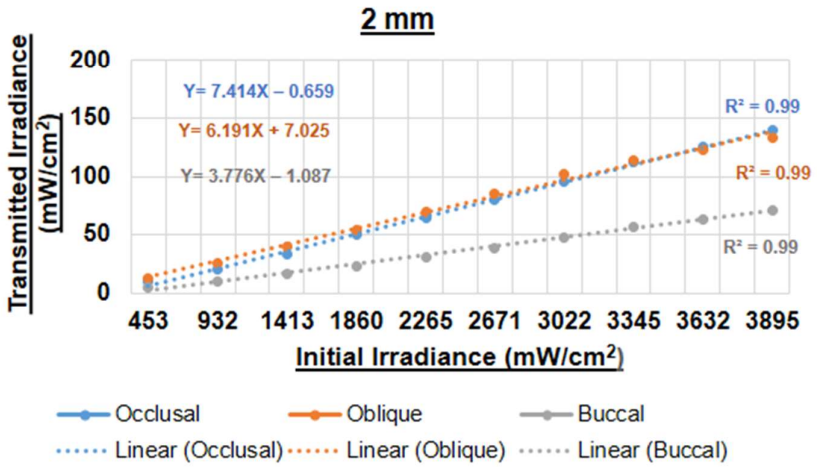

(c)

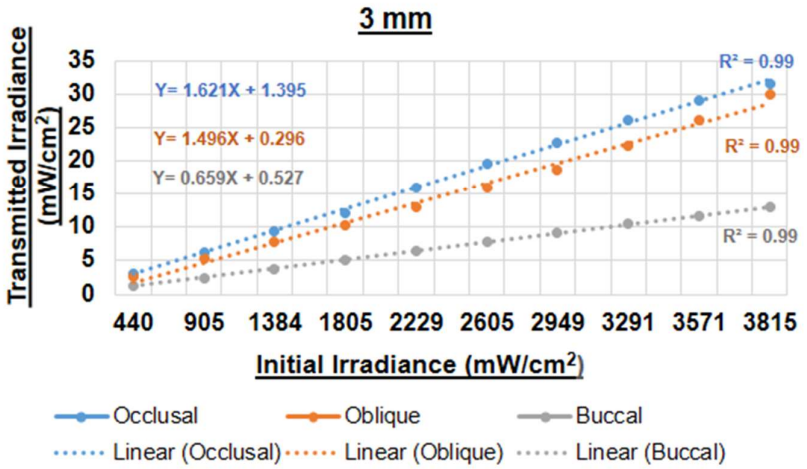

Figure 14: Scatter graphs representing mean irradiance transmitted through 1 **(a)**, 2 **(b)** and 3 **(c)** mm occlusal, oblique and buccal dentine sections in relation to the initial irradiances recorded at 1, 2 and 3 mm distance between the light source and the sensor in atmospheric air (n=5). A linear regression curve fit was applied. The formula is used to estimate the irradiance of the transmitted light on the pulpal side of dentine based on the incident irradiance.

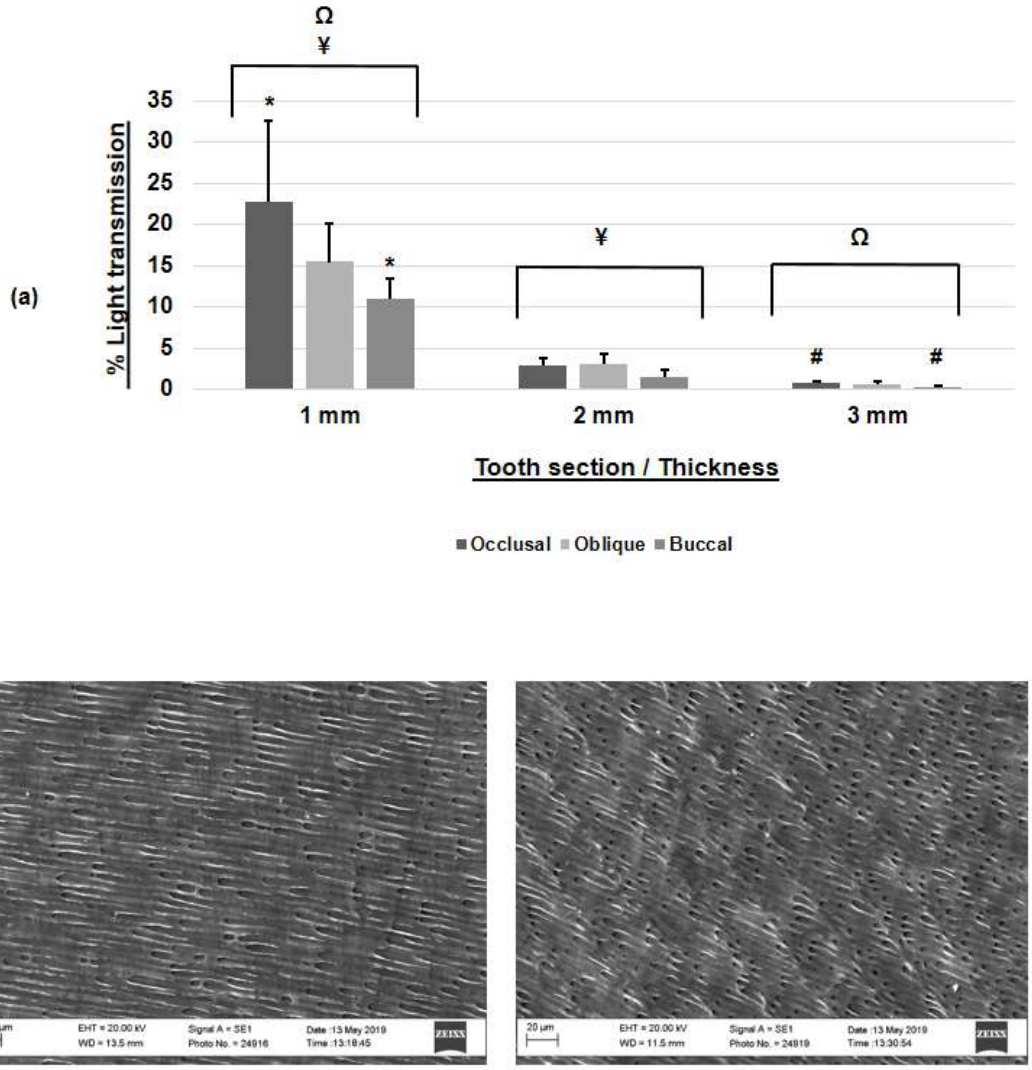

Figure 15: (a) Bar chart showing light transmission percentages through occlusal, oblique and buccal dentine at 3 separate tissue thicknesses (n=5) (mean +/- SD). Significance level set at P ≤ 0.05. Similar symbols show statistically significant differences in percentage of light transmission. (¥ and Ω P<0.001), (* and **#** P<0.05). **(b)** SEM images of buccal dentine sections at the locations where a change of orientation in tubular direction occurs. The tubules are not circular and are elongated, which occludes the light beam, limiting transmission**.**

3.2.2 Dentinal tubule density

Dentinal tubule quantification data revealed that occlusal and oblique sectioned dentine had the highest tubular density in comparison with the buccal dentine. These data correlate directly with the light transmission results where the higher tubular density encountered through the occlusal and oblique sections yielded higher percentages of light transmission. This was in comparison with the buccal sections which exhibited a lower dentinal tubular density. There was no significant differences between any outer and inner counts within the same section. Yet, both the inner occlusal and oblique counts were significantly higher than the inner buccal counts ($P=0.024$ and $P=0.004$, respectively) [see **Figure 16**].

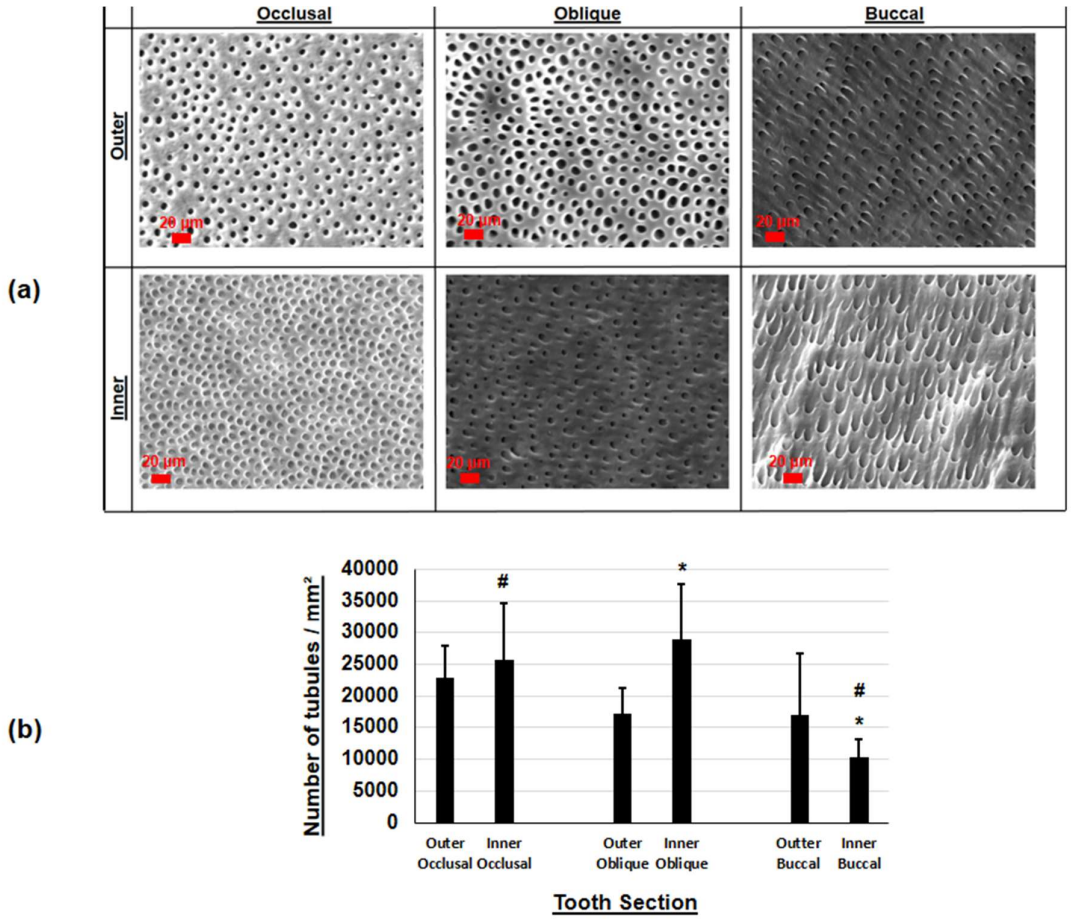

Figure 16: (a) Representative SEM images of outer (DEJ) and inner (pulp) dentine sections from each group; occlusal, oblique and buccal. These Images were used to quantify the dentinal tubules. **(b)** Bar chart showing the tubular density through occlusal, oblique and buccal dentine (n=5) (mean +/- SD). Significance level set at $P \leq 0.05$. Similar symbols indicate statistically significant differences (* and # $P<0.05$).

3.2.3 Discussion

Results of the current study indicated that the dentinal tubule orientation played a major role in the transmission of the 405 nm light, since the percentage of light transmitted through cross-sectional dissected occlusal and oblique dentine was always significantly higher than light transmitted through longitudinally dissected buccal dentine. Light was transmitted more readily along the tubules in cross-cut specimens, other than occluding perpendicular to the tubules in deeper layers of buccal dentine [see **Figure 15**]. Fried *et al*. confirmed that if light is delivered perpendicular and not along the path of the tubules, it will penetrate ~100 microns then degrades due the sigmoid pathway of the tubules. Dentine has birefringence and bi-refractive properties, meaning it exhibits two refractive indices, one due to the hydroxyapatite and the other due to the dentinal tubules structure **[51]**. Notably, the S- shaped curvatures of the dentinal tubules are less prominent beneath the cusps **[103]**.

If dentine is dissected at an angle greater than 45 degrees to the tubules, minimal to no light reflection may occur and light will be scattered in the forward half space. These findings indicate that the scattering coefficient of highly scattering dentine is zero. In cross-cut dentine, there is a relatively small angle between incident light and dentinal tubules, and so light propagates along the tubular direction as a result of multiple scattering events by collagen fibrils **[58]**. Hariri *et al.* obtained similar results confirming that the refractive index of cross-cut dentine is less than dentine cut either obliquely or longitudinally. In longitudinal and oblique dissections, hydroxyapatite crystals along with collagen are responsible for light propagation **[52]**. Light propagates

along the cross-cut tubules; however, occludes along longitudinally-cut tubules [see **Figure 15(b)**].

Although in the present study the percentage of light transmission through 1 and 3 mm occlusal sections was higher than both oblique and buccal sections, in 2 mm dentine, oblique dentine permitted the highest light transmission (3.1%). However, this percentage was slightly higher than occlusal dentine (2.9%). It is notable that the average counts of the dentinal tubules obtained in the current investigation conforms to the light transmission results obtained, especially observed through 2 mm dentine specimens. The inner oblique tubular density was higher compared with the inner occlusal dentine. This occurred most likely due to the fact that pulp horns are in closer proximity to the outer tooth surface in oblique cut section. This would result in specimens - closer to the pulp - with a higher tubular density and wider tubules **[57]** compared with the occlusal cut section.

As the teeth used in this study were extracted teeth from a cross-section of the population, standard deviations throughout the data obtained could potentially be due to heterogeneity in tooth structure **[52]**. Age is also an influential factor, as younger teeth would have wider tubules and therefore more scattering **[58]**. Type I dentine is more frequent in younger individuals while type II dentine is more prevalent in older individuals **[112]**. Furthermore, odontoblasts deposit secondary dentine at a significantly slower rate after tooth eruption and throughout life **[235]**. Variations in optical properties could occur at different zones as a result of of sclerotic dentine deposition **[123]**. It is also important to take into account that the optical characteristics of dentine can change with tooth type **[59]**. Additionally, optical

properties will most likely fluctuate if the dentine's physical condition change. Arends *et al.* measured the diameter of dentinal tubules in wet or air-dried dentine specimens in sound and demineralized dentine. Wetting did not affect sound dentine but led to an increase in demineralized dentine tubule diameter; however, this diminished as demineralisation proceeded as a result of the cariogenic bacteria's acid dissolving inter-tubular and peri-tubular dentine. Drying led to an enlargement of tubule diameter as drying time gets longer through both sound and demineralized dentine **[236]**. Uusitalo *et al.* conducted similar wetting and drying investigations; however, they assessed light curing unit transmittance at 455 nm under both conditions. They also added a third condition of EDTA etching. Light irradiance was lower in dentine compared with enamel, indicating that dentine attenuates more light. As the thickness of dentine and enamel increases the transmittance decreased. Moist dentine and enamel attenuated less light (*i.e.* transmitted more light). EDTA treatment increased the irradiance of transmitted light in dentine samples **[237]**. In contrast, Turrioni *et al.* reported that EDTA treatment had no effect on trans-dentine light propagation **[238]**.

3.3 Effects of blue light on cariogenic bacteria

3.3.1 Growth and viability

3.3.1.1 Zones of growth inhibition in bacterial biofilm lawns

Initial results for *S. mutans* lawns which were irradiated with the light source in direct contact with the underside of the agar plate indicated that the light treatment inhibited their growth. This was demonstrated as a ZOI and there was evidence of a gradual dose-response relationship. The ZOI produced by a 405 nm light at a dose of 590 J/cm^2 was significantly larger than doses of 84 and 147 J/cm^2 (P=0.05). However, there was no significant difference between any of the other irradiation doses (200, 358, 443 or 590 J/cm^2) applied using this experimental set-up [see **Figure 17**].

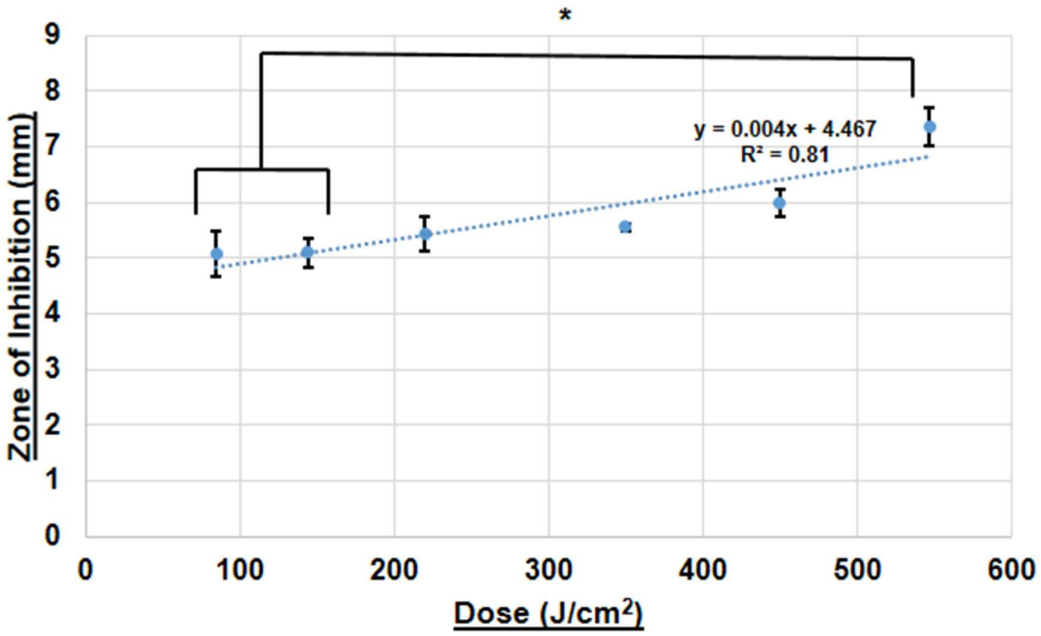

Figure 17: Scatter graph showing the effect of six increasing doses of 405 nm light irradiation on *S. mutans* lawns, when the light source was in contact with the agar plate base (mean +/- SD, n=3). Doses administered were 84, 147, 200, 358, 443 and 590 J/cm^2. An asterisk show statistically significant differences in ZOI diameters (* P=0.05). Significance level was set at P ≤ 0.05. A linear curve fit was applied, showing the direct dose-response relationship between the irradiation dose and ZOI diameteres.

To better represent the use of light in a cavity where direct application to the base or axial wall of a cavity would not be possible, further irradiation of bacterial lawns was carried out at 5 mm distance from the underside of the agar plate. With regards to results for both *S. mutans* and *E. faecalis* cultures irradiated at a 5 mm distance, data showed that 405 nm light irradiation produced a wider ZOI on *S. mutans* – compared to *E. faecalis* lawns - at all doses investigated. There was no significant differences in ZOI diameter with the range of doses investigated for either of the bacteria used between the (IT/DP) and the (IP/DT) mode. However, in general, the IT/DP mode produced wider ZOI. For the *S. mutans* analysis, delivering a dose of 110 J/cm^2 (IP/DT) resulted in a significantly smaller ZOI compared with the 573 J/cm^2 dose applied in either mode (IT/DT) (P=0.012) and (IP/DT) (P=0.016). The same dose - 110 J/cm^2 - yet in its (IT/DP) mode, exhibited a significantly smaller ZOI compared with 573 J/cm^2 (IP/DT) (P=0.047). As for *E. faecalis*, the dose of 456 J/cm^2 (IT/DP) resulted in significantly wider ZOI compared with 110 J/cm^2 (IP/DT) exposure (P=0.045). Additionally, irradiation at 573 J/cm^2 (IT/DP) led to significantly wider ZOI relative to 110 J/cm^2 (IT/DP) (P=0.013), 110 J/cm^2 (IP/DT) (P=0.001) and 154 J/cm^2 (IP/DT) (P=0.015). Moreover, irradiation at 573 J/cm^2 (IP/DT) resulted in ZOIs that were highly significantly different compared with those at 110 J/cm^2 (IT/DP) (P=0.047), 110 J/cm^2 (IP/DT) (P=0.006) and 154 J/cm^2 (IP/DT) (P=0.05) irradiation [see **Figure 18**].

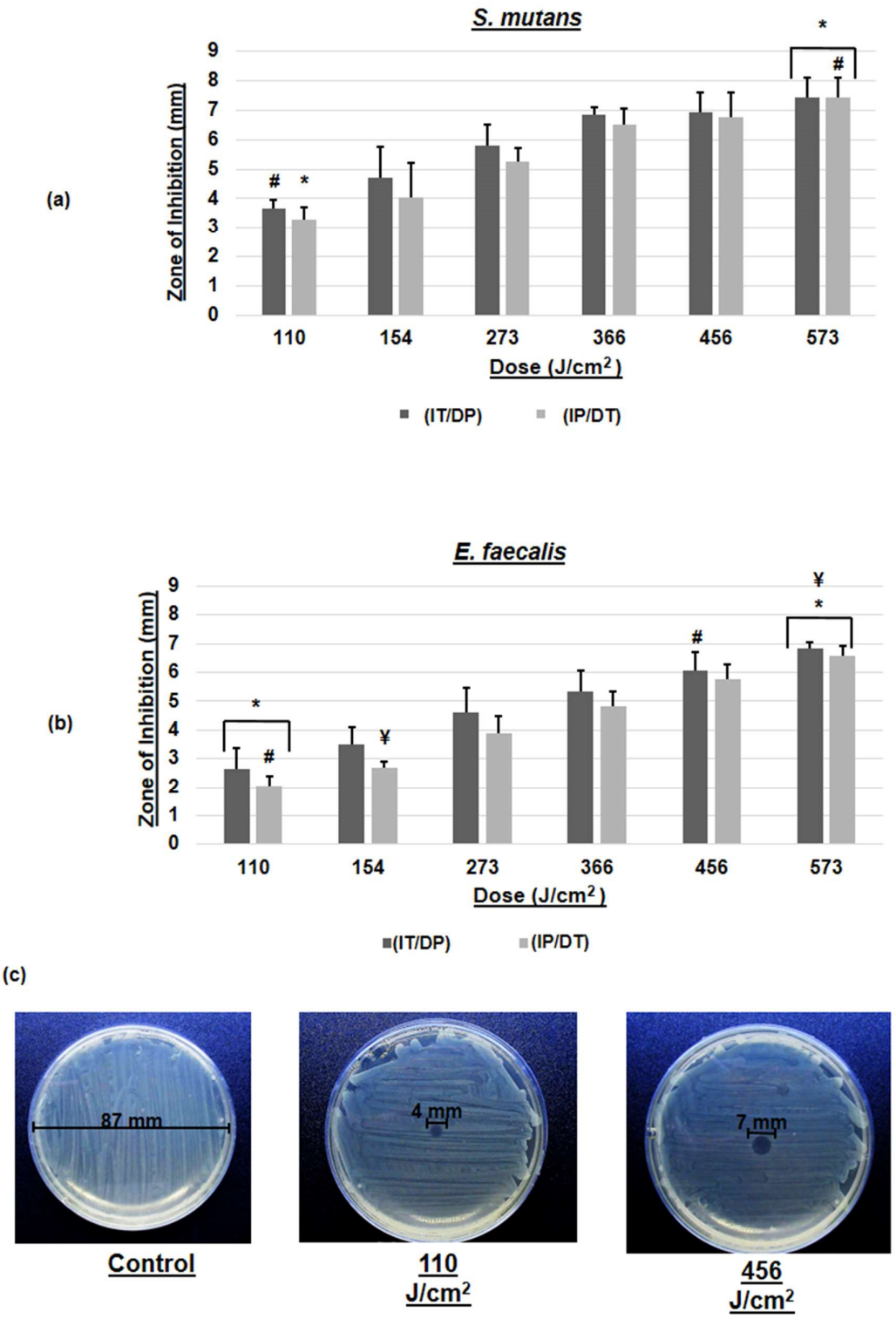

Figure 18: Bar graphs showing the effect of 405 nm light on the growth of both *S. mutans* **(a)** and *E. faecalis* **(b)** bacterial biofilm lawns when the light source was positioned at 5 mm from the agar plate base. Each dose was administrated in (IT/DP) and (IP/DT) modes (n=4, mean +/- SD). Similar symbols within each chart show statistically significant differences in ZOI diameters initiated by different doses administrated (*, # and ¥ $P<0.05$). Significance level set at $P \leq 0.05$. **(c)** Representative images showing the difference between a control plate of *S.mutans* lawns (no exposure), a plate exposed to 405 nm light at a dose of 110 J/cm^2 and at a dose of 456 J/cm^2. As illustrated, the higher dose produced a wider zone of Inhibition (7 mm) compared with the lower dose (4 mm).

3.3.1.2 Planktonic cultures

3.3.1.2.1 Irradiation effects on *S. mutans* viability

Although there was a trend identified indicating a dose response relationship, the (IT/DP) mode did not necessarily result in a decreased bacterial survival as was observed in the irradiated biofilm lawns. When irradiating planktonic cultures at a wavelength of 405 nm with a dose of 608 J/cm^2, the percentage survival was similar under both conditions (IT/DP=46.43%) (IP/DT=46.49%), although at 1254 J/cm^2 the (IP/DT) mode yielded less bacterial survival (34.86%) compared with the (IT/DP) mode (36.95%).

A dose of 1254 J/cm^2 delivered using the (IP/DT) modality produced significantly lower survival percentages compared with the 249 J/cm^2 irradiation when using either mode (IT/DP) (P=0.037) and (IP/DT) (P=0.021)**.** As was the case with irradiation of bacterial biofilms on agar, there was no significant difference on viability - within a single dose - between its (IT/DP) and (IP/DT) mode [see **Figure 19**].

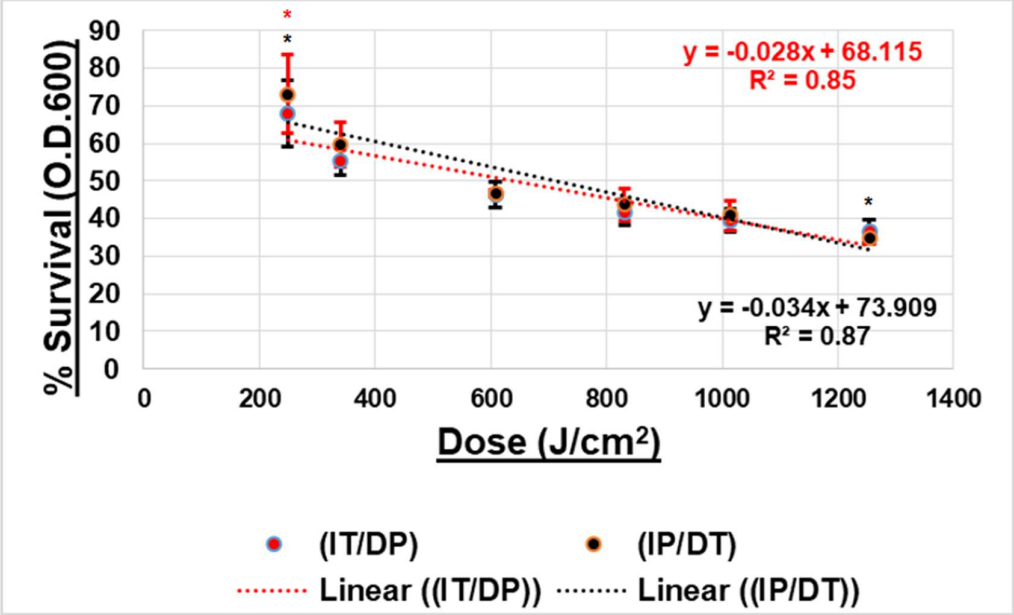

Figure 19: Scatter graph showing the effect of different 405 nm light doses on *S. mutans* planktonic culture viability. The light source delivery was in contact with the base of the well in a 96 well plate. Each dose was administrated in either (IT/DP) or (IP/DT) mode (n=3, mean +/- SD). Groups having an asterisk are statistically significantly different compared to each other (* is IT/DP, * is IP/DP) (* $P<0.05$). Significance level was set at $P \leq 0.05$. A linear regression curve fit was applied, showing the direct correlation between the light dose administered and *S. mutans* inhibition.

3.3.1.2.2 Colony counts for *S. mutans* and *E. faecalis* following 405 nm irradiation

Blue light Irradiation resulted in a 0.6 and 0.92 $\log_{10}$ (CFU/ml) reductions in bacterial growth when irradiating *S. mutans* planktonic cultures at doses of 340 and 831 J/cm^2, respectively. Both were significant reductions in colony counts compared with the non-irradiated controls (P=0.038 and P=0.002, respectively); nonetheless, there was no significant difference between colony counts using both doses. Furthermore, the 405 nm light exhibited a lower inhibitory effect on *E. faecalis* growth, as was also found when irradiating bacterial biofilm lawns directly from underneath the agar. Light treatment at 340 J/cm^2 exhibited minimal effects, only a 0.25 $\log_{10}$ (CFU/ml) reduction; however, at 831 J/cm^2 there was a significant 1.15 $\log_{10}$ (CFU/ml) reduction relative to the control (P=0.002) [see **Figure 20**].

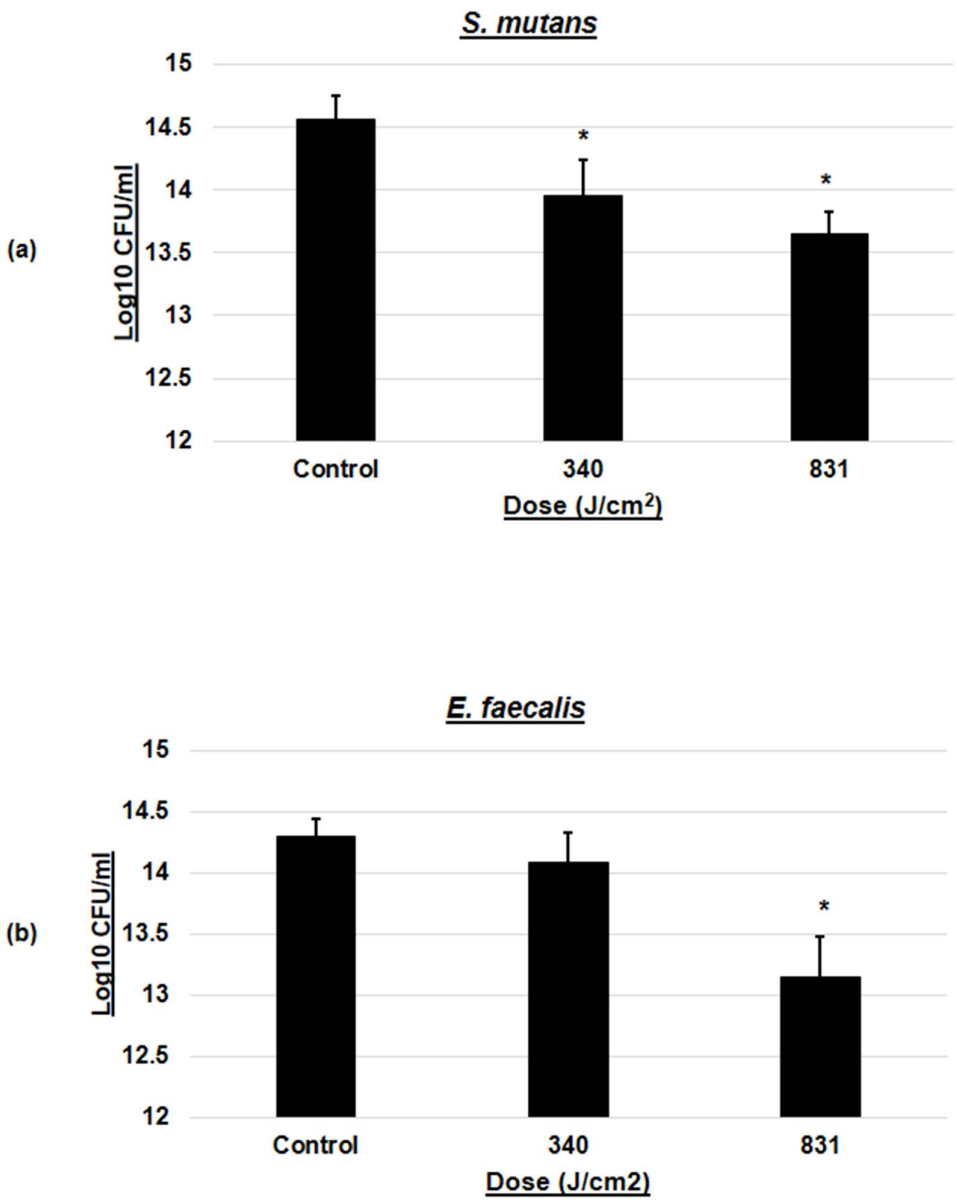

Figure 20: Bar charts showing mean +/- SD $\log_{10}$ (CFU/ml) reductions for both *S. mutans* **(a)** and *E. faecalis* **(b)** planktonic cultures in response to 405 nm light doses of 340 and 831 J/cm^2 (n=3). Irradiation parameters for 340 J/cm^2 were 378 mW/cm^2 for 15 minutes, while for 831 J/cm^2, they were 418 mW/cm^2 for 33 minutes. Asterisks represent a statistically significant difference in $\log_{10}$ (CFU/ml) reductions relative to the control (* $P<0.05$). Significance level set at $P \leq 0.05$.

3.3.1.3 Photodisinfection of *S. mutans* and *E. faecalis* biofilms

Image analysis revealed that delivering blue light (405 nm) at a dose of 340 J/cm^2 resulted in 48% ± 1.4 dead cells for *S. mutans* and 28% ± 2.2 for *E. faecalis* in biofilm cultures. Following exposure of biofilms to 830 J/cm^2, killing of 54% ± 6.4 of the *S. mutans* biofilm and 37% ± 1.8 of the *E. faecalis* biofilm was observed, respectively. There was no significant differences between the two doses investigated for each bacterial strain. However, the dose response relationship was still maintained. In addition, and consistent with all previous assay data, *E. faecalis* was more resistant to 405 nm light irradiation [see **Figure 21**].

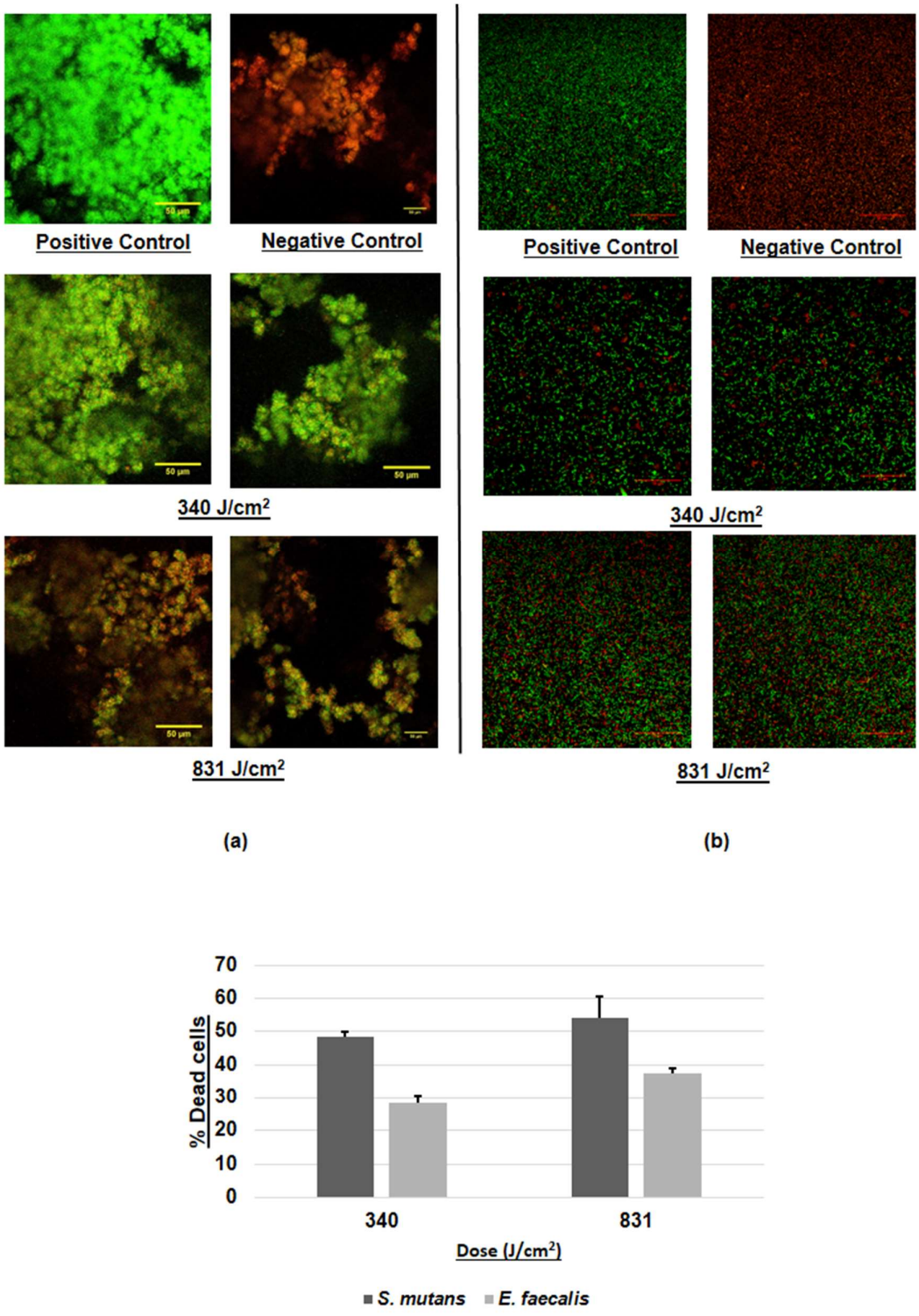

Figure 21: (a) Representative confocal microscope images demonstrating the effect of exposing *S. mutans* biofilms to 405 nm light. The dose of 340 J/cm^2 led to inhibition of 48% of the biofilm, while 831 J/cm^2 led to 54% dead cells. **(b)** Representative confocal microscope images demonstrating the effect of exposing *E. faecalis* biofilms to 405 nm light. The dose of 340 J/cm^2 led to inhibition of 28% of the biofilm, while 831 J/cm^2 led to 37% dead cells. Green represents live cells, while red represents dead cells **(c)** Bar charts showing the response of *S. mutans* and *E. faecalis* biofilms to 405 nm light doses of 340 and 831 J/cm^2 (n=3). Data is represented as the mean percentage of dead cells (+/- one SD from the mean) per biofilm. There was no statistical significant difference between the effect of the two experimented doses throughout each biofilm. Scale bar is 50 µm.

3.3.1.4 Discussion

Previous investigations have been conducted by Feuerstein *et al*. to determine the minimum inhibitory doses of three light sources on *P. gingivalis*, *F. nucleatum*, *S. mutans* and *E. faecalis*. The light sources used were a halogen lamp (400-500 nm), a plasma arc (450-480 nm) and an LED (450-480 nm). They concluded that the doses required to kill both *S. mutans* and *E. faecalis* were 7-10 times higher than the doses which were inhibitory for *P. gingivalis* and *F. nucleatum*. Interestingly, *S. mutans* and *E. faecalis* eradication was only demonstrated when using the plasma arc (450-480 nm). Inhibitory doses were 159 J/cm^2 and 212 J/cm^2 for *S. mutans* and *E. faecalis***,** respectively, when irradiating at 1 mm distance from the surface of the agar cultures **[42]**. However, results from the current study have shown that inhibition could be initiated using a 405 nm light source, at lower doses and at a greater irradiation distance. At approximately 11.5 mm irradiation distance (≈ 6.5 mm agar height plus 5 mm irradiation distance) and a dose of 110 J/cm^2, a ZOI could be initiated. This difference in outcomes compared with the literature could possibly be due to the difference in light source used. Needless to say, data from the current study confirms that *E. faecalis* is more resistant to this type of killing compared with *S. mutans* lawns. Notably, Henry *et al.* were not successful in obtaining any inhibition for both strains, using a 488-514 nm argon laser at a dose of 70 J/cm^2 **[239]**.

Data from the current study using OD survival percentages showed that 405 nm light was capable of inhibiting 27-65% of *S. mutans* planktonic cultures in a dose-response relationship. This finding was attributed to results obtained after investigating six blue

light doses ranging from 249 to 1254 J/cm^2. Furthermore, the CFU assay results showed that *E. faecalis* in planktonic suspensions showed less susceptibility towards 405 nm light compared with *S. mutans* planktonic cultures. However, this was only demonstrated at the 340 J/cm^2 but not 831 J/cm^2 doses. Light doses of 340 and 831 J/cm^2 led to a significant 0.6 and 0.92 $\log_{10}$ (CFU/ml) reductions for *S. mutans*. Conversely, 340 J/cm^2 irradiation resulted in a lower 0.25 $\log_{10}$ (CFU/ml) reduction for *E. faecalis*; however, 831 J/cm^2 irradiation resulted in a significant 1.15 $\log_{10}$ (CFU/ml) reduction – in comparison with data for *S. mutans*. These outcomes correspond with similar investigations within the literature. At a light dose as low as 5.73 J/cm^2, Hope *et al*. irradiated at 405 nm with an LED and did not show any inhibition for *E. faecalis* **[240]**. An LED array of the same wavelength inactivated most gram positive strains except for *E. faecalis* at doses of up to 72 J/cm^2 **[241].** Interestingly, *E. faecalis* was regarded as a control group in a study where a 405 nm tooth-care device did not affect the resistant strain at a slightly higher dose of 98.55 J/cm^2 **[242].** Maisch *et al.* examined the effect of combining 10% EDTA, photosan (a photosensitizer) and blue light on both *S. mutans* and *E. faecalis*. The combined treatment resulted in a more than 3 $\log_{10}$ (CFU/ml) reduction for both species, while exposure of bacteria to light alone - at a dose of 19.3 J/cm^2 - did not result in any killing **[243].** Using a similar approach, Steinberg *et al*. reported *S. mutans* viability response towards H_2O_2 and a xenon lamp (irradiation at 400-500 nm). The combined therapy was the only modality capable of achieving a 0.7-1 $\log_{10}$ (CFU/ml) reduction, while exposing the bacteria to light alone - 68 J/cm^2 - exerted no effect **[244]**.

Conversely, *S. mutans* planktonic cultures exposed to a xenon lamp (wavelengths 450-490 nm) at 686.4 J/cm^2 inhibited more than 90% of their growth in comparison with 22.88, 34.32 and 45.76 J/cm^2 which only induced inhibition when used alongside H_2O_2 **[245]**. Chebath-Taub *et al.* delivered a range of doses from a plasma arc lamp (400-500 nm); 68, 204, 340, 476 and 680 J/cm^2. All doses resulted in *S. mutans* CFU reductions; however, only significant reduction was shown at doses of 476 and 680 J/cm^2. Moreover, doses of 204, 340, 476 and 680 J/cm^2 significantly interfered with the re-formation of a new biofilm in a latent and delayed manner. This was manifested as an increase in the ratio of dead cells throughout the newly formed biofilm **[246]**. Subsequently, Cohen-Berneron *et al.* investigated three doses of 37, 112 and 262 J/cm^2 delivered from an LED (460-480 nm). Unexpectedly, these doses resulted in an increased re-growth generating a new biofilm; however, both viability and virulence factor production were impaired. Such effects were demonstrated as lower acidogenicity, aciduricity and less extracellular polysaccharide production. Their results suggested that lower doses might up-regulate genes associated with the bacteria entering into the biofilm phase **[247].**

With respect to *S. mutans* biofilms in the current study, results have demonstrated the ability of the 405 nm light to kill 48% (340 J/cm^2) and 54% (831 J/cm^2) of the bacterial cells residing within the 4 day old biofilm. The overall dose administered in De sousa *et al.*'s study falls within the same range. They irradiated *S. mutans* biofilms twice daily for 5 days (each at 72 J/cm^2). The total of 420 nm light doses of 720 J/cm^2 caused a significant reduction in extracellular polysaccharides as well as a two-fold decrease in the live biomass **[45]**. Conversely, Gomez *et al.* proposed that irradiating 12-16 hours

old *S. mutans* biofilms using a quantitative light-induced fluorescence device (380-440 nm/ peak 405 nm) could lead to significant reduction in the total biomass and viability at doses as low as 9.26 J/cm^2. This reduction was only observed in biofilms grown in sucrose free media **[46].** They indicated the same light source (9.26 J/cm^2) could significantly affect the metabolic activity of 12-16 hours old *S. mutans* biofilms grown without sucrose, with a further re-incubation period up to 6 hours. However, this pattern was different in biofilms supplemented with sucrose, resulting in lower metabolic activity at a recovery period lasting only 2 hours **[47]**. Moreover, twice daily irradiation of 5 day old biofilms (9.26 J/cm^2) resulted in a significant reduction of CFUs for *S. mutans* grown on human enamel and dentine specimens **[248],[53]**. Conversely, it was suggested that administrating H_2O_2 (30 mM) along with blue light at a dose of 68 J/cm^2 was able to reduce the viable population and ATP levels throughout an *S. mutans* biofilm. Administration of either blue light (34 and 68 J/cm^2) or H_2O_2 (3, 30 and 300 mM) - on their own - had negligible effects on *S. mutans* viability **[244]**. For *E. faecalis* biofilms, data from the current investigation revealed that 405 nm light could kill 28% and 37% of the biofilm when irradiated with a single dose of 340 and 831 J/cm^2, respectively. These findings are in contrast to those obtained by Imamura *et al.* who did not identify any form of growth inhibition using the same wavelength, even though irradiation was performed in closer proximity to the bacteria. Notably, they exposed *E. faecalis* using a radial laser tip with energy settings of up to 60 J **[249]**. Nonetheless, inhibition was possibly not initiated due to the lower irradiation parameters applied. Other studies have indicated that inhibition of *E. faecalis* biofilms is only achievable when a photosensitizer is used alongside blue light in order to obtain a synergistic

effect. Pileggi *et al.* irradiated samples pre-treated with eosin-y, rose Bengal or curcumin. They used a dental quartz-tungsten-halogen light source (380-500 nm). Although the actual exposure dose was not reported, the irradiance at the tip was 450 mW/cm^2 and the irradiation was performed for 240 seconds at a distance of 20 mm. It is therefore likely that the dose on the surface of the samples was considerably lower than 108 J/cm^2. Nonetheless, all three adjunctive treatments led to a significant decrease in viable counts within the biofilm **[250]**. Even though they employed lower irradiation parameters than the ones used in the current study, bacterial killing likely occurred at this dose as the light was supplemented with a photosensitizer.

There was a diversity among the range of inhibitory doses used in the current study. This difference between doses used to irradiate either bacterial lawns or planktonic cultures is notably due to the difference in the experimental set-up. Higher irradiation doses were required to kill bacteria in a broth medium compared with being exposed on the surface of solid agar. This was attributed to the scattering and absorption effects on the 405 nm light in the broth, thus affecting its penetration depth**.** The irradiation conditions are major modulating factors with regards to achieving disinfection **[251]**. Another reason for this issue may be due to the half-life of the ROS generated in response to light. Singlet oxygen has a very short half-life in aqueous solutions which is around 4 µs. Also, it has been estimated that the singlet oxygen can only diffuse a distance of 100 nm. So, it is essential to produce cytotoxic levels of singlet oxygen relative to the amount of photons absorbed **[252-254]**. Data presented here have shown that blue light was relatively more effective towards 3 days biofilms compared with planktonic killing. This was more evident when the dose of 340 J/ cm^2

was shown to have minimal effect on *E. faecalis* planktonic cultures (0.25 $\log_{10}$ (CFU/ml) reduction); however, it was capable of killing 28 % of cells within biofilms of the same strain. Notably, it is been reported that blue light can exert enhanced outcomes on bacteria in a biofilm phase even though bacteria in biofilms might express genes which enhance their resistance **[246],[247]**. Steinberg *et al*. demonstrated greater reductions in colony counts for *S. mutans* grown in biofilms compared with killing in planktonic cultures **[244]**. Therefore, it can be hypothesized that a growth inhibition effect was initiated on the surface of the agar due to the close proximity between the light source and the bacteria. Additionally, comparable outcomes were only obtainable at relatively higher doses to overcome the scattering effects of the broth in planktonic cultures. Irradiation of a bacterial lawn with bacteria growing in a single plane makes control of the dose easier compared with a bacterial suspension where bacteria will be at different distances from light source and therefore receive a range of different doses. However, more killing in 4 day biofilms was obtained due to the presence of a denser biomass residing at the bottom of the well notably in closer proximity to the light source. Overall this shows how various experimental set-ups affect the outcomes in studies using light.

It is worthwhile noting that only a few investigations studying the effects of blue light on cariogenic bacteria included temperature measurements **[42],[245]**. In the current investigation, the highest temperature reached at the BHI agar surface was 31.18°C, and 37.99°C in the BHI broth [see **Figure 12**]. These temperatures are within the normal range of growth for both *S. mutans* and *E. faecalis* **[233],[234]**, which excludes any potential photo-thermal killing effects.

3.3.2 Supplementation conditions affect bacterial response to blue light

3.3.2.1 Hemin increases the bacterial resistance to blue light

Supplementing the media with hemin at a concentration of 0.01 g/L did not affect the growth of both *S. mutans* and *E. faecalis*. Non irradiated controls of both species grew to similar $\log_{10}$ (CFU/ml) whether cultured in media supplemented with hemin or not [see **Figures 20** and **22**].

Overnight incubation in BHI broth containing hemin resulted in both *S. mutans* and *E. faecalis* being more resistant to blue light. Hemin supplementation also led to the loss of the dose response relationship exhibited in the previous experiments. Irradiation of *S. mutans* resulted in only 0.5 and 0.4 $\log_{10}$ (CFU/ml) reductions at doses of 340 and 830 J/cm^2, respectively. Interestingly, the 340 J/cm^2 $\log_{10}$ (CFU/ml) reduction was significant compared with the control group (P=0.002). Similarly, 340 J/cm^2 exposure did not have any effect on *E. faecalis* growth, while 830 J/cm^2 irradiation showed a limited 0.23 $\log_{10}$ (CFU/ml) reduction in growth [see **Figure 22**].

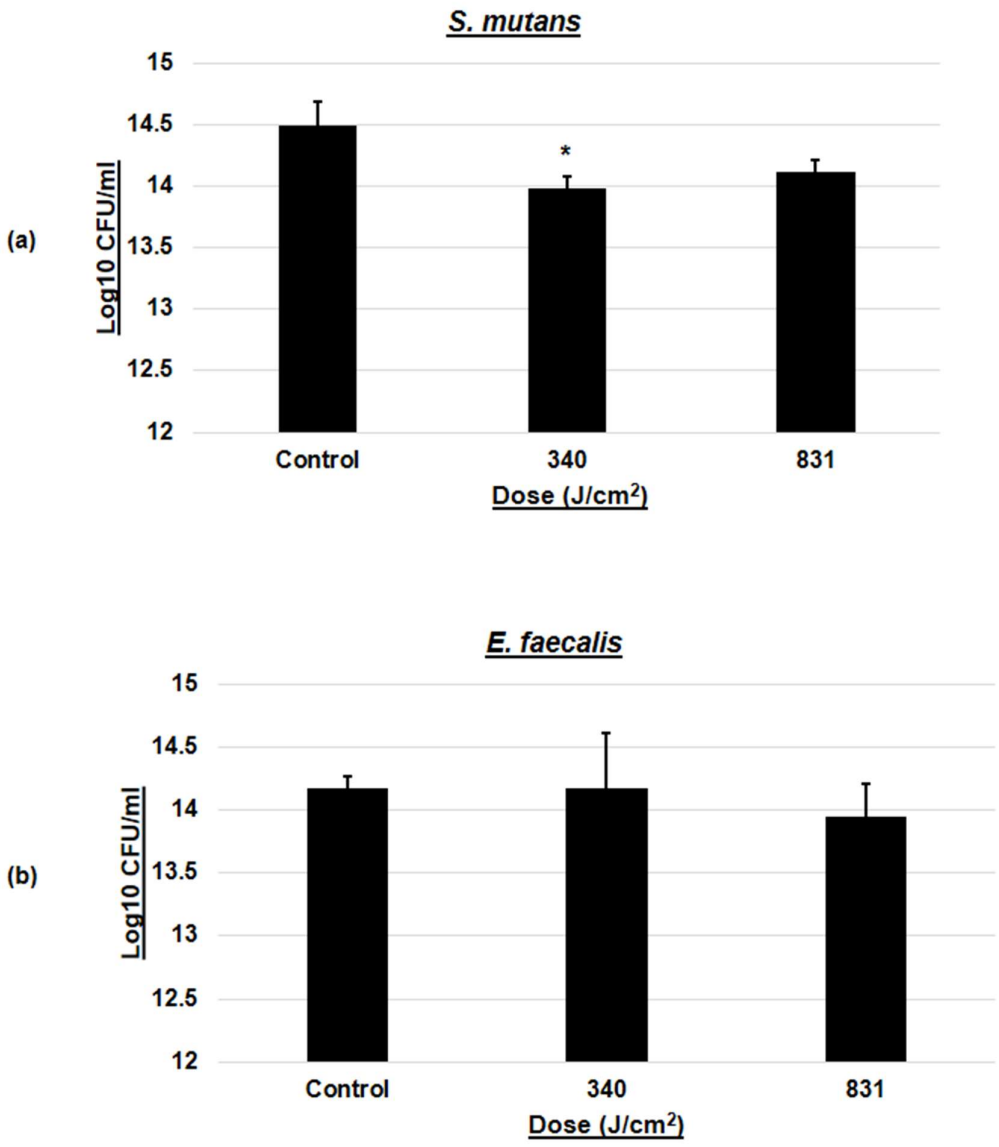

Figure 22: Bar charts showing the effect of hemin overnight supplementation on the log_{10} (CFU/ml) reductions for both *S. mutans* **(a)** and *E. faecalis* **(b)** planktonic cultures in response to 405 nm light doses of 340 and 831 J/cm^2 (n=3) (mean +/- SD). Asterisks represent a statistically significant difference in log_{10} (CFU/ml) reductions relative to the control (* P<0.05). Significance level was set at P ≤ 0.05

3.3.2.2 Aminolevulinic acid increases the susceptibility of *S. mutans* to blue light by elevating its flavin adenine dinucleotide content

Notably, ALA applied at the concentrations studied here (1 mg/ml) (6 mM) did not exert toxic effects on the bacteria of both strains studied [see **Figure 23**]. Pre-treatment of *S. mutans* planktonic cultures with ALA led to a significant 3 $\log_{10}$ (CFU/ml) reduction when light was then delivered at 831 J/cm^2. This significance difference was demonstrated in relation to the non-irradiated control samples (P=0.003), the samples treated only with ALA (P=0.016), as well as samples where only 340 J/cm^2 light was delivered (P=0.001). Conversely, ALA treatment alongside light dose of 340 J/cm^2 yielded a 1.6 $\log_{10}$ (CFU/ml) reduction, which was only statistically significant compared with its control where no ALA pre-treatment was applied (P=0.043). Light treatment on its own had minimal effect at irradiation of 340 J/cm^2 and resulted in 0.75 $\log_{10}$ (CFU/ml) reduction at a dose of 831 J/cm^2. Diversely, ALA did not potentiate the effect of the 405 nm light on *E. faecalis* as it did with *S. mutans*. Nonetheless, 831 J/cm^2 exposure resulted in a 1.12 $\log_{10}$ (CFU/ml) reduction, which was similar to the reduction obtained with the same dose applied alone. However, this reduction was statistically significant relative to the non-irradiated control group (P=0.047). As expected, 340 J/cm^2 exposure along with ALA supplementation led to only 0.45 $\log_{10}$ (CFU/ml) reduction. Without ALA pre-treatment, a light dose exposure of 340 J/cm^2 did not have any effect on growth, while 831 J/cm^2 exposure demonstrated a 0.95 $\log_{10}$ (CFU/ml) growth reduction [see **Figure 23**]. The current investigation showed a significant increase of FAD levels in *S. mutans* incubated with ALA compared with controls which did not receive ALA supplementation (P=0.02).

While *E. faecalis* controls had slightly higher FAD levels than *S. mutans*, pre-treatment with ALA did not have any significant effect on FAD content [see **Figure 24**].

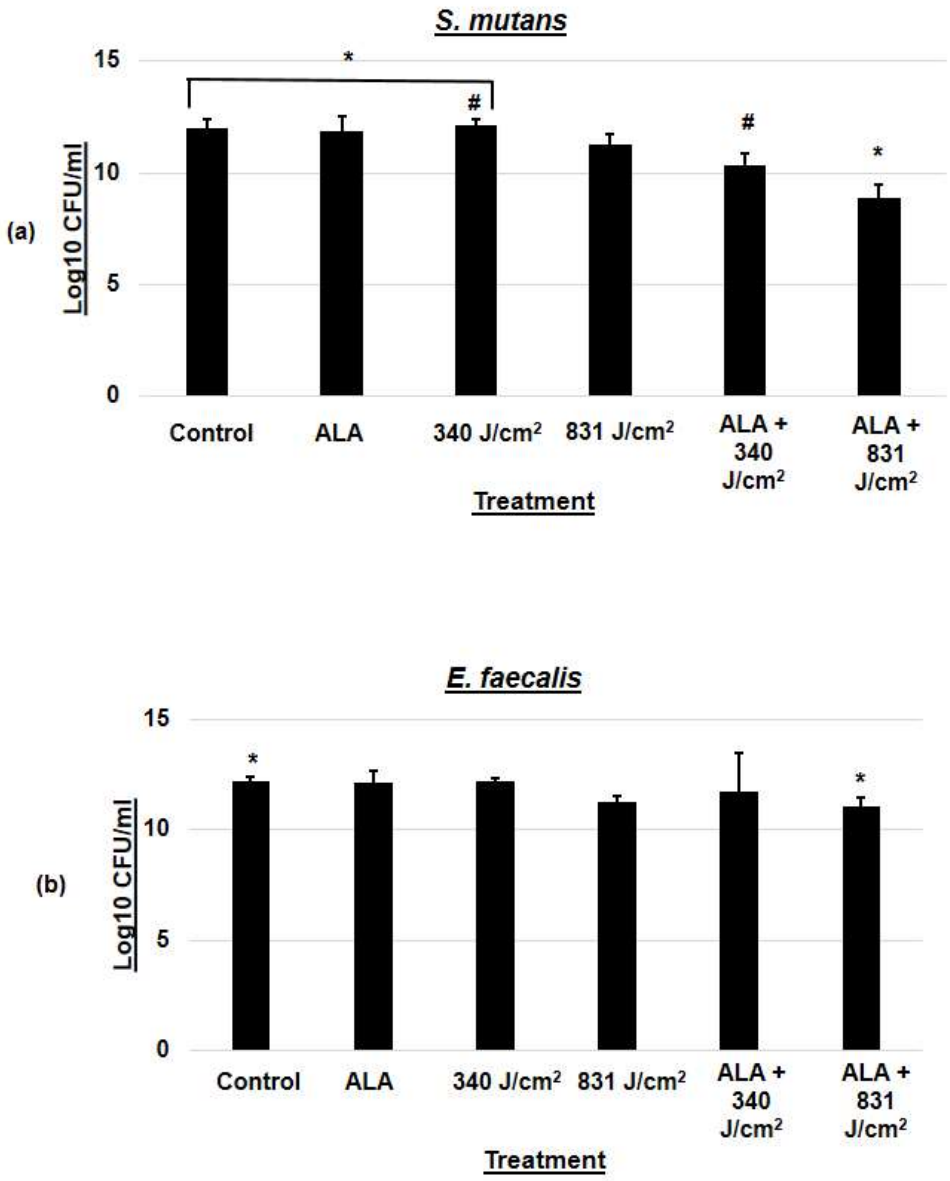

Figure 23: Bar charts showing the effect of ALA (1 mg/ml) pre-treatment on the log_{10} (CFU/ml) reductions for both *S. mutans* **(a)** and *E. faecalis* **(b)** planktonic cultures in response to 405 nm light doses of 340 and 831 J/cm^2 (n=3) (mean + /- SD). Experiments were carried out in duplicate. Similar symbols within each chart show statistically significant differences in log_{10} (CFU/ml) reductions induced by different treatments administrated (* and # $P<0.05$). Significance level was set at $P \leq 0.05$.

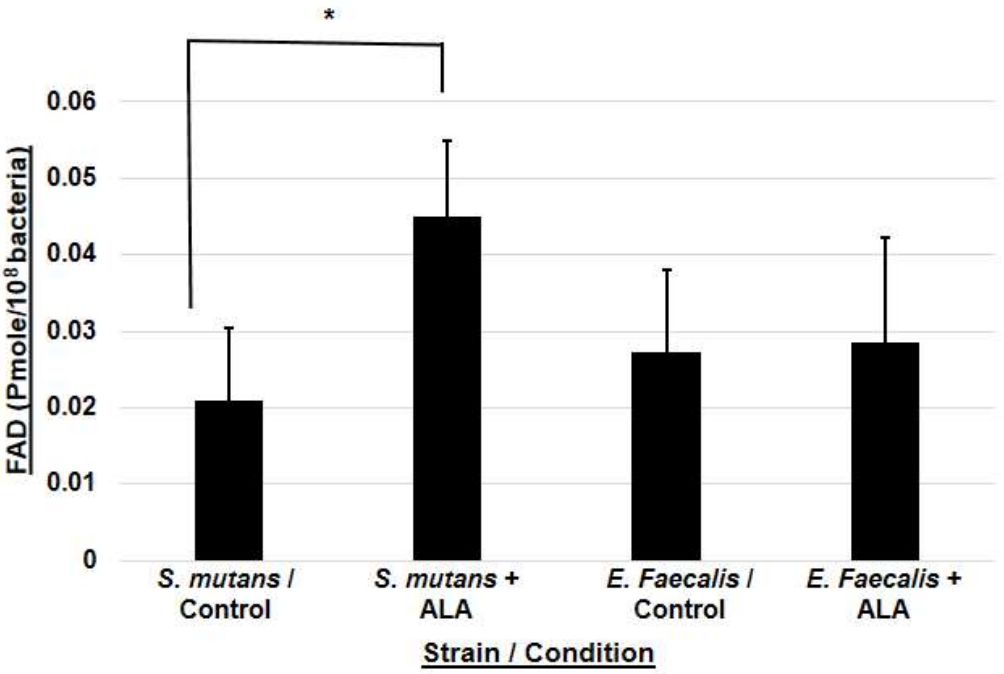

Figure 24: Bar charts showing the effect of ALA (1 mg/ml) pre-treatment on FAD content of *S. mutans* and *E. faecalis (*n=3) (mean +/- SD). Experiments were performed in triplicate. An asterisk indicate statistically significant differences in FAD content (* $P<0.05$). Significance level set at $P \leq 0.05$.

3.3.2.3 Discussion

To better elucidate the nature of the photodisinfection mechanism, a series of experiments were undertaken with the bacteria being incubated over-night with media supplemented with hemin. While this is not a photosensitizer, heme absorbs blue light **[255],[256]**, and hence the bacterial cells were washed prior to irradiation in BHI broth not supplemented with hemin. Hemin inhibits the production of ALA, and subsequently porphyrin synthesis, through a negative feedback control mechanism **[257],[258]**. Expectedly, for *S. mutans*, the 405 nm blue light resulted in 0.5 $\log_{10}$ (CFU/ml) reduction in bacterial count at a dose of 340 J/cm^2 and 0.4 $\log_{10}$ (CFU/ml) reduction at 830 J/cm^2. Since ALA supplementation enhanced the antibacterial effect of light exposure on *S. mutans*, therefore supplementing the same species with hemin should limit the production of porphyrins. Subsequently, the capability of light to kill bacteria occurred up to a certain threshold after which higher doses had no further effects. With regards to *E. faecalis*, a more resistant pattern was apparent where the 340 J/cm^2 exposure did not have any antimicrobial effect while 830 J/cm^2 exposure only showed a 0.23 $\log_{10}$ (CFU/ml) reduction. Notably, this response fits well with the failure of ALA to potentiate the inhibitory effect of blue light.

Earlier reports in the literature have stated that heme/hemin supplementation could have a toxic effect on bacteria without the application of light. Nitzan *et al.* reported that iron-containing hemin (0.01 g/L) binds to *S. aureus* rapidly, affecting its growth. This was evidenced by bacterial monitoring which indicated cessation of glucose uptake and production of CO_2. Conversely, other bacterial species such as *E. coli* and *P.*

aeruginosa were not reportedly affected by hemin even at ten times higher concentrations of supplementation. However, they attributed the toxic effect of hemin to its iron content. Notably, the antibacterial effect of hemin is not due to singlet oxygen or hydroxyl radical formation and this was confirmed by adding singlet oxygen and hydroxyl radicals' scavengers/quenchers which still did not stop the inhibitory effect of hemin on bacterial growth. Furthermore, thiol inhibited hemin's antibacterial effect although it did not have any impact on hindering the photosensitization process generated by metal-free porphyrins. These results supported the hypothesis that hemin's toxic effects are due to an oxidation-reduction process linked with a peroxide, since hemin may act on a prosthetic group in the peroxidative enzymes **[259-261]**. Conversely, hemin (0.006 g/L) showed opposite effects on lactic acid-generating bacteria, such as *L. lactis*, enhancing its growth and glucose utilization. H_2O_2 levels were also supressed after hemin addition; however, no catalase activity was detected **[262]**.

Results presented here have shown that supplementing the growth media with hemin at a concentration of 0.01 g/L did not have a negative influence on the growth of both *S. mutans* and *E. faecalis* [see **Figures 20** and **22**]. Furthermore, supplementaion increased their resistance towards the 405 nm light. Supported by results from the ALA investigations, it could be hypothesized that hemin initiated the negative feedback control for *S. mutans* and therefore restricted the photo-absorbers content. Nonetheless, there might be other explanations for why this phenomenon occurred in *S. mutans*. It has been reported that *S. mutans* expresses the SOD enzyme which has strong anti-oxidative potential. Iron can act as a co-factor in the formation of the SOD

enzyme **[245],[153]**. It is conceivable that the enzyme was highly expressed given that iron was supplemented through the hemin in the broth overnight. Another possibility is that iron was bound to the Dpr protein which sequestrates iron, preventing further hydroxyl radical formation through the Fenton reaction **[140],[158]**. The role of Dpr was further confirmed through a study by Yamamoto *et al. S. mutans'* intracellular iron content was lower when cells were transferred from anaerobic to aerobic growth conditions. This was accompanied by the synthesis of Dpr during this transition, confirming its role in iron binding and subsequent aero-tolerance **[162]**. With respect to *E. faecalis*, the results obtained from the hemin experiments were not particularly surprising, taking into consideration its enduring resistance even after pre-incubating it with ALA. However, if ALA at the concentration applied (6 mM) failed initially to produce more photo-absorbers, then there are two possible explanations: i) It is required at a higher concentration to initiate generating porphyrins relative to the ones reported in the literature **[143]** and ii) the strain studied here has not acquired the enzymatic/metabolic pathway for synthesizing porphyrins **[240],[242]** similar to these produced in *S. mutans*. However, in either case, supplementing *E. Faecalis* with hemin enhanced their resistance to oxidative stress. This could have occurred due to the emergence of catalase activity. Early studies reported the detection of catalase activity once hemin was added to *E. faecalis* grown on agar **[263]**. Furthermore, when supplemented with hemin, *E. faecalis* highly expressed features of both cytochrome bd in the cell membrane and KatA in the cytoplasm. Cytochrome bd is an essential protein for full aerobic endurance, while KatA is a gene encoding a heme-B containing catalase **[151]**. Therefore, and with regards to the outcomes obtained from the current

investigation, blue light might have exhibited a marginal inhibitory effect on *S. mutans* grown in hemin because it only expressed SOD, while *E. faecalis* expressed both cytochrome bd and catalase [see **Figure 25**].

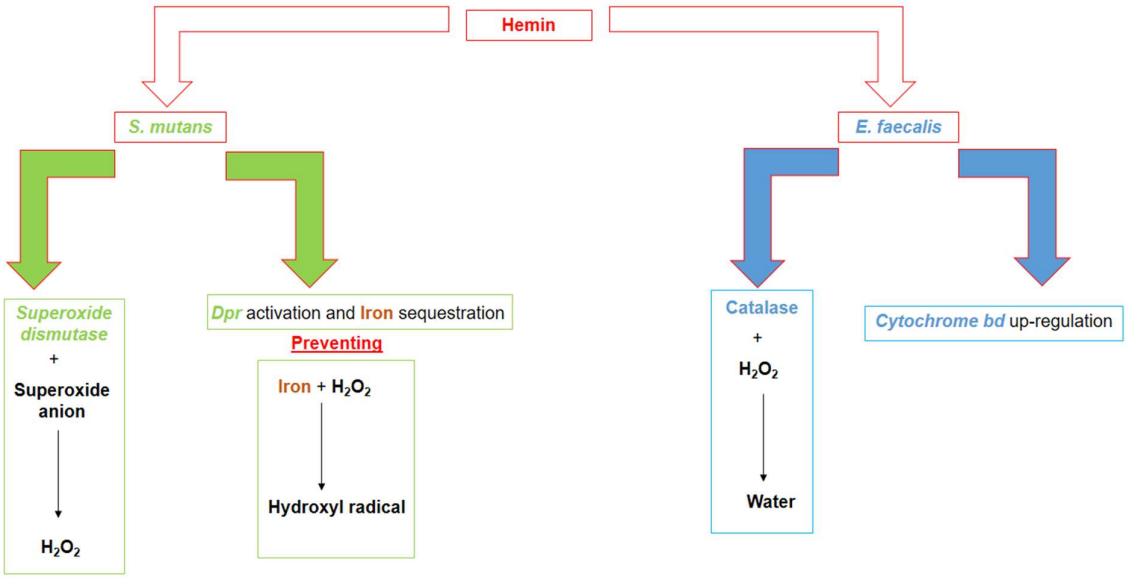

Figure 25: Schematic diagram showing the effects of hemin supplementation on both *S. mutans* and *E. facealis.* Iron in hemin leads to the activation of superoxide dismutase enzyme in *S. mutans*, converting superoxide anions to hydrogen peroxide. Iron also leads to the activation of the *Dpr* protein, sequestrating free iron and preventing the formation of hydroxyl radicals through the Fenton reaction. In *E. faecalis*, hemin leads to the activation of catalase and *cytochrome bd,* enhancing its aerobic tolerance.

To further charachterise the nature of the photodisinfection mechanism and potentially boost its effectiveness, a set of experiments were performed whereby *S. mutans* and *E. faecalis* planktonic cultures were pre-treated with ALA before blue light irradiation. ALA is the first compound in the porphyrin synthesis pathway **[34]**. ALA is not a known photosensitiser **[264]** but is a heme-protein/cytochrome intrinsic precursor **[169].** Hsieh *et al.* reported that the combination of ALA and an LED red light (635 nm) was capable of inducing significant reduction in the growth of both *S. aureus* and *P. aeruginosa*. They studied a range of concentrations of ALA at 1, 2.5, 5 and 10 mM. However, higher concentrations of ALA (5-10 mM) - on its own- showed toxicity against *P. aeruginosa*, contrary to *S. aureus* which survived at all concentrations of ALA before administration of the red light **[146]**. The same treatment modality resulted in a remarkable inhibition of the survival in antibiotic resistant staphylococcal biofilms of *S. aureus* and *S. epidermidis*. The uptake of ALA and subsequent formation of protoporphyrin 9 was confirmed by fluorescence microscopy. Irradiation from a red semiconductor laser (635 nm) did not exert any effect alone for doses up to 300 J/cm^2. Similarly, 40 mM of ALA did not exhibit any toxicity towards the biofilms **[145]**. Results from the current investigation showed that incubation of *S. mutans* planktonic cultures with ALA (6 mM) prior to 405 nm light irradiation led to a statistically significant 1.6 and 3 $\log_{10}$ (CFU/ml) reductions. These outcomes agreed with Saeed *et al.*'s which indicated that the group pre-treated with ALA showed the highest bacterial inhibition, even compared with chlorhexidine and sodium hypochlorite treatment. Notably however, while they used red light LED (635 nm), the irradiation parameters were not described other than for the exposure time of 30 seconds. Additionally, the ALA

concentration they used (125 mM) was much higher **[148]** than the one used here. Results presented here indicated that pre-treatment of *E. faecalis* cultures with ALA did not necessarily potentiate the inhibitory effect of the blue light. This was demonstrated as only 0.45 and 1.12 $\log_{10}$ (CFU/ml) reductions were achieved. When Nitzan *et al.* investigated the effect of ALA treatment (380 mM) on a wide range of Gram positive and Gram negative bacteria, *E. faecalis* was the only strain manifesting resistance to blue light (407–420 nm) at doses of 50 and 100 J/cm^2. The resulting porphyrin synthesis after ALA uptake was validated by high performance liquid chromatography; however, all the strains exhibited an obvious increased porphyrin yield except for *E. faecalis*. Moreover, *E. faecalis* viability was not affected by ALA as a treatment on its own even at this relatively high concentration **[143]**. In contrast, Liu *et al.* demonstrated that pre-treatment with either ALA or ALA methyl ester at a concentration of 10 mM exhibited an enhanced light eradication potential. *E. faecalis* was severely affected by 5.22 and 4.91 $\log_{10}$ (CFU/ml) reductions after pre-incubation with ALA and ALA methyl ester, respectively. The treatment was combined with a 633 nm red LED at a dose of 288 J/cm^2 **[149]**. Although porphyrins maximally absorb in the blue spectrum of light and ALA is the precursor of porphyrin production **[31],[35]**, previous investigations rely on red light after incubating bacterial cells with ALA. Interestingly, bacterial growth inhibition was successful which suggests that there might be another chromophore along with porphyrins and this could possibly be cytochromes **[265]**.

An important observation was noted during all ALA experiments related to a minor difference in the timing of plating the samples. Notably, the same light source used in

the current investigation demonstrated significant inhibitory effects on *S. mutans* when applied without ALA; however, the CFU assay was undertaken on the following day after re-incubating the irradiated sample for 24 hours. Conversely, when the CFU assay was performed on the same day directly after light irradiation in the ALA investigations, the light dose of 340 J/cm^2 demonstrated minimal inhibitory effects, while 831 J/cm^2 showed marginally less effect compared with the re-incubated samples. These data are supported by the reports indicating the extremely short half-life of singlet oxygen as well as its limited diffusion potential in aqueous solutions [**252-254**].

The current investigation showed a significant increase in FAD levels in *S. mutans* incubated with ALA [see **Figure 24**]. This was accompanied by a concomitant increase in *S. mutans* susceptibility *to* 405 nm blue light. Conversely, FAD levels did not change after ALA treatment in E*. faecalis*. The presence of flavo-enzymes in *E. faecalis* and their dependency on FAD has not been fully characterised **[266],[267]**. While there are several FAD constituents in *S. mutans*, results suggest that Nox-1 may act as a blue light chromophore in comparison with Nox-2 which is not simulated by FAD and generates water. Nox-1 is triggered by increasing FAD concentrations and generates H_2O_2 **[154].** Not only does FAD absorb blue light, but also produces ROS production which is essential for the inhibitory effects of light to occur. Light absorption within a chromophore does not necessarily mean that bacterial killing will take place. The chromophore has to be situated within the cell at the correct biochemical orientation for ROS production after light excitation. Previously, blue light did not show any signs of inhibition of *S. agalactiae* growth although it contains granadaene - a blue light

chromophore. Furthermore, exogenous FAD only minimally enhanced the inhibitory effects of blue light. **[268],[230].** This also highlights the issue with applying an exogenous photosensitizer, it is not clear whether ROS is generated inside the cell or generated in the media post irradiation to cause bacterial killing **[268]**.

The aero-tolerance of different bacterial species is another key factor relating to the success of photodisinfection. Notably, different bacterial species express various types and levels of chromophores as well as different antioxidant potentials **[28],[269].** It should be noted that knocking out both Nox-1 and AhpC genes did not previously affect the growth of *S. mutans* in the presence of exogenous H_2O_2. This suggests that there is either an undiscovered scavenging system **[160]** or that AhpC is only activated when an H_2O_2 gradient needs to be maintained **[270].** Moreover, H_2O_2 forming NADH oxidases are mainly found in species possessing cytochromes and heme-proteins **[154].** The significant elevation in FAD levels of *S. mutans* suggests an increase in the total redox state and ROS generation, which in turn support previous reports which indicate that bacterial species which have a blocked heme synthetic pathways can still maintain the genetic antecedents to generate membrane bound electron transport **[165].** Notably, *S. mutans* possess an incomplete TCA cycle **[156],[157]**, and it has been reported that bacteria having incomplete TCA cycle can synthesise and utilise ALA through alternative pathways **[271].** However, concentrations and distributions of intermediate compounds in the heme bio-synesthetic pathway differ according to environmental conditions and between species. In all cases the pathway is directly or indirectly linked to both the TCA cycle and cytochrome synthesis. Lactic acid produced can also reverse the function of the TCA cycle from catabolic to anabolic pathways

promoting cytochrome synthesis **[272].** This indicates that *S. mutans* can sustain aerobic metabolism amongst tolerable levels of H_2O_2.

3.4 Effects of blue light irradiation on human dental pulp cellular responses

3.4.1 Cell growth and proliferation

To investigate the effects of blue light on DPCs growth and proliferation, irradiations were performed on days 1 and 3. DPCs growth and proliferation were investigated 24 hours post initial irradiation (day 2 /cells receiving one exposure) as well as 72 hours post initial irradiation (day 4 /cells receiving two exposures). DPCs growth was investigated using the Alamar blue assay, while proliferation was investigated using the BrdU assay [refer to **sections 2.4.3.1** and **2.4.3.2**]. Alamar blue assay results showed that 405 nm blue light irradiation at range of doses appeared to negatively affect DPCs growth in a dose-dependent manner as a decreasing trend was identified. Doses administrated decreased DPCs growth by 11 – 20 % at day 2 as well as by 26 - 35 % at day 4. Notably however, no statistically significant differences were detected between different exposure groups at each time point [see **Figure 26**]. The BrdU proliferation assay results confirmed that blue light irradiation has inhibitory effects on DPCs proliferation rates, and the dose dependant trend was still evident. At day 2, the doses of 4, 5 and 6 J/cm^2 significantly decreased the cell proliferation rates compared with the non-irradiated control (P=0.039, P=0.003 and P=0.001 respectively). At day 4 the same dose-response inhibitory trend was observed, and the 4, 5 and 6 J/cm^2 groups were significantly lower than the control group (P<0.001). Notably, for the 2 J/cm^2 exposure group, proliferation rates continued to increase from day 2 till the day

4 point, as opposed to the 4, 5 and 6 J/cm^2 groups whose absorbance values were relatively similar at both time points [see **Figure 27**].

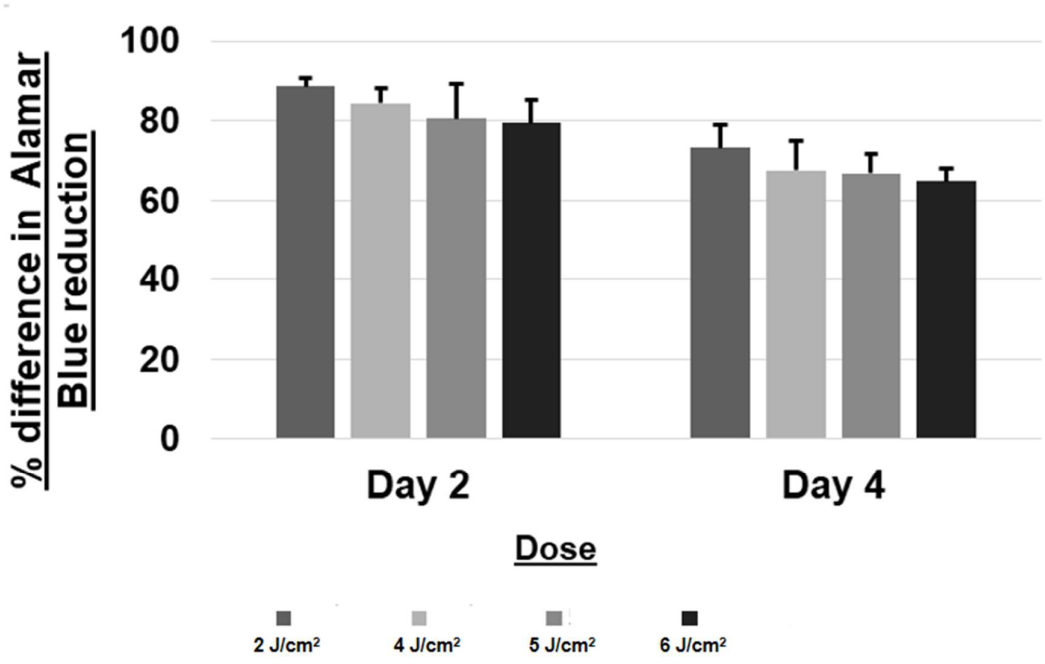

Figure 26: Bar chart showing the effect of 405 nm light irradiation on growth of DPCs (n=3) (mean +/- SD). Experiments were performed in duplicate. Alamar blue assay was carried out after 24 hours (day 2 / cells receiving 1 exposure) and 72 hours (day 4 / cells receiving 2 exposures), and the percentages of Alamar blue dye reduction were calculated relative to the non-irradiated controls. There was no statistically significant differences between any of the doses administrated on cell viability at each time point. Significance level set at $p \leq 0.05$.

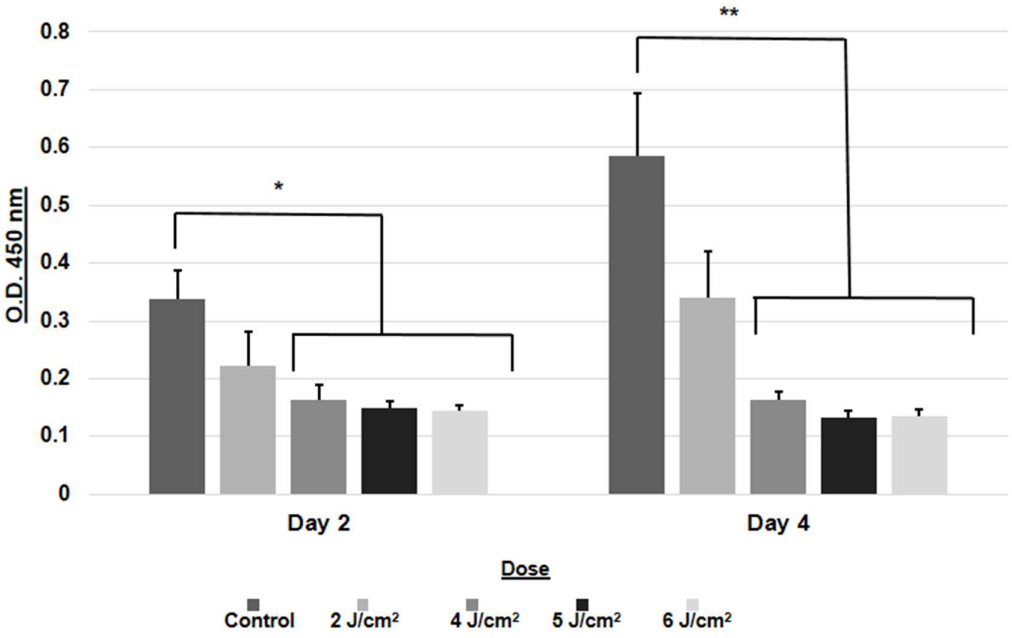

Figure 27: Bar chart showing the effect of 405 nm light on proliferation rates of DPCs (n=3) (mean +/- SD). Experiments were carried out in duplicate. BrdU assay was carried out after 24 hours (day 2 for cells receiving 1 exposure) and 72 hours (day 4 for cells receiving 2 exposures), and absorbance for samples was read at 450 nm. Asterisks represent statistically significant differences compared to the non-irradiated controls (*P<0.05) (** P<0.001). A Bonferroni post hoc test was applied for pairwise comparisons. Significance level set at $p \leq 0.05$.

3.4.2 Odontoblastic differentiation

Since ALP and DMP1 levels are central markers to odontoblastic differentiation of DPCs, they were both investigated at day 3 (cells receiving 1 exposure) and day 5 (cells receiving 2 exposures) [refer to **sections 2.4.3.3** and **2.4.3.4**]. With regards to the ALP activity, at day 3 all doses investigated lead to an increase in ALP levels compared with the non-irradiated control except for 2 J/cm^2. A dose response trend was also observed, and the stimulatory effects of 5 and 6 J/cm^2 were both significantly higher than that of 2 J/cm^2 (P=0.029 and P=0.004, respectively). At day 5, samples irradiated with blue light maintained higher ALP levels relative to the non-irradiated control although the stimulation level was lower than that observed at day 3. ALP levels in samples irradiated with 4 J/cm^2 were comparable to the control group, whereas 6 J/cm^2 resulted in the greatest stimulation (20% higher than the control); however, there were no statistically significant differences observed. Similarly, blue light irradiation enhanced DMP1 levels at day 3, and the doses of 2 and 6 J/cm^2 lead to the highest stimulation compared to 4 and 5 J/cm^2. The effects of 2 J/cm^2 were significantly higher compared with the 4 J/cm^2 (P=0.024) exposure, while there was no significant differences between DMP1 levels in the 4, 5 and 6 J/cm^2 exposure groups. At day 5 the stimulation level was lower than that detected for day 3 at all doses applied except for the 6 J/cm^2 group, where DMP1 levels continued to increase and were highly statistically significantly compared with the group irradiated with 4 J/cm^2 (P=0.002) [see **Figure 28** and **Table 4**].

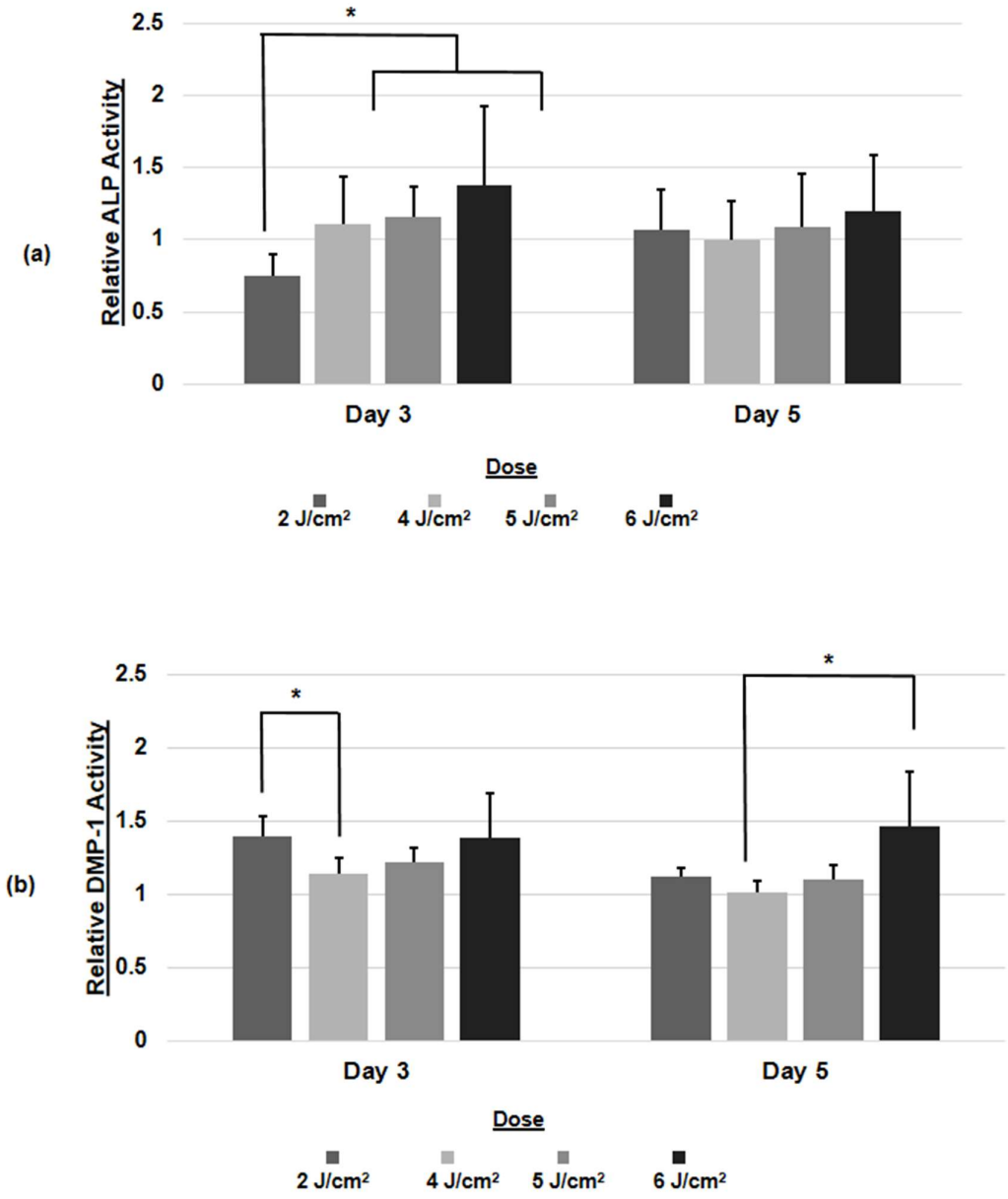

Figure 28: Bar chart showing the effect of 405 nm light on **(a)**Alkaline phosphatase (ALP) and **(b)**Dentine matrix protein-1 (DMP1) levels in DPCs (n=3) (mean +/- SD). Experiments were carried out in duplicates. ALP and DMP1 levels were investigated at day 3 (cells receiving 1 exposure) and day 5 (cells receiving 2 exposure). ALP activity was calculated in (*Unit/ml)* and DMP1 activity was calculated in (*pg/ml)* then values were relativized to the control (non-irradiated) wells in each plate. Asterisks show statistically significant differences in ALP or DMP1 levels (* P<0.05). Significance level set at $p \leq 0.05$.

Alkaline phosphatase and Dentine matrix protein-1 levels

ALP (Unit/ml) X 10^{-4}		
Dose (J/cm^2)	**Day 3**	**Day 5**
0	2.36 ± 1.56	5.14 ± 1.91
2	2.18 ± 1.45	5.19 ± 1.08
4	2.49 ± 1.85	4.85 ± 1.154
5	2.57 ± 1.42	5.34 ± 0.96
6	2.60 ± 0.78	5.93 ± 0.76
DMP1 (pg/ml)		
Dose (J/cm^2)	**Day 3**	**Day 5**
0	76.25 ± 45.08	64.42 ± 12.59
2	107.99 ± 43.22	68.19 ± 12.67
4	86.02 ± 47.86	63.90 ± 17.30
5	93.08 ± 48.49	77.35 ± 16.46
6	99.87 ± 58.99	88.40 ± 26.76

Table 4: Mean +/- SD values of of ALP (Unit/ml) and DMP-1 (pg/ml) levels in DPCs receiving no blue light as well as DPCs irradiated with 2, 4, 5 and 6 J/cm^2 (n=3). ALP and DMP1 levels were investigated at day 3 (cells receiving 1 exposure) and day 5 (cells receiving 2 exposure). Experiments were carried out in duplicates.

To evaluate the effects of 405 nm blue light on the mineralised nodule formation of DPCs, alizarin red staining was performed at days 7, 14 and 21. Cells were exposed to blue light on alternate days for 5 days (*i.e.* 3 irradiations) [refer to **section 2.4.3.5**]. Alizarin red staining showed that an exposure rate of 3 irradiations on alternate days was sufficient to stimulate mineralised nodules formation at all doses investigated. At day 7, the doses of 2, 4 and 6 J/cm^2 produced similar responses as opposed to 5 J/cm^2 which lead to the lowest degree of stimulation throughout blue light irradiated samples. At day 14, the 2 J/cm^2 group resulted in the highest mineralised nodules formation, followed by 6, 4 and 5 J/cm^2. The alizarin red stain in the 2 J/cm^2 was statistically significantly higher than the non-irradiated control at days 7 and 14 ($P=0.039$ and $P=0.017$, respectively). At day 21, 2 and 4 J/cm^2 lead the highest mineralised nodules formation, which were significant compared to the control ($P<0.001$ and $P=0.002$, respectively). Even though 5 and 6 J/cm^2 resulted in more alizarin red stain, they did not show any significant difference relative to the control [see **Figure 29**].

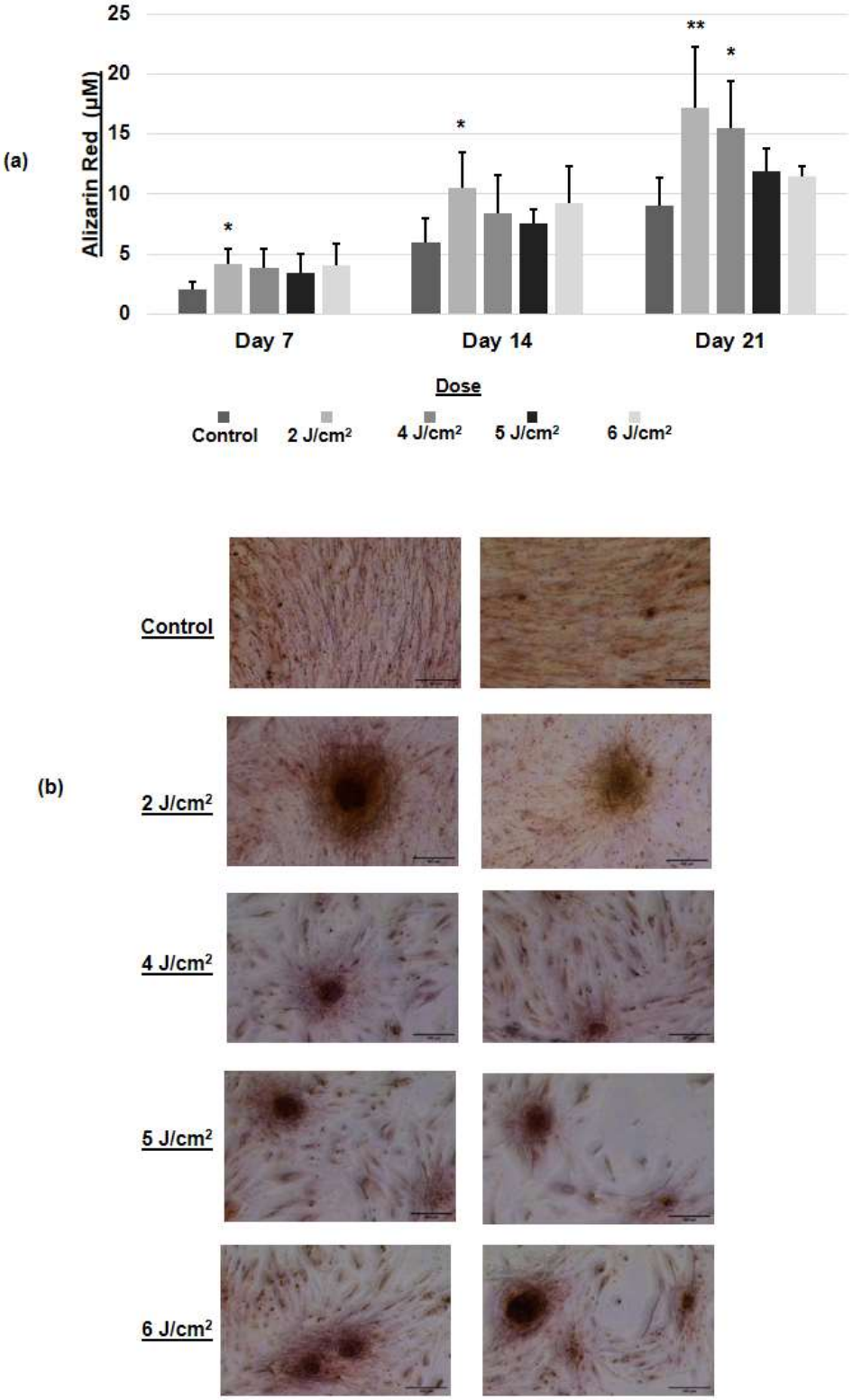

Figure 29: (a) Bar chart showing the effect of 3 irradiations (on alternate days) of blue light in stimulating mineralized nodule formation in DPCs assayed at days 7, 14 and 21 (n=3) (mean +/- SD). Experiments were performed in duplicate. Cultures were stained with alizarin red, after which alizarin red stain extraction and quantification (µM) was performed [refer to **Section 2.4.3.5**]. Asterisks represent statistically significant differences relative to its respective non-irradiated control (*P<0.05) (** P<0.001). Significance level set at $p \leq 0.05$. **(b)** Representative light microscope images of DPCs mineralised nodules stained with alizarin red at day 21 of odontoblastic differentiation. Control wells were non-irradiated, while wells receiving 405 nm light irradiation were exposed to 2, 4, 5 and 6 J/cm^2. Scale bar is 400 µm.

The effect of extended light irradiation (every other day beyond the initial 3 irradiations) on mineralized nodules formation was also investigated for the full duration of the 14 (6 irradiations) and 21 days (9 irradiations) time points. Extended blue light irradiation marginally stimulated mineral deposition at day 14 (6 irradiations) at all doses studied. However, this stimulation was much lower compared to cells receiving only 3 irradiations [see **Figures 29** and **30**]. Conversely, extended irradiation resulted in inhibitory effects at all doses at day 21 (9 irradiations), and the dose of 6 J/cm^2 resulted in statistically significantly lower mineralised nodule formation compared with the control group (P=0.027) [see **Figure 30**].

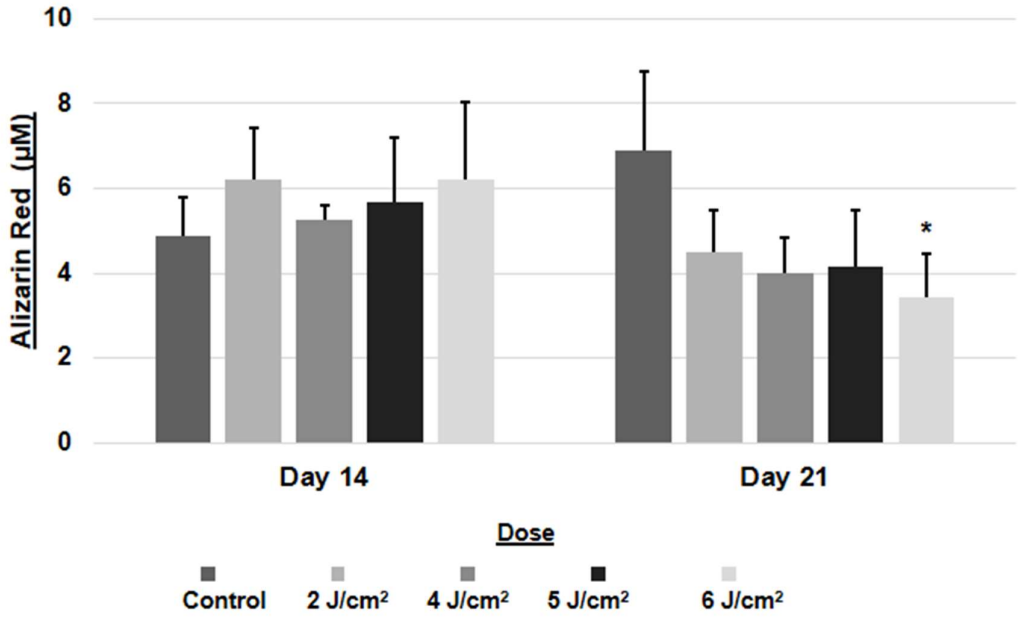

Figure 30: Bar chart showing the effect of 405 nm light irradiation on mineralized nodule formation in DPCs cultures at days 14 and 21. In order to study the effect of extended light irradiation (every other day beyond the initial 3 irradiations), cells were exposed to blue light every other day for 14 days (6 irradiations) or 21 days (9 irradiations) (n=3) (mean +/- SD). Experiments were undertaken in duplicate. Cultures were stained with alizarin red stain, after which the stain extraction and quantification (µM) was performed. Asterisks represent statistically significant differences compared with the respective non-irradiated control (* P<0.05). Significance level set at $p \leq 0.05$.

The expression of OCN - another important marker for DPCs odontoblastic differentiation - was investigated relying on PCR analysis. OCN expression was investigated on day 7 after DPCs were exposed to 405 nm blue light on alternate days for 5 days (*i.e.* 3 irradiations) [refer to **sections 2.4.3.6**]. Semi-quantitative PCR analysis showed that blue light irradiation at doses of 2 and 4 J/cm^2 up-regulated the expression of OCN in a dose-dependent manner. The effects of 4 J/cm^2 were statistically higher compared with that of the 2 J/cm^2 exposure (P=0.05) [see **Figure 31**].

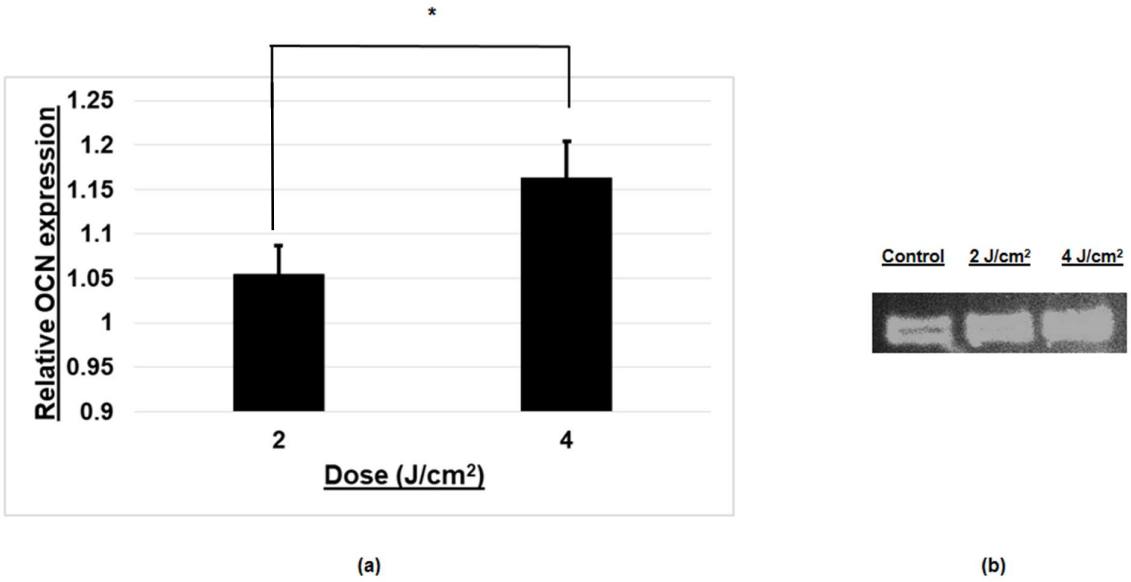

Figure 31: (a) Bar chart showing the effect of 3 irradiations (on alternate days) of 405 nm light on the expression of OCN. Expression values were normalized to GAPDH, then values were relativized to the non-irradiated controls (n=3) (mean +/- SD). The RNA was collected from 3 samples (per group in each repeat) and pooled to a single sample. An asterisk represent a statistically significant difference in the expression of OCN (* P<0.05). Significance level set at p ≤ 0.05. **(b)** Representative image of OCN agarose gel bands of non-irradiated controls as well as cells receiving blue light doses of 2 and 4 J/cm^2.

3.4.3 Discussion

The biomodulatory effects of blue light on the mineralisation processes of MSCs have only recently been investigated **[273]**. It has been reported that a blue light LED exposure could enhance the mineralisation potential of MSCs at a range of doses from 1 to 6 J/cm^2. However, investigations published in the literature have mostly focused on adapting a fixed irradiance parameter of 100 mW/cm^2 and variable irradiation times **[77],[78]**. Interestingly, R/NIR wavelengths have also shown stimulatory effects on MSCs mineralisation when applying light doses in the same range. However, R/NIR wavelengths have been more extensively studied and there has been several trends identified relating to the Arndt Schultz model for biphasic dose-dependent effects. Additionally, reciprocity between irradiance and irradiation times was evident between different studies. Moreover, enhancement of the mineralisation potential of MSCs using R/NIR light was reported to occur with either fewer exposures at higher irradiance parameters (shorter exposure times) or increased treatments at lower irradiance parameters (longer exposure times). Notably, the opposite trend was noted for blue light irradiation. Investigations adapting an irradiance of 100 mW/cm^2 required irradiation every other day for up to 28 days, while one study using an irradiance of 16 mW/cm^2 required only five exposures every two days **[273]**. Consequently, the irradiance setting of 57.7 mW/cm^2 was selected for the current investigation, irradiating DPCs for 35, 69, 90 or 104 seconds in order to deliver blue light doses of 2, 4, 5 and 6 J/cm^2.

Results from the current investigation showed that blue light inhibits DPCs proliferation; however, enhances its odontoblastic differentiation processes. The decline in proliferation occurred in a dose-response manner. The 2 J/cm^2 was the only group- among the irradiated groups- that showed continued increase in proliferation rates on day 4, unlike the 4, 5 and 6 J/cm^2 groups which gave almost the same absorbance readings on days 2 and 4. These outcomes show that 2 J/cm^2 irradiation reduced the proliferation rate, while higher doses completely arrested it. Studies applying an irradiance of 100 mW/cm^2 **[77],[78]** also showed a inhibition in proliferation; however, there are two main differences. Unlike the current investigation, cells irradiated at doses higher than 2 J/cm^2 continued to proliferate after the second blue light exposure. Moreover, the dose-response trend was not observed, for example the 2 J/cm^2 resulted in lower proliferation rates compared to 1, 4 and 6 J/cm^2.

To evaluate the effects of 405 nm blue light irradiation on the mineralisation potential of DPCs, the levels of ALP, DMP1 and OCN were investigated. These represent markers which are regarded as being central to odontoblastic differentiation of DPCs **[274]**. Results showed that 5 and 6 J/cm^2 irradiation resulted in higher ALP levels compared with the 2 and 4 J/cm^2 doses. Previous studies have demonstrated similar outcomes however different magnitudes of stimulation were reported. Zhu *et al.* irradiated gingival MSCs with an irradiance of 100 mW/cm^2 and it was reported that 2 and 4 J/cm^2 exposure resulted in the highest ALP levels compared with the 1 and 6 J/cm^2 **[77].** When using the same irradiance Yang *et al.* reported that 3 and 4 J/cm^2 yielded the highest ALP levels in relation to 1 and 2 J/cm^2 exposures when they irradiated stem

cells from the apical papilla **[78].** These data are in agreement with results from the current study, *i.e.* the higher the light dose, the greater the ALP level stimulated. Notably, the previous study also indicated that a blue light dose of 4 J/cm^2 significantly stimulated DMP1 levels. The current study showed that irradiating DPCs at 2 and 6 J/cm^2 resulted in the highest DMP1 increase, and levels continued to increase from day 3 to day 5 in the 6 J/cm^2 exposure group. However, further comparison between the studies cannot be undertaken as the only dose previously investigated was 4 J/cm^2. Results from the current study have also indicated that irradiating DPCs with 2 and 4 J/cm^2 (57.7 mW/cm^2 for 35 and 69 seconds) is capable of up-regulating the expression of OCN protein in a dose-response relationship. Reportedly, the same doses (100 mW/cm^2 for 20 and 40 seconds) as well as 3 J/cm^2 (16 mW/cm^2 for 188 seconds) have resulted in similar outcomes **[76-78]**.

Alizarin red staining showed that irradiating DPCs with 405 nm light significantly enhanced the mineralised nodule formation at days 7, 14 (2 J/cm^2) and 21 (2 and 4 J/cm^2). Irradiation at 2 and 6 J/cm^2 led to comparable results at days 7 and 14. However, at day 21 the blue light dose exposure of 2 J/cm^2 resulted in the highest calcified nodule formation, followed by doses of 4, 5 and 6 J/cm^2. Interestingly, when gingival MSCs were irradiated (at doses of 1, 2, 4 and 6 J/cm^2) using an irradiance of 100 mW/cm^2, a dose- response trend was observed at day 28 **[77].** Moreover, when apical papilla stem cells were irradiated at 1, 2, 3 and 4 J/cm^2 - using the same irradiance – the 3 J/cm^2 group resulted in the highest mineralised nodule formation followed by 2 and 4 J/cm^2 groups **[78]**.

Previous studies have reported that irradiations at time period of every other day (1 – 6 J/cm^2) at 100 mW/cm^2 (cumulative dose of 10 – 80 J/cm^2) led to enhancement in MSCs calcified nodule formation at day 28 **[77],[78].** Additionally, only 5 irradiations every two days (3 J/cm^2) at 16 mW/cm^2 (cumulative dose of 15 J/cm^2) resulted in similar outcomes at day 21 **[76].** In the current study, the cumulative blue light dose - leading to enhancement of mineralised nodule formation - after 3 irradiations on alternate days is between 6 and 18 J/cm^2. The extended irradiation on alternate days beyond the initial 3 irradiations (6 irradiations) also resulted in enhanced mineralized nodule formation at day 14 at all doses studied– delivering a cumulative dose of 12-36 J/cm^2. However, this increase was not statistically significant compared with the non-irradiated control. Contrarily, 9 irradiations (cumulative dose 18-54 J/cm^2) resulted in an inhibitory effect at all doses with the 6 J/cm^2 dose demonstrating significantly fewer nodules at day 21. When Yuan *et al.* **[223]** irradiated MSCs daily with a dose of 12 J/cm^2 (cumulative dose 70 -80 J/cm^2) at an irradiance of 20 mW/cm^2, data indicated statistically significantly lower calcified nodules formation at day 7. Collectively, these data suggest that at lower irradiance parameters, cells may require fewer exposure times.

It is notable that differences in experimental set-ups could also be the reason behind the diversity in results. In both the Zhu *et al.* and Yang *et al*. investigations, it was reported that the light source spot size was 3.5 cm in diameter (35 mm). However, proliferation was investigated in 96-well plates, ALP and mineralised nodule formation studies were performed in 35-mm dishes, and cell culture plates used for gene expression investigations were not reported. It was reported that irradiation was

performed from above the cultures at a 1 cm distance, and the standard heights of both plates were different, *i.e.* 14.5 mm for 96-well plates and 14 mm for 35-mm dishes. Moreover, the spot size is 5-6 times larger in diameter than the well's diameter in a 96-well plate (6 mm) **[77],[78].** In a study by Wang *et al.*, all plates were covered in aluminum foil except for a 4 cm^2 area / light spot size area (22.5 mm diameter). Irradiance was maintained at 16 mW/cm^2 by changing the distance between the light source and the cell culture-plates. Molecular investigations were performed in 96-well plates, while mineralised nodule studies were undertaken in 6-well plates. The location of the irradiation was not reported; however, again differences exist between the heights of 96-well plates (14.5 mm) and that of the 6-well plates (22.6 mm). Additionally, there are discrepancies between the spot size (22.5 mm) and the well in a 96-well plate (6 mm) as well as the 6-well plate diameter (34.8 mm) **[76]**. There were also no details reported regarding how the light source was characterised or where the sensor/detector was positioned during light characterisation **[76-78].** This highlights the importance of including both detailed explanation of each experimental set-up and how light is characterised, especially as blue wavelength light has the highest Rayleigh scattering **[228].** In the current investigation, the light source (7 mm diameter) was in direct contact with the black walled 96-well plate bottom and the attached cell monolayer. This experimental set-up used here ensured minimal light bleed as well as precision in both: i) light characterisation and ii) delivering the same light dose for all samples at all assays carried out.

Another important variable which should be considered is the potential effect of temperature change following light irradiation. No studies have previously reported measuring temperature changes **[76-78].** Heat dissipation in cultures depends on their thermal relaxation time as well as the irradiance, irradiation time, pulse frequency and pulse duration of the light source **[224]**. Not only can hyperthermia increase mitochondrial ROS **[225]**, but also hyperthermia is reported to enhance the osteogenic differentiaton of MSCs through the up-regulation of ALP, OSX, RUNX2, BMP2 and OPN. These effects are mediated via the heat shock protein HSP70, and its knockout alleviates the positive effects of hyperthermia **[275-277].** If the PBM mechanism involves hyperthermia, this means that the energy of lights photons absorbed in different molecules - and not only the designated chromohpore - will dictate the resulting effects. Resultantly, blue light - with higher energy per photon **[61]** - has a greater ability of causing hyperthermia compared with red light at similar irradiation doses. However, from a photo-chemical perspective, both the wavelength used and the absorption spectrum of the chromophore influence the outcomes **[224]**, and not the energy per photon. In the current study, there was no significant differences in the temperature change/decrease between the non-irradiated controls and the irradiated samples – at all doses investigated [refer to **section 3.1.3.2**]. This subsequently alleviates the hypothesis that any hyperthermic effects initiated the DPCs responses.

Chapter 4: General Discussion

Blue light has been reported to have inhibitory effects on *S. mutans* growth as well as stimulatory effects on MSCs mineralisation. However, there has been variability in experimental set-ups and irradiation parameters reported throughout the studies investigating blue light's antimicrobial and bio-modulatory effects **[45],[47],[53],[76-78]**. Consequently, this thesis aimed to elucidate 405 nm blue light interactions with dentine, *S. mutans* and DPCs in order to identify opportunities for the clinical application of a single wavelength which is able to disinfect dentine and promote the mineralisation potential. Understanding the optical properties of dentine which influences how light is penetrated through its structure will facilitate the delivery of blue light doses that: i) kill cariogenic bacteria without the need for a photosensitizer and ii) enhance mineralisation processes in DPCs.

Blue light transmission through dentine was investigated at 10 increasing power outputs of the light leading to an incident irradiance (at the outer dentine surface) of 470 - 4054 mW/cm^2. Results showed that dentine thickness, dentinal tubule orientation and density significantly affect the 405 nm blue light transmission. Light transmission decreased (i.e. absorption increased) as tissue thickness increased, while occlusal and oblique dentine allowed significantly higher blue light transmission compared with buccal dentine. This occurred due to the change in tubular orientation in the central layers of the buccal dentine as well as due to the significantly decreased inner tubular density.

To build on the results obtained following analysis of dentine's blue light transmission studies, further analyses aimed to determine 405 nm light irradiation doses that inhibited *S. mutans* activity without the need for application of a photosensitizer. The reciprocity of a range of blue light doses (110 -1254 J/cm^2) was investigated at irradiance parameters ranging from 122 to 539 mW/cm^2. Notably, *S. mutans* has been reported to lack porphyrin and heme synthesis pathway **[140]**. Accordingly, in order to elucidate the nature of the photodisinfection mechanism, this study assessed the effects of supplementing the bacteria with hemin and ALA on their blue light susceptibility. Furthermore, the bacteria's FAD levels were investigated after blue light showed significantly higher reductions in *S. mutans* cell counts post-ALA treatment. It is important to understand the factors leading to this effects within the same bacterial species as well as in comparison with appropriate control species. Therefore, a lactic acid-producing, gram positive and facultative anaerobic specie was selected, i.e. *E. faecalis*. It is strongly associated with the caries process, as well as being isolated from root canal infections and periapical disease **[278],[279]**. *E. faecalis* has demonstrated the highest resistance to direct light therapy compared with other gram positive species, and was regarded as a control specie in previous studies **[241],[242].** Notably, a better understanding and identification of antibacterial light irradiation conditions ultimately has clinical translational applications.

Results demonstrated that blue light irradiation can inhibit the growth of both *S. mutans* and *E. faecalis* as demonstrated by the ZOIs detected in the bacterial lawns. These data strongly indicate that direct blue light could inhibit initial biofilm formation **[42]**. The 405 nm wavelength irradiation also led to significant reductions in colony

counts for bacteria grown in planktonic cultures, and killed bacteria in mature biofilms. Interestingly, *E. faecalis* showed higher resistance to blue light compared with *S. mutans* at all growth conditions.

Hemin supplementation increased the bacterial resistance to blue light irradiation due to activation of the negative feedback loop limiting porphyrin production **[257],[258]** as well as providing an anti-oxidant effects **[140],[151],[153],[158],[162],[245],[263]**. Intriguingly, heme inhibits the growth of species with confirmed endogenous porphyrins **[259]**, while enhancing the growth and aero-tolerance of lactic acid-producing species where the presence of no porphyrins have been identified previously **[151],[163],[164],[262]**. It should be noted that heme acquisition and utilisation by bacteria remains a subject that has not entirely been elucidated in the literature and there are still unanswered questions concerning how bacteria utilise exogenous heme. Indeed, it is unclear as to whether exogenous or endogenously synthesised forms are preferentially taken up by the bacterial cell, and once absorbed do they exist in a free state or as a chaperone inside the bacterial cell **[167].**

Accordingly, the hypothesis that light resistance due to heme groups absorbing light and preventing light delivery to the designated chromophores cannot be excluded. ALA supplementation increased the sensitivity of *S. mutans* to blue light, which indicated that ALA likely initiated the induction of porphyrin production in *S. mutans*. This exposure was accompanied by a significant increase in FAD levels, indicating an elevation in cellular redox states. Notably, data presented here suggests that flavins are also potential blue light chromophores within *S. mutans*.

The variability identified in the inhibitory effects of 405 nm blue light on the bacterial strains studied was possibly due to the difference in the photo-absorber types and levels present as well as being due to the antioxidative potential of each strain **[28],[269]**. Furthermore, the porphyrin levels in bacteria might differ greatly in wild-type strains cultured in their natural environment **[241]**. Indeed, it has previously been reported that the antioxidative potential of each strain fluctuates depending on culture conditions **[280]**. It is notable that results from the current investigation showed that the delivery of identical reciprocal doses resulted in similar antimicrobial outcomes against *S. mutans*. This can be also observed when comparing the current irradiation parameters to other studies employing similar doses but using different irradiance settings and irradiation times **[42],[245],[246]**. This reciprocity could be observed when blue light doses were fractionated **[45]**, delivering a total cumulative dose falling within the same range of dosage as was administered in the current study. These findings demonstrate the plasticity in delivering inhibitory blue light doses for adaptation to various clinical conditions.

The final set of experiments presented in this thesis reported on the investigation of the effects of relatively lower doses of blue light (2, 4, 5 and 6 J/cm^2) on human DPCs responses. Blue light was delivered at an irradiance of 57.7 mW/cm^2 for 35, 69, 90 or 104 seconds. Results showed that 4, 5 and 6 J/cm^2 resulted in significantly lower proliferation rates compared with the non-irradiated controls at days 2 and 4. However, 5 and 6 J/cm^2 exposures resulted in the highest stimulated ALP and DMP1 levels at days 3 and 5, as well as comparable mineralized nodule formation to 2 and 4 J/cm^2 – at days 7 and 14. Nonetheless, at day 21, 2 and 4 J/cm^2 exposures resulted in

the highest mineralized nodule formation. Thus it could be hypothesized that under the current experimental set-up and irradiation parameters, higher blue light doses resulted in an arrest in proliferation rates due to the early cellular shift towards differentiation responses **[281].** The difference in the magnitude of response to each dose observed between the current study and previous investigations reported in the literature is likely due differences in cell types, light sources, experimental set-ups, irradiation parameters and exposure rates used. Of note however, concentrations of the mineralization-inducing media supplements were not always reported **[76-78].**

Chapter 5: Conclusions

Based on the results obtained from the current study, it can be concluded that when exposing the dentine of human permanent molar teeth to a 405 nm light source, targeting the light source vertically through the occlusal surface will yield the greatest transmission. If operating from a proximal / buccal / lingual surface, comparable results could be obtained if the light is targeted obliquely parallel to the tubule orientation. However, exposing the tooth to a light beam directly perpendicular to a proximal surface will lead to the lowest transmission.

Application of 405 nm direct light treatment has been shown to inhibit the growth and kill both *S. mutans* and *E. faecalis* - generating a dose-response trend - and at doses as low as 110 J/cm^2. Notably, the maximum temperatures reached following all light delivery doses investigated were within the normal incubation and growth temperatures recommended for both bacterial species **[233],[234]**, which excludes the possible effect of the photo-thermal inhibition process utilised by IR diode and CO_2 lasers **[29],[30]**. Since phototherapy is based on photoactivation of chromophores endogenous to the bacteria, it is reported that the bacteria are less likely to develop resistance to this killing process **[28]**. Potentially, greater bacterial killing would be expected in a clinical environment compared with conditions of optimal in-vitro growth conditions used here which provide a rich nutrition **[42]**. The change in bacterial susceptibility to blue light after supplementation with hemin and ALA confirmed the photo-oxidative nature of the photodisinfection mechanism. The

elevation in FAD levels of *S. mutans* supplemented with ALA also supported these outcomes.

For the potential use of the 405 nm wavelength in managing and treating carious molar dentine infections, applying an exposure time of 7 minutes with an irradiance of 251 mW/cm^2, a dose of 110 J/cm^2 could potentially be used to inhibit bacterial growth on the tooth surface. Furthermore, using the same irradiation time but with higher irradiance parameters of 280 - 325 mW/cm^2, has the potential to treat bacteria at up to a 1 mm depth within the dentinal tubules at different tooth locations. This light application regimen would therefore easily penetrate to sufficient dentine depths which have been reported for bacterially invaded tubules **[282]**. The delivery of the same dose for shorter exposure times can be achieved by either applying a higher irradiance setting or reducing the distance between the light source and the target **[247]**.

In order to achieve both antimicrobial and bio-stimulatory effects, the selected irradiance parameter would mainly depend on the location of irradiation and estimated residual dentine thickness. For example, irradiating 3 mm dentine for 7 minutes using irradiance settings between 280 and 325 mW/cm^2 will allow negligible blue light doses to reach the dental pulp tissue (0.3 - 1 J/cm^2) at different tooth locations. However, to achieve photodisinfection and PBM, it would be necessary to increase the irradiance settings to 7693 – 19,233 mW/cm^2 (allowing a 57.7 mW/cm^2 dose to reach the dental pulp) and reduce the irradiation time to 35, 69, 90 and 104 seconds. This approach would still deliver doses between 200 and 1500 J/cm^2 through the first 1 mm of the dentine tissue, potentially killing bacteria. Since the irradiance of

57.7 mW/cm^2 did not cause any rise in the MEM temperature [see **Figure 13**], this protocol is likely safe towards the pulp. However, a suitable light source would be required, as the current device used in the present investigations had a maximum irradiance of only 4054 mW/cm^2.

Notably, exposing 2 mm dentine (251 – 325 mW/cm^2 for 7 minutes) would allow blue light doses of 1.6 - 4 J/cm^2 to reach the dental pulp, which are within the bio-stimulatory range of doses investigated. However, to avoid both the biphasic PBM responses **[84-88]** arising from using different parameters and a longer irradiation time, an irradiance 1923 – 3846 mW/cm^2 could be utilised (35, 69, 90, 104 seconds). Notably, this would deliver a blue light dose of 50 – 350 J/cm^2 for photodisnfection purposes within the first 1 mm of the tissue. Irradiating 1 mm dentine (251 – 325 mW/cm^2 for 7 minutes) would permit doses of 11 – 30 J/cm^2 to reach the dental pulp, which are potentially cytotoxic to DPCs. Accordingly, and to achieve bio-stimulatory effects, it is best to increase the irradiance range up to 524 mW/cm^2 and reduce exposure time to 35, 69, 90 and 104 seconds. A blue light dose of 7 – 50 J/cm^2 would be delivered through the dentine prior to reaching the pulp; however, this is in a lower range than the inhibitory doses investigated in the current study. Nonetheless, using a different light source, previously it was reported that doses as low 9.26 J/cm^2 can kill *S. mutans* **[46]**, consequently this requires further investigation.

Chapter 6: Clinical relevance and future work

This study investigated the transmission of blue light in coronal molar dentine along with the antibacterial and bio-stimulatory effects of the same light source/wavelength. The clinical rationale is to optimise the delivery of inhibitory doses towards cariogenic bacteria as well as providing bio-stimulatory doses for DPCs, while both are *in situ* within their normal environment. Results of the current study reported on the 405 nm light propagation through molar dentine and the potential factors governing it. However, further investigations are needed which incorporate different light sources, various tooth types (i.e. anteriors / canines / premolars / molar) as well as sampling teeth from different age groups.

The reciprocity required for delivering antimicrobial blue light doses is advantageous to adapt to different conditions present in the clinical environment. ALA supplementation increased the susceptibility of *S. mutans* to blue light, which was accompanied by a significant increase in FAD levels. This results suggests that *S. mutans* is able to synthesize porphyrins and also supports the hypothesis that flavins are potential chromophores. Collectively, these data potentially provide an approach for optimising the outcomes for utilising blue light for photo-targeting *S. mutans* and disinfection of dental hard tissue, providing a wider therapeutic potential especially in view of the current issues associated with antibiotic resistance. However, the mechanisms underlying the involvement of heme-proteins, cytochromes or flavo-cytochromes still requires further elucidation. Further investigations are also needed

to confirm the types and levels of porphyrins within the bacteria under different growth conditions.

Notably, 405 nm light irradiation can potentially be used to enhance DPCs odontoblastic differentiation, and depending on the residual dentine thickness, different parameters can be adjusted to deliver the desired dose. The limited availability and high passage number of human DPCs samples used here limited the potential to investigate the odotongenic markers at further time points as well as in studying the reciprocity of blue light doses. Notably, studying different parameters would enable a better understanding of the biphasic dose-response previously reported, especially relating to the flexibility in delivering reciprocal antimicrobial doses as this may not be always the case when delivering PBM doses. Moreover, blue light PBM effects requires further studies aimed at standardizing the light sources, MSCs type/derivation/passage number, mineralising supplements concentrations, experimental set-ups and cell culture plates usage. For optimisation of this novel therapy, a concomitant development of a suitable therapeutic device is required along with *ex-vivo* models and clinical trials to demonstrate the safety and efficacy for dental phototherapy.

References

[1] Listl S, Galloway J, Mossey PA, Marcenes W. Global economic impact of dental diseases. Journal of Dental Research 2015; 94(10):1-7. https://doi.org/10.1177/0022034515602879

[2] Frencken JE, Sharma P, Stenhouse L, Green D, Laverty D, Dietrich T. Global epidemiology of dental caries and severe periodontitis – a comprehensive review. Journal of Clinical Periodontology 2017; 44 Suppl 18:S94-S105. https://doi.org/10.1111/jcpe.12677

[3] Loesche WJ. Microbiology of dental decay and periodontal disease. In: Baron S, editor. Medical Microbiology. 4th edition. Galveston (TX): University of Texas Medical Branch at Galveston; 1996. Chapter 99. Available from: https://www.ncbi.nlm.nih.gov/books/NBK8259/

[4] Love RM, Jenkinson HF. Invasion of dentinal tubules by oral bacteria. Critical Reviews in Oral Biology and Medicine 2002; 13(2):171-83. http://doi.org/10.1177/154411130201300207

[5] Heyeraas KJ, Berggreen E. Interstitial fluid pressure in normal and inflamed pulp. Critical Reviews in Oral Biology and Medicine 1999; 10(3):328-36. http://doi.org/10.1177/10454411990100030501

[6] Nagaoka S, Miyazaki Y, Liu HJ, Iwamoto Y, Kitano M, Kawagoe M. Bacterial invasion into dentinal tubules of human vital and non-vital teeth. Journal of Endodontics 1995; 21(2):70-3. http://doi.org/10.1016/S0099-2399(06)81098-8

[7] Chirnside IM. Bacterial Invasion of non-vital dentin. Journal of Dental Research 1961; 40:134-40. http://doi.org/10.1177/00220345610400010401

[8] Olgart L, Brännström M, Johnson G. Invasion of bacteria into dentinal tubules experiments in vivo and in vitro. Acta Odontologica Scandinavica 1974; 32(1):61-70. http://doi.org/10.3109/00016357409002533

[9] Michelich VJ, Schuster GS, Pashley DH. Bacterial penetration of human dentin in vitro. Journal of Dental Research 1980; 59(8):1398-403. http://doi.org/10.1177/00220345800590080701

[10] Pashley DH. Dentin conditions and disease. In: Handbook of Experimental Aspects of Oral Biochemistry. Boca Raton, FL: CRC Press 1983.

[11] Ackermans F, Klein JP, Frank RM. Ultrastructural localization of immunoglobulins in carious human dentine. Archives of Oral Biology 1981; 26(11):879-86. http://doi.org/10.1016/0003-9969(81)90146-1

[12] Okamura K. Histological study on the origin of dentinal immunoglobulins and the change in their localization during caries. Journal of Oral Pathology and Medicine 1985; 14(9):680-9. http://doi.org/10.1111/j.1600-0714.1985.tb00547.x

[13] Pekovic DD, Adamkiewicz VW, Gornitsky M. Immunoglobulins in human dental caries. Archives of Oral Biology 1988; 33(2):135-41. http://doi.org/10.1016/0003-9969(88)90057-X

[14] Hilton TJ. Keys to clinical success with pulp capping: a review of the literature. Operative Dentistry 2009; 34(5): 615–625. https://doi.org/10.2341/09-132-0

[15] Tsang P, Qi F, Shi W. Medical approach to dental caries: fight the disease, not the lesion. Pediatric dentistry 2006; 28(2):188-91.

[16] Tziafas D, Smith AJ, Lesot H. Designing new treatment strategies in vital pulp therapy. Journal of Dentistry 2000; 28(2):77-92. http://doi.org/10.1016/s0300-5712(99)00047-0

[17] Duncan HF, Cooper PR, Smith AJ. Dissecting dentine-pulp injury and wound healing responses: consequences for regenerative endodontics. International Endodontic Journal 2019; 52(3):261-266. http://doi.org/10.1111/iej.13064

[18] Tziafas D. Characterization of odontoblast-like cell phenotype and reparative dentin formation in vivo: a comprehensive literature review. Journal of Endodontics 2019; (3):241-249. http://doi.org/10.1016/j.joen.2018.12.002

[19] Mount GJ, Ngo H. Minimal intervention: early lesions. Quintessence International 2000; 31(8):535-46.

[20] Pitts NB. Clinical diagnosis of dental caries: a European perspective. Journal of Dental Education 2001; 65(10):972-8. http://doi.org/10.1177/154405910408301S03

[21] Featherstone JDB. Delivery challenges for fluoride, chlorhexidine and xylitol. BMC Oral Health 2006; 6(Suppl 1): S8. https://doi.org/10.1186/1472-6831-6-S1-S8

[22] Moshrefi A. Chlorhexidine. The Journal of the Western Society of Periodontology / Periodontal Abstracts 2002; 50(1):5-9.

[23] Yates R, Jenkins S, Newcombe R, Wade W, Moran J, Addy M. A 6-month home usage trial of a 1% chlorhexidine toothpaste: (I). Effects on plaque, gingivitis, calculus and tooth staining. Journal of Clinical Periodontology 1993; 20(2):130-8. http://doi.org/10.1111/j.1600-051X.1993.tb00327.x

[24] Gilbert R, Williams P. The oral retention and antiplaque efficacy of triclosan in human volunteers. British Journal of Clinical Pharmacology 1987; 23(5):579-83. http://doi.org/10.1111/j.1365-2125.1987.tb03094.x

[25] Pattison DI, Davies MJ. Actions of ultraviolet light on cellular structures. Experientia Supplementum 2006; (96):131-57. https://doi.org/10.1007/3-7643-7378-4_6

[26] Williams JA, Pearson GJ, Colles MJ, Wilson M. The photo-activated antibacterial action of toluidine blue O in a collagen matrix and in carious dentine. Caries Research 2004; 38(6):530-6. http://doi.org/10.1159/000080582

[27] Araújo NC, Fontana CR, Bagnato VS, Gerbi MEM. Photodynamic antimicrobial therapy of curcumin in biofilms and carious dentine. Lasers in Medical Science 2014; 29(2):629-35. http://doi.org/10.1007/s10103-013-1369-3

[28] Lipovsky A, Nitzan Y, Gedanken A, Lubart R. Visible light-induced killing of bacteria as a function of wavelength: implication for wound healing. Lasers in Surgery and Medicine 2010; 42(6):467-72. https://doi.org/10.1002/lsm.20948

[29] Dederich DN, Pickard MA, Vaughn AS, Tulip J, Zakariasen KL. Comparative bactericidal exposures for selected oral bacteria using carbon dioxide laser radiation. Lasers in Surgery and Medicine 1990; 10(6):591-94. https://doi.org/10.1002/lsm.1900100612

[30] Moritz A, Gutknecht N, Schoop U, Goharkhay K, Doertbudak O, Sperr W. Irradiation of infected root canals with a diode laser in vivo: results of microbiological examinations. Lasers in Surgery and Medicine 1997; 21(3):221-6. https://doi.org/10.1002/(sici)1096-9101(1997)21:3<221::aid-lsm1>3.0.co;2-s

[31] Hamblin MR, Viveiros J, Yang C, Ahmadi A, Ganz RA, Tolkoff MJ. Helicobacter pylori accumulates photoactive porphyrins and is killed by visible light. Antimicrobial Agents and Chemotherapy 2005; 49(7):2822-7. http://doi.org/10.1128/AAC.49.7.2822-2827.2005

[32] Lim CK, Rideout JM, Wright DJ. High-performance liquid chromatography of naturally occurring 8-, 7-, 6-, 5- and 4-carboxylic porphyrin isomers. Journal of Chromatography 1983; 282:629-41. https://doi.org/10.1016/S0021-9673(00)91640-6

[33] Bu W, Myers N, McCarty JD, O'Neill T, Hollar S, Stetson PL, Sved DW. Simultaneous determination of six urinary porphyrins using liquid chromatography-tandem mass spectrometry. Journal of Chromatography B: Analytical Technologies in the Biomedical and Life Sciences 2003; 783(2):411-23. https://doi.org/10.1016/S1570-0232(02)00703-1

[34] Bain BJ, Bates I, Laffan MA. Dacie and Lewis Practical Haematology - 12th edition. Elsevier, London 2017; 178(4).

[35] Lim CK. High-performance liquid chromatography and mass spectrometry of porphyrins, chlorophylls and bilins- In: Methods in Chromatography: Volume 2; 2009. https://doi.org/10.1142/3411

[36] Cieplik F, Tabenski LK, Buchalla W, Maisch T. Antimicrobial photodynamic therapy for inactivation of biofilms formed by oral key pathogens. Frontiers in microbiology 2014; 5:1-17. https://doi.org/10.3389/fmicb.2014.00405

[37] Castano AP, Demidova TN, Hamblin MR. Mechanisms in photodynamic therapy: part one - photosensitizers, photochemistry and cellular localization. Photodiagnosis and Photodynamic Therapy 2004; 1(4):279-293. https://doi.org/10.1016/S1572-1000(05)00007-4

[38] Strakhovskaya M, Shumarina A, Fraikin GY, Rubin A. Endogenous porphyrin accumulation and photosensitization in the yeast Saccharomyces cerevisiae in the presence of 2, 2'-dipyridyl. Journal of Photochemistry and Photobiology B: Biology 1999; 49(1):18-22. https://doi.org/10.1016/s1011-1344(98)00215-2

[39] Wakeman CA, Stauff DL, Zhang Y, Skaar EP. Differential activation of Staphylococcus aureus heme detoxification machinery by heme analogues. Journal of Bacteriology 2014; 196(7):1335-42. https://doi.org/10.1128/JB.01067-13

[40] Romiti R, Schaller M, Jacob K, Plewig G. High-performance liquid chromatography analysis of porphyrins in Propionibacterium acnes. Archives of Dermatological Research 2000; 292(6):320-22. https://doi.org/10.1007/s004030000122

[41] Wainwright M. Photodynamic antimicrobial chemotherapy (PACT). The Journal of Antimicrobial Chemotherapy 1998; 42(1):13-28. https://doi.org/10.1093/jac/42.1.13

[42] Feuerstein O, Persman N, Weiss EI. Phototoxic effect of visible light on Porphyromonas gingivalis and Fusobacterium nucleatum: an in vitro study. Photochemistry and Photobiology 2004; 80(3):412-5. https://doi.org/10.1562/0031-8655(2004)080<0412:PEOVLO>2.0.CO;2

[43] König K, Teschke M, Sigusch B, Glockmann E, Eick S, Pfister W. Red light kills bacteria via photodynamic action. Cellular and Molecular Biology 2000; 46(7):1297-303. https://doi.org/10.1016/j.chemosphere.2006.10.040

[44] Lubart R, Lipovski A, Nitzan Y, Friedmann H. Review - A possible mechanism for the bactericidal effect of visible light. Laser Therapy 2011; 20(1): 17–22. http://doi.org/10.5978/islsm.20.17

[45] De Sousa DL, Lima RA, Zanin IC, Klein MI, Janal MN, Duarte S. Effect of twice-daily blue light treatment on matrix-rich biofilm development. PLoS One 2015; 10(7): e0131941. http://doi.org/10.1371/journal.pone.0131941

[46] Gomez GF, Huang R, MacPherson M, Ferreira Zandona AG, Gregory RL. Photo inactivation of Streptococcus mutans biofilm by violet-blue light. Current Microbiology 2016; 73(3):426-433. https://doi.org/10.1007/s00284-016-1075-z

[47] Gomez GF, Huang R, Eckert G, Gregory RL. Effect of phototherapy on the metabolism of Streptococcus mutans biofilm based on a colorimetric tetrazolium assay. Journal of Oral Science 2018; 60(2):242-246. http://doi.org/10.2334/josnusd.17-0203

[48] Ricatto LGO, Conrado LAL, Turssi CP, França FMG, Basting RT, Amaral FLB. Comparative evaluation of photodynamic therapy using laser or light emitting diode on cariogenic bacteria: an in vitro study. European Journal of Dentistry 2014; 8(4):509-14. http://doi.org/10.4103/1305-7456.143634

[49] Lima JPM, Sampaio De Melo MA, Borges FMC, Teixeira AH, Steiner-Oliveira C, Nobre Dos Santos M, Rodrigues LKA, Zanin ICJ. Evaluation of the antimicrobial effect of photodynamic antimicrobial therapy in an in situ model of dentine caries. European Journal of Oral Sciences 2009; 117(5):568-74. https://doi.org/10.1111/j.1600-0722.2009.00662.x

[50] Burns T, Wilson M, Pearson GJ. Effect of dentine and collagen on the lethal photosensitization of Streptococcus mutans. Caries Research 1995; 29(3):192-7. http://doi.org/10.1159/000262068

[51] Fried D, Glena RE, Featherstone JDB, Seka W. Nature of light scattering in dental enamel and dentin at visible and near-infrared wavelengths. Applied Optics 1995; 34(7):1278-85. http://doi.org/10.1364/AO.34.001278

[52] Hariri I, Sadr A, Shimada Y, Tagami J, Sumi Y. Effects of structural orientation of enamel and dentine on light attenuation and local refractive index: an optical coherence tomography study. Journal of Dentistry 2012; 40(5):387-96. http://doi.org/10.1016/j.jdent.2012.01.017

[53] Felix Gomez GG, Lippert F, Ando M, Zandona AF, Eckert GJ, Gregory RL. Photoinhibition of Streptococcus mutans biofilm-induced Lesions in human dentin by violet-blue Light. Dentistry Journal 2019; 7(4):113. https://doi.org/10.3390/dj7040113

[54] Born M, Wolf E, Bhatia A, Clemmow P, Gabor D, Stokes A, Wilcock W. Principles of optics: electromagnetic theory of propagation, interference and diffraction of light (7th edition). Cambridge: Cambridge University Press 1999. https://doi.org/10.1017/CBO9781139644181

[55] Nikonenko NA. Optical properties of skin, tooth tissues and dental materials. Minsk BSMU 2015. Available from: http://rep.bsmu.by/bitstream/handle/BSMU/7985/366519-%D0%B8%D0%BD-%D0%B1%D1%80..pdf?sequence=3&isAllowed=y

[56] Wakefield R, D'Agostino M. Essential applications of musculoskeletal ultrasound in rheumatology. The Journal of Rheumatology 2011; 38(8):1813. https://doi.org/10.3899/jrheum.110454

[57] Zijp JR. Optical properties of dental hard tissues. Groningen: s.n. 2001. Available from: https://www.jaapzijp.nl/documents/Thesis12APR01.pdf

[58] Kienle A, Forster FK, Diebolder R, Hibst R. Light propagation in dentin: influence of microstructure on anisotropy. Physics in Medicine and Biology 2003; 48(2):7-14. http://doi.org/10.1088/0031-9155/48/2/401

[59] Pop-Ciutrila IS, Ghinea R, Perez Gomez MDM, Colosi HA, Dudea D, Badea M. Dentine scattering, absorption, transmittance and light reflectivity in human incisors, canines and molars. Journal of Dentistry 2015; 43(9):1116-1124. http://doi.org/10.1016/j.jdent.2015.06.011

[60] Mester E, Szende B, Gärtner P. The effect of laser beams on the growth of hair in mice. Radiobiologia Radiotherapia (Berl) 1968; 9(5):621-626.

[61] Hamblin MR, Demidova TN. Mechanisms of low level light therapy. SPIE Conference Proceedings 2006; 6140, 614001. https://doi.org/10.1117/12.646294

[62] Ginani F, Soares DM, Barreto, MPEV, Barboza CAG. Effect of low-level laser therapy on mesenchymal stem cell proliferation: a systematic review. Lasers in Medical Science 2015; 30(8): 2189-2194. https://doi.org/10.1007/s10103-015-1730-9

[63] Borzabadi-Farahani A. Effect of low-level laser irradiation on proliferation of human dental mesenchymal stem cells; a systemic review. Journal of Photochemistry and Photobiology B: Biology 2016; 162:577-582. https://doi.org/10.1016/j.jphotobiol.2016.07.022

[64] Kim HB, Baik, KY, Seonwoo H, Jang KJ, Lee MC, Choung PH, Chung JH. Effects of pulsing of light on the dentinogenesis of dental pulp stem cells in vitro. Scientific Reports 2018; 8(1):2057. https://doi.org/10.1038/s41598-018-19395-x

[65] Li WT, Leu YC, Wu JL. Red-light light-emitting diode irradiation increases the proliferation and osteogenic differentiation of rat bone marrow mesenchymal stem cells. Photomedicine and Laser Surgery 2010; Suppl 1:157-165. https://doi.org/10.1089/pho.2009.2540

[66] Peng F, Wu H, Zheng Y, Xu X, Yu J. The effect of noncoherent red light irradiation on proliferation and osteogenic differentiation of bone marrow mesenchymal stem cells. Lasers in Medical Science 2012; 27(3):645-653. https://doi.org/10.1007/s10103-011-1005-z

[67] Wu JY, Wang YH, Wang GJ, Ho ML, Wang CZ, Yeh ML, Chen CH. Low-power GaAlAs laser irradiation promotes the proliferation and osteogenic differentiation of stem cells via IGF1 and BMP2. PLoS One 2012; 7(9):e44027. https://doi.org/10.1371/journal.pone.0044027

[68] Wu JY, Chen CH, Yeh LY, Yeh ML, Ting CC, Wang YH. Low-power laser irradiation promotes the proliferation and osteogenic differentiation of human periodontal ligament cells via cyclic adenosine monophosphate. International Journal of Oral Science 2013; 5(2):85-91. https://doi.org/10.1038/ijos.2013.38

[69] Yang D, Yi W, Wang E, Wang M. Effects of light-emitting diode irradiation on the osteogenesis of human umbilical cord mesenchymal stem cells in vitro. Scientific Reports 2016; 6:37370. https://doi.org/10.1038/srep37370

[70] Soleimani M, Abbasnia E, Fathi M, Sahraei H, Fathi Y, Kaka G. The effects of low-level laser irradiation on differentiation and proliferation of human bone marrow mesenchymal stem cells into neurons and osteoblasts-an in vitro study. Lasers in Medical Science 2012; 27(2):423-430. https://doi.org/10.1007/s10103-011-0930-1

[71] Ateş GB, Ak A, Garipcan B, Gülsoy M. Photobiomodulation effects on osteogenic differentiation of adipose-derived stem cells. Cytotechnology 2020; 72:247–258. https://doi.org/10.1007/s10616-020-00374-y

[72] Yamakawa S, Niwa T, Karakida T, Kobayashi K, Yamamoto R, Chiba R, Yamakoshi Y, Hosoya N. Effects of Er:YAG and diode laser irradiation on dental pulp cells and tissues. International Journal of Molecular Sciences 2018; 19(8):2429. http://doi.org/10.3390/ijms19082429

[73] Wang L, Wu F, Liu C, Song Y, Guo J, Yang Y, Qiu Y. Low-level laser irradiation modulates the proliferation and the osteogenic differentiation of bone marrow mesenchymal stem cells under healthy and inflammatory condition. Lasers in Medical Science 2019; 34(1): 169-178. https://doi.org/10.1007/s10103-018-2673-8

[74] Kushibiki T, Awazu K. Controlling osteogenesis and adipogenesis of mesenchymal stromal cells by regulating a circadian clock protein with laser irradiation. International Journal of Medical Sciences 2008; 5(6):319-326. https://doi.org/10.7150/ijms.5.319

[75] Kushibiki T, Awazu K. Blue laser irradiation enhances extracellular calcification of primary mesenchymal stem cells. Photomedicine and Laser Surgery 2009; 27(3):493–498. https://doi.org/10.1089/pho.2008.2343

[76] Wang Y, Huan YY, Wang Y, Lyu P, Hamblin MR. Photobiomodulation (blue and green light) encourages osteoblastic-differentiation of human adipose-derived stem cells: role of intracellular calcium and light-gated ion channels. Scientific Reports 2016; 6: 33719. https://doi.org/10.1038/srep33719

[77] Zhu T, Wu Y, Zhou X, Yang Y, Wang Y. Irradiation by blue light-emitting diode enhances osteogenic differentiation in gingival mesenchymal stem cells in vitro. Lasers in Medical Science 2019; 34:1473–1481. https://doi.org/10.1007/s10103-019-02750-3

[78] Yang Y, Zhu T, Wu Y, Shu C, Chen Q, Yang J, Luo X, Wang Y. Irradiation with blue light-emitting diode enhances osteogenic differentiation of stem cells from the apical papilla. Lasers in Medical Science 2020; 35:1981–1988. https://doi.org/10.1007/s10103-020-02995-3

[79] Karu TI, Kolyakov SF. Exact action spectra for cellular responses relevant to phototherapy. Photomedicine and Laser Surgery 2005; 23(4):355-361. https://doi.org/10.1089/pho.2005.23.355

[80] Eichler M, Lavi R, Shainberg A, Lubart R. Flavins are source of visible-light-induced free radical formation in cells. Lasers in Surgery and Medicine 2005; 37(4):314–319. https://doi.org/10.1002/lsm.20239

[81] Lubart R, Lavi R, Friedmann H, Rochkind S. Photochemistry and photobiology of light absorption by living cells. Photomedicine and Laser Surgery 2006; 24(2):179-185. https://doi.org/10.1089/pho.2006.24.179

[82] Chen CT, Shih YRV, Kuo TK, Lee OK, Wei YH. Coordinated changes of mitochondrial biogenesis and antioxidant enzymes during osteogenic differentiation of human mesenchymal stem cells. Stem Cells 2008; 26(4):960-968. https://doi.org/10.1634/stemcells.2007-0509

[83] Lyublinskaya OG, Borisov YG, Pugovkina NA, Smirnova IS, Obidina JV, Ivanova JS, Zenin VV, Shatrova AN, Borodkina AV, Aksenov ND, Zemelko VI, Burova EB, Puzanov MV, Nikolsky NN. Reactive oxygen species are required for human mesenchymal stem cells to initiate proliferation after the quiescence exit. Oxidative Medicine and Cellular Longevity 2015; 502105 https://doi.org/10.1155/2015/502105

[84] Huang YY, Sharma SK, Carroll J, Hamblin MR. Biphasic dose response in low level light therapy - an update. Dose Response 2011; 9(4):602-618. https://doi.org/10.2203/dose-response.11-009.Hamblin

[85] Kim HB, Baik KY, Choung PH, Chung JH. Pulse frequency dependency of photobiomodulation on the bioenergetic functions of human dental pulp stem cells. Scientific Reports 2017; 15927. https://doi.org/10.1038/s41598-017-15754-2

[86] Sommer AP, Pinheiro AL, Mester AR, Franke RP, Whelan HT. Biostimulatory windows in low-intensity laser activation: lasers, scanners, and NASA's light-emitting diode array system. Journal of Clinical Laser Medicine and Surgery 2001; 19(1):29-33. https://doi.org/10.1089/104454701750066910

[87] de Freitas LF, Hamblin MR. Proposed mechanisms of photobiomodulation or low-level light therapy. IEEE Journal of Selected Topics in Quantum Electronics 2016; 22(3):7000417. https://doi.org/1010.1109/JSTQE.2016.2561201

[88] Lanzafame RJ, Stadler I, Kurtz AF, Connelly R, Peter Sr TA, Brondon P, Olson D. Reciprocity of exposure time and irradiance on energy density during photoradiation on wound healing in a murine pressure ulcer model. Lasers in Surgery and Medicine 2007; 39(6):534-42. https://doi.org/10.1002/lsm.20519

[89] Dogandzhiyska V, Angelov I, Dimitrov S, Uzunov T. In vitro study of light radiation penetration through dentin, according to the wavelength. Acta Medica Bulgarica 2015; 42(2):16-22. http://doi.org/10.1515/amb-2015-0013

[90] Ana Paula ST, Alonso JRL, Basso FG, Moriyama LT, Heling J, Bagnato VS, De Souza Costa CA. LED light attenuation through human dentin: a first step toward pulp photobiomodulation after cavity preparation. American Journal of Dentistry 2013; 26(6):319-23.

[91] Palin WM, Hadis MA, Milward MR, Carroll JD, Cooper PR. Beam profile measurements for dental phototherapy: the effect of distance, wavelength and tissue thickness. SPIE Conference Proceedings 2015; 9309 Mechanisms for Low-Light Therapy X, 930905. https://doi.org/10.1117/12.2077628

[92] Zhou X, Li Y. Supragingival microbes – In: Atlas of Oral Microbiology. Elsevier 2015; 41-65. https://doi.org/10.1016/B978-0-12-802234-4.00003-3

[93] Duggal MS, Curson MEJ. Dental disease / etiology of dental caries – In Encyclopedia of Food Sciences and Nutrition (2nd Edition). Elsevier 2003; 1746-1749.

[94] Kianoush N, Adler CJ, Nguyen KA, Browne GV, Simonian M, Hunter N. Bacterial profile of dentine caries and the impact of pH on bacterial population diversity. PLoS One 2014; 9(3):e92940. https://doi.org/10.1371/journal.pone.0092940

[95] Hamilton IR. Ecological basis for dental caries. In: Kuramitsu HK, Ellen RP Eds, Oral Bacterial ecology: The molecular basis. Horizon Scientific Press 2000; 219-274.

[96] Farges JC, Keller JF, Carrouel F, Durand SH, Romeas A, Bleicher F, Lebecque S, Staquet MJ. Odontoblasts in the dental pulp immune response. Journal of Experimental Zoology Part B: Molecular and Developmental Evolution 2009; 312B (5):425-36. http://doi.org/10.1002/jez.b.21259

[97] Shemesh M, Tam A, Steinberg D. Expression of biofilm-associated genes of Streptococcus mutans in response to glucose and sucrose. Journal of Medical Microbiology 2007; 56(Pt 11):1528-35. https://doi.org/10.1099/jmm.0.47146-0

[98] Cooper PR, McLachlan JL, Simon S, Graham LW, Smith AJ. Mediators of inflammation and regeneration. Advances in Dental Research 2011; 23(3):290-5. http://doi.org/10.1177/0022034511405389

[99] Sloan AJ. Biology of the dentin-pulp complex. In: Stem Cell Biology and Tissue Engineering in Dental Sciences. Elsevier 2015; 371-378. https://doi.org/10.1016/B978-0-12-397157-9.00033-3

[100] Levine S. Endodontics. In: Dental Secrets (4th edition). Elsevier 2015: 126-146. https://doi.org/10.1016/B978-0-323-26278-1.00007-6

[101] Gronthos S, Brahim J, Li W, Fisher LW, Cherman N, Boyde A, DenBesten P, Robey PG, Shi S. Stem cell properties of human dental pulp stem cells. Journal of Dental Research 2002; 81(8):531-5. http://doi.org/10.1177/154405910208100806

[102] Takeda T, Tezuka Y, Horiuchi M, Hosono K, Iida K, Hatakeyama D, Miyaki S, Kunisada T, Shibata T, Tezuka K. Characterization of dental pulp stem cells of human tooth germs. Journal of Dental Research 2008; 87(7):676-81. http://doi.org/10.1177/154405910808700716

[103] Nanci A. Ten Cate's Oral Histology-Development, structure, and function (9th edition). Elsevier 2017; 395-405.

[104] Arana-Chavez VE, Massa LF. Odontoblasts: the cells forming and maintaining dentine. International Journal of Biochemistry and Cell Biology 2004; 36(8):1367-73. http://doi.org/10.1016/j.biocel.2004.01.006

[105] Tziafas D. Basic mechanisms of cytodifferentiation and dentinogenesis during dental pulp repair. International Journal of Developmental Biology 1995; 39(1):281-90. http://doi.org/10.1387/IJDB.7626418

[106] Lesot H, Begue-Kirn C, Kubler MD, Meyer JM, Smith AJ, Cassidy N, Ruch JV. Experimental induction of odontoblast differentiation and stimulation during preparative processes. Cells and Materials 1993; 3(2) Article 8.

[107] Smith AJ, Tobias RS, Cassidy N, Plant CG, Browne RM, Begue-Kirn C, Ruch JV, Lesot H. Odontoblast stimulation in ferrets by dentine matrix components. Archives of Oral Biology 1994; 39(1):13-22. http://doi.org/10.1016/0003-9969(94)90029-9

[108] Smith AJ, Cassidy N, Perry H, Begue-Kirn C, Ruch JV, Lesot H. Reactionary dentinogenesis. International Journal of Developmental Biology 1995; 39(1):273-80. http://doi.org/10.1111/j.1365-2842.2005.01585.x

[109] Finkelman RD, Mohan S, Jennings JC, Taylor AK, Jepsen S, Baylink DJ. Quantitation of growth factors IGF-I, SGF/IGF-II, and TGF-beta in human dentin. Journal of Bone and Mineral Research 1990; 5(7):717-23. http://doi.org/10.1002/jbmr.5650050708

[110] Berkovitz BK, Holland GR, Moxham BJ. Color atlas oral anatomy. Wolfe Medical Publications-London 1978. https://doi.org/10.1016/0002-9416(79)90130-1

[111] Goldberg M, Kulkarni A, Young M, Boskey A. Dentin: structure, composition and mineralization. Frontiers in Bioscience 2011; (Elite Edition) 3:711–735. https://doi.org/10.2741/e281

[112] Kagayama M, Sasano Y, Sato H, Kamakura S, Motegi K, Mizoguchi I. Confocal microscopy of dentinal tubules in human tooth stained with alizarin red. Anatomy and Embryology 1999; 3:233-238. http://doi.org/10.1007/s004290050224

[113] Kienle A, Michels R, Hibst R. Magnification - a new look at a long-known optical property of dentin. Journal of Dental Research 2006; 85(10):955-959. https://doi.org/10.1177/154405910608501017

[114] Zijp JR, ten Bosch JJ. Theoretical model for the scattering of light by dentin and comparison with measurements. Applied Optics 1993; 32(4):411-415. https://doi.org/10.1364/ao.32.000411

[115] Perry A, Biel M, DeJongh O, Hefferren J. A comparative study of the native fluorescence of human dentine and bovine skin collagens. Archives of Oral Biology 1969; 14(10):1193-211. http://doi.org/10.1016/0003-9969(69)90158-7

[116] Armstrong WG, Horsley HJ. Isolation of fluorescent components from ox-bone human dentine and gelatine. Nature 1966; 211(5052):981. http://doi.org/10.1038/211981a0

[117] Spitzer D, ten Bosch JJ. The absorption and scattering of light in bovine and human dental enamel. Calcified Tissue Research 1975; 17(2):129-37. http://doi.org/10.1007/BF02547285

[118] Fujimoto D, Akiba K-ya, Nakamura N. Isolation and characterization of a fluorescent material in bovine achilles tendon collagen. Biochemical and Biophysical Research Communications 1977; 76(4):1124-9. http://doi.org/10.1016/0006-291X(77)90972-X

[119] Walters C, Eyre DR. Collagen crosslinks in human dentin: increasing content of hydroxypyridinium residues with age. Calcified Tissue International 1983; 35(4-5):401-5. http://doi.org/10.1007/BF02405067

[120] Baratieri LN, Araujo E, Monteiro Jr S. Color in natural teeth and direct resin composite restorations: essential aspects. The European Journal of Esthetic Dentistry 2007; 2(2):172-86.

[121] Berg RA, Simon JC, Fried D, Darling CL. Optical changes of dentin in the near-IR as a function of mineral content. SPIE Conference Proceedings 2017; 10044, Lasers in Dentistry XXIII, 100440M. https://doi.org/10.1117/12.2256745

[122] Mualla S. Fluorescence and dentistry. Journal of Dental and Medical Sciences 2016; 15(3):65-75.

[123] Zolotarev VM, Grisimov VN. Architectonics and optical properties of dentin and Dental Enamel. Optics and Spectroscopy 2001; 90(5):753-9. http://doi.org/10.1134/1.1374665

[124] Sirat GY, Goldstein M. Uniaxial crystal last optical element for second-and third-generation immersion lithography. SPIE Conference Proceedings 2008; 6924, Optical Microlithography XXI, 69242T. https://doi.org/10.1117/12.790828

[125] Zanin IC, Brugnera A, Goncalves RB. In vitro study of bactericidal effect of low level laser therapy in the presence of photosensitizer on cariogenic bacteria. SPIE Conference Proceedings 2002; 4610, Lasers in Dentistry VIII. https://doi.org/10.1117/12.469318

[126] Zanin ICJ, Lobo MM, Rodrigues LKA, Pimenta LAF, Höfling JF, Gonçalves RB. Photosensitization of in vitro biofilms by toluidine blue O combined with a light-emitting diode. European Journal of Oral Sciences 2006; 114(1):64-9. http://doi.org/10.1111/j.1600-0722.2006.00263.x

[127] Melo MAS, Rolim JPML, Passos VF, Lima RA, Zanin ICJ, Codes BM, Rocha SS, Rodrigues LKA. Photodynamic antimicrobial chemotherapy and ultraconservative caries removal linked for management of deep caries lesions. Photodiagnosis and Photodynamic Therapy 2015; 12(4):581-6. http://doi.org/10.1016/j.pdpdt.2015.09.005

[128] Nemezio MA, de Souza Farias SS, Borsatto MC, Aires CP, Corona SAM. Effect of methylene blue-induced photodynamic therapy on a Streptococcus mutans biofilm model. Photodiagnosis and Photodynamic Therapy 2017; 20:234-23. http://doi.org/10.1016/j.pdpdt.2017.10.025

[129] Malik Z, Hanania J, Nitzan Y. New trends in photobiology bactericidal effects of photoactivated porphyrins - an alternative approach to antimicrobial drugs. Journal of Photochemistry and Photobiology, B: Biology 1990; 5(3-4):281-293. https://doi.org/10.1016/1011-1344(90)85044-W

[130] Lipovsky A, Nitzan Y, Friedmann H, Lubart R. Sensitivity of Staphylococcus aureus strains to broadband visible light. Photochemistry and Photobiology 2009; 85(1):255-60. https://doi.org/10.1111/j.1751-1097.2008.00429.x

[131] Feuerstein O, Ginsburg I, Dayan E, Veler D, Weiss EI. Mechanism of visible light phototoxicity on Porphyromonas gingivalis and Fusobacterium nucleatum. Photochemistry and Photobiology 2005; 81(5):1186-1189. https://doi.org/10.1562/2005-04-06-ra-477

[132] Ahmed MI, Aabahalkheir AH, Aldebas, YH, Hassan EE. Antibacterial influence of omega diode laser exposure durations on Streptococcus mutans. Journal of Microbiology and Antimicrobials 2011; 3(6):136-141.

[133] Lee BS, Lin YW, Chia JS, Hsieh TT, Chen MH, Lin CP, Lan WH. Bactericidal effects of diode laser on Streptococcus mutans after irradiation through different thickness of dentin. Lasers in Surgery and Medicine 2006; 38(1):62-9. http://doi.org/10.1002/lsm.20279

[134] Al-Mamoori MHK, Hussain AK, Kodeary AK, Abed AL-Naby R. Effect of 405 nm Laser light on the cariogenic bacteria Streptococcus mutans. Journal of Babylon University for Pure and Applied Sciences 2015; 23(4).

[135] Ashkenazi H, Malik Z, Harth Y, Nitzan Y. Eradication of Propionibacterium acnes by its endogenic porphyrins after illumination with high intensity blue light. FEMS Immunology and Medical Microbiology 2003; 35(1):17-24. http://doi.org/10.1111/j.1574-695X.2003.tb00644.x

[136] Soukos NS, Som S, Abernethy AD, Ruggiero K, Dunham J, Lee C, Doukas AG, Goodson JM. Phototargeting oral black-pigmented bacteria. Antimicrobial Agents and Chemotherapy 2005; 49(4):1391-1396. http://doi.org/10.1128/AAC.49.4.1391-1396.2005

[137] Fyrestam J, Bjurshammar N, Paulsson E, Johannsen A, Östman C. Determination of porphyrins in oral bacteria by liquid chromatography electrospray ionization tandem mass spectrometry. Analytical and Bioanalytical Chemistry 2015; 407(23):7013–7023. https://doi.org/10.1007/s00216-015-8864-2

[138] Wang Y, Wang Y, Wang Y, Murray CK, Hamblin M, Hooper DC, Dai T. Antimicrobial blue light inactivation of pathogenic microbes: state of the art. Drug Resistance Updates 2017; 33-35:1–22. https://doi.org/10.1016/j.drup.2017.10.002

[139] Plavskii VY, Mikulich AV, Tretyakova AI, Leusenka IA, Plavskaya LG, Kazyuchits OA, Dobysh II, Krasnenkova TP. Porphyrins and flavins as endogenous acceptors of optical radiation of blue spectral region determining photoinactivation of microbial cells. Journal of Photochemistry and Photobiology, B: Biology 2018; 183:172-183. https://doi.org/10.1016/j.jphotobiol.2018.04.021

[140] Yamamoto Y, Poole LB, Hantgan RR, Kamio Y. An iron-binding protein, Dpr, from Streptococcus mutans prevents iron-dependent hydroxyl radical formation in vitro. Journal of Bacteriology 2002; 184(11):2931-2939. https://doi.org/10.1128/JB.184.11.2931-2939.2002

[141] Ogura SI, Maruyama K, Hagiya Y, Sugiyama Y, Tsuchiya K, Takahashi K, Abe F, Tabata K, Okura I, Nakajima M, Tanaka T. The effect of 5-aminolevulinic acid on cytochrome c oxidase activity in mouse liver. BMC Research Notes 2011; 4, 66. https://doi.org/10.1186/1756-0500-4-66

[142] Sugiyama Y, Hagiya Y, Nakajima M, Ishizuka M, Tanaka T, Ogura S. The heme precursor 5-aminolevulinic acid disrupts the Warburg effect in tumor cells and induces caspase-dependent apoptosis. Oncology Reports 2013; 31(3):1282-1286. https://doi.org/10.3892/or.2013.2945

[143] Nitzan Y, Salmon-Divon M, Shporen E, Malik Z. ALA induced photodynamic effects on gram positive and negative bacteria. Photochemical and Photobiological Sciences 2004; 3(5):430-435. https://doi.org/10.1039/b315633h

[144] Fotinos N, Convert M, Piffaretti JC, Gurny R, Lange N. Effects on Gram-negative and Gram-positive bacteria mediated by 5-aminolevulinic acid and 5-aminolevulinic acid derivatives. Antimicrobial Agents and Chemotherapy 2008; 52(4):366-1373. https://doi.org/10.1128/AAC.01372-07

[145] Li X, Guo H, Tian Q, Zheng G, Hu Y, Fu Y, Tan H. Effects of 5-aminolevulinic acid-mediated photodynamic therapy on antibiotic-resistant staphylococcal biofilm: an in vitro study. Journal of Surgical Research 2013; 184(2):1013-21. https://doi.org/10.1016/j.jss.2013.03.094

[146] Hsieh CM, Huang YH, Chen CP, Hsieh BC, Tsai T. 5-aminolevulinic acid induced photodynamic inactivation on Staphylococcus aureus and Pseudomonas aeruginosa. Journal of Food and Drug Analysis 2014; 22(3):350-355. https://doi.org/10.1016/j.jfda.2013.09.051

[147] Saeed HMM, Faraj BM, Miradan BM. Evaluation of 5-aminolevulinic acids induced photodynamic inactivation on Streptococcus mutans and Streptococcus sobrinus; by using two light emitting diode wavelengths (In vitro study). Biomedical Research 2019; 30(5). https://doi.org/10.35841/biomedicalresearch.30-19-312

[148] Saeed HMM, Faraj BM, Miradan BM. Evaluation of antibacterial effects of 5-aminolevulinic acid in combination with light emitting diode (LED: 635nm) with different disinfection methods. Photodiagnosis and Photodynamic Therapy 2020; 29, 101615. https://doi.org/10.1016/j.pdpdt.2019.101615

[149] Liu C, Zhou Y, Wang L, Han L, Lei J, Ishaq HM, Xu J. Mechanistic aspects of the photodynamic Inactivation of vancomycin-resistant Enterococci mediated by 5-aminolevulinic acid and 5-aminolevulinic acid methyl ester. Current Microbiology 2015; 70: 528–535. https://doi.org/10.1007/s00284-014-0757-7

[150] Singh AP, Bragg PD. Reduced nicotinamide adenine dinucleotide dependent reduction of fumarate coupled to membrane energization in a cytochrome deficient mutant of Escherichia coli K12. Biochimica et Biophysica Acta – Bioenergetics 1975; 396(2):229-241. https://doi.org/10.1016/0005-2728(75)90037-7

[151] Frankenberg L. Hemoproteins of Enterococcus faecalis. Filippav 4a, 222 41 Lund, Sweden 2003. Available from: https://portal.research.lu.se/portal/files/5592008/1693160.pdf

[152] Nakayama K. Nucleotide sequence of Streptococcus mutans superoxide dismutase gene and isolation of insertion mutants. Journal of Bacteriology 1992; 174(15):4928-4934. https://doi.org/10.1128/jb.174.15.4928-4934.1992

[153] Martin ME, Byers BR, Olson MO, Salin ML, Arceneaux JE, Tolbert CA. Streptococcus mutans superoxide dismutase that is active with either manganese or iron as a cofactor. Journal of Biological Chemistry 1986; 261(20):9361-9367. https://doi.org/10.1016/S0021-9258(18)67663-X

[154] Higuchi M, Shimada M, Yamamoto Y, Hayashi T, Koga T, Kamio Y. Identification of two distinct NADH oxidases corresponding to H_2O_2-forming oxidase and H_2O-forming oxidase induced in Streptococcus mutans. Journal of General Microbiology 1993; 139(10):2343-51. https://doi.org/10.1099/00221287-139-10-2343

[155] Ahn SJ, Wen ZT, Burne RA. Effects of oxygen on virulence traits of Streptococcus mutans. Journal of Bacteriology 2007; 189(23), 8519–8527. https://doi.org/10.1128/JB.01180-07

[156] Ajdić D, McShan WM, McLaughlin RE, Savić G, Chang J, Carson MB, Primeaux C, Tian R, Kenton S, Jia H, Lin S, Qian Y, Li S, Zhu H, Najar F, Lai H, White J, Roe BA, Ferretti JJ. Genome sequence of Streptococcus mutans UA159, a cariogenic dental pathogen. Proceedings of the National Academy of Sciences of the United States of America 2002; 99(22):14434-9. https://doi.org/10.1073/pnas.172501299

[157] Liu J, Wu C, Huang IH, Merritt J, Qi F. Differential response of Streptococcus mutans towards friend and foe in mixed-species cultures. Microbiology (Reading) 157(Pt 9):2433-2444. https://doi.org/10.1099/mic.0.048314-0

[158] Higuchi M, Yamamoto Y, Kamio Y. Molecular biology of oxygen tolerance in lactic acid bacteria: functions of NADH oxidases and Dpr in oxidative stress. Journal of Bioscience and Bioengineering 2000; 90(5):484-93. https://doi.org/10.1016/S1389-1723(01)80028-1

[159] Turner ME, Huynh K, Carroll RK, Ahn SJ, Rice KC. Characterization of the Streptococcus mutans SMU.1703c-SMU.1702c operon reveals its role in riboflavin import and response to acid stress. Journal of Bacteriology 2020; 203(2):e00293-20. https://doi.org/10.1128/JB.00293-20

[160] Higuchi M, Yamamoto Y, Poole LB, Shimada M, Sato Y, Takahashi N, Kamio Y. Functions of two types of NADH oxidases in energy metabolism and oxidative stress of Streptococcus mutans. Journal of Bacteriology 2009; 181(19):5940-7. https://doi.org/10.1128/JB.181.19.5940-5947.1999

[161] Baker JL, Derr A., Karuppaiah K, MacGilvray ME, Kajfasz JK, Faustoferri RC, Rivera-Ramos I, Bitoun JP, Lemos JA, Wen ZT, Quivey Jr. RG. Streptococcus mutans NADH oxidase lies at the intersection of overlapping regulons controlled by oxygen and NAD+ levels. Journal of Bacteriology 2014; 196(12):2166–2177. https://doi.org/10.1128/JB.01542-14

[162] Yamamoto Y, Fukui K, Koujin N, Ohya H, Kimura K, Kamio Y. Regulation of the intracellular free iron pool by Dpr provides oxygen tolerance to Streptococcus mutans. Journal of Bacteriology 2004; 186(18):5997-6002. https://doi.org/10.1128/JB.186.18.5997-6002.2004

[163] Brooijmans R, Smit B, Santos F, Riel JV, de Vos WM, Hugenholtz J. Heme and menaquinone induced electron transport in lactic acid bacteria. Microbial Cell Factories 2009; 8:28. https://doi.org/10.1186/1475-2859-8-28

[164] Baureder M, Hederstedt L. Heme proteins in lactic acid bacteria. Advances in Microbial Physiology 2013; 62:1-43. https://doi.org/10.1016/B978-0-12-410515-7.00001-9

[165] Ritchey TW, Seely Jr. HW. Distribution of cytochrome-like respiration in streptococci. Journal of General Microbiology 1976; 93(2):195-203. https://doi.org/10.1099/00221287-93-2-195

[166] Dailey HA, Gerdes S, Dailey TA, Burch JS, Phillips JD. Noncanonical coproporphyrin-dependent bacterial heme biosynthesis pathway that does not use protoporphyrin. Proceedings of the National Academy of Sciences of the United States of America 2015; 112(7):2210-5. https://doi.org/10.1073/pnas.1416285112

[167] Choby JE, Skaar EP. Heme Synthesis and acquisition in bacterial pathogens. Journal of Molecular Biology 2016; 428(17):3408-3428. https://doi.org/10.1016/j.jmb.2016.03.018

[168] Jansson I, Stoilov I, Sarfarazi M, Schenkman JB. Enhanced expression of CYP1B1 in Escherichia coli. Toxicology 2000; 144(1-3):211-9. https://doi.org/10.1016/s0300-483x(99)00209-7

[169] Quehl P, Hollender J, Schüürmann J, Brossette T, Maas R, Jos, J. Co-expression of active human cytochrome P450 1A2 and cytochrome P450 reductase on the cell surface of Escherichia coli. Microbial Cell Factories 2016; 15:26. https://doi.org/10.1186/s12934-016-0427-5

[170] Naradasu D, Guionet A, Miran W, Okamoto A. Microbial current production from Streptococcus mutans correlates with biofilm metabolic activity. Biosensors and Bioelectronics 2020; 162:112236. https://doi.org/10.1016/j.bios.2020.112236

[171] White GF, Edwards MJ, Gomez-Perez L, Richardson DJ, Butt JN, Clarke TA. Mechanisms of bacterial extracellular electron exchange- In: Advances in Microbial Physiology 2016; 68:87-138. https://doi.org/10.1016/bs.ampbs.2016.02.002

[172] Singh R, Geetanjali, Chauhan SMS. Electron transfer in natural and unnatural flavoporphyrins. Bioorganic Chemistry 2004; 32(3):140-169. https://doi.org/10.1016/j.bioorg.2003.11.003

[173] Karu TI. Photobiological fundamentals of low-power laser therapy. IEEE Journal of Quantum Electronics 1987; 23(10):1703 -1717. https://doi.org/10.1109/JQE.1987.1073236

[174] Karu TI. Primary and secondary mechanisms of action of visible to near-IR radiation on cells. Journal of Photochemistry and Photobiology B: Biology 1999; 49(1):1-17. https://doi.org/10.1016/S1011-1344(98)00219-X

[175] Farivar S, Malekshahabi T, Shiari R. Biological effects of low level laser therapy. Journal of Lasers in Medical Sciences 2014; 5(2):58-62. https://doi.org/10.22037/2010.v5i2.5540

[176] Karu TI, Kalendo GS, Letokhov VS, Lobko VV. Biostimulation of Hela cells by low-intensity visible light, Il Nuovo Cimento D 1982; 1(6):828-840. https://doi.org/10.1007/BF02457460

[177] Karu TI, Pyatibrat LV, Afanasyeva NI. Cellular effects of low power laser therapy can be mediated by nitric oxide. Lasers in Surgery and Medicine 2005; 36(4):307-314. https://doi.org/10.1002/lsm.20148

[178] Antunes F, Boveris A, Cadenas E. On the mechanism and biology of cytochrome oxidase inhibition by nitric oxide. Proceedings of the National Academy of Sciences of the United States of America 2004; 101(48):16774-16779. https://doi.org/10.1073/pnas.0405368101

[179] Lane N. Cell biology: power games. Nature 2006; 443(7114):901-903. https://doi.org/10.1038/443901a

[180] Wong-Riley MTT, Liang HL, Eells JT, Chance B, Henry MM, Buchmann E, Kane M, Whelan HT. Photobiomodulation directly benefits primary neurons functionally inactivated by toxins: role of cytochrome c oxidase. Journal of Biological Chemistry 2005; 280(6):4761-4771. https://doi.org/10.1074/jbc.M409650200

[181] Wong-Riley MTT, Bai X, Buchmann E, Whelan HT. Light-emitting diode treatment reverses the effect of TTX on cytochrome oxidase in neurons. NeuroReport 2001; 12(14):3033-3037. https://doi.org/10.1097/00001756-200110080-00011

[182] Karu TI, Pyatibrat LV, Kalendo GS. Photobiological modulation of cell attachment via cytochrome c oxidase. Photochemical and Photobiological Sciences 2004; 3(2):211-216. https://doi.org/10.1039/b306126d

[183] Sommer AP. Mitochondrial cytochrome c oxidase is not the primary acceptor for near infrared light—it is mitochondrial bound water: the principles of low-level light therapy. Annals of Translational Medicine 2019; 7(Suppl 1):S13. https://doi.org/10.21037/atm.2019.01.43

[184] Lubart R, Wollman Y, Friedmann H, Rochkind S, Laulicht S. Effects of visible and near-infrared lasers on cell cultures. Journal of Photochemistry and Photobiology, B: Biology 1992; 12(3):305-310. https://doi.org/10.1016/1011-1344(92)85032-P

[185] Lavi R, Shainberg A, Shneyvays V, Hochauser E, Isaac A, Zinman T, Friedmann H, Lubart R. Detailed analysis of reactive oxygen species induced by visible light in various cell types. Lasers in Surgery and Medicine 2010; 42(6):473-480. https://doi.org/10.1002/lsm.20919

[186] Finkel T. Oxidant signals and oxidative stress. Current Opinion in Cell Biology 2003; 15(2):247-254. https://doi.org/10.1016/S0955-0674(03)00002-4

[187] Janssen-Heininger YMW, Mossman BT, Heintz NH, Forman HJ, Kalyanaraman B, Finkel T, Stamler JS, Rhee SG, van der Vliet A. Redox-based regulation of signal transduction: principles, pitfalls, and promises. Free Radical Biology and Medicine 2008; 45(1):1-17. https://doi.org/10.1016/j.freeradbiomed.2008.03.011

[188] Hsu DS, Zhao X, Zhao S, Kazantsev A, Wang RP, Todo T, Wei YF, Sancar A. Putative human blue-light photoreceptors hCRY1 and hCRY2 are flavoproteins. Biochemistry 1996; 35(44):13871-1387. https://doi.org/10.1021/bi962209o

[189] Lin C, Robertson DE, Ahmad M, Raibekas AA, Jorns MS, Dutton PL, Cashmore AR. Association of flavin adenine dinucleotide with the arabidopsis blue light receptor CRY1. Science 1995; 269(5226):968-970. https://doi.org/10.1126/science.7638620

[190] Todo T, Kim ST, Hitomi K, Otoshi E, Inui T, Morioka H, Kobayashi H, Ohtsuka E, Toh H, Ikenaga M. Flavin adenine dinucleotide as a chromophore of the xenopus (6-4) photolyase. Nucleic Acids Research 1997; 25(4):764-768. https://doi.org/10.1093/nar/25.4.764

[191] Shearman LP, Sriram S, Weaver DR, Maywood ES, Chaves I, Zheng B, Kume K, Lee CC, van der Horst GT, Hastings MH, Reppert SM. Interacting molecular loops in the mammalian circadian clock. Science 2000; 288(5468):1013-1019. https://doi.org/10.1126/science.288.5468.1013

[192] Fu L, Patel MS, Bradley A, Wagner EF, Karsenty G. The molecular clock mediates leptin-regulated bone formation. Cell 2005; 122(5):803-815. https://doi.org/10.1016/j.cell.2005.06.028

[193] Griendling K, Sorescu D, Ushio-Fukai M. NAD(P)H oxidase: role in cardiovascular biology and disease. Circulation Research 2000; 86(5):494-501. https://doi.org/10.1161/01.RES.86.5.494

[194] Braunersreuther V, Jaquet V. Reactive oxygen species in myocardial reperfusion injury: from physiopathology to therapeutic approaches. Current Pharmaceutical Biotechnology 2012; 13(1):97-114. https://doi.org/10.2174/138920112798868782

[195] Starkov AA. The role of mitochondria in reactive oxygen species metabolism and signalling. Annals of the New York Academy of Sciences 2008; 1147:37-52. https://doi.org/10.1196/annals.1427.015

[196] Gross E, Sevier CS, Heldman N, Vitu E, Bentzur M, Kaiser CA, Thorpe C, Fass D. Generating disulfides enzymatically: reaction products and electron acceptors of the endoplasmic reticulum thiol oxidase Ero1p. Proceedings of the National Academy of Sciences of the United States of America 2006; 103(2):299-304. https://doi.org/10.1073/pnas.0506448103

[197] Wu RF, Ma Z, Liu Z, Terada LS. Nox4-derived H_2O_2 mediates endoplasmic reticulum signaling through local Ras Activation. Molecular and Cellular Biology 2010; 30(14):3553-3568. https://doi.org/10.1128/mcb.01445-09

[198] Kukreja RC, Kontos HA, Hess ML, Ellis EF. PGH synthase and lipoxygenase generate superoxide in the presence of NADH or NADPH. Circulation Research 1986; 59(6):612-619. https://doi.org/10.1161/01.RES.59.6.612

[199] Roy P, Roy SK, Mitra A, Kulkarni AP. Superoxide generation by lipoxygenase in the presence of NADH and NADPH. Biochimica et Biophysica Acta 1994; 1214(2):171-179. https://doi.org/10.1016/0005-2760(94)90041-8

[200] O'Donnell VB, Azzi A. High rates of extracellular superoxide generation by cultured human fibroblasts: involvement of a lipid-metabolizing enzyme. Biochemical Journal 1996; 318(Pt 3):805-812. https://doi.org/10.1042/bj3180805

[201] Boveris A, Oshino N, Chance B. The cellular production of hydrogen peroxide. Biochemical Journal 1972; 128(3):617-30. https://doi.org/10.1042/bj1280617

[202] Nathan C, Cunningham-Bussel A. Beyond oxidative stress: an immunologist's guide to reactive oxygen species. Nature Reviews Immunology 2013; 13(5):349-361. https://doi.org/10.1038/nri3423

[203] Tahara EB, Navarete FDT, Kowaltowski AJ. Tissue-, substrate-, and site-specific characteristics of mitochondrial reactive oxygen species generation. Free Radical Biology and Medicine 2009; 46(9):1283-1297. https://10.1016/j.freeradbiomed.2009.02.008

[204] Okado-Matsumoto A, Fridovich I. Subcellular distribution of superoxide dismutases (SOD) in rat liver: Cu,Zn-SOD in mitochondria. Journal of Biological Chemistry 2001; 276(42):38388-38393. https://doi.org/10.1074/jbc.M105395200

[205] Holmgren A. Antioxidant function of thioredoxin and glutaredoxin systems. Antioxidants and Redox Signaling 2000; 2(4):811-820. https://doi.org/10.1089/ars.2000.2.4-811

[206] Dröge W. Free radicals in the physiological control of cell function. Physiological Reviews 2002; 82(1):47-95. https://doi.org/10.1152/physrev.00018.2001

[207] Finkel T. Redox-dependent signal transduction. FEBS Letters 2000; 476(1-2):52-54. https://doi.org/10.1016/S0014-5793(00)01669-0

[208] Sauer H, Wartenberg M, Hescheler J. Reactive oxygen species as intracellular messengers during cell growth and differentiation. Cellular Physiology and Biochemistry 2001; 11(4):173-186. https://doi.org/10.1159/000047804

[209] Bigarella CL, Liang R, Ghaffari S. Stem cells and the impact of ROS signalling. Development (Cambridge) 2014; 22:4206-4218. https://doi.org/10.1242/dev.107086

[210] Funes JM, Quintero M, Henderson S, Martinez D, Qureshi U, Westwood C, Clements MO, Bourboulia D, Pedley RB, Moncada S, Boshoff C. Transformation of human mesenchymal stem cells increases their dependency on oxidative phosphorylation for energy production. Proceedings of the National Academy of Sciences of the United States of America 2007; 104(15):6223-6228. https://doi.org/10.1073/pnas.0700690104

[211] Valle-Prieto A, Conget PA. Human mesenchymal stem cells efficiently manage oxidative stress. Stem Cells and Development 2010; 19(12):1885-1893. https://doi.org/10.1089/scd.2010.0093

[212] Kim KS, Choi HW, Yoon HE, Kim IY. Reactive oxygen species generated by NADPH oxidase 2 and 4 are required for chondrogenic differentiation. Journal of Biological Chemistry 2010; 285(51):40294-40302. https://doi.org/10.1074/jbc.M110.126821

[213] Lyublinskaya OG, Borisov YG, Pugovkina NA, Smirnova IS, Obidina JV, Ivanova JS, Zenin VV, Shatrova AN, Borodkina AV, Aksenov ND, Zemelko VI, Burova EB, Puzanov MV, Nikolsky NN. Reactive oxygen species are required for human mesenchymal stem cells to initiate proliferation after the quiescence exit. Oxidative Medicine and Cellular Longevity 2015; 2015:502105 https://doi.org/10.1155/2015/502105

[214] Ryu JM, Lee HK, Jung YH, Lee KHKim DI, Kim JY, Ko SH, Choi GE, Chai II, Song EJ, Lee SJ, Han HJ. Regulation of stem cell fate by ROS-mediated alteration of metabolism. International Journal of Stem Cells 2015; 8(1):24-35. https://doi.org/10.15283/ijsc.2015.8.1.24

[215] Atashi F, Modarressi A, Pepper MS. The role of reactive oxygen species in mesenchymal stem cell adipogenic and osteogenic differentiation: a review. Stem Cells and Development 2015; 24(10):1150-1163. https://doi.org/10.1089/scd.2014.0484

[216] Denu RA, Hematti P. Effects of oxidative Stress on mesenchymal stem cell biology. Oxidative Medicine and Cellular Longevity 2016; 2989076. https://doi.org/10.1155/2016/2989076

[217] Matsui S, Takahashi C, Tsujimoto Y, Matsushima K. Stimulatory effects of low-concentration reactive oxygen species on calcification ability of human dental pulp cells. Journal of Endodontics 2009; 35(1):67-72. https://doi.org/10.1016/j.joen.2008.08.034

[218] Tao J, Wang H, Zhai Y, Park H, Wang J, Ji F, Zhang Z. Downregulation of Nrf2 promotes autophagy-dependent osteoblastic differentiation of adipose-derived mesenchymal stem cells. Experimental Cell Research 2016; 349(2):221-229. https://doi.org/10.1016/j.yexcr.2016.09.013

[219] Sonoda S, Mei YF, Atsuta I, Danjo A, Yamaza H, Hama S, Nishida K, Tang R, Kyumoto-Nakamura Y, Uehara N, Kukita T, Nishimura F, Yamaza T. Exogenous nitric oxide stimulates the odontogenic differentiation of rat dental pulp stem cells. Scientific Reports 2018; 8(1):3149. https://doi.org/10.1038/s41598-018-21183-6

[220] Arai M, Shibata Y, Pugdee K, Abiko Y, Ogata Y. Effects of reactive oxygen species (ROS) on antioxidant system and osteoblastic differentiation in MC3T3-E1 cells. IUBMB Life 2007; 59(1):27-33. https://doi.org/10.1080/15216540601156188

[221] Amaroli A, Agas D, Laus F, Cuteri V, Hanna R, Sabbieti MG, Benedicenti S. The effects of photobiomodulation of 808 nm diode laser therapy at higher fluence on the in vitro osteogenic differentiation of bone marrow stromal cells. Frontiers in Physiology 2018; 9:123. https://doi.org/10.3389/fphys.2018.00123

[222] Turrioni APS, Basso FG, Montoro LA, De Almeida LDFD, Costa CADS, Hebling J. Phototherapy up-regulates dentin matrix proteins expression and synthesis by stem cells from human-exfoliated deciduous teeth. Journal of Dentistry 2014; 42(10):1292-1299. http://doi.org/10.1016/j.jdent.2014.07.014

[223] Yuan Y, Yan G, Gong R, Zhang L, Liu T, Feng C, du W, Wang Y, Yang F, Li Y, Guo S, Ding F, Ma W, Idiiatullina E, Pavlov V, Han Z, Cai B, Yang L. Effects of blue light emitting diode irradiation on the proliferation, apoptosis and differentiation of bone marrow-derived mesenchymal stem cells. Cellular Physiology and Biochemistry 2017; 43(1):237-246. https://doi.org/10.1159/000480344

[224] Glavaš H, Vukobratović M, Keser T. Infrared thermography as control of handheld IPL device for home-use. Journal of Cosmetic and Laser Therapy 2018; 20(5):269-277. https://doi.org/10.1080/14764172.2017.1406607

[225] Wang Z, Cai F, Chen X, Luo M, Hu L, Lu Y. The role of mitochondria-derived reactive oxygen species in hyperthermia-induced platelet apoptosis. PLoS One 2013; 8(9):e75044. https://doi.org/10.1371/journal.pone.0075044

[226] Koçani F, Kamberi B, Dragusha E, Mrasori S, Haliti F. The cleaning efficiency of the root canal after different instrumentation technique and irrigation protocol: a SEM analysis. Open Journal of Stomatology 2012; 2:69-76. http://dx.doi.org/10.4236/ojst.2012.22013

[227] Lo Giudice G, Cutroneo G, Centofanti A, Artemisia A, Bramanti E, Militi A, Rizzo G, Favaloro A, Irrera A, Lo Giudice R, Cicciù M. Dentin morphology of root canal surface: a quantitative evaluation based on a scanning electronic microscopy study. BioMed Research International 2015; 164065. https://doi.org/10.1155/2015/164065

[228] Acton JC, Dawson PL. Particle size and scattering. In: Proteins in Food Processing. Woodhead Publishing Limited 2004; 635-636.

[229] Bumah VV, Masson-Meyers DS, Cashin SE, Enwemeka CS. Wavelength and bacterial density influence the bactericidal effect of blue light on methicillin-resistant Staphylococcus aureus (MRSA). Photomedecine and Laser Surgery 2013; 31(11):547-53. https://doi.org/10.1089/pho.2012.3461

[230] Silva DFT, Mesquita-Ferrari RA, Fernandes KPS, Raele MP, Wetter NU, Deana AM. Effective transmission of light for media culture, plates and tubes. Photochemistry and Photobiology 2012; 88(5):1211-6. https://doi.org/10.1111/j.1751-1097.2012.01166.x

[231] Miles AA, Misra SS, Irwin JO. The estimation of the bactericidal power of the blood. Journal of Hygiene 1938; 38(6):732–749. https://doi.org/10.1017/S002217240001158X

[232] Hadis MA, Cooper PR, Milward MR, Gorecki P, Tarte E, Churm J, Palin WM. The effect of UV-Vis to near-infrared light on the biological response of human dental pulp cells. SPIE Conference Proceedings 2015; 9309, Mechanisms for Low-Light Therapy X, 930906. https://doi.org/10.1117/12.2077645

[233] Ranganathan V, Akhila C. Streptococcus mutans: has it become prime perpetrator for oral manifestations?. Journal of Microbiology and Experimentation 2019; 7(4):207-213. https://doi.org/10.15406/jmen.2019.07.00261

[234] Zanoni B, Garzaroli C, Anselmi S, Rondinini G. Modeling the growth of Enterococcus faecium in bologna sausage. Applied and Environmental Microbiology 1993; 59(10):3411–3417. https://doi.org/10.1128/aem.59.10.3411-3417.1993

[235] Vishwakarma A, Sharpe P, Shi S, Ramalingam M. Biology of the dentin-Pulp complex - Chapter 29. In: Stem Cell Biology and Tissue Engineering in Dental Sciences. Elsevier 2015; 371-378.

[236] Arends J, Stokroos I, Jongebloed WG, Ruben J. The diameter of dentinal tubules in human coronal dentine after demineralization and air drying: a combined light microscopy and SEM study. Caries Research 1995; 29(2):118-21. http://doi.org/10.1159/000262052

[237] Uusitalo E, Varrela J, Lassila L, Vallittu PK. Transmission of curing light through moist, air-Dried, and EDTA treated dentine and enamel. BioMed Research International 2016; 571396. http://doi.org/10.1155/2016/5713962

[238] Turrioni APS, De Oliveira CF, Basso FG, Moriyama LT, Kurachi C, Hebling J, Bagnato VS, De Souza Costa CA. Correlation between light transmission and permeability of human dentin. Lasers in Medical Science 2012; 27(1): 191-196. https://doi.org/10.1007/s10103-011-0931-0

[239] Henry CA, Dyer B, Wagner M, Judy M, Matthews JL. Phototoxicity of argon laser irradiation on biofilms of Porphyromonas and Prevotella species. Journal of Photochemistry and Photobiology B: Biology 1996; 34(2-3):123-128. https://doi.org/10.1016/1011-1344(95)07239-X

[240] Hope CK, Strother M, Creber HK, Higham SM. Lethal photosensitisation of Prevotellaceae under anaerobic conditions by their endogenous porphyrins. Photodiagnosis and Photodynamic Therapy 2016; 13:344-346. https://doi.org/10.1016/j.pdpdt.2015.07.173

[241] Maclean M, MacGregor SJ, Anderson JG, Woolsey G. Inactivation of bacterial pathogens following exposure to light from a 405-nanometer light-emitting diode array. Applied and Environmental Microbiology 2009; 75(7): 1932–1937. http://doi.org/10.1128/AEM.01892-08

[242] Hope CK, Hindley JA, Khan Z, de Josselin de Jong E, Higham SM. Lethal photosensitization of Porphyromonas gingivalis by their endogenous porphyrins under anaerobic conditions: An in vitro study. Photodiagnosis and Photodynamic Therapy 2013; 10(4):677-682. https://doi.org/10.1016/j.pdpdt.2013.08.006

[243] Maisch T, Wagner J, Papastamou V, Nerl HJ, Hiller KA, Szeimies RM, Schmalz G. Combination of 10% EDTA, photosan, and a blue light hand-held photopolymerizer to inactivate leading oral bacteria in dentistry in vitro. Journal of Applied Microbiology 2009; 107(5):1569-78. https://doi.org/10.1111/j.1365-2672.2009.04342.x

[244] Steinberg D, Moreinos D, Featherstone J, Shemesh M, Feuerstein O. Genetic and physiological effects of noncoherent visible light combined with hydrogen peroxide on Streptococcus mutans in biofilm. Antimicrobial Agents and Chemotherapy 2008; 52(7):2626-31. https://doi.org/10.1128/AAC.01666-07

[245] Feuerstein O, Moreinos D, Steinberg D. Synergic antibacterial effect between visible light and hydrogen peroxide on Streptococcus mutans. Journal of Antimicrobial Chemotherapy 2006; 57(5): 872–876. https://doi.org/10.1093/jac/dkl070

[246] Chebath-Taub D, Steinberg D, Featherstone JDB, Feuerstein O. Influence of blue light on Streptococcus mutans re-organization in biofilm. Journal of Photochemistry and Photobiology B: Biology 2012; 116:75-78. https://doi.org/10.1016/j.jphotobiol.2012.08.004

[247] Cohen-Berneron J, Steinberg D, Featherstone JDB, Feuerstein O. Sustained effects of blue light on Streptococcus mutans in regrown biofilm. Lasers in Medical Science 2016; 31:445-452. https://doi.org/10.1007/s10103-016-1873-3

[248] Felix Gomez GG, Lippert F, Ando M, Zandona AF, Eckert GJ, Gregory RL. Effect of violet-blue light on Streptococcus mutans-induced enamel demineralization. Dentistry Journal 2018; 6(2):6. https://doi.org/10.3390/dj6020006

[249] Imamura T, Tatehara S, Takebe Y, Tokuyama R, Ohshima T, Maeda N, Satomura K. Antibacterial and antifungal effect of 405 nm monochromatic laser on endodontopathogenic microorganisms. International Journal of Photoenergy 2014; 2014:387215. https://doi.org/10.1155/2014/387215

[250] Pileggi G, Wataha JC, Girard M, Grad I, Schrenzel J, Lange N, ouillaguet S. Blue light-mediated inactivation of Enterococcus faecalis in vitro. Photodiagnosis and Photodynamic Therapy 2013; 10(2):34-40. https://doi.org/10.1016/j.pdpdt.2012.11.002

[251] Tomb RM, Maclean M, Coia JE, MacGregor SJ, Anderson JG. Assessment of the potential for resistance to antimicrobial violet-blue light in Staphylococcus aureus. Antimicrobial Resistance and Infection Control 2017; 6:100. http://doi.org/10.1186/s13756-017-0261-5

[252] Kochevar IE, Redmond RW. Photosensitized production of singlet oxygen. Methods in Enzymology 2000; 319:20-28. https://doi.org/10.1016/s0076-6879(00)19004-4

[253] Wu H, Song Q, Ran G, Lu X, Xu B. Recent developments in the detection of singlet oxygen with molecular spectroscopic methods. Trends in Analytical Chemistry 2011; 30(1):133-141. https://doi.org/10.1016/j.trac.2010.08.009

[254] Baier J, Fuß T, Pöllmann C, Wiesmann C, Pindl K, Engl R, Bäumler W. Theoretical and experimental analysis of the luminescence signal of singlet oxygen for different photosensitizers. Journal of Photochemistry and Photobiology B: Biology 2007; 87(3): 163-173. https://doi.org/10.1016/j.jphotobiol.2007.02.006

[255] Bumah VV, Morrow BN, Cortez PM, Bowman CR, Rojas P, Masson-Meyers DS, Suprapto J, Tong WG, Enwemeka CS. The importance of porphyrins in blue light suppression of Streptococcus agalactiae. Journal of Photochemistry and Photobiology B: Biology 2020; 212:111996. https://doi.org/10.1016/j.jphotobiol.2020.111996

[256] Vincent SH. Oxidative effects of heme and porphyrins on proteins and lipids. Seminars in Hematology 1989; 26(2):105-13.

[257] Dietel W, Pottier R, Pfister W, Schleier P, Zinner K. 5-Aminolaevulinic acid (ALA) induced formation of different fluorescent porphyrins: a study of the biosynthesis of porphyrins by bacteria of the human digestive tract. Journal of Photochemistry and Photobiology B: Biology 2007; 86(1):77-86. https://doi.org/10.1016/j.jphotobiol.2006.07.006

[258] Kennedy JC, Pottier RH, Pross DC. Photodynamic therapy with endogenous protoporphyrin IX: basic principles and present clinical experience. Journal of Photochemistry and Photobiology, B: Biology 1990; 6(1-2):143-148. https://doi.org/10.1016/1011-1344(90)85083-9

[259] Nitzan Y, Ladan H, Malik Z. Growth-inhibitory effect of hemin on staphylococci. Current Microbiology 1987; 14:279–284 https://doi.org/10.1007/BF01568137

[260] Nitzan Y, Ladan H, Gozansky S, Malik Z. Characterization of hemin antibacterial action on Staphylococcus aureus. FEMS Microbiology Letters 1987; 48(3):401–406. https://doi.org/10.1111/j.1574-6968.1987.tb02632.x

[261] Nitzan Y, Wexler HM, Finegold SM. Inactivation of anaerobic bacteria by various photosensitized porphyrins or by hemin. Current Microbiology 1994; 29:125–131. https://doi.org/10.1007/BF01570752

[262] Kaneko T, Takahashi M, Suzuki H. Acetoin fermentation by citrate-positive Lactococcus lactis subsp. lactis 3022 grown aerobically in the presence of hemin or Cu2+. Applied and Environmental Microbiology 1990; 56(9): 2644–2649. https://doi.org/10.1128/aem.56.9.2644-2649.1990

[263] Whittenbury R. Two types of catalase-like activity in lactic acid bacteria. Nature 1960; 187:433–434. https://doi.org/10.1038/187433a0

[264] Zhang LW, Fang YP, Fang JY. Enhancement techniques for improving 5-aminolevulinic acid delivery through the skin. Dermatologica Sinica 2011; 29(1):1-7. https://doi.org/10.1016/j.dsi.2011.02.002

[265] Hollis VS, Palacios-Callender M, Springett RJ, Delpy DT, Moncada S. Monitoring cytochrome redox changes in the mitochondria of intact cells using multi-wavelength visible light spectroscopy. Biochimica et Biophysica Acta 2003; 1607(2-3):191-202. https://doi.org/10.1016/j.bbabio.2003.09.012

[266] Chalansonnet V, Mercier C, Orenga S, Gilbert C. Identification of Enterococcus faecalis enzymes with azoreductases and/or nitroreductase activity. BMC Microbiology 2017; 17(1):126. https://doi.org/10.1186/s12866-017-1033-3

[267] Lee SC, Kim J, La IJ, Kim SK, Yoon MY. Characterization of recombinant FAD-independent catabolic acetolactate synthase from Enterococcus faecalis V583. Enzyme and Microbial Technology 2013; 52(1):54-59. https://doi.org/10.1016/j.enzmictec.2012.10.006

[268] Liang JY, Cheng CW, Yu CH, Chen LY. Investigations of blue light-induced reactive oxygen species from flavin mononucleotide on inactivation of E. coli. Journal of Photochemistry and Photobiology B: Biology 2015; 143:82-88. https://doi.org/10.1016/j.jphotobiol.2015.01.005

[269] Murdoch LE, Maclean M, Endarko E, MacGregor SJ, Anderson JG. Bactericidal effects of 405 nm light exposure demonstrated by inactivation of Escherichia, Salmonella, Shigella, Listeria, and Mycobacterium species in liquid suspensions and on exposed surfaces. Scientific World Journal 2012; 137805. https://doi.org/10.1100/2012/137805

[270] De Furio M, Ahn SJ, Burne RA, Hagen SJ. Oxidative stressors modify the response of Streptococcus mutans to its competence signal peptides. Applied and Environmental Microbiology 2017; 83(22):e01345-17. https://doi.org/10.1128/AEM.01345-17

[271] Lloyd AJ, Weitzman PD, Soll D. Icomplete citric acid cycle obliges aminolevulinic acid synthesis via the C5 pathway in a methylotroph. Journal of General Microbiology 1993; 139(12):2931-2938. https://doi.org/10.1099/00221287-139-12-2931

[272] Doss M, Philipp-Dormston WK. Regulatory link between lactate dehydrogenase and biosynthesis of porphyrin and heme in microorganisms. Enzyme 1973; 16(1):28-41. https://doi.org/10.1159/000459359

[273] Mohamad SA, Milward MR, Hadis MA, Kuehne SA, Cooper PR. Photobiomodulation of mineralisation in mesenchymal stem cells. Photochemical and Photobiological Sciences 2021; 20:699-714. https://doi.org/10.1007/s43630-021-00047-5

[274] Ching HS, Luddin N, Rahman IA, Ponnuraj KT. Expression of odontogenic and osteogenic markers in DPSCs and SHED: a review. Current Stem Cell Research and Therapy 2017; 12(1):71-79. https://doi.org/10.2174/1574888x11666160815095733

[275] Shui C, Scutt A. Mild heat shock induces proliferation, alkaline phosphatase activity, and mineralization in human bone marrow stromal cells and Mg-63 cells in vitro. Journal of Bone and Mineral Research 2001; 16(4):731-41. https://doi.org/10.1359/jbmr.2001.16.4.731

[276] Chen J, Shi ZD, Ji X, Morales J, Zhang J, Kaur N, Wang S. Enhanced osteogenesis of human mesenchymal stem cells by periodic heat shock in self-assembling peptide hydrogel. Tissue Engineering Part A 2013; 19(5-6):716-28. https://doi.org/10.1089/ten.tea.2012.0070

[277] Li C, Sunderic K, Nicoll SB, Wang S. Downregulation of heat shock protein 70 impairs osteogenic and chondrogenic differentiation in human mesenchymal stem cells. Scientific Reports 2018; 8, 553. https://doi.org/10.1038/s41598-017-18541-1

[278] Komiyama EY, Lepesqueur LSS, Yassuda CG, Samaranayake LP, Parahitiyawa NB, Balducci I, Koga-Ito CY. Enterococcus species in the oral cavity: prevalence, virulence factors and antimicrobial susceptibility. PLoS One 2016; 11(9):e0163001. https://doi.org/10.1371/journal.pone.0163001

[279] Souto R, Colombo. Prevalence of Enterococcus faecalis in subgingival biofilm and saliva of subjects with chronic periodontal infection. Archives of Oral Biology 2008; 53(2):155-60. https://doi.org/10.1016/j.archoralbio.2007.08.004

[280] Carr FJ, Chill D, Maida N. The lactic acid bacteria: a literature survey. Critical Reviews in Microbiology 2002; 28(4):281-370. https://doi.org/10.1080/1040-840291046759

[281] Robert AW, Marcon BH, Dallagiovanna B, Shigunov P. Adipogenesis, osteogenesis, and chondrogenesis of human mesenchymal stem/stromal cells: a comparative transcriptome approach. Frontiers in Cell and Developmental Biology 2020; 8, 561. https://doi.org/10.3389/fcell.2020.00561

[282] Brittan JL, Sprague SV, Macdonald EL, Love RM, Jenkinson HF, West NX. In vivo model for microbial invasion of tooth root dentinal tubules. Journal of Applied Oral Science 2016; 24(2):126–135. https://doi.org/10.1590/1678-775720150448

Appendices

Conference presentations:

Feb 2019: Oral presentation at the Oral Microbiology and Immunology group (OMIG) Symposium – Newcastle University. Title: 'Photodisinfection of dental tissue'.

Sep 2019: Oral presentation at the British society of oral and dental research (BSODR) annual meeting – University of Leeds. Title: 'Transmission of 405 nm light through dentine towards phototherapeutic applications'.

Publications:

Mohamad SA, Milward MR, Kuehne SA, Hadis MA, Palin WM, Cooper PR. Potential for direct application of blue light for photo-disinfection of dentine. J Photochem Photobiol B 2021; 215:112123. https://doi.org/10.1016/j.jphotobiol.2021.112123

Mohamad SA, Milward MR, Hadis MA, Kuehne SA, Cooper PR.Photobiomodulation of mineralisation in mesenchymal stem cells. Photochem Photobiol Sci 2021; 20:699-714. https://doi.org/10.1007/s43630-021-00047-5

Journal of Photochemistry & Photobiology, B: Biology 215 (2021) 112123

Contents lists available at ScienceDirect

Journal of Photochemistry & Photobiology, B: Biology

journal homepage: www.elsevier.com/locate/jphotobiol

Potential for direct application of blue light for photo-disinfection of dentine

Sherif A. Mohamad [a,*], Michael R. Milward [a], Sarah A. Kuehne [a,b], Mohammed A. Hadis [a], William M. Palin [a], Paul R. Cooper [a,c]

[a] Institute of Clinical Sciences, School of Dentistry, University of Birmingham, 5 Mill Pool Way, Edgbaston, Birmingham B5 7EG, UK
[b] Institute of Microbiology and Infection, University of Birmingham, 5 Mill Pool Way, Edgbaston, Birmingham B5 7EG, UK
[c] Department of Oral Sciences, Sir John Walsh Research Institute, Faculty of Dentistry, University of Otago, PO Box 56, Dunedin 9054, New Zealand

ARTICLE INFO

Keywords:
405 nm
Blue light
Light transmission
Dentinal tubules
Caries
S. mutans

ABSTRACT

The direct application of light for photo-disinfection potentially provides a safe and novel modality to inhibit or eliminate cariogenic bacteria residing upon and within dentine. This study aimed to both; characterize the pattern of transmission of 405 nm light through molar dentine at different tooth locations, as well as, determine the irradiation parameters that are antibacterial for *Streptococcus mutans* under various growth conditions, including lawns, planktonic cultures, and biofilms. To determine the amount of light (405 nm) transmitted at different anatomical tooth locations; irradiance values were recorded after blue light (470–4054 mW/cm^2) had traversed through occlusal, oblique, and buccal dentine sections; and three thicknesses - 1, 2 and 3 mm were investigated. To determine tubular density; scanning electron micrographs from 2 mm outer (dentine-enamel junction) and inner (pulp) dentine sections were analysed. For photo-disinfection studies; *S. mutans* was irradiated using the same 405 nm wavelength light at a range of doses (110–1254 J/cm^2) in both biofilm and planktonic cultures. The inhibitory effect of the irradiation on bacterial lawns was compared by measuring zones of inhibition; and for planktonic cultures both spectrophotometric and colony forming unit (CFU) assays were performed. A live/dead staining assay was utilised to determine the effect of irradiation on bacterial viability in mature biofilms. Data indicated that increasing dentine thickness decreased light transmission significantly irrespective of its orientation. Occlusal and oblique samples exhibited higher transmission compared with buccal dentine. Oblique dentine 405 nm light transmission was comparable with that of occlusal dentine independent of section thickness. An increased tubule density directly positively correlated with light transmission. Irradiation at 405 nm inhibited *S. mutans* growth in both biofilm and planktonic cultures and a dose response relationship was observed. Irradiation at doses of 340 and 831 J/cm^2 led to significant reductions in bacterial growth and viability; as determined by CFU counting and live/dead staining. Data suggests that phototherapy approaches utilising a 405 nm wavelength have therapeutic potential to limit cariogenic bacterial infections both at the surface and within dentine.

1. Introduction

Dental caries is a prevalent and debilitating disease which affects all ages and sectors of the population. Despite advancements in early detection and treatment, it remains one of the most common bacterially driven dental diseases globally and is a significant healthcare and economic burden. Advancement of the disease can cause significant pain and suffering for the patient and eventually can result in tooth loss [1,2]. The key causative factor is the initial infection by the Gram positive facultative anaerobic bacterium, *Streptococcus mutans* [3]. *S. mutans* rapidly grows on the tooth surface and ferments a range of sugars which acidifies the local environment enabling further colonisation by acidogenic and acid producing bacteria. Consequently, the conditions generated by the bacterial biofilm result in demineralisation and breakdown of the tooth's hard tissues, enabling the bacteria to infiltrate through the tooth's enamel and dentine [4–8]. Notably, *S. mutans* can be isolated from both incipient and cavitated carious lesions [9,10]. If incipient caries is untreated, deeper lesions develop, leading to pulp

* Corresponding author.
E-mail address: [redacted] (S.A. Mohamad).

https://doi.org/10.1016/j.jphotobiol.2021.112123
Received 16 August 2020; Received in revised form 31 October 2020; Accepted 5 January 2021
Available online 9 January 2021

infection, tissue necrosis, peri-apical pathologies and ultimately tooth loss [11].

Effective disease management therefore should aim to minimize *S. mutans* infection at an earlier stage as possible alongside modification of the patient's diet. The delivery of chemical antibacterial compounds (*e.g.* in toothpastes or mouth washes) to inhibit initial biofilm formation and growth is the current treatment of choice, however this approach is not always effective [12–15]. When a carious lesion is advanced, its clinical treatment involves the removal of the infected tissue which is then replaced with a restoration which aims to restore the tooth's functionality. However, these restorations have a finite lifespan and frequently re-treatment procedures are required due to secondary caries, resulting in additional tooth tissue loss over time [16].

The use of direct and indirect light therapy approaches has previously been explored for photo-disinfection of dental tissues. Photodynamic therapy (PDT) provides one such approach utilising a light-activated sensitizer to generate reactive oxygen species (ROS) which subsequently exert antibacterial action [17]. Studies have explored its potential use for the treatment of dental caries *in vitro* and *ex vivo,* using photosensitizers such as toluidine blue and curcumin activated by wavelengths of 450 nm and 633 nm, respectively. Variable results were obtained and diffusion of the photosensitizer within the biofilm was shown to be a potential limitation of this approach [18,19].

Recent studies have now indicated that direct light irradiation could be used for bacterial killing. Compared with PDT, direct light potentially results in excitation of locally derived bacterial chromophores which subsequently release ROS, exerting an antibacterial affect [20]. Intracellular porphyrins are proposed as the main endogenous photosensitizers, which have an absorption peak within the violet/blue spectral range, *i.e.* 390–425 nm [21–23]. Indeed, a recent *in vitro* study has indicated that irradiation at 405 nm could be used directly to inhibit cariogenic bacteria residing within biofilms [24]. Other *ex vivo* studies have also demonstrated the potential efficacy of direct light application for dental tissue disinfection, however, frequently, neither details of the light parameters, nor the orientation of the dentinal tissues used were reported [25–28].

Importantly, for dental applications, photo-disinfection approaches should be able to kill bacteria on the tooth surface and located within the dentinal tubules [8]. Notably, the dentine's tubular structure is complex and has an S-shaped curvature or linear orientation depending upon their location within the tooth. Furthermore, tubules are conical due to the deposition of intratubular dentine which has been deposited at increased levels at the outer dentinal margins as the tooth ages [29,30]. Consequently, dentine is optically anisotropic, and light scattering, also due to dentine's non-homogenous composition, is relatively high in the near ultraviolet - Near Infrared light spectrum. At the dentine's outer-surface scattering is lower compared with locations closer to the pulp where there is a higher dentinal tubule density with wider diameters [31].

The light dose/energy density (J/cm2) is directly related to reductions in bacterial viability and the delivered dose is dependent upon both; light irradiance/power density (W/cm2) and irradiation time (seconds). Therefore, decreased irradiation times for antibacterial action can potentially be obtained by using high energy irradiation [32]. To identify potential therapeutic irradiation parameters for use in a clinically relevant time-frame for dental tissue photo-disinfection, it is important to determine the optical characteristics of dentine at the target wavelength. Notably, differences in absorption and transmission at different anatomical tooth locations will influence how light could be delivered to disease areas. This study, for the first time, utilises the same light source, which is comprehensive photo-physically characterised, and aims to both; i) determine 405 nm light transmission through dentine, and ii) identify 405 nm light irradiation parameters that have direct antimicrobial efficacy for *S. mutans* which have the potential to be used both prophylactically and to treat different stages of carious infection.

2. Materials and methods

2.1. Dentine specimens

Seventy-five non-carious human permanent molars (aged 20–40 of approximately equal gender) were used in this study (Ethical Approval Ref.: BCHCDent398.ToothBank/REC Ref.: 14/EM/1128/IRAS Ref.: 161303). All teeth were stored at 80 °C prior to use.

2.1.1. Dentine light transmission

Teeth were fixed in acrylic blocks using impression compound sticks (Kerr®; USA) to enable sectioning. A water-cooled low speed saw (IsoMet™, BUEHLER®, USA) was used and a primary cut was made to remove the surface layer of enamel. Dentine discs (n 45); from randomly selected samples, were sliced and assigned to three main groups; cross-sectional occlusal, oblique and longitudinal buccal sections. Each group contained three sub-groups of thicknesses: 1 mm, 2 mm, and 3 mm (n 5 each). Polishing of surfaces using a carborundum stone (CARBORUNDUM®, France) was performed; after which discs were washed under running tap water and stored at room temperature in distilled water (*E*-POD®, Millitrack®, Germany) until light transmission measurements were undertaken. Compressed air was administrated to surface dry specimens prior to testing. A spectrometer; USB4000-VIS-NIR (Ocean Optics, USA); connected with 200 μm optical fibre sensor/detector and a glass cosine corrector (5 mm), were calibrated using deuterium/halogen light source DH2000 (Ocean Optics, USA). Transmission of light at 405 nm (AURA light engine®, lumencor®, USA) in each sample was recorded with the dentine disc aligned between the light source (7 mm) above, and the detector below. Specimens were oriented with the pulpal side downward [see Supp. Fig. 1]. Increasing irradiation power settings were applied to investigate the potential of delivering light which was able to penetrate the dentine and may be used for antibacterial action in a clinically relevant time-frame. An irradiance reading (mW/cm^2) was obtained for 10 increasing power outputs of the light source (470, 968, 1473, 1923, 2360, 2774, 3152, 3503, 3768, and 4054 mw/cm^2). Each reading was recorded in triplicate and an average value was calculated. The percentage of light transmitted was calculated in reference to an initial characterisation of the light source; measuring its absolute irradiance at distances of 1, 2, 3 mm between the light source and the sensor through atmospheric air. This percentage was calculated using an average of 10 measurements (*i.e.* at 10 gradual power settings) for each sample; after which, a mean from 5 measurements (per group) was calculated.

2.1.2. Dentinal tubule characterisation

Dentine discs (n 30) from non-carious molar teeth were randomly sectioned and assigned to six groups (2 mm thick) (n 5 per group). To assess the dentinal tubule density at different depths, three groups (occlusal, oblique, and buccal) were obtained with two sub-groups within each group; namely outer and inner. Outer sections were adjacent to the dentine-enamel junction (DEJ), while inner sections were located adjacent to the pulp chamber. All sectioning/slicing procedures were performed as described above. To ensure complete smear layer removal in preparation for imaging, samples were rinsed under running tap water, then each sub-group was treated in an ultrasonic bath (In-Ceram Vitasonic, VITA; Germany) for 10 min in a mixture of 5% sodium hypochlorite (Acros Organics, Fisher Scientific, UK) and 17% ethylene-diamine-tetraacetic acid (EDTA) (CanalPro EDTA 17%; COLTENE); relying on a previously published protocol [33]. This was followed by a further 10 min treatment in an ultrasonic bath of distilled water. Specimens were allowed to dry at 37 °C (Hybaid Shake 'n' Stack, Thermo-Fisher Scientific; USA) for at least 72 h before imaging. Specimens were gold sputter coated (Emitech K550X, Quorum Technologies; UK) under argon for 3 min at 20 mA at a distance of 45 mm to obtain a gold coating thickness of 21 nm. Specimens were imaged using a scanning electron microscope (SEM) (EVO MA10, Carl Zeiss; Germany). Micrographs were

captured at 2000× magnification under high vacuum and electron high tension (EHT) voltage of 20 kV. Dentinal tubule numbers were quantified using ImageJ software (National Institutes of Health; USA). Subsequently, the number of tubules per unit area (mm^2) were calculated using the following formula; *'n X 10^6/Z'*, where *'n'* is the actual tubule count per image and *'Z'* is the area of the image in μm^2 [34].

2.2. Bacteria

S. mutans (ATCC 3209) was retrieved from frozen stocks (80 °C) and incubated (37 °C) aerobically (Heracell™ 150i, ThermoFisher Scientific, USA) for 24 h on brain heart infusion (BHI) agar (Sigma-Aldrich®, USA). Subsequently, a representative colony was inoculated into 10 ml of BHI broth (Sigma-Aldrich®, USA), and incubated (37 °C) overnight (18–24 h) in a shaking incubator at 100 rpm (NB-205, N-Biotek, Korea).

2.2.1. Light irradiation characterisation in bacterial cultures

Closed plate irradiation was used to avoid cross-contamination of bacterial cultures. Irradiation (AURA light engine®, Lumencor®, USA) from beneath the plates was performed to minimize the Rayleigh scattering of blue light in air [35], and maximize its penetration within bacterial layers [36]. Light characterisation was performed with the light source at a distance of 5 mm from the underside of the culture plate to better represent the use of light in a dental cavity where direct application to a cavity wall would not be clinically feasible. To determine irradiance values, the detector USB4000-VIS-NIR (Ocean Optics, USA) was placed in contact with the agar surface orientated towards the underside of the agar dish [see Supp. Fig. 2(a)]. Using the 405 nm wavelength the irradiance readings (mW/cm^2) were obtained at 10 gradual power outputs (470–4054 mW/cm^2). Readings were recorded three times and an average was obtained. Data were used to generate a calibration curve. A calibration curve; using a similar approach was also generated for black-walled 96 well plates (4titude®; UK), with the light source placed in contact with the flat transparent underside of the well (6 mm); with the sensor in contact with the base of the well. As the diameter of the light source (7 mm) and the well were comparable, this experimental set-up ensured consistent saturation of the light beam within each black-walled well in the culture plate. No light leakage between wells was detected [see Supp. Fig. 2(b)]. Calibration curves were used to estimate irradiation doses applied using each experimental set-up; '*Dose (J/cm2) Irradiance (W/cm2) X Time (seconds)*'.

2.2.2. S. mutans viability analysis

2.2.2.1. Bacterial lawns. Overnight bacterial cultures were diluted in fresh BHI broth to an optical density (OD) of 0.1 (≃ 10^8 CFU/ml) using a 7315 spectrophotometer (Jenway, UK) with an absorbance wavelength of 600 nm. Using a sterile cotton swab (Sterilin™, Thermofisher Scientific, USA); *S. mutans* was lawned onto the BHI agar. Subsequently, a non-irradiated plate served as the negative control; while experimental plates were exposed at six increasing doses of 110, 154, 273, 366, 456, and 573 J/cm^2 – one dose per plate. Each dose was delivered using two different regimens; either with i) increased time/decreased power (IT/DP), or ii) increased power/decreased time (IP/DT) [see Table 1]. This protocol was adopted to identify optimal conditions which may have direct clinical application whilst minimising any potential heating effects. Following irradiation agar plates were incubated (37 °C) for up to 24 h. Standardized images were obtained (SX620 HS, Canon, Japan) for each plate and diameter of zones of inhibition (ZOI) were measured using ImageJ software (National Institutes of Health; USA). Each ZOI was measured at three different orientations along horizontal, vertical and diagonal axes, and an average ZOI diameter was obtained. Studies were repeated four times.

Table 1
Irradiation parameters applied when exposing *S. mutans* lawns to 405 nm light. The light source was placed at a 5 mm distance from the underside of the agar plate (see Supp. Fig. 2).

Irradiance (mW/cm^2)	Irradiation time	Dose (J/cm^2)
122	15 min	110 (IT/DP)
251	7 min + 13 s	110 (IP/DP)
172	15 min	154 (IT/DP)
251	10 min + 12 s	154 (IP/DT)
152	30 min	273 (IT/DP)
251	18 min + 6 s	273 (IP/DT)
122	50 min	366 (IT/DP)
191	31 min + 54 s	366 (IP/DT)
152	50 min	456 (IT/DP)
191	39 min + 42 s	456 (IP/DT)
191	50 min	573 (IT/DP)
251	38 min	573 (IP/DT)

2.2.2.2. Planktonic culture assay. S. mutans was grown, sub-cultured, and diluted as described above. Subsequently, 200 µl of diluted cultures were transferred into a well of a black-walled 96-well plate. Two control wells were not exposed to light in each plate and a range of doses were applied including: 249, 340, 608, 831, 1014, and 1254 J/cm^2. (IT/DP) and (IP/DT) modes were also investigated [see Table 2]. Doses were applied to individual wells in each plate. Subsequently, plates were incubated at 37 °C for up to 24 h. To determine bacterial cell viability and killing after irradiation, turbidity and colony forming units (CFU) assays were performed. For the turbidity assessment, the OD of wells was read at 600 nm using an ELx800™ Microplate Reader (BioTek™, USA). The survival rate was calculated based on the equation: *'Treated wells OD/Control wells OD X 100'*. Experiments were performed in triplicate. Two doses were investigated; 340 J/cm2 (378 mW/cm^2 for 15 min) and 831 J/cm2 (418 mW/cm^2 for 33 min) to assess reductions in colony forming units. Colony counts for samples in irradiated and non-irradiated wells were performed using the Miles and Misra method [37]. The number of colonies per millilitre (CFU/ml) was calculated using the formula: '*Average number of colonies for a dilution x 50 x dilution factor*'. Finally, 'Log10' of each (CFU/ml) was calculated. This experiment was repeated three times; each in duplicate (two plates per experiment).

2.2.2.3. Mature biofilm assay. Overnight cultures were vortexed (IEC Centra CL2, Thermofisher Scientific, USA), then centrifuged at 5000 RPM for 5 min. Afterwards, the supernatant was removed and replaced with 10 ml of sterile phosphate buffered saline (PBS), vortexed, then re-centrifuged. This step was repeated, before replacing the supernatant again with 10 ml of sterile PBS. Subsequently, the OD was adjusted to 0.5 Mcfarland standard (Pro-Lab Diagnostics, UK) (equivalent to 1.5 × 10^8 CFU/ml) using PBS. 40 µl of the diluted culture was pipetted into each well of a 96-well plate; supplemented with 160 µl of BHI broth - with 1% sucrose (Sigma-Aldrich®, USA). The cultures were incubated at

Table 2
Irradiation parameters applied when exposing planktonic cultures to 405 nm light. The light source was placed in contact with the base of a well in a 96 well plate (see Supp. Fig. 2).

Irradiance (mW/cm^2)	Irradiation time	Dose (J/cm^2)
277	15 min	249 (IT/DP)
539	7 min + 40 s	249 (IP/DT)
378	15 min	340 (IT/DP)
539	10 min + 30 s	340 (IP/DT)
338	30 min	608 (IT/DP)
539	18 min + 48 s	608 (IP/DT)
281	50 min	831 (IT/DP)
418	33 min + 7 s	831 (IP/DT)
338	50 min	1014 (IT/DP)
418	40 min + 25 s	1014 (IP/DT)
418	50 min	1254 (IT/DP)
539	38 min + 46 s	1254 (IP/DT)

37 °C, shaking at 80 rpm for four days. On the fourth day of culture, media was removed from wells; replaced with PBS, and the formed biofilms were irradiated. Two wells per 96-well plate were irradiated for each dose of 340 J/cm^2 and 831 J/cm^2. Two control wells were included containing one positive control (non-irradiated) and a negative control which included biofilm treatment with 70% ethyl alcohol for 20 min; applied immediately prior to imaging. Immediately after light delivery, the live/dead staining protocol (Filmtracer™ LIVE/DEAD™ Biofilm Viability Kit, ThermoFisher Scientific, USA) was performed. To prepare a working solution, 3 μl of SYTO® 9 stain and 3 μL of propidium iodide were added to 1 ml sterile PBS. After PBS removal from wells, 200 μl of the working solution was added to each well and the plate was incubated in the dark at room temperature for 30 min. The stains were removed by washing with PBS, and biofilms were gently disrupted by aspiration; and 100 μl was pipetted into a μ-Dish 35 mm high Glass Bottom (ibidi ®, Germany) for imaging using a confocal microscope (LSM 700, Carl Zeiss; Germany) with excitation/emission at 480/500 nm and 490/635 nm. Image analysis for quantification of the live/dead bacterial cell percentages was performed using ImageJ software. To estimate the percentage of dead cells, the following formula was used: *'(Dead Cells/Total Cell Number) X 100'*. The experiment was performed three times; in duplicates.

2.2.3. Light absorption and temperature measurement in media

The light detector USB4000-VIS-NIR (Ocean Optics, USA) was positioned beneath the agar and absolute irradiance values were obtained. These values were deducted from reference values to calculate the amount of light absorbed by the agar. The percentage of light absorbed was based on an average of 6 measurements. The amount of blue light transmitted to the surface of the BHI agar was 67.86% ± 2.03 when irradiating the plate at a 5 mm distance; indicating that the percentage of blue light absorbed before reaching the agar surface was 32.14%. For BHI broth; absorbance was determined through 200 μl fresh BHI broth in well of a 96-well plate using a microplate reader (BioTek™, USA). The transmission percentage was calculated using the formula *'Absorbance (OD) - log10 Transmittance'* [38]. Absorbance readings were obtained three times. The percentage of light transmitted through the BHI broth was calculated to be 29.36% ± 0.24. Therefore, the amount of light absorbed in the broth was 70.53%.

K- Type thermocouples attached to a TC-08 data logger (Pico Technology; UK) were used for temperature measurements. Thermocouples were either attached to the surface of the agar or positioned within wells containing 200 μl broth following generation of access portals within the plastic ware. All temperature investigations were performed at room temperature in triplicate. Temperature elevation was always directly related to the power/irradiance setting administered regardless of either; the duration of exposure or the eventual dose. Once the irradiation commenced, temperatures increased until a stationery plateau phase was reached. The highest temperature reached at the BHI agar surface was 31.18 °C, and 37.99 °C for the BHI broth [see Supp. Table 1]. Both temperatures are within the range of normal incubation and growth for *S. mutans* [39].

2.3. Statistical analysis

Light transmission through dentine and tubule quantification data were analysed using one-way ANOVA; for comparisons of more than two groups. Tukey's *post hoc* test was applied for pairwise comparisons. For antimicrobial data; the Kruskal-Wallis test was used to determine significant differences between groups. The *Bonferroni test* was applied for pair-wise comparisons. The significance value was set at $p \leq 0.05$. Data were analysed using SPSS 17 (IBM®, USA).

3. Results

3.1. Dentine light transmission

Data demonstrated that light transmission decreased as dentine thickness increased for all orientations. Percentage of light transmitted through 1 mm dentine; in all sections (occlusal, oblique, buccal), was statistically significant compared with both the 2 and 3 mm dentine specimens ($P < 0.001$). The amount of light transmitted through either occlusal or oblique sections was consistently greater than the amount of light transmitted through buccal sections at all three thicknesses studied. No significant differences were found between occlusal and oblique dentine in terms of light transmission for the thicknesses examined. In the 1 and 3 mm dentine sections, light transmission in occlusal sections was significantly greater than in buccal dentine sections (P 0.033; P 0.040, respectively). It is notable that the percentage of light transmitted through each specimen was not significantly different regardless of the light source's power output. Light therefore appeared to be transmitted along the tubules occlusally and obliquely; compared to degrading at sites of change of orientation in tubular direction buccally [see Fig. 1 & Supp. Table 2]. Dentinal tubule quantification data revealed that occlusal and oblique dentine sections exhibited the highest tubular density in comparison with the buccal dentine. These data correlated directly with the light transmission results where the higher tubular density detected in the occlusal and oblique sections yielded higher percentages of light transmission. This was in contrast to the buccal sections which exhibited a lower dentinal tubular density. There were no significant differences between any outer and inner counts within the same section. Notably, both the inner occlusal (P 0.024) and inner oblique (P 0.004) counts were significantly higher than the inner buccal counts [see Fig. 2].

3.2. S. mutans viability following irradiation

Results indicated that 405 nm light irradiation inhibited *S. mutans* growth in a dose dependent relationship based on zone of inhibition (ZOI) measurements. There were no significant differences in ZOI diameter between single doses when applied either in the IT/DP or IP/DT mode. Delivering a dose of 573 J/cm^2 in both modes; IT/DT and IP/DT resulted in a significantly greater ZOI compared with the 110 J/cm^2 (IP/DT) (P 0.012) (P 0.016). Delivery of 573 J/cm^2 IP/DT resulted in a significantly wider ZOI compared with 110 J/cm^2 IT/DP delivery (p 0.047) [see Fig. 3]. All agar plates were re-incubated for an additional 48 h; and ZOIs were still maintained indicating that the effect of 405 nm light was bactericidal rather than bacteriostatic. To address the hypothesis that 405 nm irradiation may exert an indirect affect due to i) activation of media components, or ii) degradation of nutrients, the agar was irradiated prior to the seeding of the bacterial lawn. Notably, bacteria grew over the area where the agar was illuminated and no ZOI was observed. Additionally, irradiation with the plate lid removed, directly from above, was performed and ZOIs were also observed. To address the hypothesis that blue light may be specifically degrading or sensitizing BHI agar; irradiation of bacterial lawns was conducted on Tryptone Soy Agar, similar inhibitory effects were observed.

To determine the effect of light on planktonic bacterial growth, turbidity and CFU analyses were performed following culture irradiation at 405 nm. Using turbidity measurements, a trend was detected indicating a dose response relationship using either the IT/DP or IP/DT mode of delivery. The dose of 1254 J/cm^2 delivered using the IP/DT modality produced significantly lower survival percentages compared with 249 J/cm^2 irradiation when using both modes; IT/DP (P 0.037) and IP/DT (P 0.021). As was the case with irradiation of bacterial lawns on agar, there was no significant differences; within a single dose, between its IT/DP mode and IP/DT mode [see Fig. 4(a)]. To better characterize the potential killing effects of 340 and 831 J/cm^2 irradiation, planktonic cultures of *S. mutans* were irradiated which lead to 0.6

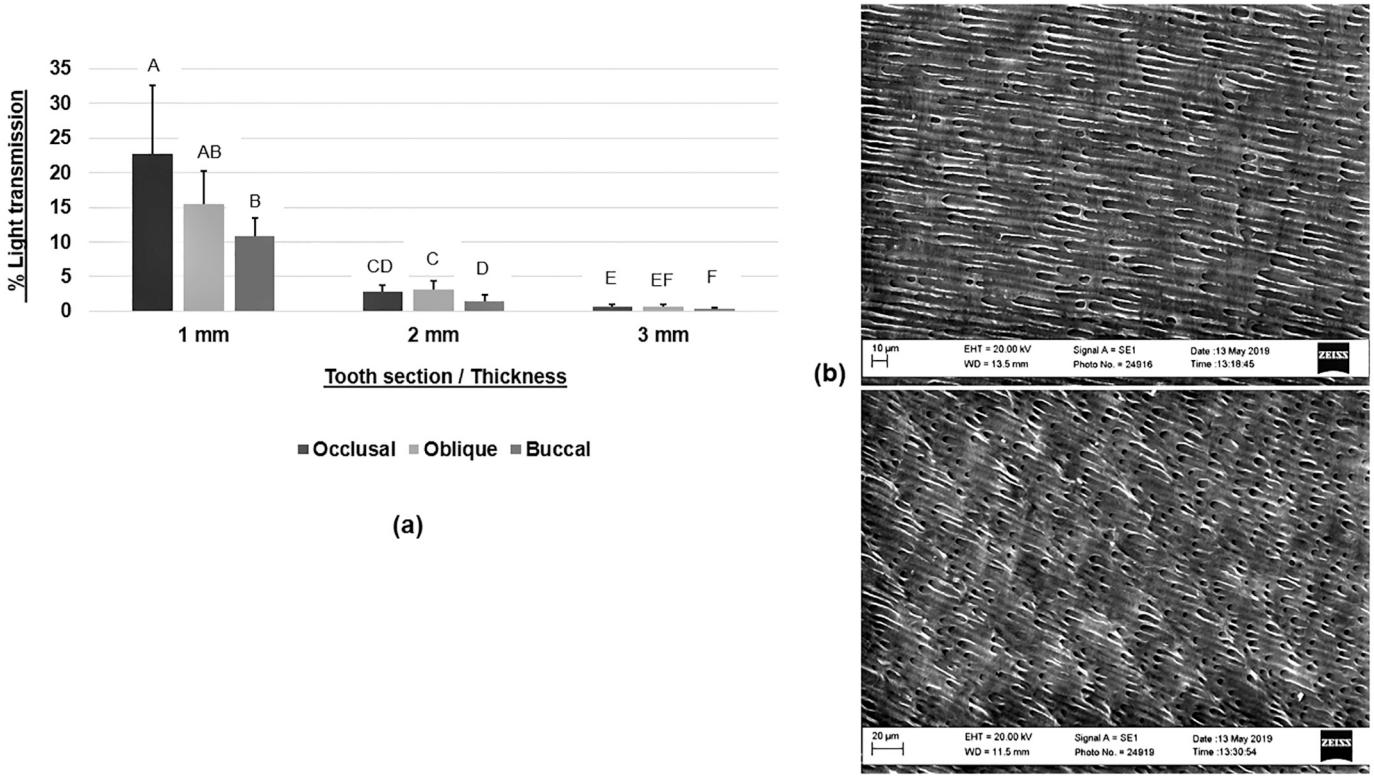

Fig. 1. (a) Bar chart showing of light transmission percentages through occlusal, oblique, and buccal dentine; at 3 separate tissue thicknesses ($n = 5$) (mean +/ S. D.). Significance level set at $P \leq 0.05$. The different letters (A-F), within each of the different thickness groups indicate statistically significant differences between the differently oriented sample groups. (b) SEM images of buccal dentine sections at the locations where a change of orientation in tubular direction occurs. The tubules are not circular, but rather elongated; occluding the light beam instead of allowing transmission.

and 0.92 log10 reductions in growth. These values were statistically significant compared with the non-irradiated controls (P 0.038) (P 0.002) [see Fig. 4(b)]. Image analysis of irradiated *S. mutans* biofilms revealed that delivery of 340 and 831 J/cm^2 light resulted in 48 ± 1.38% and 54 ± 6.38% killing, respectively [see Fig. 5]. Notably, these biofilms were irradiated solely in PBS, which therefore supports a direct antibacterial action of the light rather than this effect being due to activation of an intermediary compound as would occur due to PDT.

4. Discussion

Previously blue light has been reported to have the highest absorption and lowest penetration through dentine [40–42] whilst also having the potential to kill cariogenic bacteria [24,28]. Consequently, the current studies were performed to better characterize how 405 nm light may be applied for the treatment and management of dental disease. Data indicated that the dentinal tubule orientation played a significant role in the transmission of 405 nm light; as the percentage of light transmitted through cross-sectional dissected occlusal and oblique dentine was always significantly higher than light transmitted through longitudinally dissected buccal dentine. Fried *et al.* reported that if light is delivered perpendicular and not along the path of the tubules, it will penetrate only ~100 µm and this is in part due to dentine being a birefractive tissue as it contains hydroxyapatite crystals as well as having a complex dentinal tubule structure [43]. Interestingly, Hariri *et al.* obtained similar results to those reported here confirming that the refractive index of cross-cut dentine is less than dentine cut either obliquely or longitudinally. In longitudinal and oblique dissections, hydroxyapatite crystal and collagen orientation were reported as being key properties which influenced light propagation [44].

It is notable that considerable variation was detected in the light transmission data and this likely related to several factors. The extracted teeth used in this study were obtained from a relatively broad age range and therefore specimens would likely exhibit considerable heterogeneity in tissue structure potentially due to the presence of intratubular dentine and hence tubule width [44,45]. Furthermore, the presence of sclerotic dentine may also have been a factor influencing transmission as its presence could not be excluded [46].

Our data, along with that from several other groups, support the use of direct light application for antibacterial action against *S. mutans*. Previously, in similar studies, a range of light sources have been used including a halogen lamp (400–500 nm), a plasma arc (450–490 nm), and an LED (450–480 nm). Notably, it has been shown that *S. mutans* and *Enterococcus faecalis* lawns required a 7–10 times higher dose for killing compared with *Porphyromonas gingivalis* and *Fusobacterium nucleatum*. Furthermore, *S. mutans* eradication was only demonstrated when using the plasma arc (450–490 nm); at a dose of 159 J/cm^2 [47]. Results from the current study, however, have now shown that bacterial inhibition can be achieved using a LED light source at a wavelength of 405 nm, and lower doses than those previously reported can also be used.

Results from the current study showed that 405 nm light was capable of inhibiting *S. mutans* growth in planktonic cultures and these outcomes are in agreement with other similar studies. *S. mutans* planktonic cultures exposed to a xenon lamp (450–490 nm) at a dose of 686.4 J/cm^2 showed more than 90% growth inhibition [48]. Chebath-Taub *et al.* reported delivery of a range of doses from 68 to 680 J/cm^2 using a plasma arc lamp at wavelengths between 400 and 500 nm. All doses resulted in *S. mutans* killing and also interfered with biofilm reformation [49]. In our *S. mutans* biofilm studies results demonstrated the ability of the 405 nm light to kill 48% (340 J/cm^2) and 54% (831 J/cm^2) of bacterial cells in mature (4 days old) biofilms. Notably, the overall dose administered by De Sousa *et al.* [24] falls within the same range as was used here although they irradiated *S. mutans* biofilms twice

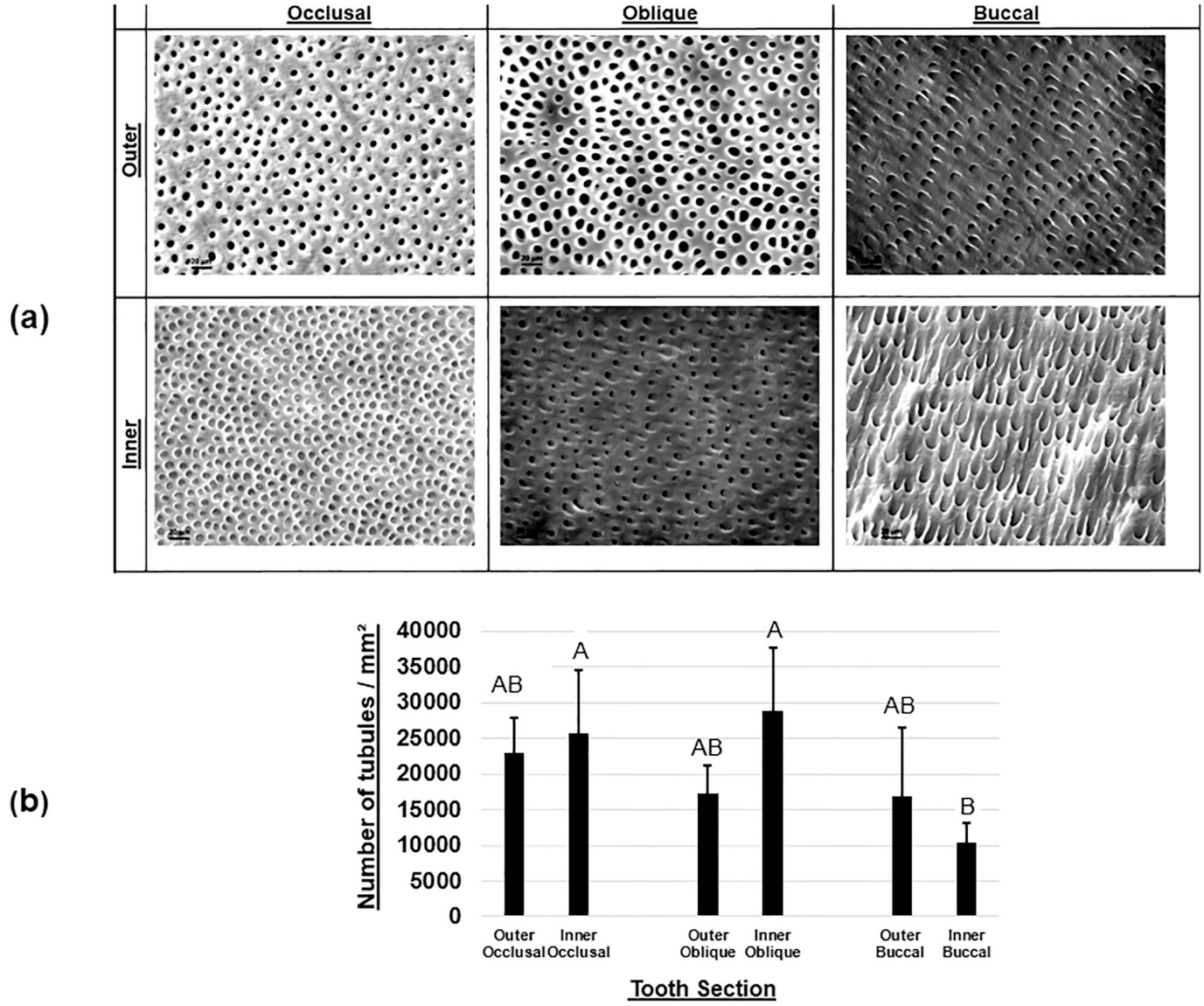

Fig. 2. (a) Representative SEM images of outer (DEJ) and inner (pulp) dentine sections from each group; occlusal, oblique, and buccal. These Images were used to quantify the dentinal tubules. (b) Bar chart showing the tubular density through occlusal, oblique, and buccal dentine (n = 5) (Mean +/ S.D.). Significance level set at $P \leq 0.05$. Different letters are statistically significantly different.

daily; for 5 days; each at 72 J/cm^2. Their irradiation protocol resulted in a significant reduction in extracellular polysaccharides, as well as, a two-fold decrease in live biomass. Gomez *et al.* [50] also proposed that irradiating 12–16 h old *S. mutans* biofilms, using a quantitative light-induced fluorescence system with a peak wavelength of 405 nm, led to a significant reduction in total biomass at doses as low as 9.26 J/cm^2. However, this reduction was only observed in biofilms grown in sucrose free media.

Results showed differences between effective antibacterial doses observed on bacterial lawns or planktonic cultures. There were also variations through light exposure reciprocity; as a longer time delivery for a given dose led to wider ZOIs. These effects likely occurred due to the variations used for the experimental set-ups. Higher irradiation doses were required to kill bacteria in a broth medium, compared with the exposure required on the surface of solid agar. Data indicated that this difference was attributable to the scattering and absorption effects on the 405 nm light in the broth, thus affecting the penetration depth. Indeed, it is well recognised that irradiation conditions, as well as, the half-life of ROS; are major modulating factors with regards to achieving disinfection [51–54]. However, there was no notable differences between the effects of the two doses investigated; on both colony counts and mature biofilms. Furthermore, it has been reported that blue light can exert enhanced bacterial killing in biofilm cultures [49,55]. Indeed, Steinberg *et al.* [56] demonstrated greater reductions in CFU counts following light irradiation for *S. mutans* biofilms compared with the levels of bacterial death detected in planktonic cultures irradiated under similar conditions.

It is therefore apparent that the direct delivery of 405 nm blue light has the potential for use to manage and treat carious infections. Based on the data presented here applying an exposure time of 7 min with an irradiance of 251 mW/cm^2, a dose of 110 J/cm^2 could be used to inhibit bacteria on the tooth surface. Using the same irradiation time but with higher irradiance parameters of 280–325 mW/cm^2, has the potential to treat bacteria at up to a 1 mm depth within dentine tubules at different tooth locations. This light application regimen would therefore easily penetrate to sufficient dentine depths which have been reported for bacterially invaded tubules [57]. Delivery of the same dose at less exposure times can be achieved by either; applying a higher power setting, or reducing the distance between the light source and the target surface [55]. Furthermore, there is the potentially that greater bacterial

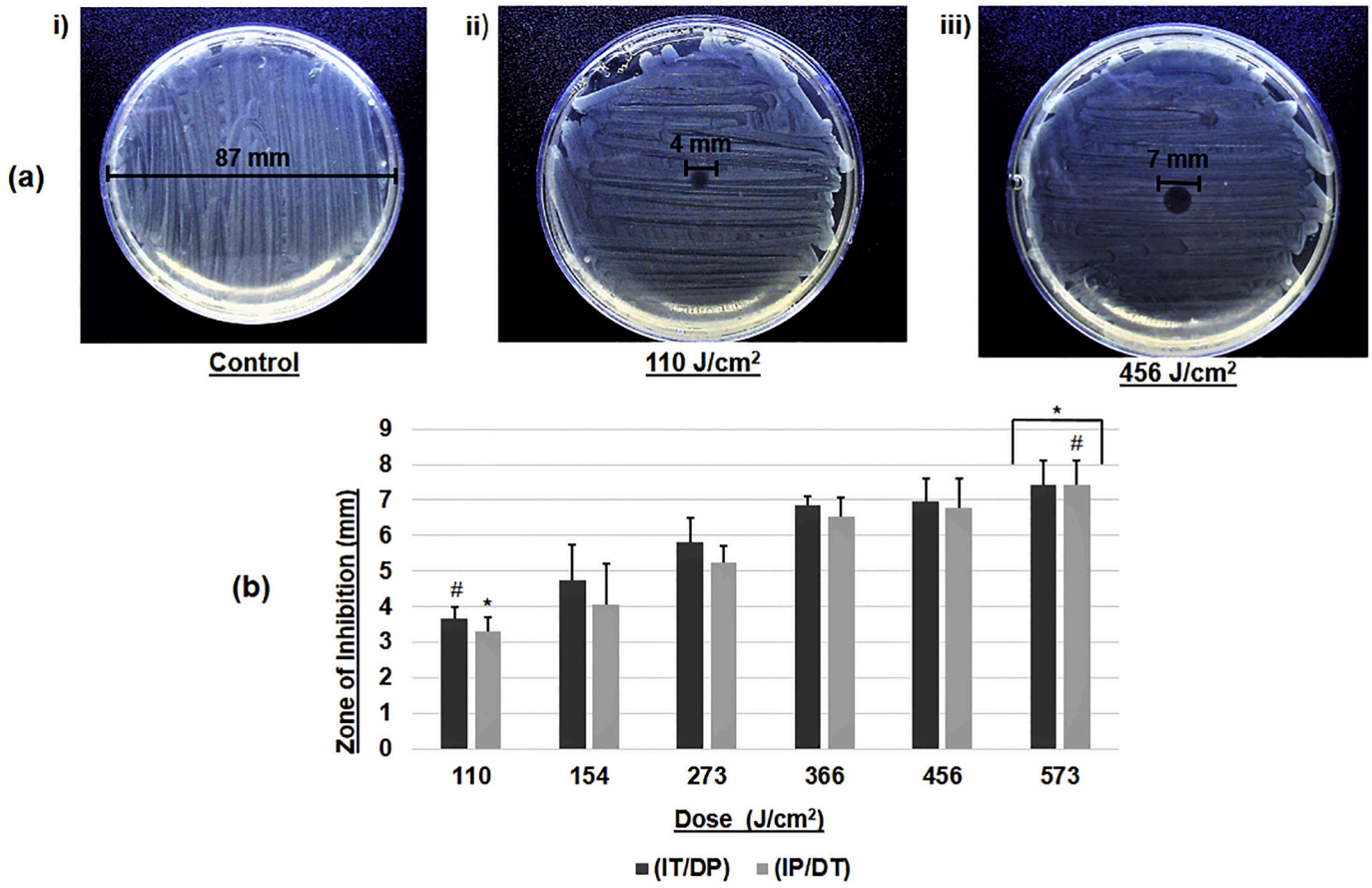

Fig. 3. (a) Representative images showing the difference between *S. mutans* i) control plate (not irradiated), ii) an agar plate exposed to 405 nm light at a dose of 110 J/cm^2, and iii) at a dose of 456 J/cm^2. As shown, the higher dose produced a greater area for the zone of Inhibition (7 mm diameter) compared with the lower dose (4 mm). (b) Bar chart showing the effect of 405 nm light on *S. mutans* lawns; when the light source was at 5 mm from agar plate bottom. Each dose was administrated in an (IT/DP) and (IP/DT) modes ($n = 4$) (Mean +/ S.D.). The same symbols show statistically significant differences. Significance level set at $p \leq 0.05$.

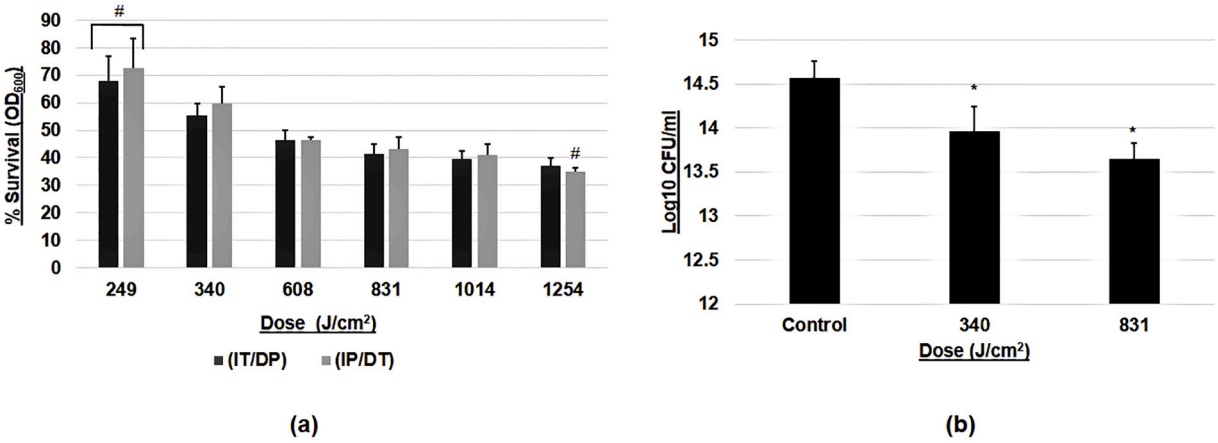

Fig. 4. Bar charts showing the effect of different 405 nm light doses on *S. mutans* planktonic cultures ($n = 3$). (a) Effect of blue light on bacterial survival percentages using OD readings at 600 nm. Each dose was administrated in either (IT/DP) or (IP/DT) mode. The same symbols show statistically significant differences. (b) Bar chart showing log10 reductions for *S. mutans* planktonic cultures; in response to 405 nm light doses of 340 and 831 J/cm^2. Irradiation parameters for 340 J/cm^2 were 378 mW/cm^2 for 15 min; while for 831 J/cm^2, were 418 mW/cm^2 for 33 min. Superscripts (*) represent a statistically significantly difference relative to the control. Significance level set at $P \leq 0.05$. Mean +/ S.D. shown.

killing at lower doses could be expected *in vivo*; as survival may not be as optimal as it is *in vitro* under the rich nutrient growth conditions used here [47]. Notably, the antimicrobial effects observed here are not based on the photo-thermal effects that are utilised by infra-red diode and carbon dioxide lasers which are potentially hazardous to healthy tissues [58,59].

To our knowledge, this is the first study which has investigated both the transmission of blue light in coronal dentine; along with determining the antibacterial effects using the same light source. The data we have presented here indicates that direct blue light delivery has the potential

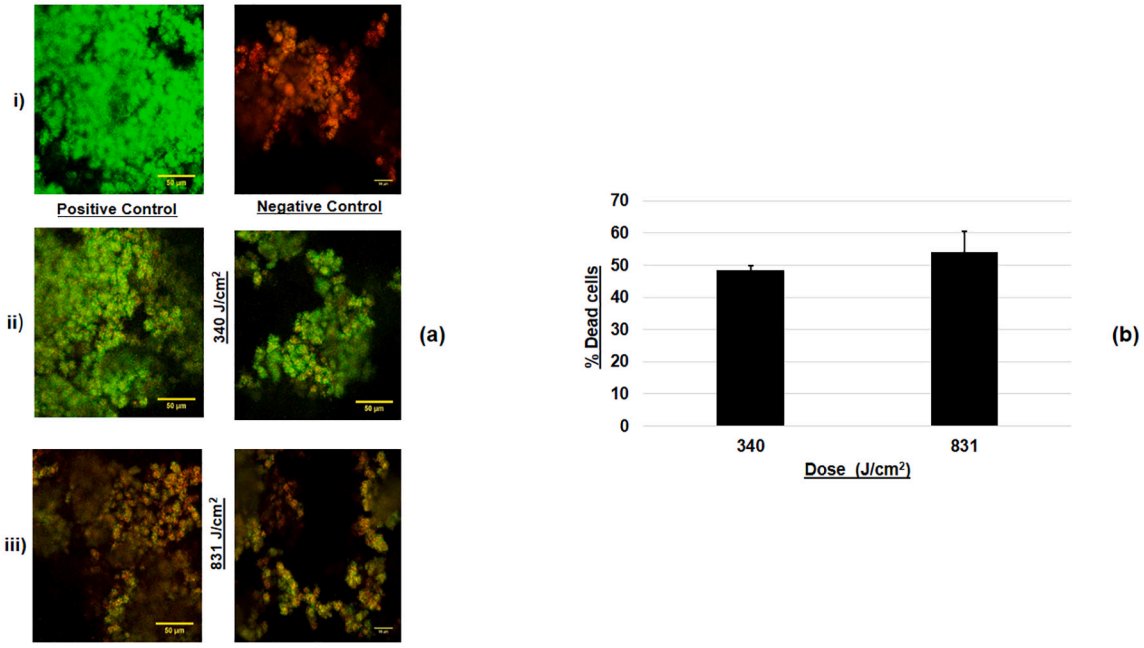

Fig. 5. (a) Representative confocal microscope images demonstrating *S. mutans* mature biofilms i) Positive and negative controls, ii) biofilm exposed to 405 nm light at a dose of 340 J/cm^2, and iii) at a dose of 831 J/cm^2. These Images were used to estimate the percentage of dead cells. (b) Bar chart showing the percentage of dead cells in response to both doses of 340 and 831 J/cm2 (n = 3) (Mean +/ S.D.). There was no statistical significant difference between the effects of the two experimental doses used.

to be used to treat and manage carious infections at different stages of disease. Our findings can therefore be used to underpin future studies which utilise well-established complex multispecies biofilm models to identify light delivery parameters for antibacterial killing which have the potential for use prophylactically and in a clinically relevant timeframe. Notably, we are also aware of the ability of 405 nm light to stimulate a positive response in host cells and tissues [60–62], therefore there is the possibility to utilise photobiomodulation to stimulate innate repair responses within the tooth through the dentine. Future translational studies will therefore require the concomitant development of a suitable therapeutic device along with further *in vitro, ex vivo* and clinical trials to demonstrate the safety and efficacy of dental phototherapy.

CRediT authorship contribution statement

Sherif A. Mohamad: Investigation, Formal analysis, Writing - original draft, Writing - review & editing. **Michael R. Milward:** Supervision, Writing - review & editing. **Sarah A. Kuehne:** Supervision, Writing - review & editing. **Mohammed A. Hadis:** Supervision. **William M. Palin:** Supervision, Writing - review & editing. **Paul R. Cooper:** Supervision, Writing - original draft, Writing - review & editing.

Declaration of Competing Interest

The authors declare that they have no known competing financial interests or personal relationships that could have appeared to influence the work reported in this paper.

Acknowledgment

The author would like to thank Soher Jayash for her generous assistance with confocal microscopy. We also acknowledge the School of Dentistry, University of Birmingham for supporting this work.

Appendix A. Supplementary data

Supplementary data to this article can be found online at https://doi.org/10.1016/j.jphotobiol.2021.112123.

References

[1] S. Listl, J. Galloway, P.A. Mossey, W. Marcenes, Global economic impact of dental diseases, J. Dent. Res. 94 (10) (2015) 1–7, https://doi.org/10.1177/0022034515602879.
[2] J.E. Frencken, P. Sharma, L. Stenhouse, D. Green, D. Laverty, T. Dietrich, Global epidemiology of dental caries and severe periodontitis – a comprehensive review, J. Clin. Periodontol. 44 (Suppl. 18) (2017) S94–S105, https://doi.org/10.1111/jcpe.12677.
[3] W.J. Loesche, Microbiology of dental decay and periodontal disease, in: Medical Microbiology, 4th edition, 1996.
[4] I.R. Hamilton, Ecological basis for dental caries, in: Oral Bacterial Ecology: The Molecular Basis, 2000.
[5] J.C. Farges, J.F. Keller, F. Carrouel, S.H. Durand, A. Romeas, F. Bleicher, S. Lebecque, M.J. Staquet, Odontoblasts in the dental pulp immune response, J. Exp. Zool. B Mol. Dev. Evol. 312B (5) (2009) 425–436, https://doi.org/10.1002/jez.b.21259.
[6] M. Shemesh, A. Tam, D. Steinberg, Expression of biofilm-associated genes of Streptococcus mutans in response to glucose and sucrose, J. Med. Microbiol. 56 (Pt 11) (2007) 1528–1535, https://doi.org/10.1099/jmm.0.47146-0.
[7] R.M. Love, H.F. Jenkinson, Invasion of dentinal tubules by oral bacteria, Crit. Rev. Oral Biol. Med. 13 (2) (2002) 171–183, https://doi.org/10.1177/154411130201300207.
[8] P.R. Cooper, J.L. McLachlan, S. Simon, L.W. Graham, A.J. Smith, Mediators of inflammation and regeneration, Adv. Dent. Res. 23 (3) (2011) 290–295, https://doi.org/10.1177/0022034511405389.
[9] X. Zhou, Y. Li, Supragingival microbes, in: Atlas of Oral Microbiology, 1st edition, 2015.
[10] M.S. Duggal, M.E.J. Curson, Dental disease/Etiology of Dental Caries, in: Encyclopedia of Food Sciences and Nutrition, 2nd edition, 2003.
[11] N.B. Pitts, Clinical diagnosis of dental caries: a European perspective, J. Dent. Educ. 65 (10) (2001) 972–978, https://doi.org/10.1177/154405910408301S03.
[12] J.D.B. Featherstone, Delivery challenges for fluoride, chlorhexidine and xylitol, BMC Oral Health 6 (Suppl. 1) (2006) S8, https://doi.org/10.1186/1472-6831-6-S1-S8.
[13] A. Moshrefi, Chlorhexidine, J. West. Soc. Periodontol. Period. Abst. 50 (1) (2002) 5–9.
[14] R. Yates, S. Jenkins, R. Newcombe, W. Wade, J. Moran, M. Addy, A 6-month home usage trial of a 1% chlorhexidine toothpaste: (I). Effects on plaque, gingivitis, calculus and tooth staining, J. Clin. Periodontol. 20 (2) (1993) 130–138, https://doi.org/10.1111/j.1600-051X.1993.tb00327.x.
[15] R. Gilbert, P. Williams, The oral retention and antiplaque efficacy of triclosan in human volunteers, Br. J. Clin. Pharmacol. 23 (5) (1987) 579–583, https://doi.org/10.1111/j.1365-2125.1987.tb03094.x.

[16] Y. Lee, Diagnosis and prevention strategies for dental caries, J. Lifestyle Med. 3 (2) (2013) 107–109.
[17] D.I. Pattison, M.J. Davies, Actions of ultraviolet light on cellular structures, EXS 96 (2006) 131–157, https://doi.org/10.1007/3-7643-7378-4_6.
[18] J.A. Williams, G.J. Pearson, M.J. Colles, M. Wilson, The photo-activated antibacterial action of toluidine blue O in a collagen matrix and in carious dentine, Caries Res. 38 (6) (2004) 530–536, https://doi.org/10.1159/000080582.
[19] N.C. Araújo, C.R. Fontana, V.S. Bagnato, M.E.M. Gerbi, Photodynamic antimicrobial therapy of curcumin in biofilms and carious dentine, Lasers Med. Sci. 29 (2) (2014) 629–635, https://doi.org/10.1007/s10103-013-1369-3.
[20] A. Lipovsky, Y. Nitzan, A. Gedanken, R. Lubart, Visible light-induced killing of bacteria as a function of wavelength: implication for wound healing, Lasers Surg. Med. 42 (6) (2010) 467–472, https://doi.org/10.1002/lsm.20948.
[21] M.R. Hamblin, J. Viveiros, C. Yang, A. Ahmadi, R.A. Ganz, M.J. Tolkoff, Helicobacter pylori accumulates photoactive porphyrins and is killed by visible light, Antimicrob. Agents Chemother. 49 (7) (2005) 2822–2827, https://doi.org/10.1128/AAC.49.7.2822-2827.2005.
[22] C.K. Lim, J.M. Rideout, D.J. Wright, High-performance liquid chromatography of naturally occurring 8-, 7-, 6-, 5- and 4-carboxylic porphyrin isomers, J. Chromatogr. 282 (1983) 629–641, https://doi.org/10.1016/S0021-9673(00)91640-6.
[23] W. Bu, N. Myers, J.D. McCarty, T. O'Neill, S. Hollar, P.L. Stetson, D.W. Sved, Simultaneous determination of six urinary porphyrins using liquid chromatography-tandem mass spectrometry, J. Chromatogr. B Anal. Technol. Biomed. Life Sci. 783 (2) (2003) 411–423, https://doi.org/10.1016/S1570-0232(02)00703-1.
[24] D.L. De Sousa, R.A. Lima, I.C. Zanin, M.I. Klein, M.N. Janal, S. Duarte, Effect of twice-daily blue light treatment on matrix-rich biofilm development, PLoS One 10 (7) (2015), e0131941, https://doi.org/10.1371/journal.pone.0131941.
[25] L.G.O. Ricatto, L.A.L. Conrado, C.P. Turssi, F.M.G. França, R.T. Basting, F.L. B. Amaral, Comparative evaluation of photodynamic therapy using LASER or light emitting diode on cariogenic bacteria: an in vitro study, Eur. J. Dent. 8 (4) (2014) 509–514, https://doi.org/10.4103/1305-7456.143634.
[26] J.P.M. Lima, M.A. Sampaio De Melo, F.M.C. Borges, A.H. Teixeira, C. Steiner-Oliveira, M. Nobre Dos Santos, L.K.A. Rodrigues, I.C.J. Zanin, Evaluation of the antimicrobial effect of photodynamic antimicrobial therapy in an in situ model of dentine caries, Eur. J. Oral Sci. 117 (5) (2009) 568–574, https://doi.org/10.1111/j.1600-0722.2009.00662.x.
[27] T. Burns, M. Wilson, G.J. Pearson, Effect of dentine and collagen on the lethal photosensitization of streptococcus mutans, Caries Res. 29 (3) (1995) 192–197, https://doi.org/10.1159/000262068.
[28] G.G. Felix Gomez, F. Lippert, M. Ando, A.F. Zandona, G.J. Eckert, R.L. Gregory, Photoinhibition of Streptococcus mutans biofilm-induced lesions in human dentin by violet-blue light, Dent. J. 7 (4) (2019) 113, https://doi.org/10.3390/dj7040113.
[29] B.K. Berkovitz, G.R. Holland, B.J. Moxham, Color atlas oral anatomy, Wolfe Med. Publ. (1978), https://doi.org/10.1016/0002-9416(79)90130-1.
[30] M. Goldberg, A. Kulkarni, M. Young, A. Boskey, Dentin: structure, composition and mineralization, Front. Biosci. (Elite Ed.) 3 (2011) 711–735, https://doi.org/10.2741/e281.
[31] J.R. Zijp, Optical Properties of Dentin. Groningen: s.n, 2001.
[32] P.J. Gwynne, M.P. Gallagher, Light as a broad-Spectrum antimicrobial, Front. Microbiol. 9 (2018) 119, https://doi.org/10.3389/fmicb.2018.00119.
[33] F. Koçani, B. Kamberi, E. Dragusha, S. Mrasori, F. Haliti, The cleaning efficiency of the root canal after different instrumentation technique and irrigation protocol: a SEM analysis, Open J. Stomatol. 2 (2012) 69–76, https://doi.org/10.4236/ojst.2012.22013.
[34] G. Lo Giudice, G. Cutroneo, A. Centofanti, A. Artemisia, E. Bramanti, A. Militi, G. Rizzo, A. Favaloro, A. Irrera, R. Lo Giudice, M. Cicciù, Dentin morphology of root canal surface: a quantitative evaluation based on a scanning electronic microscopy study, Biomed. Res. Int. 4 (2015), https://doi.org/10.1155/2015/164065.
[35] J.C. Acton, P.L. Dawson, Proteins in Food Processing, Woodhead Publishing Limited, 2004, pp. 603–604.
[36] V.V. Bumah, D.S. Masson-Meyers, S.E. Cashin, C.S. Enwemeka, Wavelength and bacterial density influence the bactericidal effect of blue light on methicillin-resistant Staphylococcus aureus (MRSA), Photomed. Laser Surg. 31 (11) (2013) 547–553, https://doi.org/10.1089/pho.2012.3461.
[37] A.A. Miles, S.S. Misra, J.O. Irwin, The estimation of the bactericidal power of the blood, J. Hyg. 38 (6) (1938) 732–749, https://doi.org/10.1017/S002217240001158X.
[38] D.F.T. Silva, R.A. Mesquita-Ferrari, K.P.S. Fernandes, M.P. Raele, N.U. Wetter, A. M. Deana, Effective transmission of light for media culture, plates and tubes, Photochem. Photobiol. 88 (5) (2012) 1211–1216, https://doi.org/10.1111/j.1751-1097.2012.01166.x.
[39] Ranganathan V, Akhila C (2019). *Streptococcus mutans*: has it become prime perpetrator for oral manifestations? J. Microbiol. Exper. 7(4):207-213. Doi:10.15406/jmen.2019.07.00261.
[40] V. Dogandzhiyska, I. Angelov, S. Dimitrov, T. Uzunov, In vitro study of light radiation penetration through dentin, according to the wavelength, Acta Med. Bulg. 42 (2) (2015) 16–22, https://doi.org/10.1515/amb-2015-0013.
[41] S.T. Ana Paula, J.R.L. Alonso, F.G. Basso, L.T. Moriyama, J. Heling, V.S. Bagnato, C.A. De Souza Costa, LED light attenuation through human dentin: a first step toward pulp photobiomodulation after cavity preparation, Am. J. Dent. 26 (6) (2013) 319–323.
[42] W.M. Palin, M.A. Hadis, M.R. Milward, J.D. Carroll, P.R. Cooper, Beam profile measurements for dental phototherapy: the effect of distance, wavelength and tissue thickness, in: Proc. SPIE 9309, Mechanisms for Low-Light Therapy X, 2015, 930905, https://doi.org/10.1117/12.2077628.
[43] D. Fried, R.E. Glena, J.D.B. Featherstone, W. Seka, Nature of light scattering in dental enamel and dentin at visible and near-infrared wavelengths, Appl. Opt. 34 (7) (1995) 1278–1285, https://doi.org/10.1364/AO.34.001278.
[44] I. Hariri, A. Sadr, Y. Shimada, J. Tagami, Y. Sumi, Effects of structural orientation of enamel and dentine on light attenuation and local refractive index: an optical coherence tomography study, J. Dent. 40 (5) (2012) 387–396, https://doi.org/10.1016/j.jdent.2012.01.017.
[45] A. Kienle, F.K. Forster, R. Diebolder, R. Hibst, Light propagation in dentin: influence of microstructure on anisotropy, Phys. Med. Biol. 48 (2) (2003) N7–14, https://doi.org/10.1088/0031-9155/48/2/401.
[46] V.M. Zolotarev, V.N. Grisimov, Architectonics and optical properties of dentin and dental enamel, Opt. Spectrosc. 90 (5) (2001) 753–759, https://doi.org/10.1134/1.1374665.
[47] O. Feuerstein, N. Persman, E.I. Weiss, Phototoxic effect of visible light on *Porphyromonas gingivalis* and fusobacterium nucleatum: an in vitro study, Photochem. Photobiol. 80 (3) (2004) 412–415, https://doi.org/10.1562/0031-8655(2004)080<0412:PEOVLO>2.0.CO;2.
[48] O. Feuerstein, D. Moreinos, D. Steinberg, Synergic antibacterial effect between visible light and hydrogen peroxide on *Streptococcus mutans*, J. Antimicrob. Chemother. 57 (5) (2006) 872–876, https://doi.org/10.1093/jac/dkl070.
[49] D. Chebath-Taub, D. Steinberg, J.D.B. Featherstone, O. Feuerstein, Influence of blue light on Streptococcus mutans re-organization in biofilm, J. Photochem. Photobiol. 116 (2012) 75–78, https://doi.org/10.1016/j.jphotobiol.2012.08.004.
[50] G.F. Gomez, R. Huang, M. MacPherson, A.G. Ferreira Zandona, R.L. Gregory, Photo inactivation of Streptococcus mutans biofilm by violet-blue light, Curr. Microbiol. 73 (3) (2016) 426–433, https://doi.org/10.1007/s00284-016-1075-z.
[51] R.M. Tomb, M. Maclean, J.E. Coia, S.J. MacGregor, J.G. Anderson, Assessment of the potential for resistance to antimicrobial violet-blue light in Staphylococcus aureus, Antimicrob. Resist. Infect. Control 6 (2017) 100, https://doi.org/10.1186/s13756-017-0261-5.
[52] I.E. Kochevar, R.W. Redmond, Photosensitized production of singlet oxygen, Methods Enzymol. 319 (2000) 20–28, https://doi.org/10.1016/s0076-6879(00)19004-4.
[53] H. Wu, Q. Song, G. Ran, X. Lu, B. Xu, Recent developments in the detection of singlet oxygen with molecular spectroscopic methods, Trends Anal. Chem. 30 (1) (2011) 133–141, https://doi.org/10.1016/j.trac.2010.08.009.
[54] J. Baier, T. Fuß, C. Pollmann, C. Wiesmann, K. Pindl, R. Engl, W. Baumler, Theoretical and experimental analysis of the luminescence signal of singlet oxygen for different photosensitizers, J. Photochem. Photobiol. 87 (3) (2007) 163–173, https://doi.org/10.1016/j.jphotobiol.2007.02.006.
[55] J. Cohen-Berneron, D. Steinberg, J.D.B. Featherstone, O. Feuerstein, Sustained effects of blue light on Streptococcus mutans in regrown biofilm, Lasers Med. Sci. 31 (3) (2016) 445–452, https://doi.org/10.1007/s10103-016-1873-3.
[56] D. Steinberg, D. Moreinos, J. Featherstone, M. Shemesh, O. Feuerstein, Genetic and physiological effects of noncoherent visible light combined with hydrogen peroxide on *Streptococcus mutans* in biofilm, Antimicrob. Agents Chemother. 52 (7) (2008) 2626–2631, https://doi.org/10.1128/AAC.01666-07.
[57] J.L. Brittan, S.V. Sprague, E.L. Macdonald, R.M. Love, H.F. Jenkinson, N.X. West, In vivo model for microbial invasion of tooth root dentinal tubules, J. Appl. Oral Sci. 24 (2) (2016) 126–135, https://doi.org/10.1590/1678-775720150448.
[58] D.N. Dederich, M.A. Pickard, A.S. Vaughn, J. Tulip, K.L. Zakariasen, Comparative bactericidal exposures for selected oral bacteria using carbon dioxide laser radiation, Lasers Surg. Med. 10 (6) (1990) 591–594, https://doi.org/10.1002/lsm.1900100612.
[59] A. Moritz, N. Gutknecht, U. Schoop, K. Goharkhay, O. Doertbudak, W. Sperr, Irradiation of infected root canals with a diode laser in vivo: results of microbiological examinations, Lasers Surg. Med. 21 (3) (1997) 221–226, https://doi.org/10.1002/(sici)1096-9101(1997)21:3<221::aid-lsm1>3.0.co;2-s.
[60] T. Kushibiki, K. Awazu, Blue laser irradiation enhances extracellular calcification of primary mesenchymal stem cells, Photomed. Laser Surg. 27 (3) (2009) 493–498, https://doi.org/10.1089/pho.2008.2343.
[61] Y. Wang, Y.Y. Huang, Y. Wang, P. Lyu, M.R. Hamblin, Photobiomodulation (blue and green light) encourages osteoblastic-differentiation of human adipose-derived stem cells: role of intracellular calcium and light-gated ion channels, Sci. Rep. 6 (2016) 33719, https://doi.org/10.1038/srep33719.
[62] T. Zhu, Y. Wu, X. Zhou, Y. Yang, Y. Wang, Irradiation by blue light-emitting diode enhances osteogenic differentiation in gingival mesenchymal stem cells in vitro, Lasers Med. Sci. 34 (7) (2019) 1473–1481, https://doi.org/10.1007/s10103-019-02750-3.

Photochemical & Photobiological Sciences (2021) 20:699–714
https://doi.org/10.1007/s43630-021-00047-5

REVIEWS

Photobiomodulation of mineralisation in mesenchymal stem cells

Sherif A. Mohamad[1] · Michael R. Milward[1] · Mohammed A. Hadis[1] · Sarah A. Kuehne[1,2] · Paul R. Cooper[3]

Received: 17 December 2020 / Accepted: 22 April 2021 / Published online: 4 May 2021

Abstract

Mesenchymal stem cells (MSCs) and photobiomodulation (PBM) both offer significant therapeutic potential in regenerative medicine. MSCs have the ability to self-renew and differentiate; giving rise to multiple cellular and tissue lineages that are utilised in repair and regeneration of damaged tissues. PBM utilises light energy delivered at a range of wavelengths to promote wound healing. The positive effects of light on MSC proliferation are well documented; and recently, several studies have determined the outcomes of PBM on mineralised tissue differentiation in MSC populations. As PBM effects are biphasic, it is important to understand the underlying cellular regulatory mechanisms, as well as, provide accurate details of the irradiation conditions, to optimise and standardise outcomes. This review article focuses on the use of red, near-infra-red (R/NIR) and blue wavelengths to promote the mineralisation potential of MSCs; and also reports on the possible molecular mechanisms which underpin transduction of these effects. A variety of potential photon absorbers have been identified which are reported to mediate the signalling mechanisms, including respiratory chain enzymes, flavins, and cryptochromes. Studies report that R/NIR and blue light stimulate MSC differentiation by enhancing respiratory chain activity and increasing reactive oxygen species levels; however, currently, there are considerable variations between irradiation parameters reported. We conclude that due to its non-invasive properties, PBM may, following optimisation, provide an efficient therapeutic approach to clinically support MSC-mediated hard tissue repair. However, to optimise application, further studies are required to identify appropriate light delivery parameters, as well as elucidate the photo-signalling mechanisms involved.

Keywords Odontoblast · Bone · Tooth · Osteogenesis · Odontogenesis · Osteoblast

1 Introduction

Repair of hard tissue following trauma or disease remains an essential therapeutic goal in rehabilitating patients back to function. Many orthopaedic patients face the challenge of delayed bone healing resulting in prolonged convalescence and the additional burden on healthcare systems. In oral disease, there is a need to promote hard tissue repair in patients suffering from diseases, such as periodontitis and caries, as well as following tooth extraction [1–3]. Regenerative therapies which utilise mesenchymal stem cells (MSCs) provide a promising therapeutic approach. MSCs can be harvested from many bodily sites, including bone marrow, adipose tissue, umbilical cord, and the dental pulp. These cells are multi-potent, can self-renew, and are capable of differentiating into mineralised tissue lineages to generate osteoblasts and odontoblast-like cells [4–6]. MSCs can proliferate to enable repopulation of the injury site, as well as being able to promote revascularization, innervation, and modulation of immune responses [7, 8]. Photobiomodulation (PBM) or low-level light therapy (LLLT) utilises light at relatively low power; inducing tissue regeneration, as well as, modulating pain and inflammation [9].

Radiant exposure (J/cm^2) is dependent upon both, the irradiance (mW/cm^2) and, irradiation time in seconds (s). The irradiance values vary according to the light source's output power, distance to target, and spot size [9]. As for pulsed light, irradiance is also affected by the duty cycle and pulse frequency [10]. PBM is known to exhibit a biphasic

✉ Sherif A. Mohamad

[1] Institute of Clinical Sciences, School of Dentistry, University of Birmingham, 5 Mill Pool Way, Edgbaston, Birmingham B5 7EG, UK

[2] Institute of Microbiology and Infection, University of Birmingham, Edgbaston, Birmingham B15 2TT, UK

[3] Department of Oral Sciences, Faculty of Dentistry, Sir John Walsh Research Institute, University of Otago, PO Box 56, Dunedin 9054, New Zealand

dose-dependent response and bio-stimulation for each specific cell type or tissue occurs only through a therapeutic window of doses [11]. This defies the reciprocity laws; meaning that if the radiant exposure was kept constant while changing the irradiance and irradiation time, the end results will not be similar [12, 13]. Consequently, the Arndt–Schulz law has provided an appropriate model to describe the dose-dependent effects of PBM. This law states that insufficient stimuli exert no effects, relatively low stimuli exert a stimulatory effects, while higher stimulus causes inhibition. If the radiant exposure is too high (higher irradiance or longer exposure times) or too low; no response or an inhibitory effect could occur. Furthermore, other irradiation parameters can also affect cellular responses, such as the mode of operation, i.e., continuous wave or pulsed, and the wavelength applied. It is important to understand that the energy of photons is dependent on the wavelength of light used, e.g., blue light photons contain more energy per photon, compared with red light. The absorption of blue light in most tissues is higher, because fundamental tissue chromophores have dominating absorption bands in the blue light region. It is therefore important to fully understand the light irradiation parameters applied to optimise the therapeutic outcomes and avoid unwanted side effects. Benefits of PBM can include regulation of the activity of growth factors, cytokines, and inflammatory mediators [9, 12, 14].

Several investigations have reported that red (620–660 nm) and near-infra-red (800–980 nm) (R/NIR) light can enhance MSC proliferation [15, 16]. Other studies have now also reported on osteo- and odonto-genic differentiation outcomes following irradiation by R/NIR light [10, 17–22]. Blue light (400–500 nm) has recently been shown capable of up-regulating the osteogenic potential of MSCs [23–27]. Even though the PBM mechanisms are not fully elucidated [9], the most widely accepted theory for the R/NIR PBM effects is in response to light absorption by cytochrome *c* oxidase (COX); which subsequently leads to stimulation of the respiratory chain and associated adenosine tri-phosphate (ATP) production [28]. The mode of action of blue light is, however, reportedly primarily mediated through a relatively small increase in reactive oxygen species (ROS) levels; after the light has been absorbed by cellular flavins [29, 30]. ROS are also secondarily generated as a result of stimulating the respiratory chain by R/NIR light [31]. Notably, the redox state of MSCs is reported as being an important modulator of both proliferation and mineralisation processes [32, 33].

A combined application of PBM and MSCs therefore offers a prospective therapeutic modality for the promotion of hard tissue repair and regeneration. However, to optimise its clinical use, the mechanisms governing their interactions need to be better understood. Indeed, it will be important to determine how different wavelengths interact with different chromophores; and subsequently determine how ROS responses may be generated resulting in the downstream molecular and cellular events. Furthermore, the accurate characterisation and reporting of irradiation parameters applied is also critical to enable optimisation of therapeutic light delivery. This review article explores potential PBM mechanisms involved in mediating MSC responses and reports on in vitro studies investigating blue and R/NIR light effects on cellular mineralisation capacity. Bibliographical searches were performed using *ScienceDirect* and *PubMed*. To identify in vitro studies reporting on the effects of blue and R/NIR light on the mineralisation potential of MSCs, the keywords used included combinations of: 'PBM', 'LLLT', 'phototherapy', 'osteogenic/odonto-genic differentiation', and 'MSCs'. Studies which only investigated light effects on proliferation were excluded; while those investigating osteo/odontogenesis were included. Subsequently, a methodological quality check was performed; in which studies lacking essential dosimetry and light characterisation parameters were not included. Studies which were included contained sufficient information for a radiant exposure to be calculated, and hence, the irradiation part of the experiment is repeatable.

2 PBM signal transduction in the red/near-infra-red spectrum

Following the absorption of photons, the resulting excited molecule exerts biologic effects by modulating intracellular metabolic pathways. Depending on the radiant exposure, light absorption can either cause increases in ATP and cyclic adenosine monophosphate (cAMP) levels resulting in downstream bio-stimulation, or destruction of cytochromes, which results in inhibitory effects. Both processes are proposed to take place within mitochondria [34]. The primary photoreceptor or chromophore which reportedly absorbs light photons is COX which is a terminal enzyme in the respiratory chain and plays a major regulatory role in the process of oxidative phosphorylation. The enzyme consists of two heme, two copper, one magnesium, and one zinc site. COX transfers electrons from cytochrome *c* to molecular oxygen, and this leads to the oxidation of ferrocytochrome *c* and the reduction of a di-oxygen molecule; inducing proton pumps from the mitochondria to the cytosol. Ultimately, the energy produced from this redox process leads to the generation of ATP [31, 35].

Karu et al. established a direct link between optical radiation, in the ultraviolet and infra-red spectrum (300–900 nm), and stimulation of both DNA and RNA synthesis in HeLa cells. DNA synthesis stimulation peaks were recorded at wavelengths of 400, 630, 680, and 760 nm, while those for RNA synthesis were detected at 400, 615, 680, 780, and 820 nm.

Data indicated that light was not absorbed directly by the nucleic acids but that light regulated their synthesis indirectly [36]. To elucidate the photo-absorber, they used a light source of a narrower spectrum (580–860 nm). Four peaks for DNA and RNA synthesis were identified; two within the red spectrum (613–623 nm and 667–683 nm), and two within the NIR spectrum (750–772 nm and 812–846 nm). These results supported the hypothesis that COX was the main endogenous chromophore; as the 613—623 nm absorbance wavelength was within the same absorbance maxima for reduced COX, while the 667- 683 nm wavelength also conformed to one of the COX intermediates, compound A (fluoromethyl-2,2-difluoro-1-trifluoromethyl vinyl ether). Moreover, peaks recorded at 750–772 nm correlated with the absorption coefficient of mitochondria; and the 812–846 nm wavelengths corresponded with oxidized COX [28]. Further studies demonstrated that cell exposure to nitric oxide (NO), a COX inhibitor, eliminated the bio-stimulatory effects of R/NIR light and this was also accompanied by significant changes in COX absorption. NO is known to compete with oxygen for binding at the COX copper (CuB) nuclear center. Notably, light reportedly dissociates the binding of NO from COX, which can then enable cellular respiration and oxygenation by reversing the hypoxic conditions in stressed cells. In turn, this increases electron transfer and ATP production, subsequently inducing transcription factors which can enhance cellular migration, proliferation, and differentiation responses [37–39]. Further studies by Wong-Riley et al. investigated the effects of five different irradiation wavelengths (670, 728, 730, 830, and 880 nm) following pre-treatment of neuronal cells with potassium cyanide; an inhibitor of COX that also binds to the CuB nuclear center. The delivered light demonstrated an ability to restore COX activity and ATP levels; with outcomes being dose-dependently related to the potassium cyanide levels applied. The most efficient wavelengths applied were 630 and 830 nm, and these correlated with the absorbance spectrum of oxidised COX. As potassium cyanide could have been bound to other proteins within the cell, such as catalase, NO synthase, cytochrome b, and cytochrome c; these data therefore did not rule these molecules out as prospective chromophores [40]. Interestingly, it has been reported that PBM effects in the R/NIR spectrum also occur due to the simultaneous production of relatively low amounts of ROS; alongside increases in ATP production. This takes place due to the shift in the cellular redox state towards higher oxidation levels, by simultaneously increasing mitochondrial ROS and decreasing cytosolic ROS [10, 31] (see Fig. 1).

3 Blue light PBM signal transduction

Several mechanisms have been reported to mediate blue light absorption and activation of downstream signalling pathways. Indeed, it is possible that more than one pathway is activated by blue light simultaneously or that sequential signalling may occur. Furthermore, differences in cell type, metabolic state, and chromophore levels likely play a pivotal role in determining the response detected. Early hypotheses have proposed that shorter wavelengths of blue light (400 nm) were absorbed by porphyrins, leading to the release of ROS; mainly in the form of singlet oxygen. Cellular mitosis is subsequently triggered via stimulation of the respiratory chain and calcium influx into the cytoplasm. Notably, however, at higher radiant exposure, molecular and cellular damaging effects could also occur due to the high reactivity of the singlet oxygen generated [36, 41].

Due to their key roles in the respiratory process, redox chain molecules are candidates for blue light signal transduction. Indeed, the flavin constituents have been proposed as chromophores; and this includes molecules such as Nicotinamide adenine dinucleotide phosphate (NADPH) dehydrogenase [35] and NAPDH oxidase. Studies have shown that hydroxyl radicals were induced in sperm cells following irradiation using blue spectrum light. Results suggested that the endogenous photosensitizer was flavin-bound; and was prevalent in the cytosol [29]. Other studies have detected increased mitochondrial ROS production after irradiating sperm cells, fibroblasts, cardiac, and skeletal muscle cells. The addition of an extracellular scavenger led to a reduction in hydroxyl radicals; findings which supported the hypothesis that ROS is produced at the cell membrane level potentially due to the sensitization of NADPH oxidase [42].

Intracellular ROS induced by light are mainly superoxide anions, hydrogen peroxide (H_2O_2), and hydroxyl radicals [43, 44], and these can be formed due to type I or type II reactions. In type I reactions, electron transfer from the excited sensitizer to oxygen produces a superoxide anion and H_2O_2, which in turn is transformed to hydroxyl radicals through Harber–Weiss or Fenton reactions. A type II reaction results in the production of singlet oxygen. Interestingly, it has been hypothesised that the type I reaction conforms closely with the ascending part of the Arndt–Schultz curve when light irradiation, up to a certain radiant exposure, results in the bio-stimulation of ROS. Longer periods of irradiation, or higher radiant exposure, correlates with the descending part of the curve; due to the elevated ROS production and activation of the cellular scavenging system which causes an imbalance in the redox state of the cell. A concomitant rise in intracellular

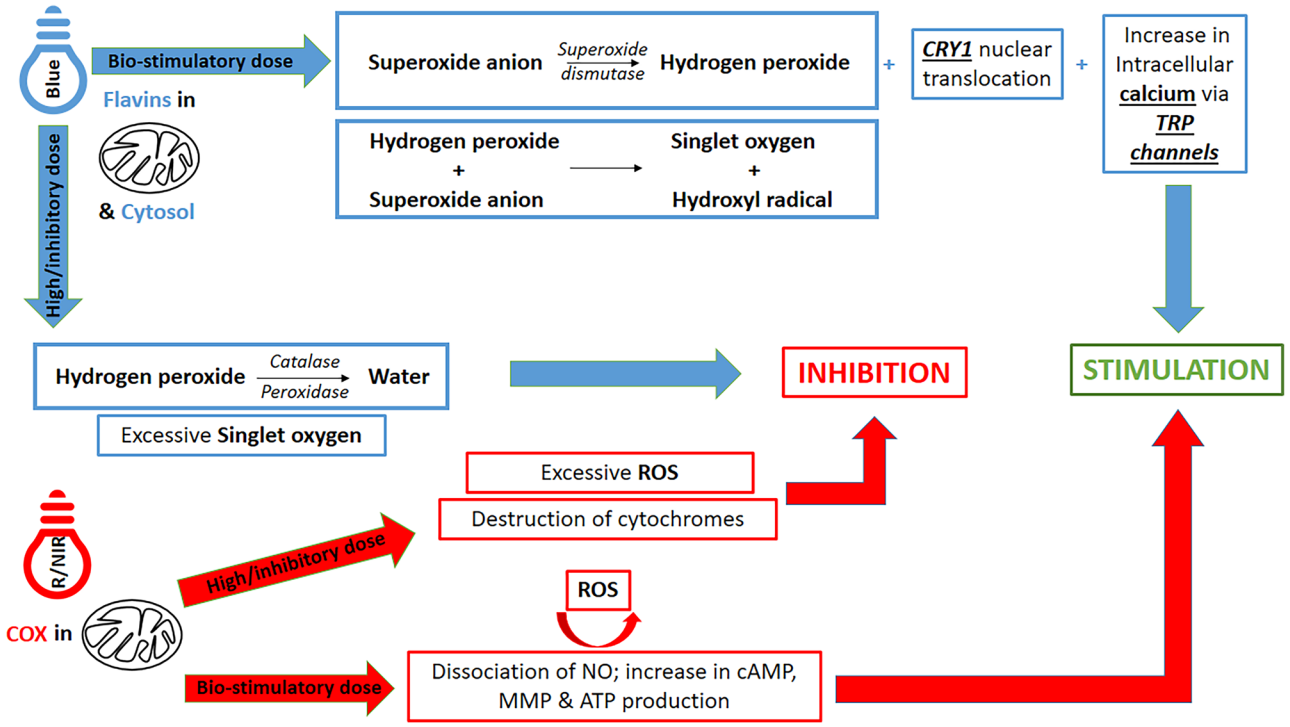

Fig. 1 Schematic diagram showing blue and red/near infra-red (R/NIR) light potential bio-modulatory mechanisms. At the stimulatory dose (i.e., radiant exposure), blue light (absorbed by flavins in both mitochondria and cytosol) induces the production of stimulatory levels of hydrogen peroxide, causing an elevation in intracellular calcium levels through transient receptor potential (TRP) channels. These effects are accompanied by decreased crytochrome-1 (CRY1) activity. R/NIR light dissociates nitric oxide (NO) bound to cytochrome *c* oxidase (COX) inside the mitochondria, enhancing cyclic adenosine monophosphate (cAMP), mitochondrial membrane potential (MMP), and adenosine tri-phosphate (ATP) production. At higher doses, blue light can cause inhibition due to the up-regulation of the scavenging system (catalase/peroxidase). Inhibitory effects of a higher dose of R/NIR light can occur due to the destruction of cytochromes. Nevertheless, both spectral ranges can cause inhibition due to the excessive production of ROS

calcium levels accompanies the ROS increase. Thus, it has been proposed that a transient increase in calcium, induced by H_2O_2, may be responsible for the bio-stimulatory effects, while more rapid increases in calcium cause inhibitory effects which are consistent with the descending part of the Arndt–Schultz curve [30] (see Fig. 1).

In addition to NADPH-dependent enzymes, flavin adenine dinucleotide (FAD) containing cryptochromes (CRY1 and CRY2) have also been proposed as blue light absorbers in humans [45]. CRY proteins are circadian rhythm regulators which modulate cell and tissue haemostasis [46, 47] (see Fig. 1). CRY1 and CRY2 specifically act as negative feedback regulators of the circadian clock and decreased levels of these molecules can increase bone formation. Increased ROS can also reset the cellular circadian clock as well as optimising cellular survival mechanisms [48–50].

4 Intracellular ROS levels regulate MSC haemostasis and fate

As has previously been highlighted, ROS can be generated within mitochondria during electron transport by a range of enzymes, including NADPH oxidase, NO synthase, mono-amide oxidase, heme oxygenase, lipoxygenase, myeloperoxidase, cyclooxygenase, and cytochrome P450 [51–53]. Other cellular locations for ROS generation include the cytosol (NO synthase/lipoxygenase), plasma membrane (NADPH oxidase/lipoxygenase) [54–57], endoplasmic reticulum (NAPDH oxidase) [58, 59], and peroxisomes [60]. In MSCs, ROS play a pivotal role in determining cell fate as well as regulation of their self-renewal. Notably, several studies have reported that the

application of exogenous ROS can stimulate mineralising marker expression in both dental pulp stem cells (DPSCs) [61] and adipose tissue-derived MSCs (ADMSCs) [62].

During homeostasis, ROS levels are regulated by a range of antioxidant/scavenging enzymes including catalases, superoxide dismutase, glutathione reductase, and glutathione peroxidase. If ROS levels reach certain thresholds; beyond the point which the scavenging enzymes can modulate, cellular injury occurs due to oxidation of several molecules, including nucleotides, lipids, and proteins [63]. Undifferentiated MSCs contain relatively low levels of ROS, and express high levels of antioxidant enzymes; however, the opposite state exists for MSCs during their proliferation and differentiation phases [32, 33, 64, 65]. During MSC differentiation, the main sources of ROS are complex I (NADH coenzyme Q oxidoreductase), complex III (ubiquinol cytochrome *c* oxidoreductase), and NADPH oxidase [66]. Similar to other cellular processes, excessive levels of ROS inhibit both proliferation and osteogenic differentiation [67].

Further evidence highlighting the role of the redox status in regulating MSC activity is highlighted by the importance of the master regulator of anti-oxidative responsive transcription factor, nuclear factor erythroid related factor-2, in the process. Its knockout increases cellular differentiation processes and bone formation [62]. Combined, these data indicate the fine balance the redox state plays in regulating cellular events and identifies a potential mechanism by which light can indirectly influence MSC fate.

5 PBM promotes MSC mineralisation processes in vitro

5.1 Red light

Red light (620–660 nm) irradiation has been reported to significantly increase the proliferation of bone marrow MSCs (BMMSCs) [17–19] and periodontal ligament stem cells [20] at radiant exposures of 1, 2, and 4 J/cm^2. Notably, osteogenic differentiation was also promoted after 2 and 4 J/cm^2, as demonstrated by up-regulation of alkaline phosphatase (ALP), osteocalcin (OCN), bone gamma-carboxyglutamic acid-containing protein [17–20], runt-related transcription factor-2 (RUNX2) [18–20], bone morphogenic protein-2 (BMP2) [19, 20], collagen-1α (Col-Iα) [18], and insulin-like growth factor-1 [19]. Importantly, data also demonstrated concomitant increases in mineral deposition [18–20] (see Table 1).

Enhanced bio-stimulatory effects in MSCs have also been observed when cultures were irradiated either once daily [20, 21] or every other day [18, 19]. Higher irradiance values and multiple exposures resulted in enhanced mineralising outcomes compared with single exposure controls [18]. It is notable that PBM effects were inhibited by culture supplementation with SQ22536, an adenylyl cyclase inhibitor; supporting the role of cAMP and respiratory chain signalling in the photo-transduction process [21].

5.2 NIR irradiation

NIR diode irradiation (810–850 nm) was reported to stimulate the proliferation [10, 21] and osteo-/odonto-genic potential of BMMSCs [21, 68], ADMSCs [22], DPSCs [10], and stem cells from human exfoliated deciduous teeth [69], at radiant exposures ranging from 77 mJ/cm^2 to 4 J/cm^2. Irradiated cell cultures exhibited higher levels of mineralisation markers, including ALP [10, 21, 22, 69], Col-Iα, Dentin matrix phosphoprotein-1 (DMP-1), and dentin sialophosphoprotein (DSPP) [69]. At relatively high radiant exposure (64 J/cm^2), diode laser (808 nm) irradiation also significantly increased mineral deposition in BMMSC cultures via the up-regulation of ALP, RUNX2, transforming growth factor-βeta 1 and Osterix (OSX) [68] (see Table 1).

5.3 Blue light

The bio-modulatory effects of blue light have only relatively recently been reported, and there has been considerable diversity in the light sources used, irradiation parameters applied, and outcomes. Yuan et al. reported that blue light (470 nm LED) adversely affected the proliferation and mineralisation potential of BMMSCs at a relatively wide range of radiant exposures from 1 to 72 J/cm^2 [70]. When gingival MSCs were treated with 420–480 nm LED irradiation at 1, 2, 4, or 6 J/cm^2, results indicated a significant reduction in proliferation rates but increases in both ALP levels and calcified nodule formation. The same light source promoted the osteogenic differentiation of stem cells from apical papilla after irradiation at 1, 2, 3, and 4 J/cm^2. These effects reportedly occurred due to up-regulation of DSPP, OCN, and DMP-1 [26, 27].

Notably, the increase in calcified nodule formation at 28 days after irradiation was observed in a dose-dependent relationship; suggesting that lower radiant exposures promoted early differentiation, while higher radiant exposures exerted enhanced effects, albeit at a more latent stage [26]. Exposure to 420 nm LED irradiation at 3 J/cm^2 also increased expression of the mineralising markers RUNX2 and OCN, in ADMSCs at 21 days. These effects were also reportedly regulated by an increase in intracellular calcium signalling [25] (see Table 2).

Continuous wave laser (405 nm) exposure at 9, 18, 27, 36, and 54 J/cm^2 was shown to enhance osteogenic differentiation in mouse BMMSCs cultures, in a dose-dependent manner. These outcomes were supported by increased ALP and OCN expression (see Table 2). Immuno-staining

Table 1 Summary of in vitro studies using different MSCs evaluating the effects of R/NIR light irradiation on mineralising phenotype differentiation

Author/year	Cells & assessment criteria/culture conditions	Light source & experimental set-up	Irradiation parameters	Main outcomes
Li et al. (2010) [17]	Rat BMMSc/Proliferation (standard media) and differentiation (mineralising media)	630 ± 5 nm C.W. LED—Bandwidth 17 nm—emitted from a 3 mm lamp. *Spot Size*: Not reported. *Exposure conditions*: Irradiation was performed from above cultures at a distance of 1.2 cm. Proliferation and differentiation assays undertaken in 96-well plates (well area 0.32 cm^2), while colony counts were performed in 10 cm dishes.	**Proliferation** *Radiant exposure*: 2 and 4 J/cm^2. Two modes were investigated; *Irradiance*: 5 mW/cm^2 *Irradiation time*: 400 and 800 s OR *Irradiance*: 15 mW/cm^2 *Irradiation time*: 133 and 266 s *Exposure rate*: single exposure OR every other day **Differentiation** *Radiant exposure*: 4 J/cm^2 *Irradiance*: 15 mW/cm^2 *Irradiation time*: 266 s. *Exposure rate*: every other day	Single exposure led to significant increase in proliferation at day 3; declined at day 5. Multiple exposures lead to further increases in proliferation at days 3 and 5; with 4 J/cm^2 (15 mW/cm^2 for 266 s) resulting in the highest proliferation rate. Red light enhanced ALP levels at day 11 and OCN expression at day 28.
Peng et al. (2012) [18]	Rat BMMSc/Proliferation and differentiation (in both; standard and mineralising media)	620 nm LED—operating in C.W. *Spot Size*: 10 cm in diameter. *Exposure conditions*: Irradiation was performed at a distance of 2 cm. Proliferation assays were undertaken in 96-well plates, and differentiation assays performed in 35-mm dishes. It was not reported as to whether irradiation was performed from above or below cultures.	*Radiant exposure*: 1, 2 and 4 J/cm^2 *Irradiance*: 6.67 mW/cm^2 *Irradiation time*: 150, 300, and 600 s. *Exposure rate*: every other day	Red light stimulated proliferation in standard media and inhibited proliferation in mineralising media. 1 and 2 J/cm^2 resulted in significant increases in proliferation at days 4 and 6; while 4 J/cm^2 was only shown to be effective at day 4. Improved differentiation outcomes only in mineralising media. Irradiation at 2 and 4 J/ cm^2 resulted in a notable increase in ALP levels at days 3, 7, and 10. Both radiant exposures led to up-regulation of Bglap at day 4, while all three radiant exposures; 1, 2, and 4 J/cm^2 up-regulated RUNX2 expression. Significant increase in calcific nodules formation by day 21 (2 and 4 J/cm^2).
Wu et al. (2012) [19]	Mouse BMMSc/Proliferation (standard media) and differentiation (mineralising media)	660 nm GaAlAs laser—operating in C.W. *Spot Size*: Not reported. Exposure conditions: Irradiation was performed from below cultures at a distance of 4 cm. Proliferation was investigated in 96-well plates, while differentiation assays were undertaken in 12-well plates.	*Radiant exposure*: 1, 2 and 4 J/cm^2 *Irradiance*: 10 mW/cm^2 *Irradiation time*: 100, 200, and 400 s *Exposure rate*: once a day	2 and 4 J/cm^2 stimulated proliferation on day 5; and an increase in ALP levels on days 3 and 5. A radiant exposure of 4 J/cm^2 up-regulated BMP2, OCN, RUNX2, and IGF1 expression. Significant differences were only noted for IGF1 levels at days 3 and 5.

Table 1 (continued)

Author/year	Cells & assessment criteria/culture conditions	Light source & experimental set-up	Irradiation parameters	Main outcomes
Soleimani et al. (2012) [21]	Human BMMSCs/Proliferation and differentiation (both assayed in mineralising media)	810 nm GaAlAs diode laser—operating in C.W. *Spot Size*: 6 mm diameter. *Exposure conditions*: Irradiation was performed from above cultures (lid removed) at a distance of 1 cm. All investigations were undertaken in 96-well plates.	*Radiant exposure*: 2 and 4 J/cm^2 *Irradiance*: 167 mW/cm^2 *Irradiation time*: 12 and 24 s. *Exposure rate*: every other day—Three exposures	Both radiant exposures induced higher proliferation rates (7th day); and increased ALP levels (days 2, 5, 7, and 10).
Wu et al. (2013) [20]	Human PDLCs/Proliferation (standard media) and differentiation (mineralising media)	660 nm GaAlAs laser- operating in C.W. *Spot Size*: Not reported. *Exposure conditions*: Irradiation was performed at a distance of 3 cm. Proliferation was investigated in 96-well plates, while differentiation was assayed in 12-well plates. It was not reported as to whether irradiation was undertaken from above or below cultures.	*Radiant exposure*: 1, 2, and 4 J/cm^2 *Irradiance*: 15.17 mW/cm^2 *Irradiation time*: 66, 132 and 264 s. *Exposure rate*: once a day	1 and 2 J/cm^2 stimulated increased proliferation by day 5; a radiant exposure of 2 J/cm^2 enhanced effects detected by day 3. 2 J/cm^2 increased ALP levels at days 3 and 5; while 4 J/cm^2 lead to ALP elevation only on day 5. Both 2 and 4 J/cm^2 led to an increase in OCN, BMP2, and RUNX2 levels at day 3. On day 5, the radiant exposure of 2 J/cm^2 significantly elevated BMP2 levels. 2 and 4 J/cm^2 significantly increased mineralised nodule formation at days 7 and 14.
Turrioni et al. (2014) [69]	SHED/Differentiation (mineralising media)	850 ± 10 nm LED operating in C.W. *Spot Size*: Not reported. *Exposure conditions*: Irradiation was carried out from below. Each diode had a collimator adhered to the underside of a well in a 24- well plate (well area 2 cm^2). All investigations were performed in 24-well plates.	*Radiant exposure*: 2 and 4 J/cm^2 *Irradiance*: 40 mW/cm^2 *Irradiation time*: 50 and 100 s. *Exposure rate*: single exposure	At 72 h post-irradiation; IR light at 2 J/cm^2 and 4 J/cm^2 stimulated increased collagen synthesis, and TP production. Irradiated cultures showed increased gene expression levels for ALP, Col-I, DMP1 and DSPP.
Kim et al. 2017 [10]	Human DPSCs/Proliferation (standard media) and differentiation (mineralising media)	810 nm LED operated in Pulsed mode. *Spot Size*: Not reported. *Exposure conditions*: Irradiation from below in 4-well plates with a reflector, light guide, and a diffuser.	*Radiant exposure*: 77 mJ/cm^2 *Irradiance*: 80.4 µW/cm^2 *Duty Cycle*: 30% *Frequency*: 1, 3, 30,300, and 3000 Hz. For molecular studies, only 300 Hz was applied *Irradiation time*: 958 s. *Exposure rate*: once daily	Irradiation enhanced proliferation after 24, 48, and 72 h; mostly with 300 Hz. Meanwhile, ALP activity was remarkably elevated at days 3 and 7. Significant increases in TGF-β1 at day 3, as well as, in DMP-1, OPN, and OCN at day 21.

Table 1 (continued)

Author/year	Cells & assessment criteria/culture conditions	Light source & experimental set-up	Irradiation parameters	Main outcomes
Amaroli et al. (2018) [68]	Mouse BMMSCs/Differentiation (mineralising media)	808 nm C.W. diode laser. *Spot Size*: 1 cm diameter. *Exposure conditions*: Irradiation was performed from above at a distance of 1 cm; with the culture lid removed and the plate was covered in aluminium foil which contained a window enable irradiation. Western blotting investigations used cultures in 24-well plates, while ALP and mineralized nodule studies were undertaken in 6-well plates.	*Radiant exposure*: 64 J/cm^2 *Irradiance*: 1 W/cm^2 *Irradiation time*: 60 s. *Exposure rate:* every 24 h	Diode laser enhanced expression of RUNX2 and OSX (days 5, 10, and 15). It also increased ALP and mineralised nodules (days 10 and 15); as well as, up-regulating TGF-β1 (days 5 and 10).
Ateş et al. (2020) [22]	Human ADMSCs/Proliferation and differentiation (only in mineralising media)	635 nm diode laser operating in C.W. Light was delivered through a 600 µm fiber and collimator. *Spot Size*: Not reported. 820 nm diode laser operating in C.W. mode. Light was delivered through a 400 µm fiber and collimator. *Spot Size*: Not reported. *Exposure conditions*: Irradiation was performed from above; and irradiance was fixed by adjusting the irradiation distance. Proliferation was investigated in 96-well plates, while differentiation assays were in 24-well plates. Plates were covered in black-out foil except for the irradiated well.	*Radiant exposure*: 0.5, 1, and 2 J/cm^2 *Irradiance*: 50 mW/cm^2 *Irradiation time*: 10, 20, and 40 s *Exposure rate*: single exposure	Using 635 nm irradiation; a radiant exposure of 0.5 J/cm^2 significantly stimulated proliferation by day 14. Irradiation at 809 nm enhanced mineral deposition at all radiant exposures; while 2 J/cm^2 was the only effective radiant exposure when employing the 635 nm wavelength.

Mineralising media was supplemented with dexamethasone, ascorbic acid, and beta-glycerophosphate

Cell type & assessment criteria/culture conditions: *BMMSCs* bone marrow MSCs, *PDLCs* periodontal ligament cells, *SHED* stem cells from human exfoliated deciduous teeth, *DPSCs* dental pulp stem cells, *ADMSCs* adipose-derived MSCs

Light source & experimental set-up: *C.W.* continuous wave, *LED* light-emitting diode, *GaAlAs* gallium–aluminium–arsenide

Main outcomes: *ALP* alkaline phosphatase, *OCN* osteocalcin, *Bglap* bone gamma-carboxyglutamic acid-containing protein, *RUNX2* runt-related transcription factor-2, *BMP2* bone morphogenic protein-2, *IGF1* insulin-like growth factor-1, *TP* total protein, *Col-I* collagen-1, *DMP1* dentine matrix protein-1, *DSPP* dentin sialophosphoprotein, *OPN* osteopontin, *OSX* osterix, *TGF-β1* transforming growth factor-beta 1

Table 2 Summary of in vitro studies using different MSCs evaluating the effects of blue light on mineralisation potential

Author/year	Cell type & assessment criteria/culture conditions	Light source & experimental set-up	Irradiation parameters	Main outcomes
Kushibiki et al. (2008–2009) [23, 24]	Mouse BMMSc/Differentiation (mineralising media) and molecular assays to detect CRY1 and PER2	405 nm C.W. laser. *Spot Size*: 500 µm circular beam. *Exposure conditions*: light attached to the clear bottom of a black 96-well plate.	*Radiant exposure*: 9, 18, 27, 36 and 54 J/cm^2 *Irradiance*: 50, 100, 150, 200, and 300 mW/cm^2 *Irradiation time*: 180 s. Exposure rate: single exposure	Irradiation significantly increased mineralised nodule formation at days 5, 7, and 14. A dose response relationship at all radiant exposures studied; and increased expression of ALP and OCN at day 5. Blue laser radiant exposures of 18, 36, and 54 J/cm^2; resulted in a notable increase in nuclear localization of CRY1 and PER2. Results were confirmed by suppression of CRY1 gene expression at 18 and 36 J/cm^2
Wang et al. (2016) [25]	Human ADMSc/Differentiation (mineralising media)	410–430 nm LED, 525–555 nm filtered lamp; as well as, 660, and 810 nm diode lasers. All operating in C.W. mode. *Spot Size*: 4 cm^2 adjusted by changing the distance between the light source and the plate. *Exposure conditions*: Molecular investigations performed in 96-well plates, while mineralised nodule studies were undertaken in 6-well plates. All plates were covered in aluminium foil. The location of the irradiation was not reported.	*Radiant exposure*: 3 J/cm^2 *Irradiance*: 16 mW/cm^2 *Irradiation time*: 188 s. *Exposure rate*: every 2 days over the course of 3 weeks—Five exposures	Blue (420 nm) and green (540 nm) light irradiation resulted in the highest expression levels for RUNX2 (days 7 and 14), OSX, and OCN (day 21). This was relative to non-irradiated controls, red, and NIR light. Blue and green light resulted in highest intracellular calcium levels.
Yuan et al. (2016) [70]	Mouse BMMSc/Proliferation (standard media) and differentiation (mineralising media)	470 nm LED C.W. *Spot Size*: Not reported. *Exposure conditions*: Irradiation distance, location, and culture plates used were not reported.	*Radiant exposure*: 1.2, 6, 12, 36, and 72 J/cm^2 *Irradiance*: 20 mW/cm^2 Irradiation time: 1, 5, 10, 30, 60 min. *Exposure rate*: Single exposure for proliferation/viability assays; meanwhile, cells were irradiated 10 min daily for differentiation assays	At all radiant exposures, blue light exposure resulted in a considerable reduction in proliferation and cell counts; 6 h post-irradiation. At all exposures, there was significant reductions in ALP levels and calcific nodule formation at day 7.

Table 2 (continued)

Author/year	Cell type & assessment criteria/culture conditions	Light source & experimental set-up	Irradiation parameters	Main outcomes
Zhu al. (2019) [26]	Human GMSCs/Proliferation and differentiation (only in mineralising media)	420–480 nm LED—operating in C.W. *Spot Size*: 3.5 cm in diameter. *Exposure conditions*: Irradiation was performed from above cultures at 1 cm distance. Proliferation was investigated in 96-well plates, while ALP and mineralised nodules formation studies were in 35-mm dishes. Plates used for gene expression investigations were not reported.	*Radiant exposure*: 1, 2, 4, and 6 J/cm^2 *Irradiance*: 100 mW/cm^2 *Irradiation time*: 10, 20, 40, and 60 s *Exposure rate*: every other day	All radiant exposures reduced proliferation rates for up to 9 days. ALP levels in exposure groups were higher than the controls at days 7 and 14. The radiant exposure of 2 and 4 J/cm^2 showed the highest ALP levels. Increases in expression of all three genes; Col-I, OCN, and Runx2 at day 7 following exposure to 2 and 4 J/cm^2 Significant increases in mineralised nodules after 28 days at all radiant exposures were observed.
Yang et al. (2020) [27]	Human SCAP/Proliferation and differentiation (only in mineralising media)	420–480 nm LED – C.W. *Spot Size*: 3.5 cm in diameter. *Exposure conditions*: Irradiation was performed from above cultures at a 1 cm distance. Proliferation was investigated in 96-well plates, while ALP and mineralised nodules formation were investigated in 35-mm dishes. Culture plates for gene expression studies were not reported.	*Radiant exposure*: 1, 2, 3, and 4 J/cm^2 *Irradiance*: 100 mW/cm^2 *Irradiation time*: 10, 20, 30, and 40 s *Exposure rate*: every other day	All radiant exposures decreased proliferation rates for up to 10 days. 3 and 4 J/cm^2 showed the highest ALP levels at days 7 and 14. Up-regulation of DSPP, OCN, and DMP1 at days 7 and 14; after exposure to 4 J/cm^2 Irradiation at 2, 3, and 4 J/cm^2 resulted in significant increases in mineralised nodules formation after 28 days.

Cell type & assessment criteria/culture conditions: *BMMSCs* bone marrow MSCs, *ADMSCs* adipose-derived MSCs, *GMSCs* gingival MSCs, *SCAP* stem cells from apical papilla

Light source & experimental set-up: *C.W.* continuous wave, *LED* light-emitting diode

Main outcomes: *ALP* alkaline phosphatase, *OCN* osteocalcin, *CRY1* cryptochromes-1, *PER* period, *RUNX2* runt-related transcription factor-2, *OSX* osterix, *Col-I* collagen-1, *DSPP* dentin sialophosphoprotein, *DMP1* dentine matrix protein-1

confirmed the nuclear accumulation of the clock proteins, CRY1 and Period-2. CRY1 down-regulation occurred in a dose-dependent manner, at levels above 18 J/cm^2, and the authors proposed that blue light was able to reset the circadian clock in MSCs. Notably, however, 664 and 808 nm light irradiation did not affect the expression of CRY1 [23, 24].

The application of transient receptor potential channel antagonists, including capsazepine and SKF96365, have been shown to abolish the bio-stimulatory effects of blue light, suggesting involvement of light-gated channels in the PBM mechanism. The original enhancement in mineralisation processes reportedly occurred via an ROS-mediated mechanism, accompanied by an increase in intracellular calcium, which was transduced by light-gated ion channels [25, 29, 30].

6 Discussion and Conclusions

This review has outlined the different PBM mechanisms reported to enhance the mineralisation potential of MSCs, using either blue or R/NIR light. Studies have shown that light in the R/NIR spectrum can have positive bio-stimulatory effects on MSCs in terms of both proliferation and mineralising phenotype differentiation. These effects predominantly occur using both continuous-wave LEDs and lasers at relatively low radiant exposures of up to 4 J/cm2 [17–21]. The majority of the studies reporting multiple irradiations did not specify the exact number of treatments applied to the MSCs except for the study by Soleimani et al. [21], which utilised an estimated cumulative radiant exposure of 6–12 J/cm^2. Assuming that in studies where multiple irradiations were applied throughout the full duration of the mineralised nodules formation assay, the cumulative radiant exposure would be in the range of 10–50 J/cm^2 [17–20]. Interestingly, it was also reported that multiple NIR laser irradiations at much higher radiant exposures of 64 J/cm^2 [68] could enhance osteogenic processes.

Relating to the Arndt Schultz model for the biphasic dose-dependent effects, several irradiation parameters trends were observed. With regards to R/NIR light, different combinations of irradiances and irradiation times were used to deliver a range of radiant exposures from 0.5 to 4 J/cm^2. With multiple red light (620–660 nm) irradiations, 1 and 2 J/cm^2 enhanced proliferation—compared with 4 J/cm^2- when irradiation was undertaken at 6.67 and 15 mW/cm^2. However, 2 and 4 J/cm^2 resulted in enhanced proliferation—in comparison with 1 J/cm^2—at 10 mW/cm^2 [18–20]. Moreover, a single exposure of 0.5 J/cm^2 at 50 mW/cm^2 significantly enhanced proliferation compared with 1 and 2 J/cm^2 [22]. Conversely, 2 and 4 J/cm^2 enhanced the mineralisation processes in a dose-dependent manner regardless of the irradiance or irradiation time [17–20, 22]. As for NIR light (808–850 nm), differentiation was also stimulated in a similar dose-dependent trend using 2 and 4 J/cm^2 when MSCs were irradiated once (40 mW/cm^2) or up to three irradiations (167 mW/cm^2) [21, 69]. Notably, when employing a single irradiation at 50 mW/cm^2, 0.5 and 2 J/cm^2 resulted in higher mineralised nodules formation compared with 1 J/cm^2 [22]. All these trends were common using both lasers and LEDs, indicating that successful phototherapy approaches depend on the irradiation parameters, rather than the light delivery source [12].

Several studies investigated different irradiation modes to optimise light delivery. *Li* et al. studied the effects of 2 and 4 J/cm^2 (630 nm LED)—on BMMSCs—delivered in two modes, 5 mW/cm^2 (400 and 800 s) or 15 mW/cm^2 (133 and 266 s); they also studied single or multiple irradiations. Their results showed that multiple irradiations at 15 mW/cm^2 for 266 s resulted in the highest proliferation rates [17]. Moreover, Kim et al. reported that pulsed 810 nm LED light was more effective in enhancing ALP levels in DPSCs, compared with continuous-wave irradiation. They examined the effects of a range of duty cycles (0–60%) at a fixed pulse frequency (1 Hz), which typically resulted in a range of radiant exposures (0.8–154 mJ/cm^2). The duty cycle indicates the percentage of time the light is on over the entire 'on–off' cycle. A duty cycle of 30% resulted in the most hyperpolarized cytoplasmic membrane potential. At fixed frequency (1 Hz) and duty cycle (30%), cells exhibited similar ALP levels when irradiated at both 77 mJ/cm^2 and 2.3 J/cm^2—at variable irradiation times. Additionally, at fixed radiant exposure (77 mJ/cm^2), and duty cycle (30%), a frequency of 300 Hz resulted in highest ALP levels when studying a range of different frequency settings; 1–3000 Hz. These results indicated that the duty cycle and pulse frequency are the main parameters influencing DPSC response, as opposed to the radiant exposure. Nonetheless, the radiant exposure settings applied [10] were much lower compared with other studies investigating the effects of continuous-wave R/NIR light [17–22, 69]. This violates the Arndt–Schulz law if both continuous and pulsed irradiation are hypothesised to enhance mineralisation relying on the same photo-chemical mechanism.

For blue LED irradiation, induction of MSC osteogenic differentiation and inhibition of proliferation occurred as a result of multiple irradiations at radiant exposures within a range from 1 to 6 J/cm^2, utilising an irradiance of 100 mW/cm^2 (cumulative 10—80 J/cm^2) [26, 27]. However, at much lower irradiance (16 mW/cm^2), longer exposure times, and only five irradiations, 3 J/cm^2 (cumulative 15 J/cm^2) was required to stimulate MSCs mineralisation [25].

At higher radiant exposures; multiple blue LED irradiations (12 J/cm^2) inhibited osteogenesis [70], while single blue laser irradiation (9—54 J/cm^2) stimulated mineralisation [23, 24]. Compared with LEDs, both blue and NIR

lasers were shown to enhance MSCs mineralisation only at considerably higher radiant exposure. Further investigation, especially using the higher energy of blue light photons, is required to ensure that irradiation does not lead to injury of local tissues. Intriguingly, enhancement of the mineralisation potential of MSCs using R/NIR light was reported to occur with either fewer treatments at higher irradiance parameters (40–167 mW/cm^2) (shorter exposure times), or increased treatments at lower irradiance (6–15 mW/cm^2) (longer exposure times). However, the converse was the case for blue light irradiation, since MSCs irradiated at 16 mW/cm^2 required only five exposures compared with cultures irradiated at 100 mW/cm^2 every other day. Reciprocity between irradiance and exposure times was evident throughout various R/NIR investigations, which was not reported for blue light studies [17–22, 25–27, 69].

Notably, as is highlighted in Tables 1 and 2, there were variations among the experimental conditions regarding the type of MSCs culture-ware used, location of irradiation source, and irradiation distance. Remarkably, different studies reported using fixed irradiance values, even though irradiation was carried out in different culture dishes within the same study. The use of different size culture-ware will clearly result in the generation of different irradiance at target, different cell densities, and different light–cellular interaction. Despite this, to address this issue, the studies by Ateş et al. [22] and Wang et al. [25] reported adjusting the irradiation distance within the various culture-plate setups to enable maintenance of the same spot size and irradiance. Other differences in experimental set-up were also reported in attempts to maintain homogeneity of delivered light and decrease bleed. For example, in some designs, the culture-ware plate lid was removed before covering the entire plate with aluminium foil except for a window to enable the light source to be used to deliver the light from above the culture at a fixed distance [68]. Other designs relied on changeable distance to target while keeping the light spot and aluminium foil window size fixed [25]. While the aluminium foil can cause multiple light reflections and affect the light–cellular interaction, some authors preferred covering the plates with blackout foil or using black-walled well plates [22–24].

Another important variable which should be considered is the potential effect of temperature change following light irradiation. Only the two studies of Li et al. [17] and Turrioni et al. [69] reported measuring thermal affects. In the first study, red LED (630 nm) irradiation resulted in less than 0.26 °C temperature increase in the media, while in the latter study, no significant rise in temperature was detected at up to 2 min of 850 nm LED irradiation. In vivo, the heat dissipation in cultures depends on their thermal relaxation time, as well as the irradiance, irradiation time, pulse frequency, and pulse duration of the light source [71]. It is also notable that non-irradiated controls in all the experimental designs studied were kept outside the incubator for the same amount of time it took their counterparts to be irradiated. This means that depending on the local temperature, the irradiated samples might experience a rise in temperature below their thermal tolerance, which may not be the case in a clinical setting. While PBM is generally accepted as a non-thermal response [9], the effect of hyperthermia cannot be totally ruled out specially it is known to lead to an increase in mitochondrial ROS production [72]. Notably, hyperthermia is reported to enhance the osteogenic differentiation of BMMSC's via the up-regulation of ALP, OSX, RUNX2, BMP2, and osteopontin. These effects are mediated by the heat shock protein (HSP70), and its knockout alleviated the positive effects of hyperthermia [73–75]. If the phototherapy mechanism involves hyperthermia, this would mean that total energy of all light photons absorbed in different molecules—aside/alongside the chromophore—will dictate the resulting effects. Therefore, generally, this means that blue light—with higher energy per photon [14]—exhibits a greater ability to cause hyperthermia compared with red light with similar number of photons. However, from a photo-chemical prospective, both the wavelength used and the absorption spectrum of the chromophore influence the outcomes [71]; and not the energy per photon. Therefore, with the variations among experimental setups, light sources, cultures dishes, and the lack of any media absorption measurements, hyperthermia cannot be excluded. It also means that the inclusion of appropriate thermal controls should be included in all studies.

Interestingly, R/NIR and blue light enhanced osteogenic events in MSCs when cultured in mineralising-inductive media, containing dexamethasone, ascorbic acid, and beta-glycerophosphate. No irradiation conditions were reportedly able to stimulate differentiation in cultures maintained in unsupplemented media. Notably, R/NIR was able to stimulate MSC proliferation in mineralising-inductive media, while blue light could inhibit proliferation irrespective of the MSC culture media used. These findings highlight potential differences in the mode of action between R/NIR and blue light, and indicate the need for a conducive environment to enable PBM effects, i.e., the presence of supportive culture conditions.

Data summarised here support PBM of MSC mineralisation events as conforming with the Arndt–Schulz law, with relatively low radiant exposure enhancing cell fate determination, while much higher levels are inhibitory of both proliferation and differentiation. The inhibitory effects of higher radiant exposure of light potentially occur due to either the direct interference of photons on chromophore function, or indirectly due to excessive ROS production [76] or hyperthermia [71, 72]. R/NIR light stimulates the mineralisation potential of MSCs via stimulation of cAMP, respiratory chain signalling, and ROS production. Blue light

enhanced mineralisation primarily through relatively small increases in ROS levels; however, the precise involvement of the CRY protein in light absorption and subsequent redox signalling still remains to be entirely elucidated [77–79]. To ensure the safety of PBM, thorough characterisation of light irradiation parameters and the further investigations are required for the use of blue and NIR lasers at high radiant exposure. The combined application of PBM and MSCs could offer a prospective modality for hard tissue regenerative medicine in the future provided that the underlying pathways of light–cellular interactions are fully understood, and irradiation parameters are standardised. The light parameters applied should be optimised for delivery, taking into account the absorption of the light within the target tissue while maintaining the safety of host tissues.

Declarations

Conflict of interest On behalf of all authors, the corresponding author states that there is no conflict of interest.

References

1. Zhang, K., Wang, S., Zhou, C., Cheng, L., Gao, X., Xie, X., Sun, J., Wang, H., Weir, M. D., Reynolds, M. A., Zhang, N., Bai, Y., & Xu, H. H. K. (2018). Advanced smart biomaterials and constructs for hard tissue engineering and regeneration. *Bone Research., 6*, 31. https://doi.org/10.1038/s41413-018-0032-9
2. Schmidt-Bleek, K., Marcucio, R., & Duda, G. (2016). Future treatment strategies for delayed bone healing: An osteoimmunologic approach. *Journal of the American Academy of Orthopaedic Surgeons, 24*(10), e134–e135. https://doi.org/10.5435/JAAOS-D-16-00513
3. Frencken, J. E., Sharma, P., Stenhouse, L., Green, D., Laverty, D., & Dietrich, T. (2017). Global epidemiology of dental caries and severe periodontitis—A comprehensive review. *Journal of Clinical Periodontology, 44*(Suppl 18), S94–S105. https://doi.org/10.1111/jcpe.12677
4. Hass, R., Kasper, C., Böhm, S., & Jacobs, R. (2011). Different populations and sources of human mesenchymal stem cells (MSC): A comparison of adult and neonatal tissue-derived MSC. *Cell Communication and Signaling, 9*, 12. https://doi.org/10.1186/1478-811X-9-12
5. Song, M., Lee, J. H., Bae, J., Bu, Y., & Kim, E. C. (2017). Human dental pulp stem cells are more effective than human bone marrow-derived mesenchymal stem cells in cerebral ischemic injury. *Cell Transplantation, 26*(6), 1001–1016. https://doi.org/10.3727/096368916X694391
6. Couble, M. L., Farges, J. C., Bleicher, F., Perrat-Mabillon, B., Boudeulle, M., & Magloire, H. (2000). Odontoblast differentiation of human dental pulp cells in explant cultures. *Calcified Tissue International, 66*(2), 129–138. https://doi.org/10.1007/PL00005833
7. Park, K. S., Kim, Y. S., Kim, J. H., Choi, B., Kim, S. H., Tan, A. H. K., Lee, M. S., Lee, M. K., Kwon, C. H., Joh, J. W., Kim, S. J., & Kim, K. W. (2010). Trophic molecules derived from human mesenchymal stem cells enhance survival, function, and angiogenesis of isolated islets after transplantation. *Transplantation, 89*(5), 509–517. https://doi.org/10.1097/TP.0b013e3181c7dc99
8. Caplan, A. I., & Dennis, J. E. (2006). Mesenchymal stem cells as trophic mediators. *Journal of Cellular Biochemistry, 98*(5), 1076–1084. https://doi.org/10.1002/jcb.20886
9. Huang, Y. Y., Sharma, S. K., Carroll, J., & Hamblin, M. R. (2011). Biphasic dose response in low level light therapy—An update. *Dose Response, 9*(4), 602–618. https://doi.org/10.2203/dose-response.11-009.Hamblin
10. Kim, H. B., Baik, K. Y., Seonwoo, H., Jang, K. J., Lee, M. C., Choung, P. H., & Chung, J. H. (2018). Effects of pulsing of light on the dentinogenesis of dental pulp stem cells in vitro. *Science and Reports, 8*(1), 2057. https://doi.org/10.1038/s41598-018-19395-x
11. Sommer, A. P., Pinheiro, A. L., Mester, A. R., Franke, R. P., & Whelan, H. T. (2001). Biostimulatory windows in low-intensity laser activation: Lasers, scanners, and NASA's light-emitting diode array system. *Journal of Clinical Laser Medicine & Surgery, 19*(1), 29–33. https://doi.org/10.1089/104454701750066910
12. de Freitas, L. F., & Hamblin, M. R. (2016). Proposed mechanisms of photobiomodulation or low-level light therapy. *IEEE Journal of Selected Topics in Quantum Electronics, 22*(3), 7000417. https://doi.org/10.1109/JSTQE.2016.2561201
13. Lanzafame, R. J., Stadler, I., Kurtz, A. F., Connelly, R., Peter, T. A., Sr., Brondon, P., & Olson, D. (2007). Reciprocity of exposure time and irradiance on energy density during photoradiation on wound healing in a murine pressure ulcer model. *Lasers in Surgery and Medicine, 39*(6), 534–542. https://doi.org/10.1002/lsm.20519
14. Hamblin, M. R., & Demidova, T. N. (2006). Mechanisms of low level light therapy. *Proceedings of SPIE, 6140*, 614001. https://doi.org/10.1117/12.646294
15. Ginani, F. F., Soares, D. M., Barreto, M. P. E. V., & Barboza, C. A. G. (2015). Effect of low-level laser therapy on mesenchymal stem cell proliferation: a systematic review. *Lasers in Medical Science, 30*(8), 2189–2194. https://doi.org/10.1007/s10103-015-1730-9
16. Borzabadi-Farahani, A. (2016). Effect of low-level laser irradiation on proliferation of human dental mesenchymal stem cells; a systemic review. *Journal of Photochemistry and Photobiology B: Biology, 162*, 577–582. https://doi.org/10.1016/j.jphotobiol.2016.07.022
17. Li, W. T., Leu, Y. C., & Wu, J. L. (2010). Red-light light-emitting diode irradiation increases the proliferation and osteogenic differentiation of rat bone marrow mesenchymal stem cells. *Photomedicine and Laser Surgery, Suppl, 1*, S157–S165. https://doi.org/10.1089/pho.2009.2540
18. Peng, F., Wu, H., Zheng, Y., Xu, X., & Yu, J. (2012). The effect of noncoherent red light irradiation on proliferation and osteogenic differentiation of bone marrow mesenchymal stem cells. *Lasers in Medical Science, 27*(3), 645–653. https://doi.org/10.1007/s10103-011-1005-z
19. Wu, J. Y., Wang, Y. H., Wang, G. J., Ho, M. L., Wang, C. Z., Yeh, M. L., & Chen, C. H. (2012). Low-power GaAlAs laser irradiation promotes the proliferation and osteogenic differentiation of stem

cells via IGF1 and BMP2. *PLoS ONE, 7*(9), e44027. https://doi.org/10.1371/journal.pone.0044027
20. Wu, J. Y., Chen, C. H., Yeh, L. Y., Yeh, M. L., Ting, C. C., & Wang, Y. H. (2013). Low-power laser irradiation promotes the proliferation and osteogenic differentiation of human periodontal ligament cells via cyclic adenosine monophosphate. *International Journal of Oral Science, 5*(2), 85–91. https://doi.org/10.1038/ijos.2013.38
21. Soleimani, M., Abbasnia, E., Fathi, M., Sahraei, H., Fathi, Y., & Kaka, G. (2012). The effects of low-level laser irradiation on differentiation and proliferation of human bone marrow mesenchymal stem cells into neurons and osteoblasts-an in vitro study. *Lasers in Medical Science, 27*(2), 423–430. https://doi.org/10.1007/s10103-011-0930-1
22. Ateş, G. B., Ak, A., Garipcan, B., & Gülsoy, M. (2020). Photobiomodulation effects on osteogenic differentiation of adipose-derived stem cells. *Cytotechnology, 72*, 247–258. https://doi.org/10.1007/s10616-020-00374-y
23. Kushibiki, T., & Awazu, K. (2008). Controlling osteogenesis and adipogenesis of mesenchymal stromal cells by regulating a circadian clock protein with laser irradiation. *International Journal of Medical Sciences, 5*(6), 319–326. https://doi.org/10.7150/ijms.5.319
24. Kushibiki, T., & Awazu, K. (2009). Blue laser irradiation enhances extracellular calcification of primary mesenchymal stem cells. *Photomedicine and Laser Surgery, 27*(3), 493–498. https://doi.org/10.1089/pho.2008.2343
25. Wang, Y., Huan, Y. Y., Wang, Y., Lyu, P., & Hamblin, M. R. (2016). Photobiomodulation (blue and green light) encourages osteoblastic-differentiation of human adipose-derived stem cells: Role of intracellular calcium and light-gated ion channels. *Scientific Reports, 6*, 33719. https://doi.org/10.1038/srep33719
26. Zhu, T., Wu, Y., Zhou, X., Yang, Y., & Wang, Y. (2019). Irradiation by blue light-emitting diode enhances osteogenic differentiation in gingival mesenchymal stem cells in vitro. *Lasers in Medical Science, 34*, 1473–1481. https://doi.org/10.1007/s10103-019-02750-3
27. Yang, Y., Zhu, T., Wu, Y., Shu, C., Chen, Q., Yang, J., Luo, X., & Wang, Y. (2020). Irradiation with blue light-emitting diode enhances osteogenic differentiation of stem cells from the apical papilla. *Lasers in Medical Science, 35*, 1981–1988. https://doi.org/10.1007/s10103-020-02995-3
28. Karu, T. I., & Kolyakov, S. F. (2005). Exact action spectra for cellular responses relevant to phototherapy. *Photomedicine and Laser Surgery, 23*(4), 355–361. https://doi.org/10.1089/pho.2005.23.355
29. Eichler, M., Lavi, R., Shainberg, A., & Lubart, R. (2005). Flavins are source of visible-light-induced free radical formation in cells. *Lasers in Surgery and Medicine, 37*(4), 314–319. https://doi.org/10.1002/lsm.20239
30. Lubart, R., Lavi, R., Friedmann, H., & Rochkind, S. (2006). Photochemistry and photobiology of light absorption by living cells. *Photomedicine and Laser Surgery, 24*(2), 179–185. https://doi.org/10.1089/pho.2006.24.179
31. Farivar, S., Malekshahabi, T., & Shiari, R. (2014). Biological effects of low level laser therapy. *Journal of Lasers in Medical Sciences, 5*(2), 58–62. https://doi.org/10.22037/2010.v5i2.5540
32. Chen, C. T., Shih, Y. R. V., Kuo, T. K., Lee, O. K., & Wei, Y. H. (2008). Coordinated changes of mitochondrial biogenesis and antioxidant enzymes during osteogenic differentiation of human mesenchymal stem cells. *Stem Cells, 26*(4), 960–968. https://doi.org/10.1634/stemcells.2007-0509
33. Lyublinskaya, O. G., Borisov, Y. G., Pugovkina, N. A., Smirnova, I. S., Obidina, J. V., Ivanova, J. S., Zenin, V. V., Shatrova, A. N., Borodkina, A. V., Aksenov, N. D., Zemelko, V. I., Burova, E. B., Puzanov, M. V., & Nikolsky, N. N. (2015). Reactive oxygen species are required for human mesenchymal stem cells to initiate proliferation after the quiescence exit. *Oxidative Medicine and Cellular Longevity*. https://doi.org/10.1155/2015/502105
34. Karu, T. (1987). Photobiological fundamentals of low-power laser therapy. *IEEE Journal of Quantum Electronics, 23*(10), 1703–1717. https://doi.org/10.1109/JQE.1987.1073236
35. Karu, T. (1999). Primary and secondary mechanisms of action of visible to near-IR radiation on cells. *Journal of Photochemistry and Photobiology B: Biology, 49*(1), 1–17. https://doi.org/10.1016/S1011-1344(98)00219-X
36. Karu, T. I., Kalendo, G. S., Letokhov, V. S., & Lobko, V. V. (1982). Biostimulation of Hela cells by low-intensity visible light. *Il Nuovo Cimento D, 1*(6), 828–840. https://doi.org/10.1007/BF02457460
37. Karu, T. I., Pyatibrat, L. V., & Afanasyeva, N. I. (2005). Cellular effects of low power laser therapy can be mediated by nitric oxid. *Lasers in Surgery and Medicine, 36*(4), 307–314. https://doi.org/10.1002/lsm.20148
38. Antunes, F., Boveris, A., & Cadenas, E. (2004). On the mechanism and biology of cytochrome oxidase inhibition by nitric oxide. *Proceedings of the National Academy of Sciences of the United States of America, 101*(48), 16774–16779. https://doi.org/10.1073/pnas.0405368101
39. Lane, N. (2006). Cell biology: Power games. *Nature, 443*(7114), 901–903. https://doi.org/10.1038/443901a
40. Wong-Riley, M. T. T., Liang, H. L., Eells, J. T., Chance, B., Henry, M. M., Buchmann, E., Kane, M., & Whelan, H. T. (2005). Photobiomodulation directly benefits primary neurons functionally inactivated by toxins: Role of cytochrome c oxidase. *Journal of Biological Chemistry, 280*(6), 4761–4771. https://doi.org/10.1074/jbc.M409650200
41. Lubart, R., Wollman, Y., Friedmann, H., Rochkind, S., & Laulicht, S. (1992). Effects of visible and near-infrared lasers on cell cultures. *Journal of Photochemistry and Photobiology, B: Biology, 12*(3), 305–310. https://doi.org/10.1016/1011-1344(92)85032-P
42. Lavi, R., Shainberg, A., Shneyvays, V., Hochauser, E., AIsaac, A., Zinman, T., Friedmann, H., & Lubart, R. (2002). Detailed analysis of reactive oxygen species induced by visible light in various cell type. *Lasers in Surgery and Medicine, 42*(6), 473–480. https://doi.org/10.1002/lsm.20919
43. Finkel, T. (2003). Oxidant signals and oxidative stress. *Current Opinion in Cell Biology, 15*(2), 247–254. https://doi.org/10.1016/S0955-0674(03)00002-4
44. Janssen-Heininger, Y. M. W., Mossman, B. T., Heintz, N. H., Forman, H. J., Kalyanaraman, B., Finkel, T., Stamler, J. S., Rhee, S. G., & van der Vliet, A. (2008). Redox-based regulation of signal transduction: Principles, pitfalls, and promises. *Free Radical Biology and Medicine, 45*(1), 1–17. https://doi.org/10.1016/j.freeradbiomed.2008.03.011
45. Hsu, D. S., Zhao, X., Zhao, S., Kazantsev, A., Wang, R. P., Todo, T., Wei, Y. F., & Sancar, A. (1996). Putative human blue-light photoreceptors hCRY1 and hCRY2 are flavoproteins. *Biochemistry, 35*(44), 13871–21387. https://doi.org/10.1021/bi962209o
46. Lin, C., Robertson, D. E., Ahmad, M., Raibekas, A. A., Jorns, M. S., Dutton, P. L., & Cashmor, A. R. (1995). Association of flavin adenine dinucleotide with the Arabidopsis blue light receptor CRY1. *Science, 269*(5226), 968–970. https://doi.org/10.1126/science.7638620
47. Todo, T., Kim, S. T., Hitomi, K., Otoshi, E., Inui, T., Morioka, H., Kobayashi, H., Ohtsuka, E., Toh, H., & Ikenaga, M. (1997). Flavin adenine dinucleotide as a chromophore of the Xenopus (6–4)photolyase. *Nucleic Acids Research, 25*(4), 764–768. https://doi.org/10.1093/nar/25.4.764
48. Shearman, L. P., Sriram, S., Weaver, D. R., Maywood, E. S., Chaves, I., Zheng, B., Kume, K., Lee, C. C., Gvan der Horst, G.

T., Hastings, M. H., & Reppert, S. M. (2000). Interacting molecular loops in the mammalian circadian clock. *Science, 288*(5468), 1013–1019. https://doi.org/10.1126/science.288.5468.1013
49. Tamaru, T., Hattori, M., Ninomiya, Y., Kawamura, G., Varès, G., Honda, K., Mishra, D. P., Wang, B., Benjamin, I., Sassone-Corsi, P., Ozawa, T., & Takamatsu, K. (2013). ROS stress resets circadian clocks to coordinate pro-survival signals. *PLoS ONE, 8*(12), e82006. https://doi.org/10.1371/journal.pone.0082006
50. Fu, L., Patel, M. S., Bradley, A., Wagner, E. F., & Karsenty, G. (2005). The molecular clock mediates leptin-regulated bone formation. *Cell, 122*(5), 803–815. https://doi.org/10.1016/j.cell.2005.06.028
51. Griendling, K., Sorescu, D., & Ushio-Fukai, M. (2000). NAD(P)H oxidase: Role in cardiovascular biology and disease. *Circulation Research, 86*(5), 494–501. https://doi.org/10.1161/01.RES.86.5.494
52. Braunersreuther, V., & Jaquet, V. (2012). Reactive oxygen species in myocardial reperfusion injury: From physiopathology to therapeutic approaches. *Current Pharmaceutical Biotechnology, 13*(1), 97–114. https://doi.org/10.2174/138920112798868782
53. Starkov, A. A. (2008). The role of mitochondria in reactive oxygen species metabolism and signalling. *Annals of the New York Academy of Sciences, 1147*, 37–52. https://doi.org/10.1196/annals.1427.015
54. Kukreja, R. C., Kontos, H. A., Hess, M. L., & Ellis, E. F. (1986). PGH synthase and lipoxygenase generate superoxide in the presence of NADH or NADPH. *Circulation Research, 59*(6), 612–619. https://doi.org/10.1161/01.RES.59.6.612
55. Roy, P., Roy, S. K., Mitra, A., & Kulkarni, A. P. (1994). Superoxide generation by lipoxygenase in the presence of NADH and NADPH. *Biochimica et Biophysica Acta, 1214*(2), 171–179. https://doi.org/10.1016/0005-2760(94)90041-8
56. O'Donnell, V. B., & Azzi, A. (1996). High rates of extracellular superoxide generation by cultured human fibroblasts: Involvement of a lipid-metabolizing enzyme. *Biochemical Journal, 318*(Pt 3), 805–812. https://doi.org/10.1042/bj3180805
57. Nathan, C., & Cunningham-Bussel, A. (2013). Beyond oxidative stress: An immunologist's guide to reactive oxygen species. *Nature Reviews Immunology, 13*(5), 349–361. https://doi.org/10.1038/nri3423
58. Gross, E., Sevier, C. S., Heldman, N., Vitu, E., Bentzur, M., Kaiser, C. A., Thorpe, C., & Fass, D. (2006). Generating disulfides enzymatically: Reaction products and electron acceptors of the endoplasmic reticulum thiol oxidase Ero1p. *Proceedings of the National Academy of Sciences of the United States of America, 103*(2), 299–304. https://doi.org/10.1073/pnas.0506448103
59. Wu, R. F., Ma, Z., Liu, Z. L. S., & Terada, L. S. (2010). Nox4-derived H2O2 mediates endoplasmic reticulum signaling through local Ras activation. *Molecular and Cellular Biology, 30*(14), 3553–3568. https://doi.org/10.1128/mcb.01445-09
60. Boveris, A., Oshino, N., & Chance, B. (1972). The cellular production of hydrogen peroxide. *The Biochemical Journal, 128*(3), 617–630. https://doi.org/10.1042/bj1280617
61. Matsui, S., Takahashi, C., Tsujimoto, Y., & Matsushima, K. (2009). Stimulatory effects of low-concentration reactive oxygen species on calcification ability of human dental pulp cells. *Journal of Endodontics, 35*(1), 67–72. https://doi.org/10.1016/j.joen.2008.08.034
62. Tao, J., Wang, H., Zhai, Y., Park, H., Wang, J., Ji, F., & Zhang, Z. (2016). Downregulation of Nrf2 promotes autophagy-dependent osteoblastic differentiation of adipose-derived mesenchymal stem cells. *Experimental Cell Research, 349*(2), 221–229. https://doi.org/10.1016/j.yexcr.2016.09.013
63. Bigarella, C. L., Liang, R., & Ghaffari, S. (2014). Stem cells and the impact of ROS signalling. *Development (Cambridge), 22*, 4206–4218. https://doi.org/10.1242/dev.107086
64. Valle-Prieto, A., & Conget, P. A. (2010). Human mesenchymal stem cells efficiently manage oxidative stress. *Stem Cells and Development, 19*(12), 1885–1893. https://doi.org/10.1089/scd.2010.0093
65. Kim, K. S., Choi, H. W., Yoon, H. E., & Kim, I. Y. (2010). Reactive oxygen species generated by NADPH oxidase 2 and 4 are required for chondrogenic differentiation. *Journal of Biological Chemistry, 285*(51), 40294–40302. https://doi.org/10.1074/jbc.M110.126821
66. Atashi, F., Modarressi, A., & Pepper, M. S. (2015). The role of reactive oxygen species in mesenchymal stem cell adipogenic and osteogenic differentiation: A review. *Stem Cells and Development, 24*(10), 1150–1163. https://doi.org/10.1089/scd.2014.0484
67. Denu, R. A., & Hematti, P. (2016). Effects of oxidative stress on mesenchymal stem cell biology. *Oxidative Medicine and Cellular Longevity*. https://doi.org/10.1155/2016/2989076
68. Amaroli, A., Agas, D., Laus, F., Cuteri, V., Hanna, R., Sabbieti, M. G., & Benedicenti, S. (2018). The effects of photobiomodulation of 808 nm diode laser therapy at higher fluence on the in vitro osteogenic differentiation of bone marrow stromal cells. *Frontiers in Physiology, 9*, 123. https://doi.org/10.3389/fphys.2018.00123
69. Turrioni, A. P. S., Basso, F. G., Montoro, L. A., De Almeida, L. D. F. D., Costa, C. A. D. S., & Hebling, J. (2014). Phototherapy up-regulates dentin matrix proteins expression and synthesis by stem cells from human-exfoliated deciduous teeth. *Journal of Dentistry, 42*(10), 1292–1299. https://doi.org/10.1016/j.jdent.2014.07.014
70. Yuan, Y., Yan, G., Gong, R., Zhang, L., Liu, T., Feng, C., Du, W., Wang, Y., Yang, F., Li, Y., Guo, S., Ding, F., Ma, W., Idiiatullina, E., Pavlov, V., Han, Z., Cai, B., & Yang, L. (2017). Effects of blue light emitting diode irradiation on the proliferation, apoptosis and differentiation of bone marrow-derived mesenchymal stem cells. *Cellular Physiology and Biochemistry, 43*(1), 237–246. https://doi.org/10.1159/000480344
71. Glavaš, H., Vukobratović, M., & Keser, T. (2018). Infrared thermography as control of handheld IPL device for home-use. *Journal of Cosmetic and Laser Therapy, 20*(5), 269–277. https://doi.org/10.1080/14764172.2017.1406607
72. Wang, Z., Cai, F., Chen, X., Luo, M., Hu, L., & Lu, Y. (2013). The role of mitochondria-derived reactive oxygen species in hyperthermia-induced platelet apoptosis. *PLoS ONE, 8*(9), e75044. https://doi.org/10.1371/journal.pone.0075044
73. Shui, C., & Scutt, A. (2001). Mild heat shock induces proliferation, alkaline phosphatase activity, and mineralization in human bone marrow stromal cells and Mg-63 cells in vitro. *Journal of Bone and Mineral Research, 16*(4), 731–741. https://doi.org/10.1359/jbmr.2001.16.4.731
74. Chen, J., Shi, Z. D., Ji, X., Morales, J., Zhang, J., Kaur, N., & Wang, S. (2013). Enhanced osteogenesis of human mesenchymal stem cells by periodic heat shock in self-assembling peptide hydrogel. *Tissue Engineering Part A, 19*(5–6), 716–728. https://doi.org/10.1089/ten.tea.2012.0070
75. Li, C., Sunderic, K., Nicoll, S. B., & Wang, S. (2018). Downregulation of Heat Shock Protein 70 Impairs Osteogenic and Chondrogenic Differentiation in Human Mesenchymal Stem Cells. *Science and Reports, 8*, 553. https://doi.org/10.1038/s41598-017-18541-1
76. Sommer, A. P. (2019). Mitochondrial cytochrome c oxidase is not the primary acceptor for near infrared light—It is mitochondrial bound water: the principles of low-level light therapy. *Annals of Translational Medicine, 7*(Suppl 1), S13. https://doi.org/10.21037/atm.2019.01.43
77. Arai, M., Shibata, Y., Pugdee, K., Abiko, Y., & Ogat, Y. (2007). Effects of reactive oxygen species (ROS) on antioxidant system and osteoblastic differentiation in MC3T3-E1 cells. *IUBMB Life, 59*(1), 27–33. https://doi.org/10.1080/15216540601156188

78. Consentino, L., Lambert, S., Martino, C., Jourdan, N., Bouchet, P. E., Witczak, J., Castella, P., El-Esawi, M., Corbineau, F., d'Harlingue, A., & Ahmad, M. (2015). Blue-light dependent reactive oxygen species formation by Arabidopsis cryptochrome may define a novel evolutionarily conserved signaling mechanis. *New Phytologist, 206*(4), 1450–1462. https://doi.org/10.1111/nph.13341

79. Jourdan, N., Martino, C. F., El-Esawi, M., Witczak, J., Bouchet, P. E., d'Harlingue, A., & Ahmad, M. (2015). Blue-light dependent ros formation by arabidopsis cryptochrome-2 may contribute toward its signaling role. *Plant Signaling and Behavior, 10*(8), e1042647. https://doi.org/10.1080/15592324.2015.1042647